

# **NOVEL APPROACHES TO IRON CHELATION THERAPY: NOVEL COMBINATIONS AND NOVEL COMPOUNDS**

**Dr Evangelia Vlachodimitropoulou Koumoutsea**

**BSc, MBBS**

**King's College London**

**A thesis submitted for the degree of PhD**

**University College London (UCL)**

From work performed at  
the Department of  
Haematology, University  
College London,  
72 Huntley Street,  
London, WC1E 6BT

'I, Evangelia Vlachodimitropoulou Koumoutsea confirm that the work presented  
in this thesis is my own. Where information has been derived from other sources,

I confirm that this has been indicated in the thesis.'

ITHACA by C.P. Cavafy

*As you set out for Ithaka  
hope the voyage is a long one,  
full of adventure, full of discovery.  
Laistrygonians and Cyclops,  
angry Poseidon—don't be afraid of them:  
you'll never find things like that on your way  
as long as you keep your thoughts raised high,  
as long as a rare excitement  
stirs your spirit and your body.  
Laistrygonians and Cyclops,  
wild Poseidon—you won't encounter them  
unless you bring them along inside your soul,  
unless your soul sets them up in front of you.*

*Hope the voyage is a long one.  
May there be many a summer morning when,  
with what pleasure, what joy,  
you come into harbors seen for the first time;  
may you stop at Phoenician trading stations  
to buy fine things,  
mother of pearl and coral, amber and ebony,  
sensual perfume of every kind—  
as many sensual perfumes as you can;  
and may you visit many Egyptian cities  
to gather stores of knowledge from their scholars.*

*Keep Ithaka always in your mind.  
Arriving there is what you are destined for.  
But do not hurry the journey at all.  
Better if it lasts for years,  
so you are old by the time you reach the island,  
wealthy with all you have gained on the way,  
not expecting Ithaka to make you rich.*

*Ithaka gave you the marvelous journey.  
Without her you would not have set out.  
She has nothing left to give you now.*

*And if you find her poor, Ithaka won't have fooled you.  
Wise as you will have become, so full of experience,  
you will have understood by then what these Ithakas mean.*

## ACKNOWLEDGEMENTS

After a 5 year journey, the day to put the finishing touch to my thesis has come. It has been a period of intense learning for me, not only scientifically but also personally. I am extremely happy to be in a position to write this note of thanks, as I consider this one of my biggest achievements to date.

This journey has allowed me to consolidate a number of relationships. I would like to first and foremost express my sincere gratitude to my supervisor Prof. John Porter for welcoming me into his team. Despite my slightly unconventional research path he has been unwavering in his support, patience, motivation, enthusiasm, and encouragement. I could not have imagined having a better mentor.

I would like to express my appreciation to Dr. Anna David for her support and advice in both my clinical and academic work. A special thank you goes to Dr. Panicos Shangaris for his encouragement and invaluable support with the mouse work. Special thanks also goes to Prof. Robert Hider for his constant support throughout this time with his enthusiasm and immense knowledge on medicinal chemistry as well as Dr. Yu-Lin for his contribution of invaluable compound combination speciation plots. Many thanks to Dr. Daniel Stuckley and Laurence Jackson from the UCL Centre for Advanced Biomedical Imaging (CABI) for a brilliant collaboration. I would also like to acknowledge Prof. Richard Naftalin, who introduced me to the world of research and who has encouraged and supported me every step of the way, up until today.

I would like to thank all my fellow labmates, particularly Dr. Maciej Garbowski and Dr. Edith Weiner for all the guidance, stimulating discussions, and sleepless nights spent working together, plus all the fun we have had collaborating over the last 5 years. Huge thanks to Dr. Srichairatankool and our team from Thailand, Pimpi, and Adchara who spent many months tirelessly working with us.

I would like to express my profound gratitude to my mother, dog Hector, aunt Stamatia and cousin Dimitri and to all of my family for their unconditional love and support. I would also like to thank my friends Lizzie, Neil, Igor, Maria and my Kolyan for putting up with me when times were rough, supporting me during my write up and seeing me through this journey.

Finally, I gratefully acknowledge the Onassis Foundation, Greece, and Novartis UK, for their financial support which has made this thesis possible.

## SUMMARY

Iron overload is an inevitable consequence of repeated blood transfusions required to sustain life in a wide array of haematological conditions such as thalassaemia, aplastic anaemia, and myelodysplastic syndromes (MDS). Without iron chelation therapy, death from cardiotoxic effects of iron overload usually ensues in the second decade. Iron chelation therapy with subcutaneous Desferrioxamine (DFO) infusions at least 5 nights per week has been shown unequivocally to prolong life expectancy in thalassaemia major. However, although this molecule is remarkably free of toxic side effects at treatment doses, patient compliance is often poor, and iron overload still leads to death today.

One of the scopes of this Ph.D. was to develop a cellular model that would allow the testing of novel chelating agents used alone or in combination with established chelators. Our *in vitro* model of iron overload was able to elucidate several principles regarding the interactions of chelators within cells. It allowed for the first time a detailed interrogation of synergy as opposed to additivity of action of licensed chelators when used in combination, which has now been published. This model is also relevant to the development of new chelators and was used to demonstrate the iron binding properties of Eltrombopag (ELT), a drug used to manage ITP, at clinically achievable concentrations. ELT is a powerful intracellular iron chelator that decreases storage iron and enhances iron removal when in combination with commercially available iron chelators. In clinical use, donation of chelated iron by ELT to these chelators offers established routes for elimination of chelated iron. Furthermore, we extensively investigated the iron mobilising properties of the naturally occurring flavonoid quercetin and its principle metabolites. For the first time we showed that quercetin and its metabolites can act as a shuttle when combined with licensed chelators and provided a unique structure-function analysis of flavonoids with regards to iron and ferritin mobilisation and antioxidant capacity as a function of Fe(II) binding.

A further goal of this thesis was to establish an iron-overloaded humanised thalassaemia mouse model that could be used to examine whether the same principles which determine iron release from cell cultures also influence the oral efficiency of iron chelators, *in vivo*. We utilised iron dextran to achieve cardiac iron loading confirmed by histology and MRI investigations. Iron overloaded mice were treated with a combination of the flavonoid quercetin and the iron chelator Deferasirox (DFX), and we established the value of this in combination in terms of cardiac iron mobilisation. Our novel humanised  $\beta$  thalassaemia iron-overloaded mouse model demonstrating cardiac iron loading is a first-in-kind development, and the novel application of MRI will provide a useful tool for studying iron chelators, the pathophysiology and disease progression, blood transfusion regimens and cellular/gene therapy in iron overload in the future. Our findings *in vivo* support the contention that our cellular model is a useful screening tool for new compounds, both for toxicity and efficacy.

**Keywords:** Iron, Chelator, Hepatocyte, Cardiomyocyte, Thalassaemia



## Table of Contents

NOVEL APPROACHES TO IRON CHELATION THERAPY: NOVEL COMBINATIONS AND NOVEL COMPOUNDS.....	1
ACKNOWLEDGEMENTS .....	3
LIST OF ABBREVIATIONS.....	16
Chapter 1 INTRODUCTION .....	17
1.1 Objective of this work.....	17
1.2 The need for safe and effective iron chelation.....	17
1.3 Principles of iron chelation therapy .....	22
1.4 Design of chelators: properties for maximal oral efficacy.....	27
1.5 Properties to minimise toxicity: design of chelators.....	31
1.6 Chelator Evaluation .....	34
1.7 Commercially available iron chelators .....	44
1.8 Other chelators that have reached clinical trials .....	51
1.9 Conclusions.....	53
Chapter 2 MATERIALS AND METHODS.....	54
2.1 Iron chelators and substances tested for iron chelation activity .....	54
2.2 Cell Lines .....	54
2.3 Cellular Methods.....	54

2.4	Flowchart of final cellular iron loading model .....	59
2.5	Ferritin quantification .....	59
2.6	Determination of intracellular reactive oxygen species (ROS) levels using a fluorimetric method .....	60
2.7	Preparation of heat-inactivated human serum.....	61
2.8	Animal Study .....	62
2.9	Drug Combination Analysis .....	66
2.10	Statistical analysis.....	67
Chapter 3	HEPATOCYTE AND CARDIOMYOCYTE CULTURES; Development of a model to study iron mobilisation by chelators.....	68
3.1	Introduction.....	68
3.2	Iron and the human liver .....	69
3.3	Iron Uptake Mechanisms .....	72
3.4	Developing the cellular model; the approach .....	76
3.5	Establishing optimal medium for iron loading in HuH7 cells .....	76
3.6	Establishing the number of media changes for optimal iron loading .....	80
3.7	Establishing the optimal cell washing technique .....	80
3.8	Regime for iron loading and washing of H9C2 cardiomyocyte cells.....	83

3.9	Cell damage in HuH7/H9C2 assessed by Tryptan blue, AO/PI staining and LDH release .....	85
3.10	Time course of and concentration dependence of intracellular iron mobilisation with DFO, DFP and DFX monotherapy .....	86
3.11	Iron release with low membrane-permeable hydrophilic iron chelators ...	91
3.12	Effect of iron loadin or iron chelation of cellular ferritin in HuH7 and H9C2 cells.	93
3.13	Discussion .....	97
3.14	Conclusion .....	98
Chapter 4	THE INFLUENCE OF COMBINATION OF COMMERCIALY AVAILABLE IRON CHELATORS ON RELEASE OF CELLULAR IRON. ....	100
4.1	Introduction.....	100
4.2	Chelator speciation plots and their relevance to synergistic chelator combinations .....	100
4.3	Comparison of cellular iron mobilisation with monotherapy and combinations in HuH7 cells .....	104
4.4	Effect of chelator combinations on the intracellular iron pool after 8 hours in cardiomyocytes (H9C2).....	107
4.5	Differentiation of synergy vs. additivity of chelator combinations using isobolograms .....	109
4.6	Indexes of synergy with the three combinations.....	111

4.7	Insights into synergistic mechanisms using the hydroxypyridinones CP40 and CP44 as probes.....	116
4.8	Discussion.....	118
4.9	Conclusion.....	121
Chapter 5 ELTROMBOPAG IS A POWERFUL CHELATOR OF IRON(III), THAT MOBILISES INTRACELLULAR STORAGE IRON ALONE OR IN COMBINATION WITH CLINICALLY ESTABLISHED CHELATORS.....		
		122
5.1	Introduction.....	122
5.2	Material and methods.....	123
5.3	Results.....	127
5.4	Discussion.....	142
5.5	Conclusion.....	146
Chapter 6 THE INFLUENCE OF FLAVONOIDS ON CELLULAR IRON MOBILISATION ALONE OR IN COMBINATION WITH CLINICALLY AVAILABLE IRON CHELATORS.....		
		147
6.1	Introduction.....	147
6.2	Chemistry of flavonoids.....	148
6.3	Dietary uptake and metabolism of flavonoids in humans.....	151
6.4	Flavonoids and their biological activities.....	152
6.5	Dietary uptake, metabolism and toxicology of Quercetin.....	155

6.6	Materials and Methods.....	159
6.7	Results.....	161
6.8	Synergistic chelation of Quercetin combined with otherwise ineffective hydroxyxyridinone CP40.....	180
6.9	Discussion.....	182
6.10	Conclusion.....	186
Chapter 7	DEVELOPMENT OF AN IRON-OVERLOADED MOUSE MODEL FOR TESTING THE ORAL EFFICACY OF IRON MOBILISATION WITH FLAVONOIDS ALONE OR IN COMBINATION WITH OTHER IRON CHELATION.....	187
7.1	Rationale for developing a murine model where cardiac iron overload is achieved.....	187
7.2	Mouse models of cardiac iron-overload.....	187
7.3	Development of the iron overloaded murine mouse model.....	192
7.4	Results.....	195
7.5	Discussion and conclusion.....	209
7.6	Testing the flavonoid quercetin in our animal model.....	211
Chapter 8	CONCLUSIONS AND FUTURE PERSPECTIVES.....	220
8.1	The value of the <i>in vitro</i> cultures and <i>in vivo</i> mouse model for investigating iron chelators.....	220
8.2	Limitations of the cellular culture system in investigating iron chelators.....	222

8.3	Future developments and perspectives .....	225
8.4	Conclusion .....	225
	APPENDICES .....	227

## List of Tables

Table 1 Estimated global annual births with major haemoglobinopathies. ....	20
Table 2 Overview of cellular systems used to study the efficacy and toxicity of chelators .	38
Table 3 Methods used to iron-load animals. ....	43
Table 4 Properties, pharmacokinetics, and metabolism of commercially available iron chelators.....	50
Table 5 Percentage of intracellular iron removed by chelators in HuH7 and H9C2 .....	90
Table 6 Iron chelator characteristics.....	101
Table 7 Combination Indices of chelators in cardiomyocytes (H9C2).....	112
Table 8 Combination indices of chelators in hepatocytes (HuH7).....	113
Table 9 Chelator DRI in hepatocytes (HuH7). ....	114
Table 10 Chelator Dose reduction in cardiomyocytes (H9C2). ....	114
Table 11 Comparison of the structure and iron binding properties of ELT and other chelators.....	128
Table 12 Comparison of percentage of intracellular iron mobilised at 8h in a cardiomyocyte (H9C2) and a hepatocyte (HuH7) cell lines by clinically available chelators or ELT, alone (top panel) or in combination (lower panel). ....	131
Table 13 Comparison of ROS generation in cardiomyocyte (H9C2) and a hepatocyte (HuH7) cell lines is shown after addition of clinically available chelators or ELT, alone (top panel) or in combination (lower panel) over 90 minutes at the concentrations shown. .....	134
Table 14 Food sources of dietary flavonoids. ....	147
Table 15 Percentage viability assessed by the LDH assay following 12 hours of treatment with quercetin and its metabolites at 30µM. ....	162
Table 16 Percentage iron release from hepatocyte (HuH7) and cardiomyocyte (H9C2) cells following 8 hours of treatment with commercially available chelators at 30µM and quercetin at 30µM.....	163
Table 17 Synergy Index 'α' for the combination treatment of commercially available chelators with quercetin in cardiomyocyte (H9C2) cells.....	180
Table 18 Heart, liver and spleen tissue iron.....	198
Table 19 Changes in haematological parameters secondary to iron loading with iron dextran.....	200
Table 20 Total 'blue' iron containing area count from the histology images in Figure 70 . .....	218
Table 21 Total number of 'blue' pixels in the histology images in Figure 70 .....	218

## List of Figures

Figure 1 Illustration of the three commercially available iron chelators and their denticity. .....	29
Figure 2 Rhodotorulic Acid (RA) structure (Grady et al, 1979) .....	51
Figure 3 Structures of the iron chelators Desferrithiocin, Deferitricin, Deferitazole .....	53
Figure 4 AO/PI staining following 8 hours of treatment with DFO at 30 $\mu$ M ibe. ....	56
Figure 5 Trypan blue staining in HuH7 cells following 8 hours of chelator treatment.....	57
Figure 6 Ferrosine assay standard curve. ....	58
Figure 7 Rat (A) and human (B) ferritin standard curve.....	60
Figure 8 Effect of varying the concentration of DCF on ROS production in HuH7 cells.....	61
Figure 9 Sample Isobologram .....	67
Figure 10 FAC/FBS loading regime in HuH7 cells.....	78
Figure 11 Total iron concentration of RPMI media and RPMI media containing 10% FBS (A) and NTBI content (B).....	79
Figure 12 HuH7 iron following 1 or 2 changes of 10% FBS media, each for 10 hours.....	80
Figure 13 Effect of washing HuH7 cells with PBS for different time intervals on cellular protein.....	81
Figure 14 Effect of washing HuH7 cells with different agents before and after chelator exposure on iron detection. ....	82
Figure 15 Iron loading of H9C2 with FAC/10% FBS-DMEM media over one (A) or two (B) 10 hour periods. ....	84
Figure 16 LDH viability assay in H9C2 following 8 hours of chelator treatment.....	86
Figure 17 HuH7 intracellular iron mobilisation with DFO, DFP and DFX monotherapy at increasing concentrations at 4 hours of treatment.....	87
Figure 18 HuH7 intracellular iron mobilisation time course with DFO, DFP and DFX monotherapy at (A) 10 $\mu$ M and (B) 30 $\mu$ M.....	88
Figure 19 H9C2 intracellular iron decrements time course with DFO, DFP and DFX monotherapy at 30 $\mu$ M ibe. ....	89
Figure 20 H9C2 intracellular iron mobilisation at 8 hours with increasing concentrations of DFO, DFP, and DFX. ....	90
Figure 21 Decrements in cellular iron after an 8 hour treatment with 100 $\mu$ M CP40/CP46 in A. HuH7 B. H9C2.....	92
Figure 22 Effect of one and two 10 hours treatments of 10% FBS containing media on ferritin concentration in (A) HuH7 and (B) H9C2 cells.....	94
Figure 23 Ferritin in (A) HuH7 and (B) H9C2 cells treated with commercially available chelators for 8 hours.....	96
Figure 24 DFO, DFX, and DFP combination speciation plots at pH 7.4 .....	102



Figure 25 Treatment of HuH7 cells with a combination of (A) DFO and DFX, (B) DFO and DFP, and (C) DFP and DFX for 8 hours and (D) DFP and DFP for 4 hours. ....	104
Figure 26 Treatment of H9C2 cells with a combination of (A) DFO and DFX, (B) DFO and DFP and (C) DFP and DFX for 8 hours.....	107
Figure 27 Commercial chelator combination isobolograms in HuH7 cells. ....	109
Figure 28 Commercial chelator combination isobolograms in H9C2 cells. ....	110
Figure 29 Synergy Index 'α' for the combination treatment of commercially available chelators in hepatocyte (HuH7) and cardiomyocyte (H9C2) cells. ....	111
Figure 30 Treatment of chelator monotherapy combined with CP40 for 8 hours in HuH7 cells.....	116
Figure 31 Structure of Eltrombopag and its iron complex.....	127
Figure 32 Cellular iron release from hepatocyte HuH7 (A) or cardiomyocyte H9C2 cells (B) by ELT is shown as a function of ELT concentration. ....	128
Figure 33 Hepatocyte HuH7 (A) and Cardiomyocyte H9C2 (B) cell viability following an 8-hour treatment with ELT.....	129
Figure 34 Comparison of the effect of ELT on ferritin and total cellular iron mobilisation in hepatocyte HuH7 (A) and cardiomyocyte H9C2 cells (B) is shown. ....	131
Figure 35 The time-course for ROS inhibition by ELT and other chelators.....	133
Figure 36 Rate of ROS production following chelation treatment in (A) HuH7 and (B) H9C2 cells.....	134
Figure 37 The speciation of iron(III) in the presence of ELT as a function of pH. [Fe] <sub>total</sub> =1μM; [ELT] <sub>total</sub> =10μM. ....	137
Figure 38 The proportions of ELT species bound to iron(III) at equilibrium, with increasing ELT concentrations, in the presence of (a) 1μM DFO, (b) 3μM DFP, (c) 2μM DFX.....	138
Figure 39 The effect of serum and albumin on the iron mobilisation by ELT is shown in HuH7 cells.....	138
Figure 40 Cellular iron retention mobilisation is shown in previously iron loaded HuH7 cells, after 8 hours of exposure to ELT 3μM and/or CP40 33μM ibe as single agents and combination over an 8 hour period.....	140
Figure 41 Core flavonoid structure.....	148
Figure 42 Structures of the different flavonoid groups.....	149
Figure 43 Flavonoid binding site for trace metal ions indicated by Men <sup>+</sup> (A)(Kumar & Pandey, 2013) and complexes formed between quercetin and Fe (III) and Fe (II) (B). ....	153
Figure 44 Structure of quercetin and its principal metabolites.....	157
Figure 45 Tryptan blue viability staining in HuH7 cells following a 12 hour treatment with quercetin and its metabolites at 30μM. ....	161
Figure 46 Time course of change in intracellular iron content using monotherapy with quercetin and its metabolites at (A) 3 μM and (B) 30μM and in HuH7 cells.....	165

Figure 47 Concentration dependence for change in cellular iron at 8h after monotherapy with quercetin and its metabolites in HuH7 cells.....	166
Figure 48 Concentration dependent ROS inhibition by Quercetin and its metabolites and commercially available chelators in cardiomyocytes (A) and hepatocytes (B). .....	167
Figure 49 The time-course for ROS inhibition by DFO 1 $\mu$ M ibe, Quercetin, Quercetin-3-glucoside and Quercetin metabolites at 1 $\mu$ M in HuH7 cells.....	169
Figure 50 Ferritin decrements at 8h with quercetin or DFX, DFP or DFO in (A) cardiomyocyte H9C2 cells and (B) in hepatocyte HuH7 .....	171
Figure 51 Ferritin decrements at 8h with quercetin and its metabolites in (A) cardiomyocyte H9C2 cells and (B) in hepatocyte HuH7.....	173
Figure 52 Decrements in HuH7 cellular iron by DFO/DFX/DFP combined with Quercetin or its metabolites.....	176
Figure 53. Decrements in cellular iron in H9C2 cells by combinations of Isorhamnetin with clinically available iron chelators following 8 hours of treatment. (A) DFO-Isorhamnetin, (B) DFP-Isorhamnetin, (C) DFX-Isorhamnetin. ....	177
Figure 54 Quercetin and commercially available chelator combination isobolograms in HuH7 cells.....	179
Figure 55 Cellular iron mobilisation is shown in previously iron loaded HuH7 cells, after 8 hours of exposure to quercetin 3 $\mu$ M and/or CP40 33 $\mu$ M ibe as single agents and combination .....	181
Figure 56 Schematic representation of mouse iron loading model.....	193
Figure 57 Iron in the heart, liver and spleen following iron-loading in mice and a 4 week re-equilibration period.....	196
Figure 58 Perls stain of the heart of iron loaded mice demonstrating iron in the myocardium .....	197
Figure 59 Perls stain of the heart of iron loaded mice demonstrating iron in the myocardium in mice sacrificed directly after the 4 week iron loading treatment or 4 weeks later. ....	198
Figure 60 Comparison of the weight of mice (A) and their heart, liver and spleen weights (B) post sacrifice. ....	201
Figure 61 Mice spleen volumes. ....	202
Figure 62 T2 relaxation times in iron-loaded mice. ....	204
Figure 63 T2* relaxation times in iron-loaded mice .....	205
Figure 64 T1 relaxation times in iron-loaded mice. ....	206
Figure 65 Cardiac function following iron loading. ....	207
Figure 66 Cardiac T2* to iron calibration curve. ....	208
Figure 67 Schematic representation of DFX/Quercetin combination treatment in iron-overloaded mice .....	212

<b>Figure 68 Tissue iron content of the (A) heart, (B) liver and (C) spleen of iron-loaded mice treated with DFX/Quercetin .....</b>	<b>214</b>
<b>Figure 69 Perls staining of heart, liver and spleen tissue in iron loaded mice following DFX/Quercetin treatment.....</b>	<b>216</b>
<b>Figure 70 Perls stain images from Figure 69, following Image J modification to enable blue stained iron pixel quantification.....</b>	<b>217</b>

## LIST OF ABBREVIATIONS

CNS	Central nervous system
CSF	Cerebrospinal fluid
DFO	Desferrioxamine
DFP	Deferiprone
DFX	Deferasirox
ELT	Eltrombopag
FAC	Ferric ammonium citrate
HPO	Hydroxypyridinone
ip	Intraperitoneal
iv	Intravenous
LIP	Labile iron pool
LVEF	Left ventricular ejection function
MDS	Myelodysplastic Syndrome
MW	Molecular weight
NTBI	Non-transferrin bound iron
RA	Rhodotorulic Acid
RES	Reticuloendothelial system
ROS	Reactive oxygen species
sc	Subcutaneous
Tf	Transferrin

## **Chapter 1 INTRODUCTION**

### **1.1 Objective of this work**

The initial purpose of the work carried out in this thesis was to develop an *in vitro* cellular model for the screening of new iron chelators which will provide useful information about the likely relative efficacy and toxicology of iron chelators *in vivo*.

The second purpose was to identify new approaches to iron chelation, either when used as monotherapy or in combination with established chelators. A cell culture model was therefore developed and applied to closely compare single agent chelation with combined use of iron chelators. We also wished to examine the ability of chelators to access intracellular iron pools and abrogate or enhance further the damaging effects of iron overload. Additional objectives were to develop a humanised thalassaemic murine model of iron overload that will allow screening of new chelators and predict toxicology and efficacy of chelation in humans.

In this chapter, the clinical need to identify new oral iron chelators for the management of transfusional iron overload is discussed as well as current knowledge of the chemical and biological requirements of such chelators and their merits and limitations. The advantages and limitations of other available models for evaluating iron chelators both *in vivo* and *in vitro* are also discussed, in order to put into context the potential value of the novel hepatocyte/cardiomyocyte and animal model.

### **1.2 The need for safe and effective iron chelation**

The most established application of iron chelation treatment is the management of transfusional iron overload. Iron overload occurs from repeated blood transfusions, but it can also be a result of excess absorption of iron from the gut, as is the case in hereditary haemochromatosis. Patients who receive 25 units of blood per year, if they are not treated with chelation therapy, will by the age of fifteen years be at risk from the effects of iron overload due to deposition in critical tissues such as the heart, since there is no physiological mechanism for removing this iron (Borgna-Pignatti & Marsella, 2015). Alternatively, an excess of 100 units of blood is equivalent to 20-25g of iron, and will cause cellular, and organ damage through a mechanism such as lipid peroxidation and therefore must be removed prior to this event. Whereas iron loading

from excessive iron absorption can be treated by phlebotomy, transfusional iron loading usually results from conditions associated with anaemia, thereby precluding this option. Iron chelation therapy, defined as the removal of excess iron using iron-binding molecules, is the only therapeutic option unless the underlying cause of the anaemia is corrected.

Repeated blood transfusions will in principle result in iron overload in any condition. There are a number of anaemias which are known to be associated with transfusional siderosis and patients would benefit from the availability of orally active iron chelators. These include aplastic anaemia, myelodysplasia, pyruvate kinase deficiency and red cell aplasia. Iron overload may also occur in other anaemias where sporadic transfusion is more typical or where transfusion is not usually given for the anaemia as such- for example in sickle cell disease. However, worldwide,  $\beta$  thalassaemia major patients are the ones who would benefit the most frequently from regular oral iron chelation therapy.

Individuals with  $\beta$  Thalassaemia major become symptomatic of severe anaemia by 6 months of age and requires blood transfusions to sustain life, with the rapid consequent accumulation of excess iron. Globally, there are more than 300,000 births annually with severe haemoglobinopathies. The majority of these occur in developing countries with low-to-middle income (Weatherall, 2010). The majority of potentially transfusion-dependent thalassaemia patients reside in Asia, with an estimated 21,639 births annually with  $\beta$  thalassaemia (and  $E\beta$  thalassaemia) (**Table 1**). Despite the introduction of effective antenatal diagnosis and prevention programs there are still approximately 1,347  $\beta$  thalassaemia homozygote births annually in Europe (Latest World Health Organisation (WHO) statistics, 2008). In some countries  $\beta$  thalassaemia is prevalent yet the clinical infrastructure to support safe and regular blood transfusions is lacking therefore treatment with iron chelators is secondary consideration. In other countries transfusional support of thalassaemic patients is available, but chelation treatment for example with DFO is prohibitively expensive. In the UK, in 2014 the annual costs of DFO, DFP and DFX treatment were approximated to £1,994- £9,303, £4,993 and £7,665- £20,000 respectively, excluding blood transfusion. In a Taiwanese study in 2006, it was estimated that the lifetime cost of blood transfusions accompanied by chelation therapy treatment vs. haematopoietic stem cell transplantation was \$363,149

vs. \$110,588 (Ho et al, 2006). Based on economic considerations, transplantation has advantages over combined transfusion and chelation therapy. Favourably reported results include a 93% 3-year rejection-free survival in previously well-chelated patients without liver fibrosis and hepatomegaly (Lucarelli et al, 1993). This compares to 91% survival free of cardiac disease after 15 years for patients that maintain their ferritin below 2500 $\mu$ g/L on conventional DFO treatment (Olivieri et al, 1994). While the use of oral chelation therapy improves patient compliance and thus prognosis, in developing countries with a high incidence of severe thalassaemia syndromes the health costs are still likely to be prohibitive. Therefore, advances in either chelation or stem cell transplantation need to be accompanied by an active screening and prevention program for thalassaemia syndromes, if the limited health resources are not to be overwhelmed in these countries.

**Table 1 Estimated global annual births with major haemoglobinopathies.** (World Health Organisation, 2008)

<b>Annual Births</b>	<b>Sickle cell disorders</b>	<b><math>\beta</math> thalassaemias</b>	<b><math>\alpha</math> thalassaemias</b>	<b>Affected births (Total)</b>	<b>Annual births (1000s) (Total)</b>
<b>Africa</b>	233 289	1 520	11	234 819	22 895
<b>Americas</b>	9 047	533	422	10 022	16 483
<b>Eastern Mediterranean</b>	6 491	9 715	1	16 207	16 776
<b>Europe</b>	1 292	1 347	162	2 800	10 459
<b>South-East Asia</b>	26 037	21 693	1 383	49 114	38 139
<b>West Pacific</b>	13	7 601	10 524	18 138	23 914
<b>Total</b>	276 168	42 409	13 466	332 043	128 667

Despite the above economic considerations, there is a major need for improvement in patient compliance with iron chelation therapy. There is no doubt that based on the accumulated clinical experience with DFO, iron chelation is of proven efficacy in prolonging life expectancy in thalassaemia major. The life expectancy of patients with  $\beta$  thalassaemia major did not exceed 20 years (Zurlo et al, 1989) prior to the use of DFO, initially by the intramuscular (i.m) (Barry et al, 1974) and later the subcutaneous (s.c) route (Propper et al, 1976).

There are numerous studies showing the value of DFO in reducing liver iron (Cohen et al, 1989; Flynn et al, 1982; Olivieri et al, 1996) and producing negative iron balance



(Silvestroni et al, 1982) while prolonging life expectancy (Brittenham et al, 1994; Modell et al, 1982; Olivieri et al, 1994). Patients are treated lifelong for 8 hours per day, often overnight, with pumps which deliver DFO via subcutaneous hypodermic needles, which is associated with considerable challenges with compliance, particularly in older children and adolescents. Poor treatment compliance leads to a significant reduction in life expectancy (Brittenham et al, 1994; Gabutti & Piga, 1996; Olivieri et al, 1994). Compliance with oral chelators has been shown to be greater, with DFP showing a 95% compliance compared to a 70% with DFO (Olivieri et al, 1996).

A further consideration regarding the need for new iron chelators is that as treatment is life-long from an early age, there is a need for a high therapeutic safety margin. For example, DFO is remarkably well tolerated provided doses are kept within the therapeutic ratio. Side effects have been observed at high doses relative to the degree of iron overload including ototoxicity (Porter et al, 1989a), retinal disturbances (Marcus et al, 1984), growth retardation (De Virgiliis et al, 1988; Piga et al, 1988a) and bony deformities (Olivieri et al, 1992a). However, because of the inconvenience of administration, cost and poor compliance with DFO, and often the suboptimal results with the current oral options, there is a clear need for further affordable, safe and effective orally administered iron chelation. Orally absorbed chelators, namely DFP and DFX are now available (see below) but these agents can also have problems with patient acceptance and tolerability that can limit overall effectiveness.

A large focus of this thesis is the development of a model that will screen novel iron chelating compounds intended for the management of excess iron, but it should be noted that iron chelators are of potential interest for the management of a variety of other disorders where there is, for example, free radical-mediated tissue damage. Iron chelators have been tested for a potential role in rheumatoid arthritis (Magaro et al, 1990; Yoshino et al, 1984), post-ischaemic perfusion injury (Badylak & Babbs, 1986; Niu et al, 2014), organ transplantation (Bradley et al, 1986; Schaefer et al, 2014), adult respiratory distress syndrome (Marx & van Asbeck, 1996; Ritter et al, 2006) and as anti-cancer agents, due to their modulating effect on cell proliferation with promising results (Salis et al, 2014). However, chelators designed specifically for these various purposes

may require different physiochemical properties, biodistribution and enzyme interactions from compounds intended for the management of iron overload.

### **1.3 Principles of iron chelation therapy**

There are two objectives of iron chelation treatment in the management of excess iron; primarily the production of a negative iron balance and thereby removal of excess body iron, and secondly the detoxification of the excess iron until the primary objective is accomplished. It is well established that iron is essential for normal cell function. Excess iron, however, is harmful to tissues and overwhelms mechanisms that usually protect against free radicals. Optimal iron chelation in iron overload should remove excess iron from where it is harmful without chelating it from where it is required for physiological function. In this chapter, the properties of iron chelation that are necessary for efficient chelation of iron, producing a negative iron balance without toxic effects will be considered.

#### **1.3.1 The achievement of negative iron balance and safe tissue iron concentrations**

Iron content is 40-50mg per kilogram of body weight in humans, on average. The majority of body iron is present as haemoglobin (30mg/kg) within circulating red blood cells. Muscle tissue contains a further 4mg/kg iron in muscle tissue, and 2mg/kg is present in cells as iron-containing enzymes. The remaining body iron is present in storage form as ferritin or haemosiderin mainly in the spleen, liver and bone marrow. In males, the average storage iron is 769mg and 323mg in females. By contrast, in iron overloaded conditions, over 25g can be found to accumulate as 'storage iron.' This excess iron will be present in most body tissues. However, maximum quantity is found in the liver.

In humans, iron metabolism is of a conservative nature, and there is no physiological pathway for elimination of this additional iron. Iron absorption is usually in the order of 1-2mg per day, and is matched by insensible losses. Approximately 11mg of dietary iron is required daily to keep pace with losses as iron absorption is relatively inefficient. Two-thirds of iron losses in humans are through the gut through exfoliation of mucosal cells and loss of red blood cells and one-third is from exfoliation of skin and urinary

tract epithelial cells. In women, to this may be added menstrual losses (mean 0.6mg/day) and pregnancy (mean 2.7mg/day) (McLaren, 1980). The major turnover of body iron, amounting to some 20mg/day, is through the plasma compartment as iron is released from the breakdown of effete red cells in the mononuclear system, which is then released onto transferrin for subsequent delivery to bone marrow erythroid precursors which are found in bone marrow. Approximately 10% of recycled plasma iron turnover is taken up by hepatocytes.

Increased gastrointestinal iron absorption over prolonged periods of time or ongoing blood transfusions will result in the development of iron overload. Iron absorption occurs predominantly in the upper gastrointestinal tract and is regulated by the intestinal mucosa. Under normal circumstances, iron absorption is in equivalence with insensible losses. The efficiency of iron absorption increases when iron stores are depleted, such as in anaemic states, but there appears to be no mechanism for shutting off iron absorption in iron overload states. Furthermore, iron absorption is increased in many conditions associated with ineffective erythropoiesis even in the presence of iron overload (Cavill et al, 1975). In hereditary haemochromatosis, excess iron absorption occurs with normal iron content diets and without evidence of ineffective erythropoiesis.

The distribution of excess iron from hereditary haemochromatosis differs from that seen in the early stages of transfusional iron overload. In the former, the excess gastrointestinal absorption results in an early accumulation of hepatocellular iron, whereas early transfusional siderosis begins with the excess accumulation of iron in mononuclear cells. However, in the majority of chronically transfusionally iron overloaded patients, hepatocellular iron predominates in terms of tissue iron concentration. The most significant clinical consequence of chronic iron deposition in the liver is cirrhosis, usually developing in the fourth and fifth decades of life in hereditary haemochromatosis. In transfusional iron overload, significant siderosis in myocardial tissues is usually seen after approximately 100 units of blood have been transfused. Myocardial damage leading to cardiac failure is a frequent cause of death in thalassaemia major patients in their second and third decades unless chelation therapy is given (Brittenham et al, 1994; Wolfe et al, 1985). The lethal concentration of

myocardial iron is significantly less than that of hepatocellular iron. For example, liver iron concentrations of 40mg/g dry weight are unlikely to cause acute liver decompensation in the short term but myocardial iron nearly ten times less than this are associated with cardiomyopathy and heart failure (Carpenter et al, 2011).

Excess iron is deposited in all body tissues except for the brain, striated muscle, and the nervous tissue. It is unevenly distributed and has a preference for liver, endocrine system and myocardium. In addition to heart failure and cirrhosis, this may lead to multiple endocrine failures such as diabetes mellitus, hypogonadotropic hypogonadism, hypoparathyroidism, and hypothyroidism (Gabutti & Piga, 1996; Zurlo et al, 1989).

Venesection is an option for patients who absorb excess iron but possess a good reserve of endogenous erythropoiesis, such as patients with hereditary haemochromatosis. However, patients with sideroblastic anaemia, often have an adequate erythropoietic reserve and thus do not require blood transfusion, but this is not sufficient to allow for venesection, and therefore also require management with iron chelation to prevent iron overload.

In transfusion dependent anaemias, it has been estimated that an iron chelator must induce between 0.25-0.4mg/kg of iron excretion daily to prevent the accumulation of iron (Gordeuk et al, 1987). A slightly higher excretion of iron will potentially be required in unsplenectomised thalassaemia patients. The transfusion requirements in unsplenectomised patients may increase by even up to threefold (Modell, 1977). Further to this is absorption through the gut, which accounts for a further 1-4mg/day, which can increase several folds in ineffective erythropoiesis (Pippard & Weatherall, 1984). Thus a target in excess of 0.4mg/kg/day in splenectomised patients and typically around 0.5mg/kg/day in patients with an intact spleen may be a more realistic estimate of the required iron excretion to be induced by chelators.

Measurement of iron excreted through the urine and faeces is important in the assessment of iron balance, and this can vary greatly at different time points in the transfusion cycle and furthermore, between individuals (Pippard et al, 1982). In principle, the effectiveness of iron chelators may decrease as the iron load is reduced, necessitating dose changes (occasionally to toxic levels) to reach a negative iron

balance. Ideally, a normalisation of all tissue iron should be achieved as all excess tissue iron concentrations can cause harm. In principle, this can be achieved by matching the iron input rate from transfusion with iron excretion with chelators. In practice, iron chelation is limited by low efficiency of chelation and by increased toxicity at low levels of iron overload. If DFO was 100% efficient (i.e., 100% of the administered drug was excreted bound to iron), then 6mg/kg daily would be adequate. However, a typically used dose is 40-60mg/kg daily, which makes it only 10% efficient. However, DFP, which is orally active is even less efficient at 3.8% (al-Refaie et al, 1995).

Normal concentrations of liver iron are 1-1.8 mg/gr liver dry weight but mildly increased concentrations, such as those seen in heterozygotes for hereditary haemochromatosis (3-7mg/g liver dry weight), do not appear to affect life expectancy and are not associated with cardiac or liver complications. Liver iron of 7-15mg/gr liver dry weight is associated with increasing likelihood of liver and cardiac injury and concentrations above 15mg/gr dry pose a significant threat of early death secondary to cardiac complications (Brittenham et al, 1994). Concentrations below the target of 3-7mg/gr liver dry weight can be achieved using currently available chelation treatment.

### **1.3.2 Minimisation of iron-mediated free radical injury**

Physiologically, the potential for iron to generate toxic free radicals is abrogated by being bound to ligands such as transferrin. However, in situations where there is iron overload, these protective mechanisms become saturated and non-transferrin bound plasma iron (Hershko, 1978) as well as increased quantities of intracellular iron are potentially available to participate in free radical generating reactions.

Iron is particularly important as it is present at sufficient concentrations in tissues and because of the favorable redox potential of the Fe(II)/Fe(III) couple. The iron-catalysed reaction between superoxide and hydrogen peroxide was first described by Haber and Weiss in 1934 and involves the sequential reduction and re-oxidation of Fe(III). This reaction generates hydroxyl radicals that can damage a variety of biomolecules by peroxidations including proteins, DNA and membrane lipids.

Any putative chelator should make iron unavailable to participate in such reactions, whether present as Fe(II), Fe(III) or as larger complexes. When iron is coordinated by a chelator, depending on the stability of this reaction and depending on the extent to which the free electrons in the iron atom are protected, the iron may still have the potential to participate in free radical producing reactions. For example, EDTA which only coordinates one free electron does not diminish the reactivity of iron salts in the Fenton reaction and indeed may catalyse such reactions (Gutteridge & Halliwell, 1989). Conversely, DFO which surrounds the iron more completely is a powerful inhibitor of lipid peroxidation (Gutteridge et al, 1979).

Thus, while iron chelators used clinically in the treatment of excess iron should produce a negative iron balance, they should also ideally decrease the propensity of iron to participate in free radical producing reactions. Thus while it may take a considerable period of time to remove all the excess iron from iron loaded patients, a well-designed chelator should ideally decrease the damage caused by the iron before and during the removal of iron.

### **1.3.3 Prevention of Non-Transferrin Bound Iron (NTBI) uptake**

As part of progressing iron overload, there is an increasing saturation of transferrin noted, and once this exceeds 75%, there is a gradual appearance of NTBI (Le Lan et al, 2005). Unlike transferrin, the uptake of NTBI into cells is much less regulated, similar to its distribution (Oudit et al, 2003). Unlike transferrin-bound iron, NTBI is taken up rapidly by hepatocyte cells (Brissot et al, 1985) as well as myocytes (Link et al, 1989). In cardiomyocytes, NTBI has been noted to be taken up 200x more rapidly than transferrin bound iron and participate in free radical generation, lipid peroxidation and organelle dysfunction (Link et al, 1989). NTBI uptake appears to be restricted to tissues that are normally known to accumulate iron, and L-type calcium channels (Oudit et al, 2006) and zinc transporters (Liuzzi et al, 2006) are thought to facilitate uptake.

Chelators should prevent the uptake of NTBI into parenchymal cells, as the abnormal pattern of iron distribution secondary to iron overload is directly correlated to this (Oudit et al, 2003). 24-hour protection from uptake of NTBI is a desirable property and an important target for chelation therapy. NTBI has a rapid turnover, however, it

reappears rapidly in the circulation in the absence of chelators (Porter et al, 1996). Standard doses of DFO are not able to eliminate NTBI, and chelation can be optimised by giving DFP during the day and a DFO infusion during the night, or by a once-daily dosing of DFX, which provides 24-hour cover (Piga et al, 2006).

### **1.3.4 Further objectives of iron chelation**

Adding to the principle objectives of achieving a negative iron balance and preventing generation of harmful free radicals, there are a number of other desirable properties for chelators. A chelator should not redistribute iron in the body. Furthermore, the chelator should not interact unduly with essential iron-containing enzymes. The compounds should also be reasonably inexpensive to synthesise as they are also intended for use in developing countries with limited economic resources. The following section will consider the design of iron chelators so as to maximise iron excretion while minimising toxicity.

## **1.4 Design of chelators: properties for maximal oral efficacy**

### **1.4.1 Properties for high Fe<sup>3+</sup> affinity**

Iron commonly exists in the iron(III) (ferric), and iron(II) (ferrous) oxidative states. Iron(III) is the predominant species under anaerobic conditions as it is known to be generally more stable than iron(II). For a ligand to, therefore, be an effective chelator, it must be able to bind iron(III) effectively. Due to its possessing high charge density, the iron(III) molecule binds tightly to atoms such as hydroxypyridinones and catecholates. How stable an iron complex will be is determined by how many iron-coordinating groups are provided by each iron chelating ligand. Common examples of electron donor atoms are oxygen and nitrogen. Nitrogen has three unpaired electrons in its *p* orbital vs. two of oxygen.

For example, iron(II) is in its most stable form when coordinated by 6 oxygen atoms. There are various ways by which these 6 oxygen atoms may be supplied., such as, for example, when three chelating ligands each provide two oxygen atoms (bidentate chelators), or two chelator molecules providing three oxygen atoms (tridentate chelators), or one ligand provides all six of these oxygen atoms (hexadentate chelation).

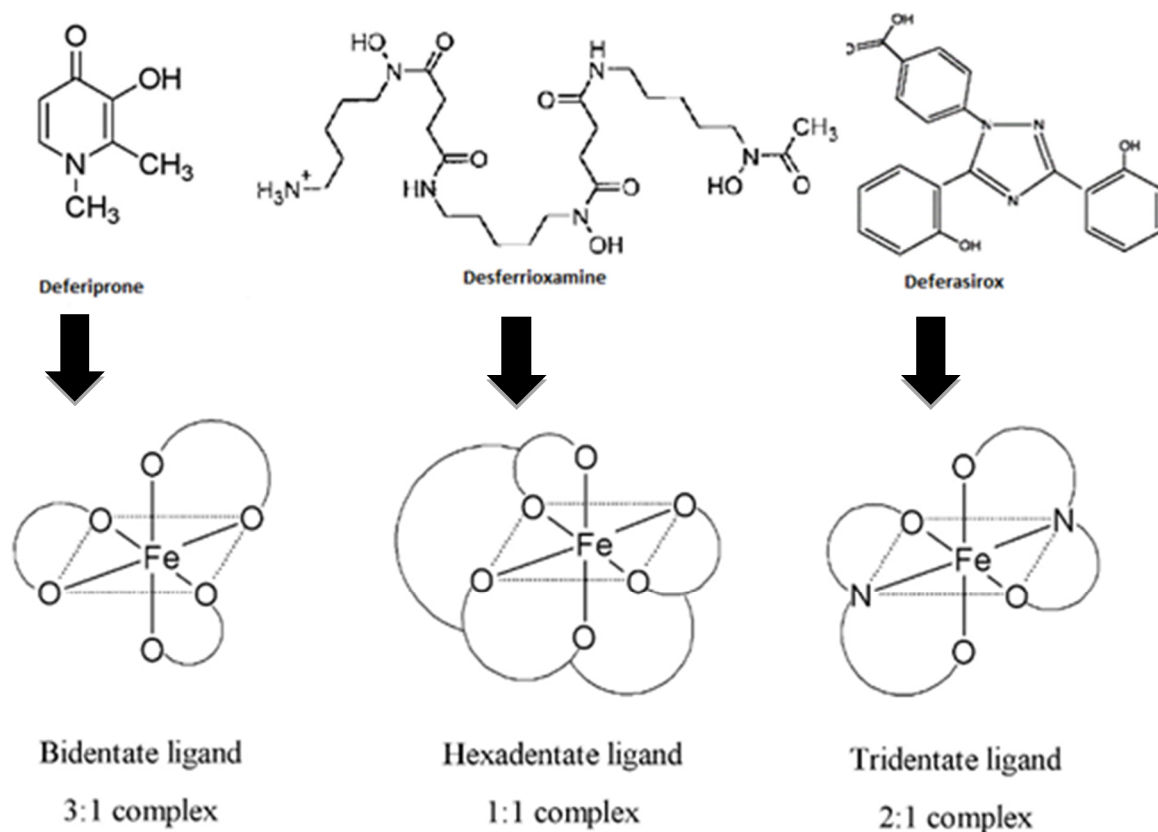
When a chelating molecule is hexadentate, it has a stability advantage compared to its bidentate counterparts (Streater et al, 1990). There is greater kinetic stability, thus making the complex much more stable at lower concentrations. The binding power of a hexadentate chelator is higher at low chelator concentrations ( $<20\mu\text{M}$ ) than equivalent bidentate ligands and is, therefore, a more effective iron scavenger at low concentrations, and dissociation and redistribution of iron is much less likely within the body. **Figure 1** shows the structures and denticity of the three commercially available iron chelators.

The stability constant alone does not fully reflect this concentration dependent 'chelate effect.' The use of a term called the pM, defined as  $-\log(\text{Fe(III)})$  under defined conditions (e.g., when  $\text{pH}=7.4$ ,  $\text{chelator}_{(\text{total})}=10\mu\text{M}$  and  $(\text{Fe(III)})_{\text{total}}=1\mu\text{M}$ ), is in many ways more useful (Hider et al, 1996; Motekaitis & Martell, 1991). A compound with a high pM, under these conditions (i.e. a low concentration of free metal), a compound will have an advantage over another with a low pM, even if the stability constant for the chelator in question appears less favourable. This is because the concentration of free iron is given by this term at physiologically relevant free iron concentrations and clinically achievable chelator concentrations. The importance of this concept can be illustrated by contrasting the pM for the bidentate acetohydroxamic acid (pM =12.5) with that of DFO (pM=26.3) (Motekaitis & Martell, 1991). Thus although the difference in the stability constant is relatively small (28.3 for acetohydroxamic acid vs. 30.99 for DFO), the difference in the pM value is large; a feature resulting from the higher denticity of DFO.

Another disadvantage of bidentate ligands is that they can participate in the generation of hydroxyl radicals. When at low concentrations there is formation of complexes which are partially dissociated (2:1 and 1:1). Therefore, purely from a chemical point of view, a chelator that is hexadentate is suited better to scavenge iron than its bidentate or tridentate equivalent.



**Figure 1 Illustration of the three commercially available iron chelators and their denticity.** (Adapted from Hider & Zhou, 2005).



#### 1.4.2 Uptake through the oral route

There are two main factors that affect oral absorption of a drug, namely its lipid solubility, and molecular weight. The compound may be absorbed by transcellular diffusion through the enterocyte or by the paracellular route. Absorption by the latter route is usually relatively minor as only a fraction of the surface available is used, compared with the transcellular route which occurs through most of the surface area (95%) of the small intestine. There is a molecular weight cut-off for the paracellular route that is thought to be approximately 400 Da and that for the transcellular route about 500 Da (Hider et al, 1996; Travis & Menzies, 1992). For effective treatment, large quantities of chelator (1-2g daily) need to be absorbed, making the necessity for efficient absorption particularly pertinent. Ligands that are more lipid soluble are more efficiently absorbed than their hydrophilic counterparts (Leo et al, 2002). When a ligand has a neutral charge, for example, hydroxypyridinones, it is more effectively taken up than, for example, DFO, which is charged in its iron free state.

### 1.4.3 Access to chelatable iron pools

It is clear that if a chelator cannot gain access to the iron pool, then it is irrelevant how strongly it can bind iron(III) as there will be no effective mobilisation from cells. A key property for an oral chelator is how effectively it can cross cell membranes, allowing it to be absorbed from the gastrointestinal tract and reach into tissues such as hepatocytes and cardiomyocytes. A large number of molecules penetrate cell membranes through the process of simple diffusion, and therefore, neutrally charged drugs enter the intracellular compartment more rapidly than charged molecules. As already stated, neutral charge also has the advantage of more effective gastrointestinal absorption, compared to charged agents. Equally, such chelators enter the cytoplasm of cells more easily. For example, DFO which is a charged ligand is highly unlikely to be orally bioavailable. On the other hand, hydroxypyridinones that do not have a charge under physiological conditions are readily taken up through the gut mucosa. Furthermore, for a compound to be orally active, the ligand should not be broken down in the acidic stomach conditions, and be able to resist enzymatic action. Therefore, when designing chelator molecules, groups containing esters, hydroxamates and amides are not suitable.

Following chelation of iron in the intracellular compartment, the ligand-iron complex should cross the cell membrane in order to exit the cell. Hence, the iron complex, as well as the free ligand, must be water soluble and be uncharged. Out of the iron-chelating molecules known to possess a high affinity for binding iron, the hydroxamates, and the hydroxypyridinones are known to possess these properties.

Lipid solubility is a desirable quality of the unbound chelator as it enables quicker access through cell membranes. However the rate of intracellular compartment entry should be modulated as too rapid diffusion can lead to the chelator penetrating the blood-brain barrier, leading to potentially serious neurotoxicity. For the free and bound forms of chelator to be transported through the plasma and be excreted in the urine, a further requirement is that it is adequately water soluble. Thus, a tricky balance is required between lipid solubility that will allow penetration of cell membranes, and hydrophilic properties in order to limit toxicity to the central nervous system (CNS).

An approach that can be adopted to limit toxicity and maximise iron chelation is the combination of a ligand that is hydrophilic extracellularly at high concentrations, with a lipophilic compound at smaller quantities, aiming to obtain a synergistic mode of action (Vlachodimitropoulou Koumoutsea et al, 2015). A key aim of this thesis is to elucidate this optimal balance and to closely examine synergy/additivity of action between commercially available iron chelators. A further strategy would be to design a compound with high extraction by first-pass metabolism in the liver which is subsequently metabolised to a hydrophilic chelator with low penetration of other tissues thereby limiting the toxicity. Such a combination of properties would also minimise the redistribution of chelated metals (May & Williams, 1979). In this proposed scheme, hepatocyte iron would be excreted with the unmetabolised drug in faeces whilst macrophage-derived iron would be excreted by the metabolised drug in the urine.

#### **1.4.4 Long half-life of the free chelator**

Although DFO is a widely used iron chelator. However one of its major disadvantages is that its plasma half-life is particularly short, which compromises its efficiency to around 10%. The longer the iron free drug circulates in the plasma, the greater the potential to chelate extracellular iron and to remove non-transferrin bound iron (NTBI). Therefore, a long plasma half-life is desirable with respect to extracellular chelation. For intracellular chelation, the labile iron pool is finite but constantly turned over. Hence a sustained uptake of chelator into cells is preferable to a short-term uptake with wide fluctuations in intracellular chelator concentrations. The metabolism of chelators and chelator complexes has a critical bearing on half-life. If the iron free ligand is rapidly metabolised (in liver or plasma), to a moiety which cannot bind iron, then the effective plasma half-life is reduced.

### **1.5 Properties to minimise toxicity: design of chelators**

#### **1.5.1 Selectivity for Fe<sup>3+</sup>**

To minimise long-term toxicity, a ligand that is highly specific for iron(III) is desired. For example, even though DTPA appears to be highly selective and 11-fold more stable in terms of its binding to iron compared to zinc, side effects related to zinc deficiency are well documented in humans (Pippard et al, 1986). Above are discussed the reasons

why hexadentate ligands have a higher selectivity for iron(III) compared to their bidentate counterparts. The selectivity of a chelator is directly related to how closely the electron orbital configuration of the iron molecule is coordinated by oxygen atoms. There are certain bacterial siderophores that possess a structure which is close to ideal, such as enterobactin, which has a good selectivity for iron(III) and a particularly high affinity, possesses a particularly close fit.

### **1.5.2 Limited lipophilicity**

As described above, the importance of membrane lipid solubility is pivotal for the free ligand to access the intracellular chelatable iron pools. However, this lipophilicity should be limited. Molecules demonstrate toxicity *in vitro* as well as *in vivo*, often in a way that directly correlates to the lipophilicity of the compound. Firstly, iron-ligand complexes are more likely to participate in the generation of free radicals and secondly access to the CNS will be greater if the compounds are lipophilic.

### **1.5.3 Iron-chelator complex rapid elimination**

Following binding of the ligand to iron, there is commonly a change in the charge of the molecule, which can affect lipid solubility. The properties of the new molecule should permit excretion in the bile (faecal route) or in the urine. This is primarily to reduce the risk of iron redistribution if the complex is unstable and because certain complexes may pose a toxicity risk. Iron chelated in hepatocytes can potentially be excreted in the bile by an active mechanism. However, other cells lack this, and there is a possibility of increased toxicity by the chelator complex building up intracellularly if it is stable and particularly hydrophilic.

### **1.5.4 Minimal reabsorption or redistribution of iron**

Following iron binding of the ligand, the charge of the complex can differ depending on the ratio of iron: chelator interaction and the specifics of the binding site. The resulting charge of the iron-ligand will have a significant impact on the distribution of iron. For example, DFO that forms a charged iron complex tends not to be able to cross cell membranes, thus posing less of a risk for iron redistribution. Furthermore, the potential of donation of iron to transferrin by the complexed ligand is something that

can affect iron redistribution and should be taken into consideration. This property becomes of particular importance when the saturation of transferrin is not 100%. Another factor that needs to be taken into account is the potential of reabsorption of iron via the enterohepatic system. From the moment the iron-chelate is secreted into the bile, there should be no re-uptake through the gastrointestinal system. A number of factors that limit this re-absorption, namely that if the chelator complex is not of neutral charge, and if there is an increase in the molecular weight. Furthermore, reabsorption of iron is also correlated to the stability of the new molecule during its excretion process in the gut.

### **1.5.5 Low CSF penetration**

The penetration of molecules into the central nervous system is directly correlated to their lipophilicity (Levin, 1980; Oldendorf, 1974). Previously, it has been proposed that the neurotoxic side effects of DFO could potentially be related to it gaining access through the blood-brain (Blake et al, 1985) and blood-retinal (Arden et al, 1984) barrier. However, it should be noted that DFO has a particularly low toxicity when used to manage iron overload, and this may, in fact, be related to its inability to access the cerebrospinal fluid (CSF) because of its high molecular weight and hydrophilicity. In fact, hydroxypyridinones which are more lipophilic have been linked to greater CNS toxicity (Gyparaki et al, 1987; Porter et al, 1990). In general, compounds which are hexadentate have a higher molecular weight than bidentate chelators, which limits their general cell membrane penetration and also their access to the CSF.

### **1.5.6 No acceleration of growth of micro-organisms**

Bacterial siderophores (DFO, enterobactin, etc.) are naturally occurring and therefore may accelerate the growth of bacteria, something which is less likely with their non-naturally occurring counterparts. However, Ferrioxamine (FO) has been shown to increase the pathogenicity of *Yersinia enterocolitica* in mice and to enhance its growth *in vitro* (Robins-Browne & Prpic, 1983; 1985). Future iron chelators should preferably, therefore, be tested for their effects on known pathogenic organism before they are introduced into humans.

### **1.5.7 Targeting excess iron pools while sparing iron-containing enzymes**

Iron is essential for the normal function of all cells, particularly those rapidly dividing. An ideal chelator should be able to target tissues where iron is present in excess but is not in high demand. In an ideal scenario, a chelator should spare iron chelation in areas of high demand such as the bone marrow where iron is both an essential part of the enzyme ribonucleotide reductase as well as for the production of haemoglobin in erythroid precursors. However, in hepatocytes iron chelation would be ideal as these cells are the major site of excess iron deposition and may offer an excretion pathway for the iron chelate complex through the bile.

## **1.6 Chelator Evaluation**

### **1.6.1 Chelator's coordination of iron(III) and other metals**

A key determination is the affinity constant of a molecule for iron compared to other biologically important metals, and it is important to establish how selective for iron(III) a chelator actually is. There are a number of ways for this to be determined, and these include studies with EDTA or spectrophotometrically (Taylor et al, 1988) or potentiometric titration (Kline & Orvig, 1992). The stability constants for the tribasic cations  $\text{Ga}^{3+}$  and  $\text{Al}^{3+}$  as well as dibasic  $\text{Cu}^{2+}$ ,  $\text{Zn}^{2+}$ ,  $\text{Ca}^{2+}$ , and  $\text{Mg}^{2+}$ , should also be determined to ascertain the likely specificity of iron binding. Generally speaking, bidentate chelators will have greater specificity for tribasic cations than dibasic cations (Hider & Hall, 1991).

### **1.6.2 The physiochemical characteristics of the chelator**

The iron binding constant and  $\text{pM}$  are important to determine as this gives an indication of the efficacy of the metal binding at low chelator concentrations (Motekaitis & Martell, 1991). It is also important to establish the  $\text{pK}_a$  values of any titratable group in order to calculate the proportion of chelator that possesses zero net charge at physiological  $\text{pH}$ . This value can be determined with potentiometric as well as spectrophotometric methods (Taylor et al, 1988).

A further useful molecular property to establish is lipid solubility. This can be expressed as the  $K_{\text{part}}$  or otherwise known as the partition coefficient of the molecule between n-Octanol and water (pH 7.4). This allows for an indication of how quickly a chelator will be able to cross cell membranes and may be determined spectrophotometrically (Dobbin et al, 1993). A value of 1 denoted solubility approximately equal in lipid and aqueous phases. Knowledge of the  $K_{\text{part}}$  allows for a prediction regarding a potential oral route of administration of the compound.

### **1.6.3 Characterising the iron(III) complex**

The  $K_{\text{part}}$  of the iron(III): ligand should be calculated, and it gives an estimate of the speed at which the complex will cross cell membranes and be excreted via the kidney. The ability of ligands and their complexes to remove or donate iron to transferrin or ferritin respectively under a variety of chelate and protein concentrations should be investigated. The concentrations of chelator to be tested should be similar to the ones that are found *in vivo*.

### **1.6.4 Evaluation of chelators in cells**

Once it is established that a molecule has desirable properties in terms of its affinity for iron and its specificity, biological pathways are required to screen often a wide variety of candidate molecules. A mechanism for screening of both activity and toxicity that is rapid and requires only small quantities of chelators in which several compounds can be compared simultaneously is desirable. The above advantages are all present when using cell cultures as compared to *in vivo* models where a large number of animals are required for testing often of one compound. Commencing screening with a cellular model will allow assessing numerous chelators for efficiency and toxicity, and determining molecules should progress to testing in animals. Previously used models have included cells in culture, primary cell lines and cells in suspension, and indeed over the last few years the principals of the basic cellular models have not changed markedly, but they have developed.

Red cells are easily accessible and are a simple system to study radiolabelled chelator complexes and their movement across cell membranes, as a predictor of their behaviour

*in vivo* (Hider et al, 2002). Commercially available cell lines these days are commonly used, and they can be easily purchased. This avoids the difficulties involved in isolating primary cell suspensions. They have been used to evaluate specific actions of chelators, particularly when large numbers of cells are required. For example, K562 ( a human erythroleukaemia cell line) cellular models have been used to test the interaction of chelators with the different iron pools (Hoyes & Porter, 1993), their effect on cell proliferation (Blatt & Stitely, 1987), DNA synthesis and cell cycle (Hoyes et al, 1992; Nocka & Pelus, 1988) and the inhibition of iron-containing enzymes such as ribonucleotide reductase (Cooper et al, 1996). The Caco cell line has been used to study successfully the properties of chelators which determine iron absorption from the gut (Hamilton et al, 1994). HuH7 cells have been used to investigate synergy vs. additivity of action of commercially available iron chelators (Vlachodimitropoulou Koumoutsea et al, 2015).

Several primary cell systems have proved useful in testing compounds for the management of iron overload, such as hepatocytes and cardiomyocytes. Primary hepatocytes enable the examination of the effect of various chelators on liver parenchymal cells. The hepatocyte is key to the treatment of excess iron as 80% of iron accumulation occurs in the liver. It is also a key cell of drug metabolism. The majority of data concerning DFP and iron chelation has been generated in hepatocyte cellular models (Laub et al, 1985; Rama et al, 1981). More recently, combinations of commercially available iron chelators were studied in hepatocytes to distinguish between synergy and additivity of action with regards to iron mobilisation (Vlachodimitropoulou Koumoutsea et al, 2015). Kidney cells (MDCK) have been used to investigate the effect of naturally occurring flavonoid compounds on iron uptake (Vlachodimitropoulou et al, 2011).

Primary cardiomyocytes can be utilised to represent the effects of chelators on the clinically significant effects of iron overload on the heart. The effect of a series of hydroxypyridinones on iron mobilisation from myocytes has been studied (Hershko et al, 1991). Models involving macrophages have also been used to examine iron mobilisation by DFO (Kleber et al, 1981); in this work there was no iron shuttling to transferrin detected over a period of 9 hours, making the relevance of transferrin to iron



chelated from the spleen, liver and bone marrow seem doubtful. A similar model has been used to investigate the binding of iron released from macrophages onto transferrin (Saito et al, 1986), which suggests that binding of iron(III) to transferrin does not require active uptake or binding of transferrin to macrophages. Thus, chelators will bind iron released from macrophages independently of their ability to enter cells. Such a model is, therefore, unlikely to uncover any major differences between chelators with respect to their access to intracellular iron pools. Primary thymocytes have been used to compare the effects of chelators on apoptosis of these cells (Maclean et al, 2001). This model appears to correlate with the relative effects of iron chelators on thymic atrophy *in vivo*. An overview of the use of cells that lead to establishing the basic principles of action of iron chelators is given in **Table 2** .

**Table 2 Overview of cellular systems used to study the efficacy and toxicity of chelators**

<b>SYSTEM</b>	<b>PURPOSE</b>	<b>OBSERVATIONS</b>	<b>REF</b>
<b>Myocardial cells</b>	Iron mobilisation  Cell toxicity	Hydroxypyridinones are more effective than DFO  Chelators reduce lipid peroxidation	(a)
<b>Hepatocyte cultures</b>	Iron mobilisation  Cell toxicity  Chelator combination	Comparison of hydroxypyridinones, DFO derivatives  Relates to lipid solubility  Synergistic mode of action of commercially available iron chelation	(b, c)  (d)  (e)
<b>MDCK cells</b>	Iron mobilisation by flavonoids	Quercetin can shuttle iron out of cells via the GLUT1 transporter	(f)
<b>Caco cells</b>	Chelator GI absorption	Model of chelator absorption	(g)
<b>K562 cells</b>	Cell proliferation  Cell cycle  DNA synthesis  Subcellular distribution  Ribonucleotide reductase	Independent of lipid solubility with prolonged exposure  Late G1/S arrest  Parallels anti-proliferative effects  More rapid uptake and iron release by hydroxypyridinones than DFO  Hydroxypyridinones faster than DFO	(h)      (i)   (j)
<b>Bone marrow</b>	Proliferation	Relative <i>in vitro</i> effects do not parallel <i>in vivo</i> effects	(k)
<b>Thymocytes</b>	Apoptosis	DFO, DFP, and hydroxypyridinones induce apoptosis in thymocytes by chelating zinc and iron.	(l)

*Cited References:* (a) (Hershko et al, 1991); (b) (Baker et al, 1985); (c) (Laub et al, 1985); (d) (Dobbin et al, 1993); (e) (Vlachodimitropoulou Koumoutsea et al, 2015); (f) (Vlachodimitropoulou et al, 2011); (g) (Hamilton et al, 1994); (h) (Hoyes et al, 1992); (i) (Hoyes & Porter, 1993); (j) (Cooper et al, 1996); (k) (Cunningham et al, 1994); (l) (Maclean et al, 2001)

### **1.6.5 Evaluation in animal models**

The numerous advantages of using cells to evaluate iron chelators have been discussed above. However, there are several limitations of using cellular systems. Firstly, compound metabolism in plasma may be significant, and this will not necessarily occur *in vitro*. Secondly, the drug pharmacokinetics cannot be studied using the *in vitro* model. Thirdly, such as for example in the case of DTPA, there are certain chelators that only act extracellularly yet *in vivo* can produce a significant amount of iron excretion via the urine. However, once a target organ has been identified (for example the bone marrow), it may subsequently be useful to study the mechanism of toxicity *in vitro*.

Animals can be used to evaluate long or short term effects of the compounds in question. Short term models, in addition to comparing the efficacy and acute toxicity of novel compounds, can identify the main iron pools on which chelators act. Longer term administration is essential to uncover potential toxicity and to relate this to the effects on tissue non-haem iron.

The lack of a universal animal model in assessing the relative efficacy of new chelators is an issue to date. Animal testing should be reasonably reproducible and allow for the testing of several compounds at the same time. These models generally measure urinary and faecal iron excretion, often using radioactive iron to label defined iron pools. In the first instance, the study should be able to establish if compounds are excreted in the urine or faeces and whether they are orally active. Subsequent aims are determination of tissues of action of the molecules and whether there is the danger of iron reabsorption and redistribution.

Ideally, once a test substance has been shown to significantly mobilise iron in one species, its effects should be confirmed in a further animal model. This is to allow for differences between animals such as rats and humans in the basal iron turnover and elimination, and in the amount of iron either excreted in faeces or urine (Finch et al, 1978). The choice of species for longer-term evaluation of compounds is also critical with respect to metabolism of the drug in question. For example, with hydroxypyridinones, there is marked interspecies variability in toxicity which also parallels interspecies efficacy and correlates with the variability of inactivation of the drug by glucuronidation at the iron binding site (Porter et al, 1993). With DFO, drug metabolism in the hamster is closer to than seen in humans than the rat and therefore is a more relevant model for pharmacokinetic studies as well as efficacy evaluation (Steward et al, 1996).

If a compound proves comparable to current treatment progression to subacute evaluation will be required. Such studies identify potential target organs for toxicity and satisfy requirements for clinical administration of the drug. Subacute toxicity and efficacy evaluation needs to include a cohort of iron loaded animals in order to determine whether any toxicity observed is dependent on the degree of iron loading (Porter et al, 1993; Porter et al, 1991; Wong et al, 1997). A summary of methods which have been used in animal studies to investigate efficacy and toxicology of iron chelators will be discussed next.

#### *Methods of iron loading*

Initially, screening models used iron loaded animals by hypertransfusion (Grady et al, 1976; Gralla & Burgess, 1982; Graziano et al, 1974; Hershko, 1978) or chemical iron loading (Awai et al, 1979; Gyparaki et al, 1987; Longueville & Crichton, 1986). The distribution in these models ideally should mirror human iron overload. **Table 3** shows examples of methods used to iron-load animals. Iron loading is most physiologically achieved with hypertransfusion, however, in the past, there has been concern regarding inconsistent results with test substances in different models. Some of these can be attributed to the differences in re-equilibration times after hypertransfusion (Pitt et al, 1979). Furthermore, iron overloading using blood transfusions requires time and technical expertise. Because of this, some groups have used iron dextran (Bergeron et

al, 1992; Gyparaki et al, 1987) as a loading medium. Iron dextran is initially loaded in the reticuloendothelial system (RES), however, it then redistributes into cellular tissues after redistribution has occurred. Models using ferrocene for iron loading in rats have also been described (Longueville & Crichton, 1986) and are of value for assessing liver iron mobilisation in particular. Yet another way of loading animals with iron is using carbonyl iron by the oral route (Nielsen et al, 1993; Wong et al, 1997) but this takes longer and is less efficient than TMH-ferrocene (Nielsen et al, 1993).

#### *Animals with genetic mutations used to investigate iron transport*

Mouse mutants have been used for over 40 years in the investigation of iron transport. One of the first mutant mice was the 'hpx mouse' in 1978 which when homozygous dies secondary to severe deficiency of serum transferrin. This mouse consolidated knowledge regarding the essential role of transferrin and provided insight into atransferrinaemia (Bernstein, 1987). The 'mk mouse' was discovered in 1960, which has severe impairment in iron absorption from the gut as well as a defective iron uptake mechanism in erythroid precursors. Bone marrow transplant in this species showed that in this model the erythroid iron-uptake defect is independent of intestinal iron absorption (Edwards & Hoke, 1972). A number of haemochromatosis mouse models have been developed to investigate iron overload, mainly involving knockout of the HFE gene (Bahram et al, 1999; Levy et al, 1999; Zhou et al, 1998). More recently, the benefits of DFX were demonstrated in a mouse model of juvenile haemochromatosis which has iron deposition in the heart, liver, and pancreas, with a mutation in the haemojuvelin/(HFE2) gene (Nick et al, 2009). Organ damage and response to iron chelation has also been investigated in a number of thalassaemic mouse models (Sanyal et al, 2013; Schmidt et al, 2015; Yatmark et al, 2015), with the more recently developed humanised model of  $\beta$ -thalassaemia, which is blood transfusion dependent in its heterozygous form, providing a very promising model for future research (Huo et al, 2010).

### *Choice of further species*

Following an initial investigation in rodent models such as those described above, some investigators have used primate models to evaluate iron chelators prior to clinical trials (Bergeron et al, 1993; Bergeron et al, 1992; Bergeron et al, 1996). This is clearly very expensive and arguably has limitations shared with other animal models. Firstly, the iron metabolism in primates is significantly less conservative (0.15% in monkeys vs. 0.03% in humans) (Finch et al, 1978). Secondly, the metabolism of chelators has been shown to have an important bearing on both the efficacy and toxicology of chelators but varies between species (Porter et al, 1993). Thus there is no certainty that the chelator metabolism in monkeys will be the same in humans. Therefore, the use of primates may add little to the rodent models.

**Table 3 Methods used to iron-load animals.**

<b>Loading Material</b>	<b>Species</b>	<b>Methods and effects</b>	<b>Ref.</b>
<b>Hypertransfusion</b>	Rats	2 i.v. injections of 20ml packed RBC/kg Days -4 & -1	(a)
<b>Iron dextran</b>	1) Mice and rats	Total 180mg (9 doses over 2 weeks). Iron in cardiac interstitium and to a lesser extent in myocytes  Weekly i.p. iron dextran 100mg/kg x4. Wait 4 weeks before animal cull.	(b)  (c)
	2) Gerbil	1gr/kg loading dose, followed by 500mg/kg weekly for 6 weeks. Stable liver and heart haemosiderosis. Liver scarring 1-3 months after loading.  200mg/kg for 10 weeks. Cardiomyocyte iron loading noted	(d)  (e)
	3) Monkeys	i.v. infusion 200-300mg/kg x3 over 10 days.	(f)
<b>TMH - Ferrocene</b>	Rats	1gr/kg of ferrocene to diet/day for 2-4 weeks. Stable hepatocellular loading after ferrocene stopped.	(g)
<b>Carbonyl Iron</b>	Rats	2% carbonyl iron. Hepatocellular carcinoma may complicate dietary hepatic iron overload in the absence of fibrosis/cirrhosis	(h)

(a) (Hershko, 1978), (b) (Yatmark et al, 2014), (c) (Porter et al, 1993), (d) (Otto-Duessel et al, 2008), (e) (WOOD et al, 2011), (f) (Bergeron et al, 1992), (g) (Florence et al, 1992), (h) (Asare et al, 2006)

## 1.7 Commercially available iron chelators

### 1.7.1 Desferrioxamine (DFO)

DFO belongs to the hydroxamate group and possesses a high affinity and selectivity for iron(III). It forms complexes with iron(III) without a change in net charge on binding, which is ideal for clinical iron chelation. DFO is highly selective for iron(III) with a stability constant for the latter of  $10^{30}$  (Motekaitis & Martell, 1991) compared to that of the next most avidly bound metal, namely aluminium with a stability constant  $10^{25}$  followed by copper with  $10^{14}$  and zinc at  $10^{11}$ . DFO is also a hexadentate ligand so it will tend to scavenge iron efficiently at low concentrations of chelator (as evidenced by its high pM) (**Table 4**). The iron-chelate complex ferrioxamine (FO) will be relatively stable compared with bidentate ligands, limiting the potential for the redistribution of iron. The fact that DFO has a low lipophilicity when it is complexed with iron is also of importance (Porter et al, 1988), as this form does not penetrate cell membranes easily and therefore is less likely to re-distribute iron around the body. Thus, uptake of DFO is slow in cells, and this has been demonstrated in cells such as the K562 cell line *in vitro*, where concentrations approaching those outside cells are not seen for approximately 4hours (Hoyes & Porter, 1993) (Cooper et al, 1996). Hepatocytes, however, appear to have a facilitated uptake mechanism for DFO. The FO also has a positive charge that tends to retard the egress of the iron complex from cells such as cardiomyocytes (Porter et al, 2005). In hepatocytes, however, an active excretion mechanism exists for excretion in bile. Furthermore, metabolism of DFO to metabolite B, which has a negative charge, allows egress of this metabolite from hepatocytes (Porter et al, 2005). DFO enters most cells more slowly than DFP because of its low lipid solubility, its high molecular weight and its charge (Porter et al, 2005).

Hydroxamates have several drawbacks. They are not very resistant to gastro-intestinal breakdown when taken up by the oral route (Keberle, 1964; Summers et al, 1988), limiting their oral activity. In addition, as mentioned previously, the high molecular weight of DFO and its positive charge, further contribute against oral bioavailability. Other disadvantages of DFO are that it has a very short plasma half-life (5-10 minutes) (Lee et al, 1993; Summers et al, 1988) and that it promotes the growth of *Yersinia enterocolitica in vivo* (Robins-Browne & Prpic, 1983; 1985). The fact that it is rapidly



metabolised and excreted is clearly a disadvantage, as DFO must be administered by continuous s.c. or i.v. infusion. However, the long-term efficacy of DFO is well established (Brittenham et al, 1994; Zurlo et al, 1989). It has been shown that it prolongs life expectancy (Brittenham et al, 1994) and despite being administered daily over many years, if the doses are kept below 50mg/kg, DFO is remarkably well tolerated with limited side-effects.

The large majority of toxicity noted by DFO is related to the dose; thus skeletal growth effects and audiometric and retinopathic toxicity are more likely at higher doses. Clinical presentations of ocular toxicity include night or colour vision disturbances or decreased visual acuity, particularly with continuous 24h infusions. These complications occurred not infrequently in the early phase studies which used DFO doses of 100 mg/kg/day, but rarely occur today as significantly lower doses are typically used in clinical practice (Davies et al, 1983). Drug-related ototoxicity is typically symmetrical, high-frequency sensorineural (Porter et al, 1989b). Certain complications, such as neurotoxic effects, occur when iron levels are low, and DFO continues to be administered, and even coma has been described. Audiometric and retinopathic complications can also be seen with low ferritin levels (Porter et al, 1989b) (less than 1000 mg/L) (Olivieri et al, 1986). If the use of DFO leads to toxic effects, treatment should be withheld temporarily and restarted when symptoms or signs have improved. In children: doses greater than 40 mg/kg have been linked to an increased risk of impaired growth and skeletal changes. Retardation of growth was noted when DFO was started earlier than 3 years of age or at higher doses (De Virgillis et al, 1988; Piga et al, 1988b). A short trunk may arise because of metaphyseal changes in the spine, and a rickets-like picture and genu valgum may also occur (Olivieri et al, 1992b). Other reactions such as skin irritation, allergies, and *Yersinia enterocolitica* infections, are less clearly dose-related.

### **1.7.2 Deferiprone (DFP)**

DFP belongs to the hydroxypyridinone group, which was initially designed by Hider and colleagues (Hider et al, 1996) , and is a bidentate iron chelator (3:1). Due to its low molecular weight and uncharged nature under physiological conditions both as the free ligand and when complexed with iron, it has the desirable properties of rapid oral

absorption and subsequent biodistribution. DFP is less hydrophilic than DFO with about one-third of the molecular weight (**Table 4**) but is still not truly lipophilic, being about 5 times more soluble in water than lipid (Porter et al, 1990). The simple stability constant for iron(III) is about six times higher than for DFO. However more clinically relevant is the pM, which is 20 and lower than that of DFO at 26.6 (Hider et al, 1996). Thus while iron(III) binding is efficient at high concentrations of DFP, at lower chelator concentrations such as 10 $\mu$ M and at clinically relevant iron concentrations of 1 $\mu$ M, DFO will bind iron more effectively than DFP. The lower pM also increases the potential to redistribute iron within the body (Pippard et al, 1989) with the potential formation of incomplete 1:1 and 1: 2 iron-chelate complexes which theoretically could participate in the generation of hydroxyl radicals (Dobbin et al, 1993). There is a potential advantage to the low pM, however, because as chelatable iron concentration fall in tissues, the risk of over-chelation, such as occurs with DFO, may be less.

DFP was selected for studies in humans, firstly in 3 patients with myelodysplasia (Kontoghiorghes et al, 1987) and then in thalassaemia major patients (al-Refaie et al, 1992; Kontoghiorghes et al, 1990a). Early short-term evaluation in previously poorly chelated patients showed that DFP can increase urinary iron excretion at levels sufficient in some cases to induce a reduction in serum ferritin and a negative iron balance at doses between 75 to 100mg/kg/day (Kontoghiorghes et al, 1987). In a further study involving previously poorly chelated patients, a dose of 75mg/kg/day resulted in iron excretion which correlated with reduction of serum ferritin as well as with DFO induced urinary iron excretion (Olivieri et al, 1990). Furthermore, DFP has proved superior to DFO in thalassaemia major patients in preventing cardiac events (Borgna-Pignatti et al, 2006) and reducing cardiac iron loading assessed by MRI T2\*(Pennell et al, 2006) and has thus established its role in iron chelation therapy.

In assessment of the value of DFP for clinical use, the reported efficacy has to be weighed against the reported unwanted effects. Animal toxicology confirms a dose and time-dependent suppression of the bone marrow in several animal species both in iron overloaded and non- overloaded states (Porter et al, 1989a) as well as thymic atrophy and teratogenic effects at doses close to the therapeutic dose in humans (Berdoukas et al, 1993). Bone marrow related toxicity has also been reported in clinical studies, with

rates of agranulocytosis in subjects taking the drugs estimated to be approximately 3-4%, and with mild neutropaenia in a further 4% (al-Refaie et al, 1995; al-Refaie et al, 1992). Unlike laboratory animals, this effect appears unpredictable at currently prescribed doses. Neutropaenia may last from 7 to 127 days (Hoffbrand, 1994; Hoffbrand et al, 1989); reintroduction of the drug will induce a rapid reduction in the neutrophils and is contraindicated. Arthropathy, affecting most commonly the knees, may be more seen with high levels of iron overload (Kellenberger et al, 2004) possibly suggesting an effect of the iron complex. The frequency of arthropathy increases over time, from 6% at 1 year to 13% at 4 years (Cohen et al, 2003). This often requires cessation of treatment and usually resolves once treatment is withheld. Other side effects include nausea in 8% of subjects taking current clinical doses, fluctuation in liver function tests (transaminases) in 44% and mild zinc deficiency in 14%. The effect of dose on tolerability has not been studied systematically. All patients treated with DFP require weekly blood tests because of the risk of agranulocytosis. Progression of liver fibrosis has been reported (Olivieri et al, 1998) but not confirmed in other studies (Wanless et al, 2002).

### **1.7.3 Exjade (DFX)**

DFX has the chemical formula 4-[3,5-bis(2-hydroxyphenyl)-1,2,4-triazol-1-yl]benzoic acid and its molecular weight is 373 (**Table 4**). The tridentate structure results in the chelator binding iron(III) in a 2:1 ratio. The stability of this complex as estimated by the pM values is intermediate between DFO and DFP (**Table 4**). DFX is lipophilic but highly protein bound in plasma. Despite the protein binding, good tissue penetration with faster mobilisation of tissue iron than DFO is seen (Nick et al, 2003; Vlachodimitropoulou Koumoutsea et al, 2015). Mobilisation of myocyte iron appears to be efficient (Glickstein et al, 2006; Hershko et al, 2001) and has been confirmed in studies with iron overloaded gerbils (Wood et al, 2005b).

The drug has low water solubility and is given as an oral suspension once daily. More recently a tablet preparation has been developed by the pharmaceutical company Novartis, and it is clinically available in the USA but not yet in Europe. Pharmacokinetics by the oral route were examined in the first Phase I randomised double-blind study using single doses, in 24 patients with thalassaemia major who

received single doses of dispersible tablets (2.5 to 80 mg/kg) (Galanello et al, 2003). Absorption was rapid with a plasma half-life of 11 to 19 hours, supporting a once daily administration regimen. Metabolism occurs at several sites but predominantly by glucuronidation in the liver at a position not involved in iron coordination (Porter et al, 2003). Elimination of this and other metabolites was predominantly faecal. Excretion of DFX and its complex in the urine is limited to less than 0.1%. The final elimination of DFX, the iron complex, and metabolites appears to be by hepatobiliary anion transport and dose adjustment is required for patients with hepatic impairment.

DFX has been approved for use in the treatment of transfusional iron overload and has a more favourable side-effect profile compared to DFP (Goldberg et al, 2013). At the initial phase III trial it showed a significant reduction in serum ferritin but failed to meet its primary endpoint of reduction of liver iron, likely as a result of underdosing (Cappellini et al, 2006b). However, subsequent studies have proven the efficacy of DFX in controlling as well as reducing iron burden, at doses greater than 30mg/kg/day (Porter et al, 2008; Taher et al, 2009a; Taher et al, 2009b). Larger prospective studies with defined dosing regimens then followed. 192 patients with  $\beta$  thalassaemia with a T2\* from 5 to 20 ms, left ventricular ejection fraction (LVEF) of 56% or more, serum ferritin more than 2500 $\mu$ g/L, liver iron more than 10 mg Fe/gr dry weight (Pennell et al, 2010) patients were followed up for up to 3 years. A significant improvement in myocardial T2\* from 14.6 to 17.4 ms was seen at 1 year at a mean dose of 33 mg/kg/day (Pennell et al, 2010). In patients with baseline T2\* values less than 10 ms initially, the T2\* also significantly improved from 7.4 to 8.2 ms over the period of a year. The response rate for improvement of myocardial T2\* at 1 year was 70% in this study. In this study, 71 subjects continued taking DFX into the 3rd year. 68.1% of patients with baseline T2\* 10 to <20 ms normalised myocardial T2\* and 50.0% of patients with baseline T2\* >5 to <10 ms improved to 10 to <20 ms. There were no deaths and no significant changes to the function of the left ventricular function reported (Pennell et al, 2012). CORDELIA is a randomized controlled trial of DFX (target dose 40mg/kg) versus DFO, that studied myocardial iron mobilisation in  $\beta$  thalassaemia major (Pennell et al, 2014). In this study, the myocardial T2\* improved with DFX from 11.2ms at baseline to 12.6ms at 1 year (Pennell et al, 2014). At 2 years (Pennell et al, 2015) sustained improvement was seen with myocardial T2\* increasing from 11.6 to 15.9 ms with

improvement across all subgroups, and with LVEF remaining stable. These studies have included only patients with normal LVEFs, and no significant changes have been seen (Pennell et al, 2011).

More than 3000 patients have been studied in prospective trials of DFX, where the frequency of unwanted effects have been reported. Most studies lasted 1 year, but several have been extended up to 5 years. Discontinuation rates are generally lower than those seen with long-term DFP administration. The most common adverse effects are generally mild to moderate gastrointestinal events, such as abdominal pain, nausea and vomiting, diarrhoea, and constipation, occurring in approximately 15% of patients with thalassaemia (Cappellini et al, 2006a), and somewhat higher numbers of older patients with myelodysplasia. Skin rashes occur early in approximately 10% of patients (Cappellini et al, 2006a). One-third of patients had a mild dose-dependent increase in serum creatinine, occurring within a few weeks of starting or increasing therapy. These increases were usually not progressive and reversed or stabilised when doses were adjusted. Occasional cases of renal failure have been reported. It is important to monitor serum creatinine and to decrease or interrupt the dose if creatinine increments exceed 30% or if the creatinine increases above the normal range. Failure to do this can result in renal injury, and regular monitoring of urinary protein is therefore recommended. Liver enzyme changes, judged to be related to DFX, occurred in less than 1% of patients. Improvement or stabilisation in liver pathology in patients with  $\beta$  thalassaemia receiving DFX for at least 3 years has been noted (Deugnier et al, 2011) Audiometric effects and lens opacities did not differ significantly from the control arm treated with DFO, (Cappellini et al, 2006a) and no clearly related drug-related agranulocytosis has been observed in clinical trials. In paediatric patients, growth and development proceeded normally (Aydinok et al, 2012b). Data from the five phase II/III studies show no inhibitory effects on growth (Cappellini et al, 2011).

**Table 4 Properties, pharmacokinetics, and metabolism of commercially available iron chelators.**

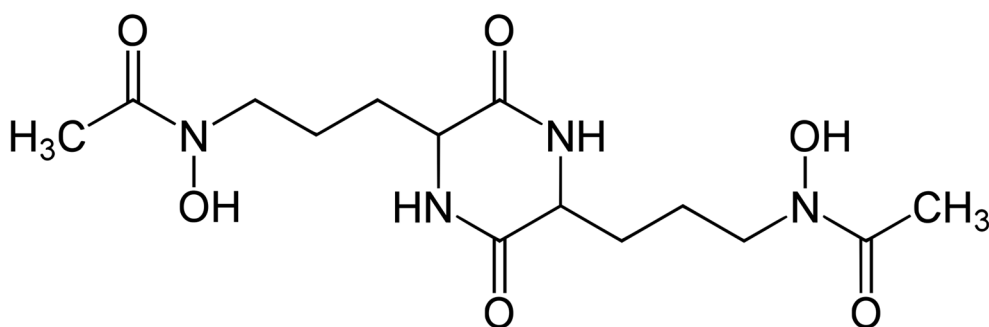
Compound	Desferrioxamine (DFO)	Deferasirox (DFX)	Deferiprone (DFP)
Molecular weight	561	373	139
Chelator : Iron binding ratio	1:1	2:1	3:1
Stability constant (log $\beta_n$ )	33	26.5	37.1
pM	26.6	22.5	20.5
Charge of free complex	1+	1-	0
Charge of iron complex	1+	3-	0
Lipid solubility of free ligand (Log $K_{part}$ )	-2.0	+6.3	-0.8
Lipid solubility of iron complex (log $K_{part}$ )	-1.5	Not known	-1.1
Route of absorption	S.C., I.V. , I.M.	Oral	Oral
Route of iron excretion	Urinary and faecal	Faecal	Urinary
Max plasma levels ( $\mu$ M) Of iron free drug	7-10 (Porter et al, 2005)	80 (Galanello et al, 2003)	90-450 (Kontoghiorghes et al, 1990b)
Concentration of iron complex	complex remains similar (about 7 $\mu$ M) with ascending doses but the iron-free drug and metabolites increase (Porter et al, 2005)	Complex accounts for about 10% of plasma drug (Waldmeier et al, 1993)	Complex correlates with urine iron excretion and predicts response to therapy (Aydinok et al, 2012a)
Elimination of iron complex	Urine + faeces Iron complex removed more slowly than free drug.	Faeces	Urine
Metabolism	Intrahepatic to metabolite B (Porter et al, 1998).	>90% eliminated in faeces, 60% unmetabolised. Metabolism mainly in the liver to glucuronides. Oxidative metabolism by cytochrome P450 accounts for < 10%. (Waldmeier et al, 1993)	Glucuronide formed in liver does not bind iron (Kontoghiorghes et al, 1990b)
Dose mg/kg/day	30-60 5-7 x/week	20-40 once daily	75-100 in 3 divided doses
Chelation efficiency(%) (% of drug excreted iron bound)	13	27	7
Main Adverse effects	Ocular, auditory, bone growth retardation local reactions, allergy	Gastrointestinal increased creatinine, Hepatitis	Gastrointestinal, arthralgia, agranulocytosis/n eutropenia

## 1.8 Other chelators that have reached clinical trials

### I. *Rhodotorulic Acid (RA)*

RA is a hydroxamate that occurs naturally and is produced by *Rhodotorula pilimanae*, similarly to DFO (Grady et al, 1979) (**Figure 2**). However, unlike DFO it is not a hexadentate ligand (binds in  $\text{Fe}_2\text{RA}_3$  ratio), and it also has a lower water solubility. RA proved more effective than DFO in hyper transfused rats (Grady et al, 1979), and this was attributed to its higher renal excretion. Initial both long and short term toxicity studies including histological examination in rats, mice, and monkeys as well as pharmacokinetic studies in rats, monkeys, and dogs seemed encouraging. However, RA was eliminated from further development, as in addition to being orally inactive, clinical trials were associated with unacceptable inflammation at the sites of intramuscular/subcutaneous injections (Grady et al, 1979).

**Figure 2** Rhodotorulic Acid (RA) structure (Grady et al, 1979)



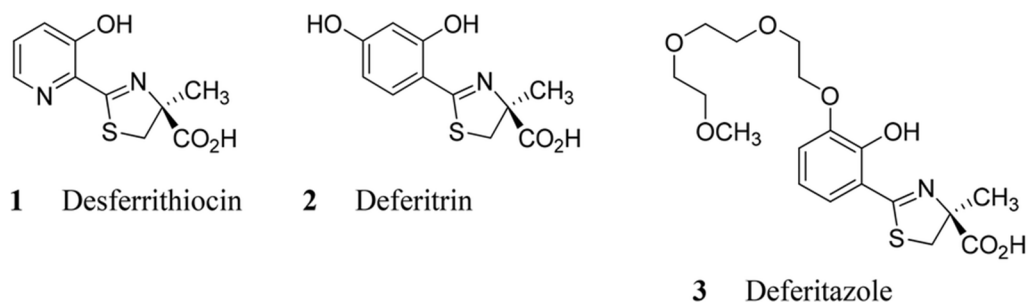
## II. Desferrithiocin, Deferitirin, and Deferitazole

Desferrithiocin is a naturally occurring siderophore that was isolated from *Streptomyces antibiotics* in 1865 (Bergeron et al, 1991) and is tridentate, forming 2:1 complexes with Fe(III) (**Figure 3**). It has a high binding constant ( $\text{Log}\beta_2=29.6$ ) and a good selectivity for iron, similar to that of DFO but it also retains an appreciable affinity for other metals such as aluminium ( $\text{Log}\beta_2=22.6$ ) and zinc ( $\text{Log}\beta_2=15.3$ ). Desferrithiocin is three times more effective when administered orally than DFO given parenterally to rats (Longueville & Crichton, 1986). However, it has been reported to cause CNS related deaths in mice, progressive weight loss, renal toxicity and neurological complications in animals. Further *in vitro* and *in vivo* studies suggested that the toxicity was more likely related to the iron complex ferrithiocin than the desferrithiocin itself (Baker et al, 1992).

Whilst desferrithiocin was excluded from further development, largely because of the renal toxicity, it was found that relatively minor modifications to the structure profoundly alter the activity/toxicity profile of the drug. Deferitirin which has a phenol ring substitution instead of the pyridyl ring (**Figure 3**), showed promising iron mobilisation in phase I clinical trials but presented unacceptable for further use in patients due to renal toxicity at higher doses (Barton, 2007). In order to overcome nephrotoxicity, a number of derivatives were created, of which Deferitazole or otherwise known as FBS0901 or SSP-004184 or SPD602 was the most promising (**Figure 3**). A number of clinical trials involving Deferitazole were conducted around the world; however results appeared inconclusive resulting in treatment being stopped in 2014.



**Figure 3 Structures of the iron chelators Desferrithiocin, Deferitrin, Deferitazole**



### 1.9 Conclusions

In this chapter, the need for further safe and effective orally active iron chelators has been described. Furthermore, the properties of iron chelators that are needed for such a goal and the methods for assessing such compounds pre-clinically have been examined. By investigating the relationship between structure, efficacy, and toxicity of related compounds those with a wider therapeutic safety margin may in principle be identified. The primary objective of the work in this thesis has been to develop a cellular system for screening a large number of compounds (often available in small quantities) which is predictive of how such compounds will behave *in vivo*. In the ensuing chapters the development of such a model is described (**Chapter 3**) and its predictive value is then tested in our newly developed iron overloaded humanised thalassaemia mouse model (**Chapter 7**).

## Chapter 2 MATERIALS AND METHODS

### 2.1 Iron chelators and substances tested for iron chelation activity

- I. DFO, DFP, Quercetin, Isorhamnetin, Quercetin 3- $\beta$ -D- glucoside (Sigma-Aldrich, USA)
- II. Eltrombopag (Generon, UK)
- III. Quercetin-3-D-glucuronide, (HWI Pharma Solutions, Germany)
- IV. Kaempferol (Calbiochem, Canada)
- V. DFX, CP20, and CP40 were supplied in powder form by R.C.Hider from King's College London University.

### 2.2 Cell Lines

#### a) HuH7 hepatocyte cell line

Tissue: Human hepatocellular carcinoma

Organism: *Homo sapiens*

Purchased: Sigma-Aldrich England, UK

#### b) H9C2 cardiomyocyte cell line

Tissue: Heart/Myocardium

Organism: *Rattus norvegicus*, rat

Purchased: ATCC England, UK

### 2.3 Cellular Methods

#### 2.3.1 Maintenance of hepatocyte HuH7 and cardiomyocyte H9C2 cells

##### *Cell culture*

HuH7 cells and H9C2 cells were grown in tissue culture flasks in RPMI 1640 containing L-glutamine and DMEM media respectively. The media contained 10% (vol./vol.) FBS and cells were maintained at 37°C in a humidified atmosphere (5% CO<sub>2</sub>). RPMI was supplemented with 0.02% penicillin/0.5% gentamicin while penicillin/streptomycin was added to DMEM. Cells were cultured at densities between 2-7 x 10<sup>5</sup> to maintain exponential growth. Cells were quantitated using a Neubauer counting chamber as well

as an automated cell counter calibrated for our cell lines as per manufacturer's instructions.

### *Freezing*

Cells were frozen periodically in media containing 10% FBS and 10% DMSO. They were plunged into liquid nitrogen (-180°C).

### *Thawing*

Cells maintained in liquid nitrogen were thawed at 37°C in a water bath. Cold media was added to a final volume of 20ml. Subsequently, the cells were then washed twice with media before being suspended in culture medium and placed in a 37°C incubator.

### **2.3.2 Plating procedure**

Cells were suspended in media to a final concentration of  $0.4 \times 10^6$ /ml and 0.5ml added to each well in a 24 well plate. Cells were cultured at a temperature of 37°C at conditions of 5% CO<sub>2</sub> – 95% air. An initial series of experiments were undertaken to ascertain the optimal plating number of cells/well in a 24 well plate. The optimal number of cells for confluence is just under  $1 \times 10^6$ /well. Below this confluence fell, and above this, the cells became superimposed. In such cases viability was poor, and the cells failed to adhere during experiments.

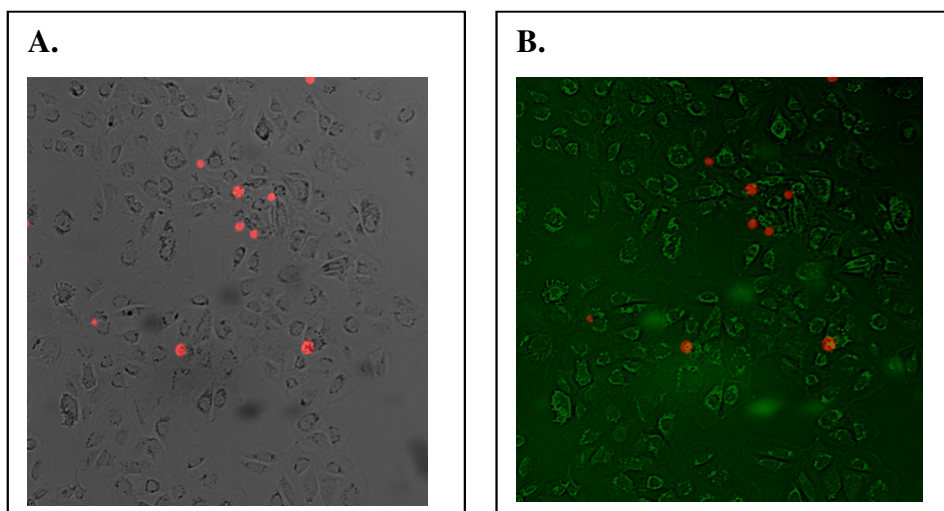
The plating technique was found to be critical to achieving a high-quality monolayer. Volumes of medium less than 0.5ml lead to a tendency for cells to be unevenly distributed in the well with crowding of the cells in the circumference and in the middle of the well. Great care was taken while plating to gently but thoroughly mix to achieve an even distribution, avoiding a vortex effect. Any deviation for even plating leads to sheets of cells coming away at later time points.

### 2.3.3 Cell viability

#### a) Dye: Fluorescence method; Acridine Orange (AO)/Propidium Iodide (PI)

This approach was generally preferred for viability assessment and was frequently used to ensure viability >98% as compound cell damage causes iron release independently of the chelation mechanism. AO and PI are nuclear staining dyes. PI is permeable to dead cells and stains red while AO crosses the membranes of live/dead cells and binds to nucleic acids, staining green. Microscope images were captured with the aid of UV light where appropriate and analysed using the software Image J (**Figure 4**).

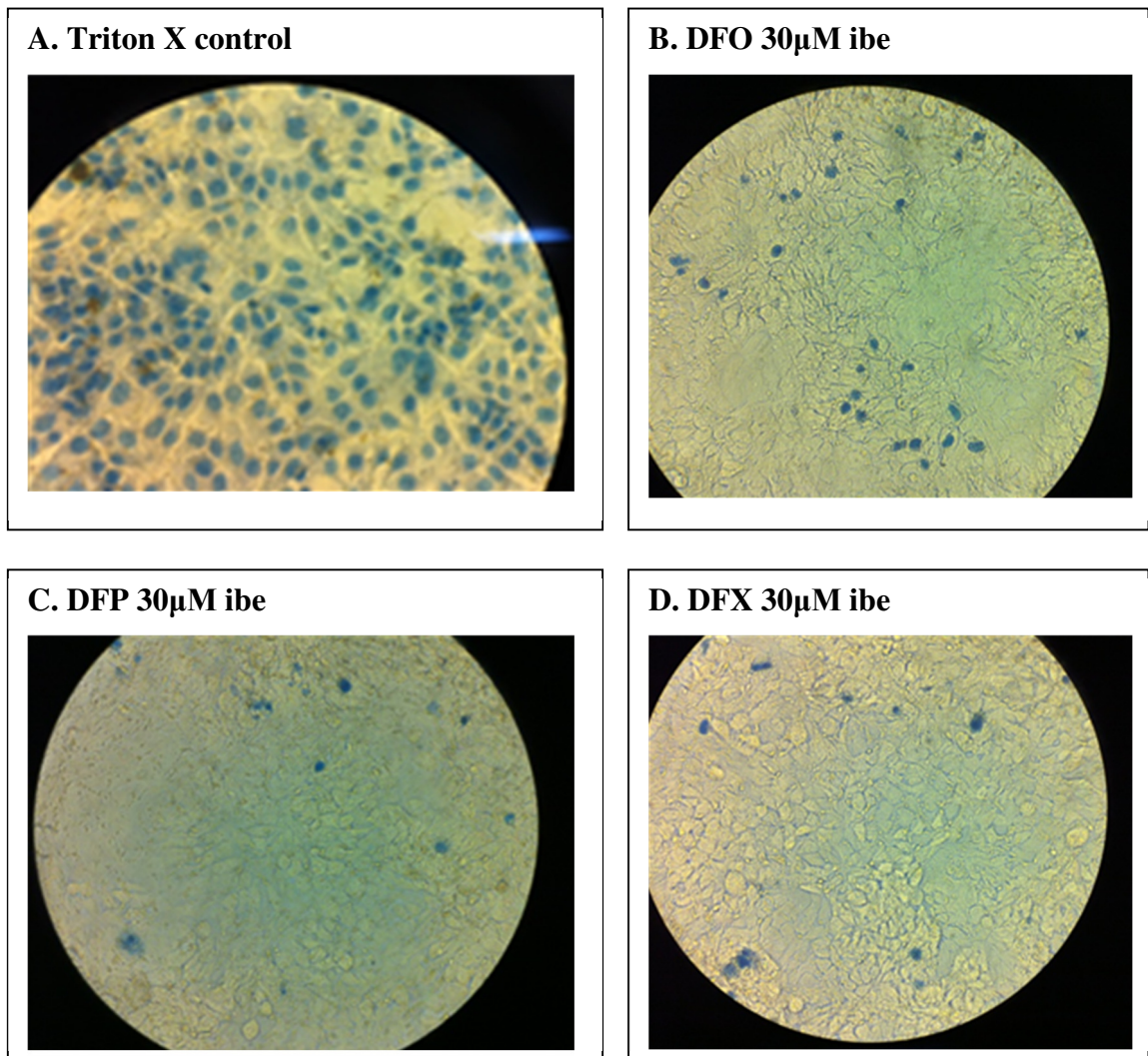
**Figure 4 AO/PI staining following 8 hours of treatment with DFO at 30 $\mu$ M ibe.** A. Dead cells stained red by PI. B. Green AO staining, with dead red stained AO cells, superimposed.



#### b) Dye: Trypan blue method

A solution of 50/50 (vol./vol.) of trypan blue solution in PBS was added, and they were then incubated at room temperature for 10 minutes to allow the dye to be taken up into non-viable cells. The cells were then counted in a Neubauer chamber or directly visualized under the microscope, with the dead cells appearing blue (**Figure 5**).

**Figure 5 Trypan blue staining in HuH7 cells following 8 hours of chelator treatment.**



*c) Lactate Dehydrogenase Assay*

Viability was also assessed using the 'LDH Cytotoxicity Detection Kit' by Takara Bio Inc, which gives a quantitative comparison of early cell damage between 'treatment' and 'control.' This is a colorimetric assay and measures LDH activity leaked by damaged cells into the supernatant.

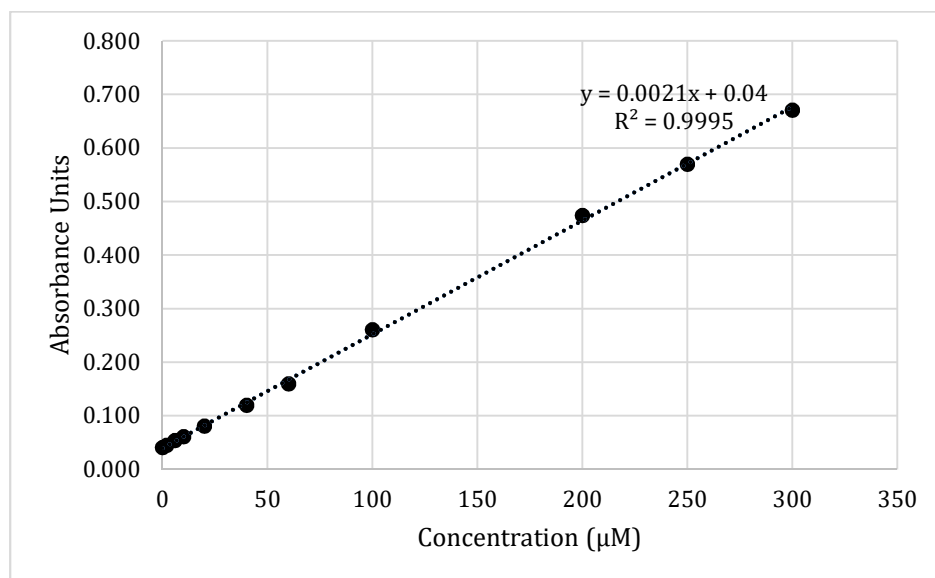
### **2.3.4 Cellular protein concentration determination**

The Coomassie (Bradford) Assay protocol was used for to determine cellular protein (Bradford, 1976). Briefly, 250  $\mu$ L of Bradford reagent was mixed with 5  $\mu$ L of cell lysate (duplicates) on a shaker for half a minute in a 96 well plate. The mixture was left to stand for 10 minutes. Absorbance was recorded at 595nm and compared to standards of bovine serum albumin ( $\mu$ g/ml), used to generate a standard curve.

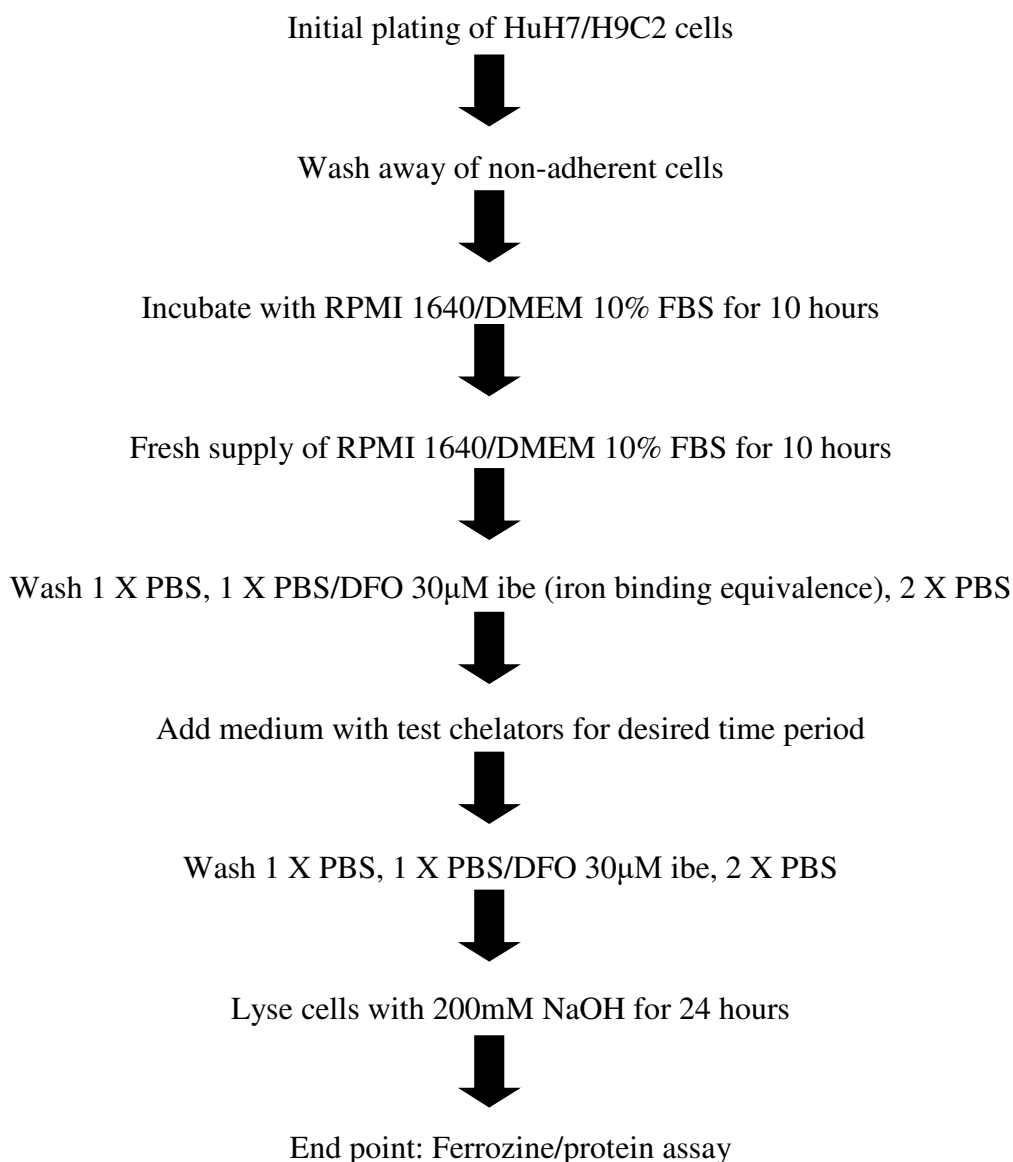
### 2.3.5 The ferrozine assay

Following treatment, the cells were washed four times including one wash containing DFO at 30µM and 3 PBS washes and lysed with 200µl of 200 mmol/l NaOH per well in a 24 well plate overnight. 5 µL were isolated for protein determination in duplicates. The ferrozine assay (on 190µl aliquots) was used to determine iron concentration (Riemer et al, 2004) with modifications. Briefly, 200µL of 10mM HCL and 200µL of the iron-releasing agent (1.4M HCL and 4.5% (w/v) KMnO<sub>4</sub>) were added and incubated for 2 hours at room temperature on a plate shaker. 120 µL of iron-detection reagent (6.5mM ferrozine, 6.5mM neocuproine, 2.5M ammonium acetate, and 1M ascorbic acid dissolved in iron free HPLC grade water) were then added to each well for 30 minutes. Absorbance was recorded in a plate reader at 562nm. Standard curve interpolation was used to calculate the iron content. A range of atomic absorption iron standards (0-300µM) of equal volume were prepared in a similar manner to unknowns (**Figure 6**). Intracellular iron was normalised against protein content. The sensitivity of the assay is noted to be as low as 1µM.

**Figure 6** Ferrozine assay standard curve.



## 2.4 Flowchart of final cellular iron loading model

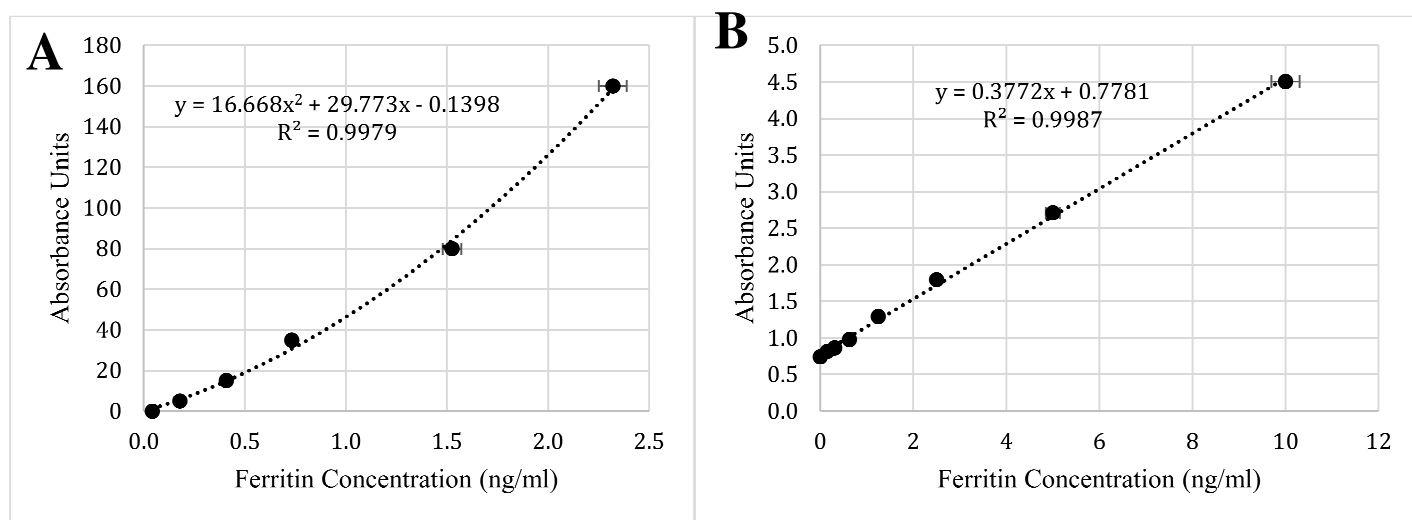


## 2.5 Ferritin quantification

Human and rat tissue ferritin were recorded by commercially available enzyme-linked immunosorbent assay (ELISA) kits (Cusabio, Wuhan, China and My BioSource, San Diego, USA respectively) according to the instructions provided by the manufacturer for recording ferritin of cell lysates. In brief, adherent cells were rinsed once with ice-cold PBS. The cells were scraped off the plate and stored in PBS (pH 7.2-7.4) at -20°C overnight. 2 freeze-thaw cycles were carried out in order to disturb cell membranes, and the resulting lysates were centrifuged for 5 minutes at 5000 g at 2-8°C, and the supernatants collected. Samples as well as standards are exposed to a conjugated

antibody specific to ferritin. The wells are then washed to remove unbound reagent, and a substrate solution is added to the wells. Colour develops in proportion to the amount of ferritin-bound during the initial step. The colour development is stopped, and the intensity of the colour is measured. **Figure 7** shows the standard curves for the rat (A) and human (B) ferritin ELISA.

**Figure 7 Rat (A) and human (B) ferritin standard curve.**

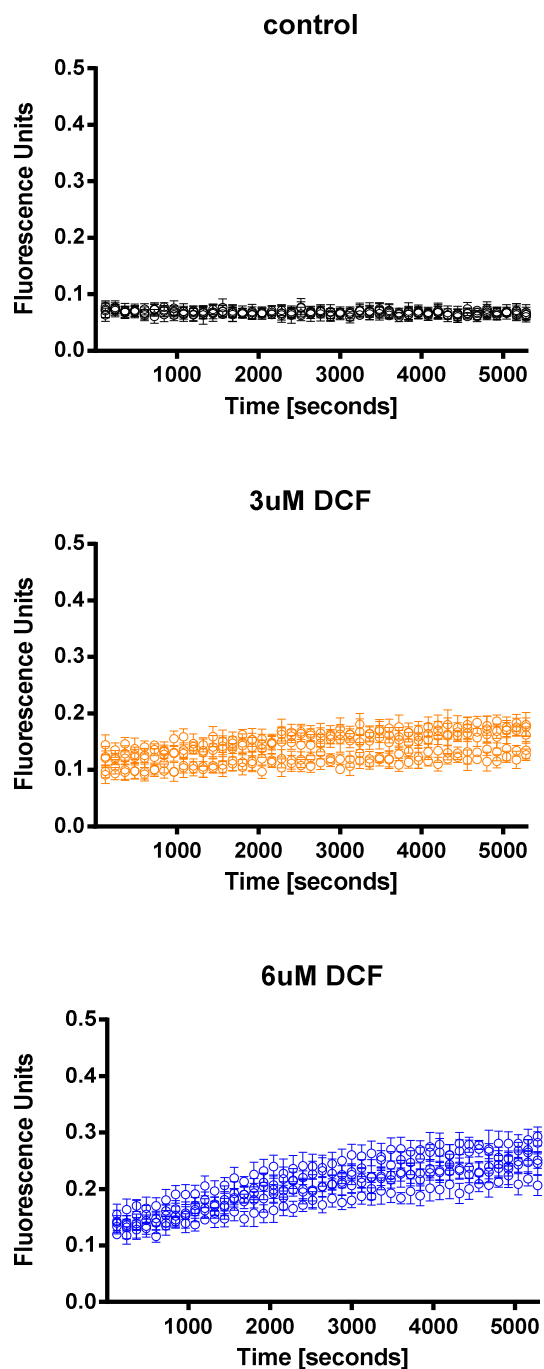


## 2.6 Determination of intracellular reactive oxygen species (ROS) levels using a fluorimetric method

We chose the fluorescent probe 5,6-carboxy-2',7'- dichlorofluorescein diacetate (DCFH-DA) (Molecular Probes, Leiden, Netherlands) to detect intracellular ROS. The non-fluorescent DCFH-DA is cleaved to DCFH when in the intracellular compartment and yields the highly fluorescent probe DCF in the presence of hydrogen peroxide ( $H_2O_2$ ) intracellularly. Therefore, the dichlorofluorescein (DCF) fluorescence signal directly correlates to the amount of intracellular ROS. Corning 24-well plates (Sigma-Aldrich, MA, USA) were used, and cells were pre-incubated with  $6\mu M$  H2DCF-DA for 30 minutes at  $37^\circ C$ . Chelators were then added and the resulting fluorescence cells treated with chelators as well as control were read throughout the treatment period in the plate reader (excitation 504 nm, emission 526 nm). The rate of change of production of ROS was calculated over 60 – 90 minutes. **Figure 8** demonstrated the effect of varying the concentration of DCF on ROS production.



Figure 8 Effect of varying the concentration of DCF on ROS production in HuH7 cells.



## 2.7 Preparation of heat-inactivated human serum

Following venipuncture by an experienced phlebotomist from volunteer healthy lab donors, following informed consent, in a red-top vacutainer tube, coagulation was allowed over a period of 30 minutes. The sample was then spun at 3000 rpm for 10

minutes, and the serum aspirated and heated in the water bath at 56°C over a period of 1 hour.

## **2.8 Animal Study**

### **2.8.1 Specification and Housing**

All animal work carried out conformed with the Animals (Scientific Procedures) Act 1986 and university guidelines. A humanised mouse model of thalassaemia (Heterozygous knockin  $\gamma^{\text{HPFH}}\delta\beta^0/\gamma\beta^{\text{A}}$  thalassaemia mice) (Huo et al, 2010) was kindly donated by Dr. A.David from the Institute for Women's Health, at UCL. All mice were male and between 4 and 5 months of age. Animals were grouped in cages having previously been earmarked for ease of individual identification. The environment was controlled, with a temperature of 25+/-2 °C and 12 hour light/dark cycles. Standard chow diet (Harlan Laboratories, Inc. Stoughton Rd, USA) and water were provided *ad libidum*. Normal chow diet contains moisture 12%, crude protein 24%, fat 4.5%, fiber 5%, metabolic energy 3040 kcal/kg, phosphorus 0.9%, calcium 1%, sodium 0.2%, magnesium 0.23%, potassium 1.17%, manganese 171 ppm, copper 22 ppm, zinc 100 ppm, iron 180 ppm, cobalt 1.82 ppm, vitamin K 5 mg/kg, selenium 0.1%, vitamin D 4000 IU/kg, vitamin A 20000 IU/kg, vitamin E 100 mg/kg, vitamin B1 20 mg/kg, vitamin B2 20 mg/kg, vitamin B6 20 mg/kg, vitamin B12 20 mg/kg, folic acid 6 mg/kg, niacin 100 mg/kg, biotin 0.4 mg/kg and choline chloride 1500 mg/kg.

## 2.8.2 Iron loading and chelation treatment

### Establishing the iron loaded mouse model

*Humanised Control:* Humanized  $\gamma\beta^A/\gamma\beta^A$  control mice (n=7). These control mice received 0.1ml of IP PBS 5 days/week for 4 weeks

*Iron-loaded:* Heterozygous knockin  $\gamma^{\text{HPFH}}\delta\beta^0/\gamma\beta^A$  thalassaemia mice received intraperitoneal injections of iron dextran solution (10mg (0.1ml) daily for 4 weeks (5days/week)). A further month was allowed for re-equilibration of iron following the iron overloading.

*Thalassaemia Control:* Heterozygous knockin  $\gamma^{\text{HPFH}}\delta\beta^0/\gamma\beta^A$  thalassaemia mice. These mice received PBS injections with the same regime as the mice undergoing iron loading.

### Chelation treatment

Iron-loaded animals were randomly assigned to the following three groups: iron chelation treatment with DFX 30mg/kg daily (n=7), Quercetin 300mg/kg daily (n=5), or combination of DFX 30mg/kg and Quercetin 300mg/kg daily (n=7). Hydroxypropyl cellulose 0.5% was chosen as the vehicle medium as previously described (Sumi et al, 2013), which was received by the control group (n=7). Treatment was administered orally by gavage and mice were observed immediately before dosing each day and again at least 15 minutes after the dose, for any adverse effects. Body weights were observed throughout and at the end of the study.

## 2.8.3 In vivo Magnetic Resonance Imaging (MRI)

This was carried out by Laurence Jackson (Ph.D. student), under the direct supervision of Dr. Daniel Stuckley at the Centre for Advanced Biomedical Imaging (CABI). This collaboration had as a primary aim to determine if MRI can be used to assess and

quantify excess iron distribution in a murine model of thalassaemia by comparing this with a histological and biochemical assessment of tissue iron. Imaging was performed using a 9.4T MR system (Agilent Technologies, Santa Clara, USA) equipped with 1000mT/m gradient inserts and a 39mm volume resonator RF coil (RAPID Biomedical, Rimpar, Germany). Using MRI, T1, T2, and T2\* relaxation rates were measured in the myocardium, liver and spleen in addition to cardiac function and spleen volume measurements. The animals were observed using a monitoring system (SA Instruments, Stony Brook, NY) which recorded the ECG trace, respiration rate, and internal temperature. Animals were anaesthetised under a mixture of isoflurane and oxygen with physiological measurements used to maintain anaesthesia.

#### **2.8.4 Measurement of iron overload in tissues**

Animals were anaesthetized and blood drawn from within the ventricle following thoracotomy. The blood collection was carried out under terminal anaesthesia, which was achieved by the injection of 0.8 ml of 1.25% Tribromoethanol solution (Avertin Sigma- Aldrich, UK). From the cardiac puncture, an average of 0.5-1 ml of blood collection was achieved using a pre heparinised 26G syringe in 0.5ml EDTA tubes. Each animal was weighed, and haemoglobin (Hb) estimated using a HemoCue machine (Hemocue, Sweden). The heart, spleen, and liver were isolated, weighed and then stored in paraformaldehyde (PFA) 4% solution in PBS (Santa Cruz Biotechnology, Germany).

#### **2.8.5 Bothwell Method (Bothwell et al, 1964): Tissue Iron Quantification**

##### REAGENTS

- *Iron free reagents, water, glassware*
- *Working standard iron solution (2µg/ml)*
- *Acid Solution (3M hydrochloric acid and 10% trichloroacetic acid). Into a 500ml volumetric flask containing 200ml iron free water, 50g trichloroacetic acid, and 1.5moles hydrochloric acid (129ml concentrated 36% hydrochloric acid). Dissolve and make up to volume with iron free water. (stable for 2 months in a dark bottle).*
- *Chromogen reagent (0.1% bathophenanthroline sulphonate and 1% thioglycolic acid). Place 100mg disodium 4,7- diphenyl -1, 10-phenanthroline disulphonate in a 100ml flask which contains 50ml iron free water. Add 1ml*

*concentrated (100%) thioglycolic (mercaptoacetic) acid and make up to volume with iron free water. (Stable for one month in a dark brown bottle)*

- *Working chromogen reagent. Prepare on the day:*
  - 1: volume of the 0.1% chromogen reagent
  - 5: volumes of saturated sodium acetate ( $\text{CH}_3\text{COONa} \cdot 3\text{H}_2\text{O}$ ) – iron content less than 0.0002% (0.2ppm)
  - 5: volumes iron free water.

## THE METHOD

1. *Weigh, e.g., 1g of tissue. Cut into small pieces*
2. *Transfer pieces to 50ml Erlenmeyer flask, add 10ml of acid solution*
3. *Stopper the flask lightly with a glass stopper of large marble*
4. *Place the flask in an oven at 65 degrees for 20 hours*
5. *Solution 1 - After cooling to room temperature, transfer 0.2ml of the clear yellow solution to a test tube and add 10ml of working chromogen reagent. Mix the contents of the tube and allow to stand for at least 10 minutes*
6. *Solution 2 – Prepare a reagent blank by adding 10ml of the working chromogen reagent to 0.2ml of acid solution. Following mixing, allow to stand for at least 10 minutes.*
7. *Solution 3 -Prepare a standard by adding 2ml of working iron standard solution to 8.2 ml of the working chromogen reagent. Mix and allow to stand for at least 10 minutes.*
8. *Measure the optical densities of the three solutions at 535 $\mu\text{m}$  against a distilled water blank*

## CALCULATIONS

Tissue iron concentration ( $\mu\text{g Fe/g}$  dry tissue)

$= \text{O.D. Tissue Extract} - \text{O.D. blank} / \text{O.D. Iron standard} - \text{O.D. blank} \times 200 / \text{Tissue dry weight(g)}$

### **2.8.6 Perls' Prussian Blue Staining**

Tissue slide preparation and staining was performed by Central Diagnostic Services, University of Cambridge, Queen's Veterinary School Hospital. Liver, heart, pancreas, and spleen initially fixed in paraformaldehyde 4% solution in PBS were trimmed and embedded in paraffin. In brief, sections were washed and dehydrated with distilled water with xylene and ethanol. They were then stained with Prussian blue stain (potassium ferrocyanide and hydrochloric acid). Stained sections were further dehydrated by ethanol and xylene and mounted onto slides using Permount medium for

microscopic examination. Slides were scanned at the Center for Cell & Molecular Dynamics, UCL, London and analysed using the ZEN software (ZEISS, 2012).

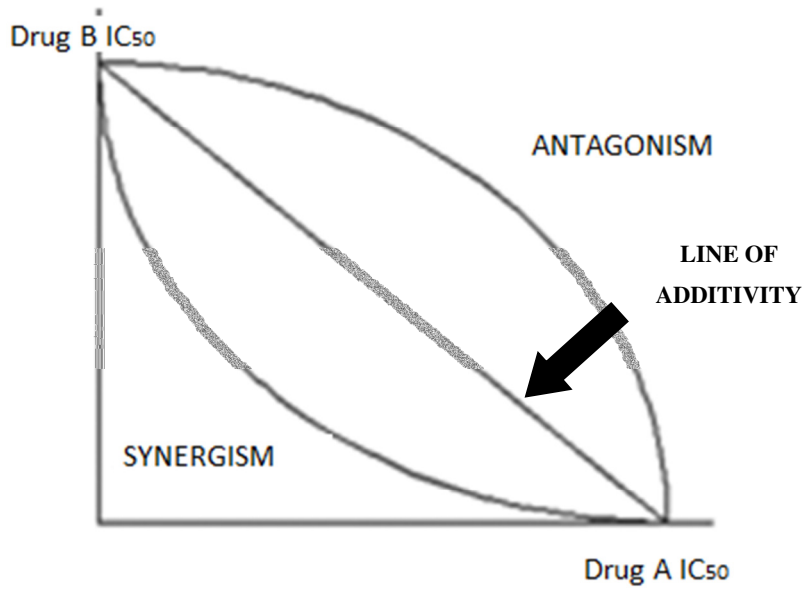
## 2.9 Drug Combination Analysis

As reviewed by Tallarida (Tallarida, 2006), two drugs with a similar action can produce an exaggerated or diminished effect in combination. Isobolograms can be used to provide a quantitative assessment of the combined effect and provide further insight into distinguishing synergism vs. additivity. Making this distinction is based on the classic definition of additivity which explains that each constituent will be contributing to the resulting effect in accordance with its individual potency. Thus, the relative potency of each agent allows a calculation of the predicted effect of dose pairs to determine the equivalent contribution of either agent and ascertain the exaggerated component of the actual obtained effect.

Isobolograms can be constructed for any desired chelation effect, for example, 50% of half maximal following the desired time of chelator treatment. If a 50% response is chosen, as it can be seen in **Figure 9**, the axis intercepts show the IC<sub>50</sub> for each chelator when in monotherapy (i.e. the potency). The straight line on the graph that connects these two intercept points is known as ‘the line of additivity’, and shows the locus of all such dose pairs, which based on their known potencies should result in the exact same chelation effect. If the actual resulting effect of the dose pairs is noted to be above the line, the two compounds are antagonists, whereas when a curve is noted below the line, this indicates a super-additive effect and thus synergy of action of the two compounds.

To further quantify this effect we looked at the *synergy index*  $\alpha$ , which is equivalent to  $(1 - 1/R) \times 100\%$  where R= difference between the area under the line and the area under the curve. This index is a way of determining how much the resulting effect actually surpasses the one expected by the simple additivity action of the two compounds.

**Figure 9 Sample Isobologram**



## **2.10 Statistical analysis**

Data presented are shown as mean  $\pm$  SEM for  $n$  determinations, represented as error bars on the graphs. Comparisons between categorical data were conducted using the chi-squared test or the Fisher's exact test in the case where the variables were categorical, and the Mann-Whitney U test for continuous variables. Analysis of variance was adopted to establish differences between groups with post-test Bonferroni correction, where appropriate. The statistical software packages SPSS 21 (SPSS Inc., Chicago, IL) and GraphPad Prism 5 were used for data analysis and construction of isobolograms.

## **Chapter 3 HEPATOCYTE AND CARDIOMYOCYTE CULTURES; Development of a model to study iron mobilisation by chelators**

### **3.1 Introduction**

In this chapter, experiments were undertaken to develop a model that enables the study of chelator interactions and intracellular iron pools. Two cell lines were chosen, the human hepatocellular carcinoma cell line (HuH7) and the rat cardiomyocytes (H9C2). This system, using the cardiomyocyte cell line H9C2 was developed because heart failure secondary to iron overload is the main cause of death in transfusional iron overload. The hepatocyte is the major cell type in which excess iron is stored and is an important source of iron excretion for example by DFO. As well as being the major site of iron storage in iron overload, the hepatocyte is an important target of iron-mediated damage where unstable iron laden lysosomes release their contents, thereby triggering a sequence of events leading to cell-mediated fibrogenesis and finally cirrhosis (Myers et al, 1991; Tsukamoto et al, 1995).

Before performing experiments to examine the effect of new chelators on iron release, it was necessary to firstly characterise the behavior of the cardiomyocyte and hepatocyte culture models, with particular reference to the effect of physiological iron binding proteins on iron uptake and release. An important objective in designing the model was to identify a method of loading iron that was as physiological or 'pathophysiological' as possible and did not require the use of radioactive tracers. One of the first models of cardiomyocyte iron loading developed used radioactivity and demonstrated that non-transferrin bound iron is taken up by an excess of 5-fold more rapidly than transferrin-bound iron in these cells (Link et al, 1985). In hepatocytes, much more than cardiomyocytes, there is an abundance of saturable transferrin receptors on the cell surface (between 37,000 and 66,000). We initially designed our experiments using 10% fetal bovine serum (FBS), which contains transferrin at normal serum concentrations and could act as a source of iron for the cells. While much is known about iron uptake from transferrin into hepatocytes, mechanisms controlling iron release and the importance of transferrin to this process are less well understood. It was, therefore, important to understand the interaction of transferrin with our cells in culture and



develop an efficient way of iron loading, before examining how iron chelators may modify iron status.

As will be shown later in the chapter, however, FBS also contains other sources of iron that are not bound to transferrin, namely NTBI. NTBI is a major conduit through which iron is taken into cells in iron overload conditions. Uptake into cells that are susceptible to iron overload from NTBI is very rapid. Therefore iron loading cells from serum that contains NTBI is potentially a 'pathophysiological' way to iron load cells that has clinical relevance. Other methods of loading iron such as by using ferric ammonium citrate (FAC) are also evaluated here.

In this chapter, the experiments which helped to determine the optimal model to be used in our study of chelators will be described. Additionally, experiments will be shown which address how hepatocytes and cardiomyocytes differ in their interaction with chelators. These differences have clinical implications for the potential efficacy and toxicity of chelators.

Before describing the model, I will present a brief review of intracellular iron metabolism with the hepatocyte as the particular reference.

### **3.2 Iron and the human liver**

In humans, liver amounts to 10% of total body iron in normal subjects or about 400mg. Of this iron, 98% is found in hepatocytes, 1.5% in Kupffer cells and 0.5% in endothelial cells (Bacon & Tavill, 1984). Therefore, the hepatocytes contain the vast majority of liver iron. Kupffer cells contain only a small proportion of body iron in healthy individuals, and together with other reticuloendothelial cells in the spleen and bone marrow, are major sites of iron turnover where red blood cells are broken down and iron liberated from haemoglobin. This iron is subsequently released for binding and transport by plasma transferrin, which has a long plasma half-life of 7 to 10 days and can repeat numerous plasma to cell iron cycles (Bomford & Munro, 1985; Young & Bomford, 1984).

Within the hepatocyte, about 70% of the iron is present as storage iron (50% in the form of ferritin and 12% as haemosiderin), 12% in haem-containing molecules and other forms include transferrin and some labile plasma iron. Any remaining iron is present as non-haem containing enzymes (Bailey-Wood et al, 1975; Selden & Peters, 1979; Van Wyk et al, 1971; Zuyderhoudt et al, 1978).

### **3.2.1 Storage iron**

The predominant form of iron storage is ferritin which is a large molecule of MW 440,000 and can accommodate up to 4500 iron atoms stored in the form of polymeric iron hydroxide and ferric oxyhydroxide. Each ferritin molecule consists of 24 subunits with a varied proportion of either heavy (H) acidic subunits or lighter (L) basic subunits. Depending on the tissue type, these subunits vary. The H-ferritin subunits are predominant in the heart and kidney, whereas the L predominate in the liver and spleen. Plasma ferritin correlates with body iron stores and consists almost exclusively of L and 'G' subunits. The 'G' subunit represents glycosylation of subunits (Cragg et al, 1981). Iron stimulates the formation of L subunits and promotes apoferritin aggregation into a shell. For cytosolic iron to be incorporated into ferritin, it must first be reduced to ferrous iron (Treffry & Harrison, 1979). Once inside the protein shell, the ferrous iron is oxidised back to ferric iron and following a process of hydrolysis it polymerises to ferric oxyhydroxide phosphate. Iron is incorporated faster onto partially filled ferritin than apoferritin (Hoy & Jacobs, 1981). The release of iron from ferritin requires reduction of ferric back to ferrous iron (Sirivech et al, 1974) or catabolism of the protein. Release is very slow and triggered by reducing agents or low pH. Physiological release of iron from ferritin requires the molecule to be catabolised.

Haemosiderin is present only in tissues, and predominately in hepatocytes and macrophages in the absence of iron overload. It is thought to be formed following degradation of ferritin by lysosomes (Weir et al, 1984). It is an insoluble deposit of degraded ferritin protein and ferric hydroxide polymers which give a positive Prussian blue reaction (Wixom et al, 1980).

### 3.2.2 Iron utilised for essential proteins and enzymes

There are a number of haem proteins that contain iron, including haemoglobin, myoglobin, catalase, peroxidases and cytochromes. The relative amounts of haem proteins depend on the cell type. For example, in liver cells the amount of haemoglobin and myoglobin synthesized is insignificant. In the mitochondrion, iron distribution is heterogenous with one-third present as haem proteins (cytochromes), one-third in iron-sulphur clusters (succinate dehydrogenase, reduced NADH-ubiquinone, cytochrome C) and one-third as non-haem, non-sulphur, transit pool.

Iron Sulphur proteins are a large class of molecules containing iron atoms bound to sulphide. In eukaryotes their principle function is as redox mediators in the mitochondrial electron transport chain, acting together with cytochromes to facilitate this process. Furthermore, they are involved in the citric acid cycle which catalyses the stereospecific dehydration and rehydration reaction involved in the conversion of citrate to isocitrate (Beinert & Kennedy, 1989).

There is also a group of non-haem, non-sulphur enzymes containing iron. This disparate group of enzymes is potentially important with respect to chelators because unlike haem iron-containing compounds, the iron on these proteins can potentially be chelatable. Chelation can lead to inactivation and inhibition of enzyme function and knowledge of this is of potential interest in view of unwanted inhibitory effects of iron chelators. An important member of this group is the ribonucleotide reductase responsible for the catalysis of the reduction of ribonucleotides to deoxyribonucleotides, and essential prerequisite to the synthesis of DNA (Thelander & Reichard, 1979). It is conceivable that the antiproliferative effects of iron chelators in tumour cells (Hoyes et al, 1992; Roth et al, 2012) relates to the inhibition enzymes directly by the chelators.

There are several oxygenases in mammalian tissues that depend on ferrous iron for their maximal activity. *Propyl* and *lysyl hydroxylase* are essential for the synthesis of hydroxylysine and hydroxyproline which are unique constituents of collagen (Cumming et al, 1978). *Phenylalanine hydroxylase* has high activity in liver and catalyses the hydroxylation of L-phenylalanine to L-tyrosine and provides the body with a source of tyrosine. *Tyrosine hydroxylase* further hydroxylates L-tyrosine to L-Dopa,

levels of which are low in Parkinson's disease. Other enzymes thought to require iron are *lipxygenases*, involved in a variety of oxygenation reaction of fatty acid substrates. There is interest in the design of chelators that could inhibit these enzymes for the treatment of atherosclerosis.

### **3.2.3 Transit iron and labile iron pool (LIP)**

Delivery of iron to hepatocytes is primarily via transferrin, which is synthesized in its free form within the hepatocyte. Once liberated from transferrin in the acidic endosome, iron egress from the endosome is via the Nramp2 transporter (Fleming et al, 1998), and then it enters a small labile iron pool (LIP) which is destined either for incorporation into storage iron or is utilised in proteins and enzymes described above. A number of groups have provided evidence of this chelatable iron pool, in several cell types including reticulocytes, marrow cells, and intestinal epithelial cells. Iron entering cells becomes transiently chelatable before being incorporated into ferritin (Pippard et al, 1982). This pool can be rapidly chelated with DFO, EDTA or transferrin (White et al, 1976). Experiments using the fluorescent probe calcein have suggested that in K562 cells LIP is present at 0.4 $\mu$ M with a transit time of 2 hours (Breuer et al, 1995). LIP increases with acute iron loading but rapidly reduces with a t<sub>1/2</sub> of 27 minutes (Breuer et al, 1996), and is chelatable by hydroxypyridinones and other chelators (Zanninelli et al, 1997).

## **3.3 Iron Uptake Mechanisms**

### **3.3.1 Iron uptake through transferrin (Tf)**

One of the major conduits through which extracellular iron enters cells is through transferrin. This is the primary mechanism by which iron is delivered to hepatocytes. Transferrin is a glycoprotein of MW 80,000, with an N and a C iron(III) binding domain. Each iron(III) is coordinated between two tyrosines, one histidine and one aspartic acid and indirectly to an arginine with bicarbonate acting as a bridging ligand (Bailey et al, 1988). Under normal iron status, plasma transferrin is approximately saturated by one-third. At 20% saturation, the iron-free form is predominant (57%) with only 3% diferric form and the remainder consisting of monoferric species FeN-Tf (14%) and FeC-Tf (26%). The proportion of diferric TF rises with saturation (Leibman & Aisen, 1979)

Between 37,000 and 66,000 saturable transferrin receptors are found on each hepatocyte and together with unsaturable non-specific uptake processes this gives a maximal rate of iron uptake of  $9 \times 10^5$  to  $1 \times 10^6$  molecules/cell/minute (Thorstensen, 1988; Trinder et al, 1990; Young & Bomford, 1984). It has been previously shown in hepatocytes that diferric transferrin is taken up at 35x the rate of apotransferrin, and that monoferric transferrin uptake is twice that of apotransferrin (Young & Aisen, 1981). Transferrin receptor expression reflects cellular iron requirements (Sutherland et al, 1981). Iron uptake from transferrin occurs through receptor-mediated endocytosis (Dautry-Varsat et al, 1983; Klausner et al, 1983). Diferric transferrin binds to the receptor and the complex becomes localized in clathrin-coated pits. These pits bud off from the cell surface to form clathrin-coated vesicles which lose their coats and fuse to form an endosome. A proton pump ATPase in the endosomal membrane acidifies the vesicle to approximately pH5.5. Iron dissociates from transferrin because of the acidic conditions and is transported across into the cytosol (Bomford & Munro, 1985). The newly formed apotransferrin remains firmly bound to the transferrin receptor while it remains within cells and is recycled to the cell surface (Dautry-Varsat et al, 1983; Klausner et al, 1983; Leverence et al, 2010). This process is thought to take between 3 and 5 minutes. The iron removed enters the LIP prior to incorporation into ferritin, haem proteins or other iron-containing molecules. It was believed that apotransferrin dissociates from the transferrin receptor following exposure to the neutral pH at the cell membrane, however, it is now known that the apotransferrin- transferrin receptor complex remains intact until iron-loaded Tf which has a higher affinity for the receptor displaces apotransferrin ((Leverence et al, 2010).

Receptor-mediated endocytosis of transferrin iron has an established role in iron uptake. However, there is also evidence to support an endocytosis-independent pathway of iron uptake from transferrin (Irie & Tavassoli, 1987; Trinder et al, 1996). Alternative proposed pathways include associated reduction of iron from transferrin, which is then transported across the cell membrane (Cole & Glass, 1983; Hodgson et al, 1994; Morley & Bezkorovainy, 1985; Oshiro et al, 1993; Thorstensen & Romslo, 1988; 1990). Iron release from Tf is a complex multifactorial process dependent on a number of factors including pH, anion binding, the presence of chelators, and the 'lobe' location of iron on Tf. Release of iron from the N- lobe of the molecule is thought to be rapid at (17.7

+/-2.2 min) while removal of iron from the C- lobe slow (0.65 +/-0.06/min) (Luck & Mason, 2012). Furthermore, release of iron from the N-lobe is accelerated by the absence or iron from the C-lobe (Luck & Mason, 2012).

### **3.3.2 Ferritin uptake, synthesis control, and turnover of iron**

Physiologically the most important pathway for iron uptake in hepatocytes is from transferrin; however other routes are known to contribute. These can be exploited in the design of *in vitro* models and *in vivo* animal models to probe the availability and the kinetics of iron availability from different pools to chelation.

Ferritin from plasma is almost exclusively cleared by hepatocytes (Unger & Hershko, 1974). Ferritin clearance is influenced by glycosylation; rat ferritin has a low glycosylation and is rapidly cleared by hepatocytes whereas human plasma ferritin has a high glycosylation and is cleared relatively slowly. This implies that in states of poorly controlled diabetes ferritin iron clearance will be further delayed. Liver-derived ferritin has a half-life of 50 hours (Worwood, 1982) vs. spleen-derived ferritin which is cleared more quickly (Cragg et al, 1983).

Ferritin uptake is typically via receptor-mediated endocytosis, however, it cannot be rapidly exocytosed in a similar way to transferrin. Ferritin is taken from endosomes to lysosomes (Radisky & Kaplan, 1998) where the iron is liberated after catabolism of the protein coat, and the iron is incorporated into newly formed ferritin molecules of haemosiderin (Hershko et al, 1973). Within hepatocytes, the bulk of ferritin is turned over regularly and degraded by proteolysis with the subsequent release of iron to the labile intracellular pool. It was previously estimated that ferritin is turned over intracellularly with a half-life of about 72 hours (Drysdale & Munro, 1965). Ferritin release from hepatocytes reflects cellular iron content or may also reflect cellular iron damage.

Ferritin levels are the result of the balance between ferritin synthesis and degradation. Synthesis is upregulated when cytosolic iron is high to provide capacity for storage iron. Iron binding proteins bind to iron-responsive elements (IREs) on ferritin mRNA, enhancing ferritin synthesis (Rouault, 2006). In conditions of iron demand, ferritin is

degraded by a process known as autophagy, where it is delivered to lysosomes (Radisky & Kaplan, 1998). This process is modulated by cargo molecules such as NCOA4 (Mancias et al, 2014). Ferritin is depleted of iron and then ubiquitinated followed by degradation (De Domenico et al, 2006).

### **3.3.3 Uptake of plasma NTBI**

Iron that is non-transferrin bound is often present in pathology and is also taken up by cells (Baker et al, 1981; Fawwaz et al, 1967). NTBI appears in plasma when influx exceeds iron efflux, and when Tf saturation is >75%. NTBI is known to be increased in iron overload, decreased transferrin iron clearance, ineffective erythropoiesis as well as erythroid hypoplasia. NTBI is multispecied and can take a number of forms such as iron-citrate, bound albumin complexes, glycated protein-iron complexes or iron-chelate complexes (Garbowski et al, 2016). NTBI uptake often requires calcium (Oudit et al, 2003; Wright et al, 1986), and can be inhibited by divalent cations such as zinc and manganese (Wright et al, 1986). In iron overloaded mice with cardiomyopathy, tissue iron was shown to be significantly decreased in mice by blocking of L-type voltage-dependent  $Ca^{2+}$  channels (LVDC) with amlodipine and verapamil (Oudit et al, 2003). ZIP 14 is another metal iron transporter present in the liver, heart, and pancreas that has been identified as a candidate route for NTBI (Pinilla-Tenas et al, 2011). The rate of hepatocyte uptake of NTBI is increased in perfused livers of iron deficient animals (Zimelman et al, 1977) although the opposite effect is seen in intact animals, where iron overload increases liver uptake and iron deficiency decreases liver uptake. Similarly, high rates of iron uptake are observed if iron is complexed to citrate or fructose (Brissot et al, 1985). In hepatocytes, NTBI delivered is found within lysosomes (Batey et al, 1981) as ferritin within 30 minutes (Wright et al, 1986).

### **3.4 Developing the cellular model; the approach**

In view of the importance of hepatocytes as cells for iron storage, iron uptake and as a major source of chelatable iron, it was decided to commence the development of our cell system using HuH7 cells and then extend our study to cardiomyocytes in order to study the effects of iron chelators on iron mobilisation. The journey to establishing our model consisted of numerous experiments undertaken over a period of 5-6 months,

looking at the most effective and physiological form of iron for loading, different regimes for cell washing and viability challenges following chelator treatment.

### **3.5 Establishing optimal medium for iron loading in HuH7 cells**

A monolayer cell culture system was chosen in an attempt to create a reliable model for the study of iron release with chelators by minimising cell membrane damage, viability loss, and iron leakage, as is seen for example when agitating cells in suspension (Bailey-Wood et al, 1975; Baker et al, 1985). For the above reasons, a density of 200,000 cells per well was noted to be the most appropriate in 24 well plates. The cells were then allowed to settle for 24 hours reaching an average of 60% confluency, and non-adherent or partially adherent dead cells were washed off. The monolayers were then pulsed with RPMI 1640 media containing either 20 $\mu$ M FAC or 10% FBS for 24 hours. The supernatant was then aspirated, and a fresh supply of RPMI 1640 was added containing either 20 $\mu$ M FAC or 10% FBS for a further 24 hours. At the end of the 48 hours in total cells were noted to have reached 90% confluency; the medium was decanted and the cells rinsed on two occasions with PBS solution followed by a wash with PBS/DFO 30 $\mu$ M ibe and a final PBS wash. Iron content was determined via the ferozine assay as described in the methods **Section 2.3.5** and adjusted for protein, following overnight cell lysis with 200mM NaOH.

The iron content of cells was shown to be tripled in the presence of FAC and almost quadrupled in the presence of 10% FBS following two 24 hour incubations (**Figure 10**). The iron content of RPMI 1640 supplemented with 10% FBS was 25 $\mu$ M. The NTBI content was kindly measured by Dr. M. Garbowski in our laboratory, and the method is described in **Section 5.2.7**. In 100% FBS, the NTBI content was 3.31 $\pm$ 0.23  $\mu$ M, and 0.29 $\pm$ 0.05  $\mu$ M in RPMI media containing 10% FBS (**Figure 11**). Whilst Tf uptake is a known mechanism of iron acquisition, NTBI is a very rapidly taken up form of iron (Brissot et al, 1985). Using serum known to contain transferrin to effectively iron load cells was particularly appealing as we aimed to use physiological iron binding proteins and mechanisms as much as possible to examine iron uptake and release. Ferric ammonium citrate (FAC) also proved to be effective in increasing intracellular iron content. However, there was concern regarding iron binding on the extracellular membrane as well as on plastic wear, introducing error in intracellular iron assessment.



Hepatocytes have between 37,000 and 66,000 transferrin receptors on the cell surface (Young & Bomford, 1984), and transferrin is the major uptake pathway for iron in these cells, as described above (**Section 3.3.1**).

**Figure 10 FAC/FBS loading regime in HuH7 cells.** Cells were treated with RPMI media containing 10% FBS or 20 $\mu$ M FAC for 24 or 48 hours. Adherent cells were rinsed four times, including one wash containing DFO at 30 $\mu$ M and 3 x PBS washes. The cells were then lysed with 200mM NaOH. Intracellular iron concentration was determined using the ferrozine assay and normalised for total cellular protein in each well. Results are mean  $\pm$  SEM of quadruplicates in one experiment.

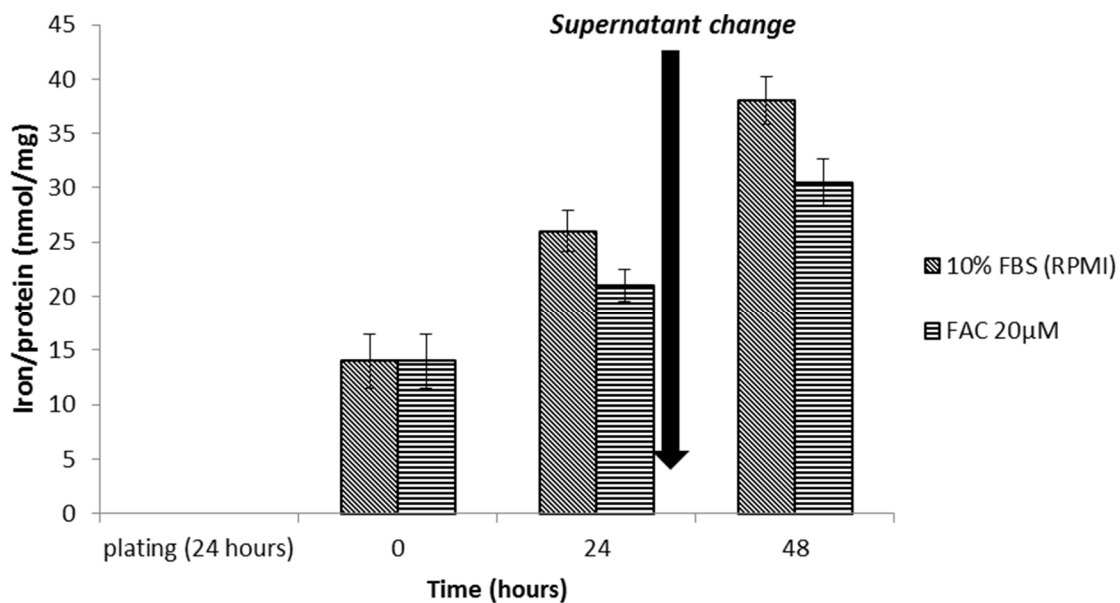
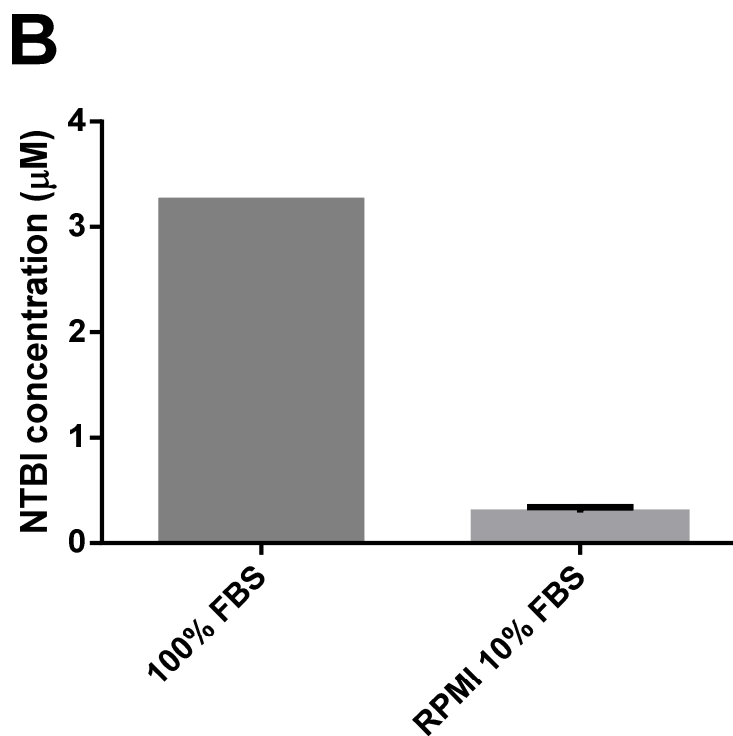
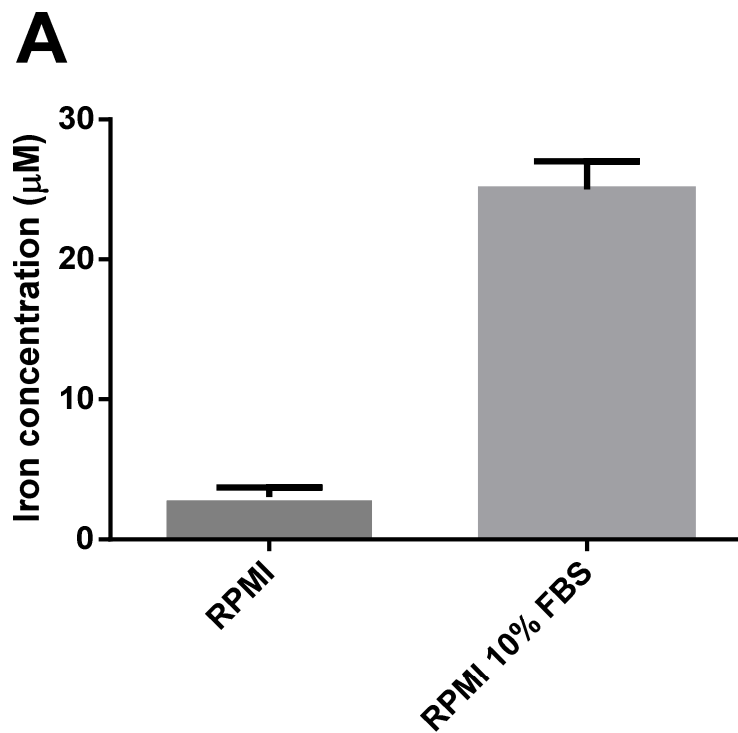


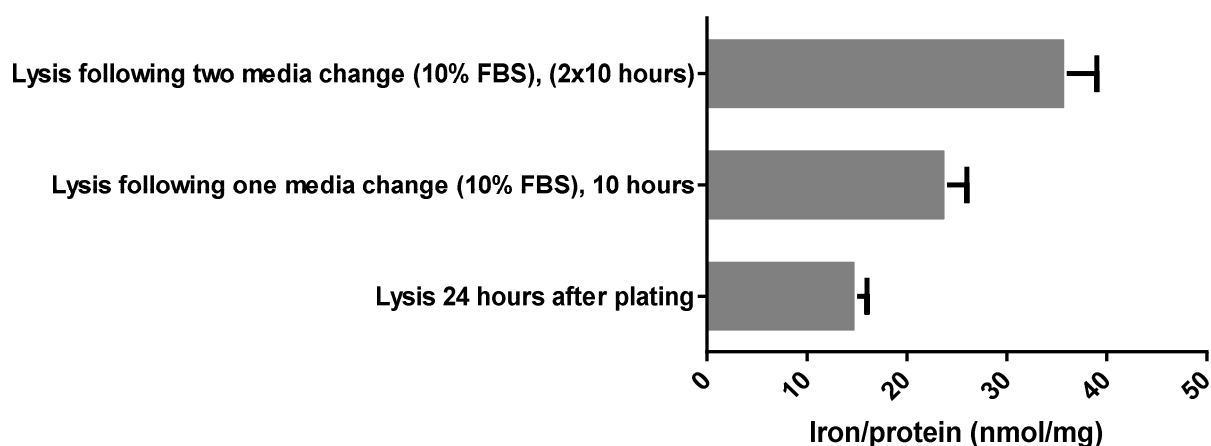
**Figure 11** Total iron concentration of RPMI media and RPMI media containing 10% FBS (A) and NTBI content (B). The ferrozine assay described in the methods Section 2.3.5 was used to determine media iron content.



### 3.6 Establishing the number of media changes for optimal iron loading

We investigated the number of changes of FBS containing media required to iron load the cells, and whether a shorter time period than the 24 hours used above could be adopted. HuH7 cells were exposed to RPMI 1640 media supplemented with 10% FBS changed once or two times, for 10-hour treatments. Cells were then washed as above (PBS solution followed by a wash with PBS/DFO 30 $\mu$ M ibe and a final PBS wash). Total iron content was determined via the ferozine assay as described in the methods **Section 2.3.5** and adjusted for protein, following overnight cell lysis with 200mM NaOH. The findings (**Figure 12**) indicate that two ten hour incubations with RPMI 1640 containing 10% FBS doubled the initial iron content. The intracellular iron content, in this case, was similar compared to two 24 hour treatments (**Figure 10**), indicating that a shorter time of iron loading can be adopted.

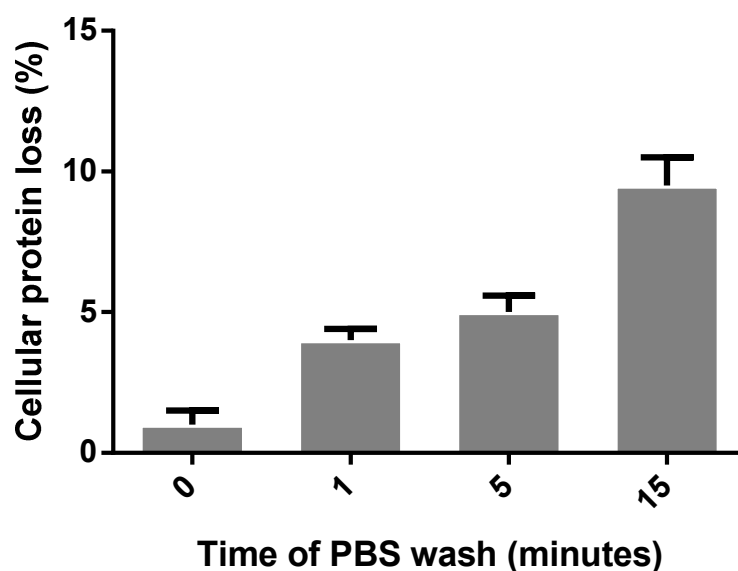
**Figure 12 HuH7 iron following 1 or 2 changes of 10% FBS media, each for 10 hours.** Cells were treated with RPMI media containing 10% FBS for zero, one or two 10- hour periods. Adherent cells were rinsed four times, including one wash containing DFO at 30 $\mu$ M ibe and 3 x PBS washes. The cells were then lysed with 200mM NaOH. Intracellular iron concentration was determined using the ferozine assay and normalised for total cellular protein in each well.



It should be taken into account when estimating iron release that in a culture system that various iron species may be adherent to the cell membrane or the plastic wear. It was thus important to establish an optimal washing regimen that would not lead to excessive

cell loss and would minimise this bias. Hepatocytes were pulsed as previously described with RPMI containing 10% FBS for two ten hour intervals. **Figure 13** shows the results of protein loss following PBS washing for 0, 1, 5 and 15 minutes. Washing with PBS for longer than 5 minutes compromised cellular protein by more than 5%, indicating cell loss due to increasing proportions of non-adherent cells during this washing process.

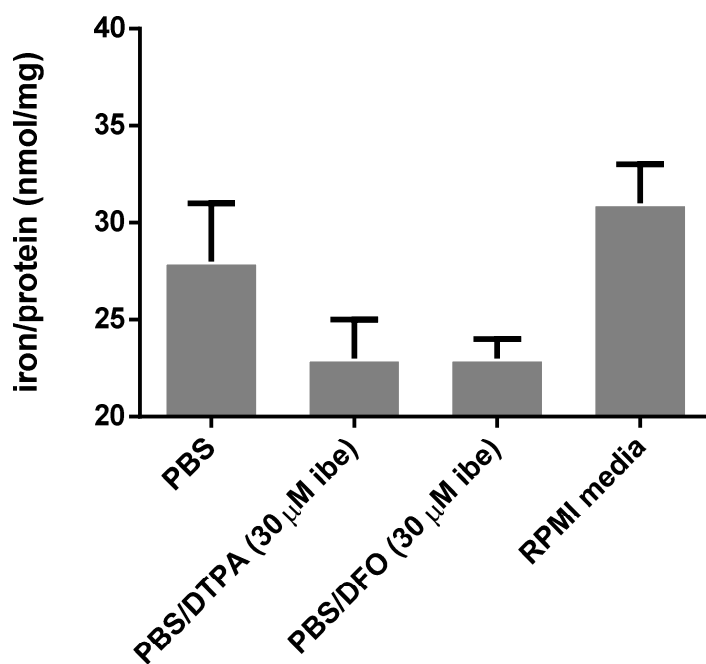
**Figure 13** Effect of washing HuH7 cells with PBS for different time intervals on cellular protein. 24 hours after plating, cells were washed with PBS for 0, 1, 5 and 15 minutes and cellular protein quantified as described in methods.



In order to establish the best approach to minimising non-specific extracellular iron adherence to cell membranes, iron-loaded HuH7 cells were then washed at room temperature prior as well as following an 8 hour DFO 30 $\mu$ M treatment using a variety of regimens. These included 4 x PBS, PBS/DTPA (+3 x PBS), PBS/DFO (+3 x PBS), and 4 x RPMI media (see **Figure 14**). Following iron loading with two 10-hour changes of RPMI media containing 10% FBS, the cellular iron content is 36 $\mu$ M $\pm$ 2.1. An expected decrease in intracellular iron following treatment with DFO 30 $\mu$ M for 8 hours was best noted when washing was carried out with PBS/DTPA and PBS/DFO. Each wash had a duration of about a minute. Washing with media and PBS were likely not effective at removing extracellular iron and reflect the iron-releasing effects of DFO.

Furthermore, further washing with media could potentially prove to be a further source for NTBI leading to further iron contamination (See **Section 5.2.7** for calculation of NTBI concentration in media). Based on the above data, the washing regime was finalised to 1 x PBS, 1 x PBS/DFO 30 $\mu$ M ibe, 2 x PBS prior to as well as post-chelator exposure. PBS/DTPA wash was not adopted, aiming to keep exposure to different chelators to a minimum.

**Figure 14 Effect of washing HuH7 cells with different agents before and after chelator exposure on iron detection.** 24 hours after plating, cells were iron loaded with two ten-hour changes of 10% FBS-containing RPMI media. Cells were then washed with PBS, PBS DTPA (30 $\mu$ M ibe), PBS/DFO (30 $\mu$ M ibe), and RPMI media before and after 8 hours of 10 $\mu$ M DFO treatment. The cells were then lysed with 200mM NaOH. Intracellular iron concentration was determined using the ferrozine assay and normalised for total cellular protein in each well.

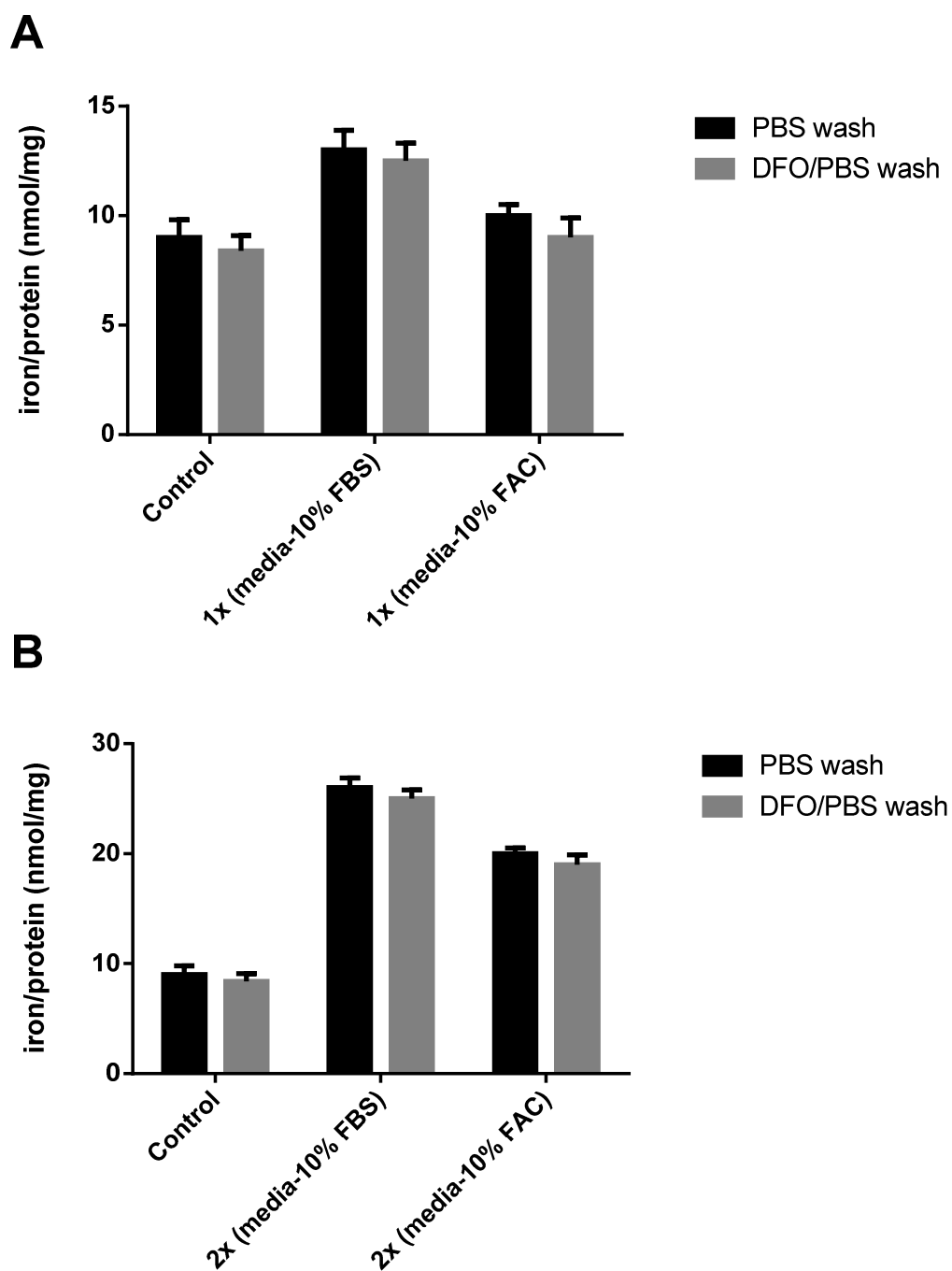


### 3.8 Regime for iron loading and washing of H9C2 cardiomyocyte cells

Despite the much-reduced expression of transferrin receptors on the cell membrane of cardiomyocytes in G0 phase compared to hepatocytes (Gatter et al, 1983), it is known that they play an important role in cardiac iron uptake as their absence leads to cardiomyopathy and heart failure in mice (Xu et al, 2015), most likely as a consequence of NTBI uptake when transferrin becomes saturated (Oudit et al, 2006). A model of iron

pre-loading of H9C2 cells was developed so as to load iron into cells at sufficient final concentrations for intracellular iron to reach levels where reliable cellular iron determination could be obtained using the ferrozine assay. When 10% FBS is added to DMEM, the total iron concentration in the media increases from an average of 1 $\mu$ M to 22 $\mu$ M. The NTBI content of DMEM containing 10% FBS was 0.33 $\mu$ M  $\pm$ 0.04 and was kindly measured by Dr M. Garbowski in our laboratory (the method is described in **Section 5.2.7**). When the total cellular iron accumulation was compared using FAC or 10% FBS, 10% FBS incubations resulted in more reproducible and higher final cellular iron concentrations than those achieved with FAC both with one and two 10 hour treatments (**Figure 15 A, B**). It was found that adequate iron loading was achieved after two changes of incubation medium (**Figure 15 B**). Furthermore, washing with 1 x PBS, 1 x PBS/DFO 30 $\mu$ M ibe, 2 x PBS proved superior at removing extracellular iron compared to PBS alone (**Figure 15 A, B**). In subsequent experiments reported, pre-loading of H9C2 was achieved using two 10 hour changes of media containing 10% FBS, also improving consistency between experiments across cell lines.

**Figure 15 Iron loading of H9C2 with FAC/10% FBS-DMEM media over one (A) or two (B) 10 hour periods.** Cells were treated with DMEM media containing 10% FBS for one or two 10- hour periods and were rinsed four times. Intracellular iron concentration was determined using the ferrozine assay and normalised for total cellular protein in each well.



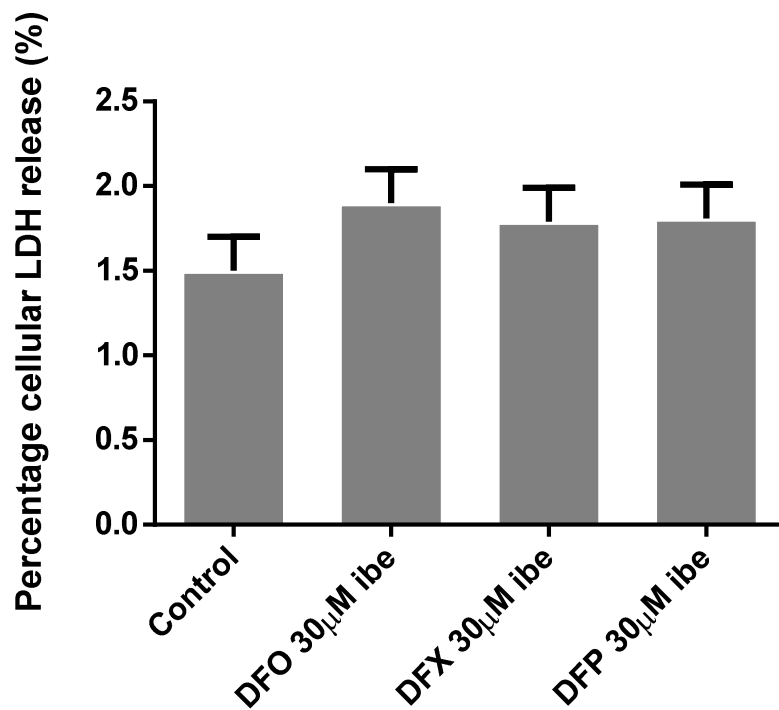


### **3.9 Cell damage in HuH7/H9C2 assessed by Trypan blue, AO/PI staining and LDH release**

The viability of hepatocytes has a critical influence on cellular iron release (Porter et al, 1988), as any compound leading to cell damage can cause iron release independently of the chelation mechanism. Prior to comparing chelator iron release effects we thus ensured that viability was consistently > 98%. Dye exclusion techniques provide a good estimate of cell viability and membrane integrity, and this was tested using both 0.4% Trypan blue solution as well as Acridine Orange (AO)/Propidium Iodide (PI) (**Section 2.3.3**) viability staining. The commercially available colorimetric LDH assay was also used (**Section 2.3.3**).

Following loading of HuH7/H9C2 as described above (**Section 3.8**) with two 10 hour treatment periods with RPMI/DMEM containing 10% FBS, cells were incubated with media without FBS, but with the maximum intended for use concentration of iron chelators. A sample of viability testing using Trypan blue solution in hepatocytes can be seen in **Figure 5**, and using the Acridine Orange (AO)/Propidium Iodide (PI) viability staining in **Figure 4**. A further sample of the LDH colorimetric viability assay using maximal concentration of iron chelators in cardiomyocytes is shown below (**Figure 16**). Viability was maintained >98% with all three licensed chelators in both cell types, and was re-assessed when using novel compounds or chelator combinations.

**Figure 16 LDH viability assay in H9C2 following 8 hours of chelator treatment.** Cells were iron loaded with two 10-hour changes of 10% FBS containing media and rinsed as in **Figure 15**. Cells were then treated for 8 hours with the maximum experimentally used concentration of DFO/DFX and DFP. % cellular LDH release was calculated using the LDH assay as described in the methods (**Section 2.3.3**)



### 3.10 Time course and concentration dependence of intracellular iron mobilisation with DFO, DFP and DFX monotherapy

The cellular iron content expressed as nmol/mg of cell protein has been investigated as a function of time in the presence of DFP, DFX or DFO in hepatocytes and cardiomyocytes. The cells were exposed to two 10 hour treatment periods with RPMI/DMEM containing 10% FBS to iron load the cells, and were then incubated with media without FBS, but with chelators at either 10 $\mu$ M ibe or 30 $\mu$ M ibe for different time periods. At 4h a significant decrease in cellular iron is seen with DFP and DFX as low as 10 $\mu$ M ibe but DFO shows minimal effect in HuH7 cells at this time (**Figure 17**). However by 8h DFO was as effective as DFP and DFX in hepatocytes (**Figure 18 A,B, Table 5**). Similar findings at 8h are seen in cardiomyocytes where DFO shows similar iron release as DFX and DFP (**Figure 19, Figure 20**). Iron mobilisation as a proportion of baseline cellular iron was found to be between 18.6 % and 25.9 % in cardiomyocytes and 39.0 % to 47.2 % in hepatocytes (**Table 5**). The results are consistent with a slower

access of DFO to intracellular iron pools than the other chelators (Hoyes & Porter, 1993; Porter et al, 2005; Vlachodimitropoulou Koumoutsea et al, 2015).

**Figure 17** HuH7 intracellular iron mobilisation with DFO, DFP and DFX monotherapy at increasing concentrations at 4 hours of treatment. Cells were loaded with iron using two 10-hour changes of 10% FBS containing media, rinsed before and after chelation treatment, exposed to chelators for 4 hours, and cellular iron/protein determined as in **Figure 15**.

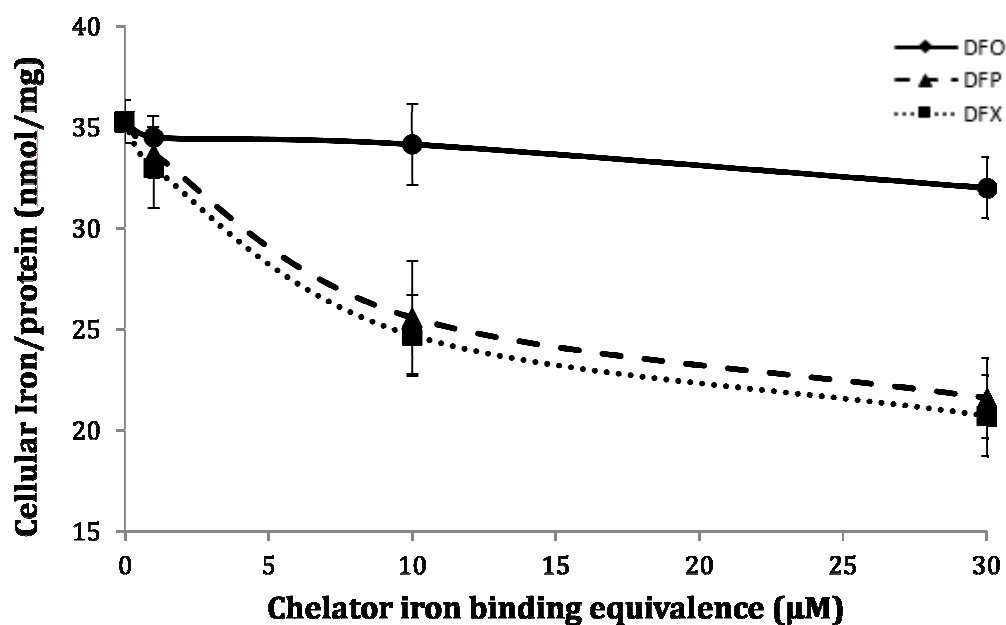


**Figure 18** HuH7 intracellular iron mobilisation time course with DFO, DFP and DFX monotherapy at (A) 10 $\mu$ M and (B) 30 $\mu$ M. Cells were loaded with iron using two 10-hour changes of FBS containing media, rinsed before and after chelation treatment, exposed to chelators for 0, 1, 4 and 8 hours, and cellular iron/protein determined as in **Figure 15**. Results shown are the mean  $\pm$  SEM of 4 replicates in one experiment.

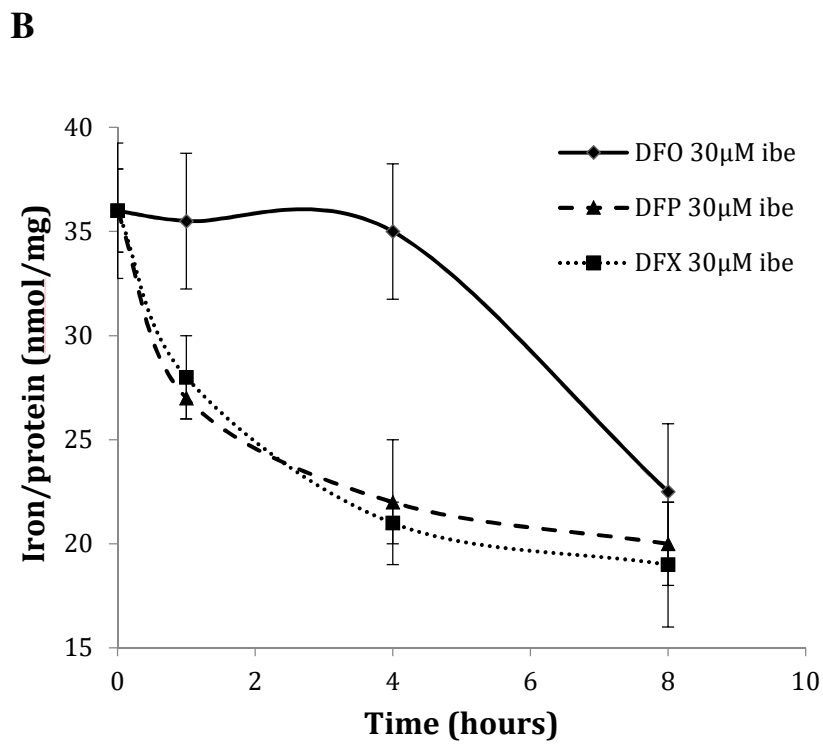
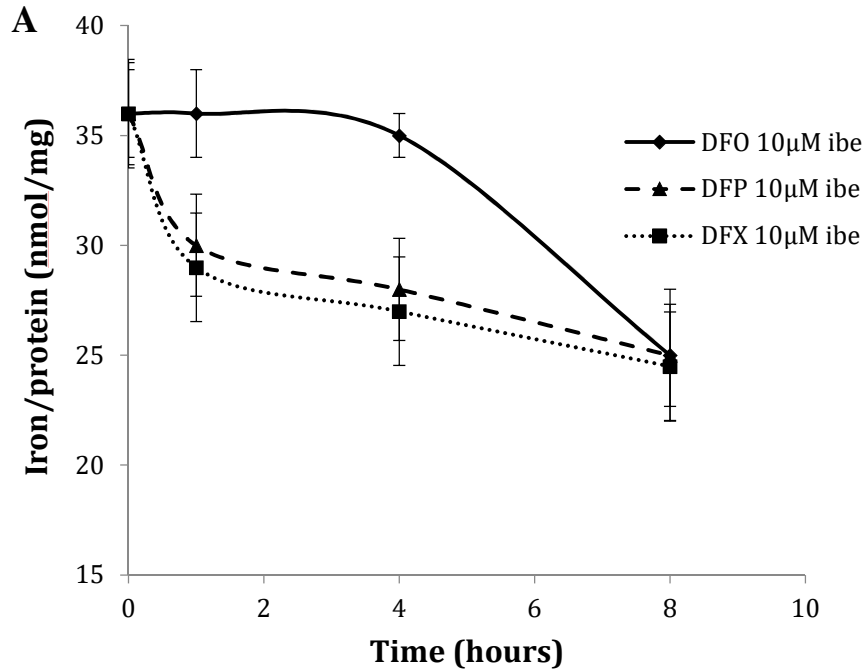


**Figure 19 H9C2 intracellular iron decrements time course with DFO, DFP and DFX monootherapy at 30 $\mu$ M ibe.** Cells were loaded with iron using two 10-hour changes of FBS containing media, rinsed before and after chelation treatment, exposed to chelators for 0, 1, 4 and 8 hours, and cellular iron/protein determined as in **Figure 15**. Results shown are the mean  $\pm$  SEM of 3 replicates in one experiment.

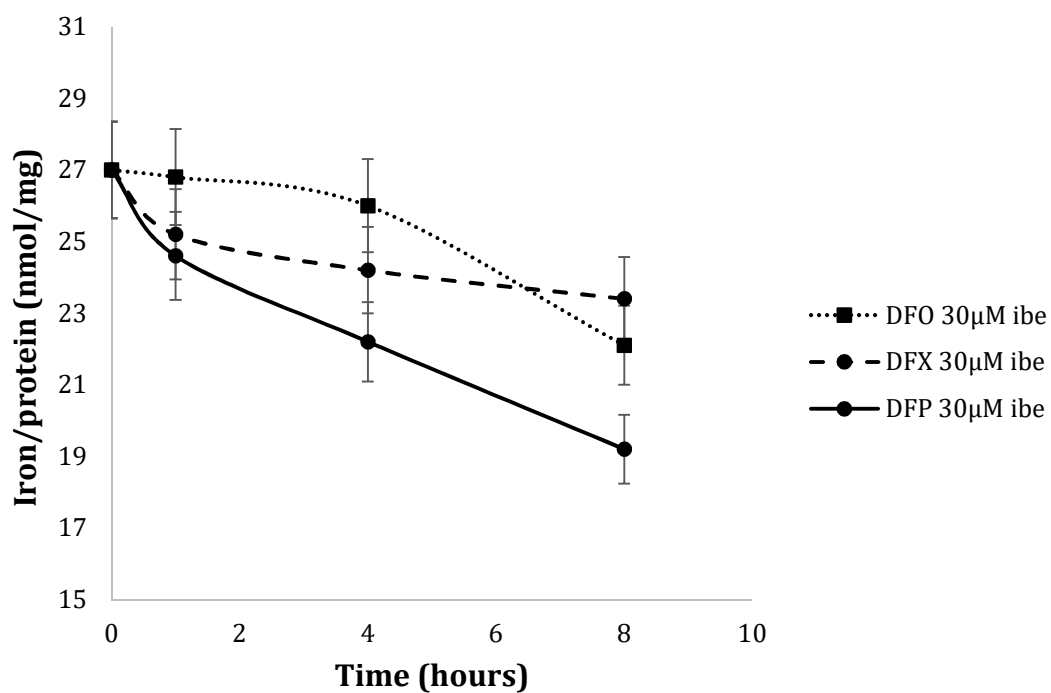


**Figure 20 H9C2 intracellular iron mobilisation at 8 hours with increasing concentrations of DFO, DFP, and DFX.** Cells were loaded with iron using two 10-hour changes of 10% FBS containing media, rinsed before and after chelation treatment with 3x PBS washes and one containing PBS/DFO 30 $\mu$ M ibe, exposed to chelators for 8 hours, and cellular iron/protein determined as in **Figure 15**. Results shown are the mean  $\pm$  SEM of 4 replicates in one experiment.

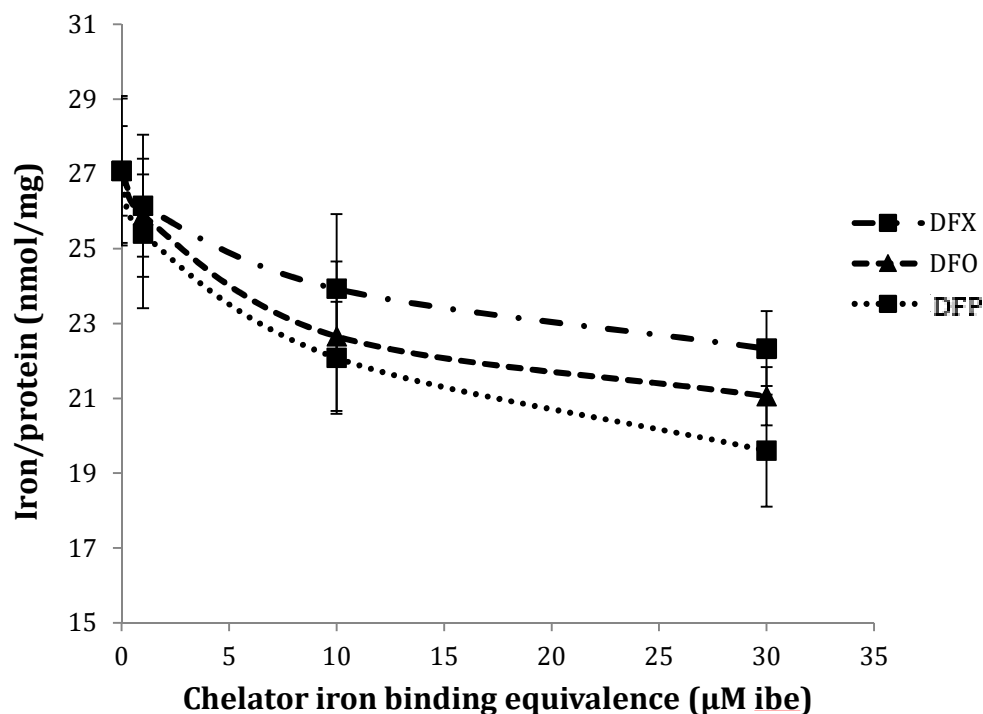


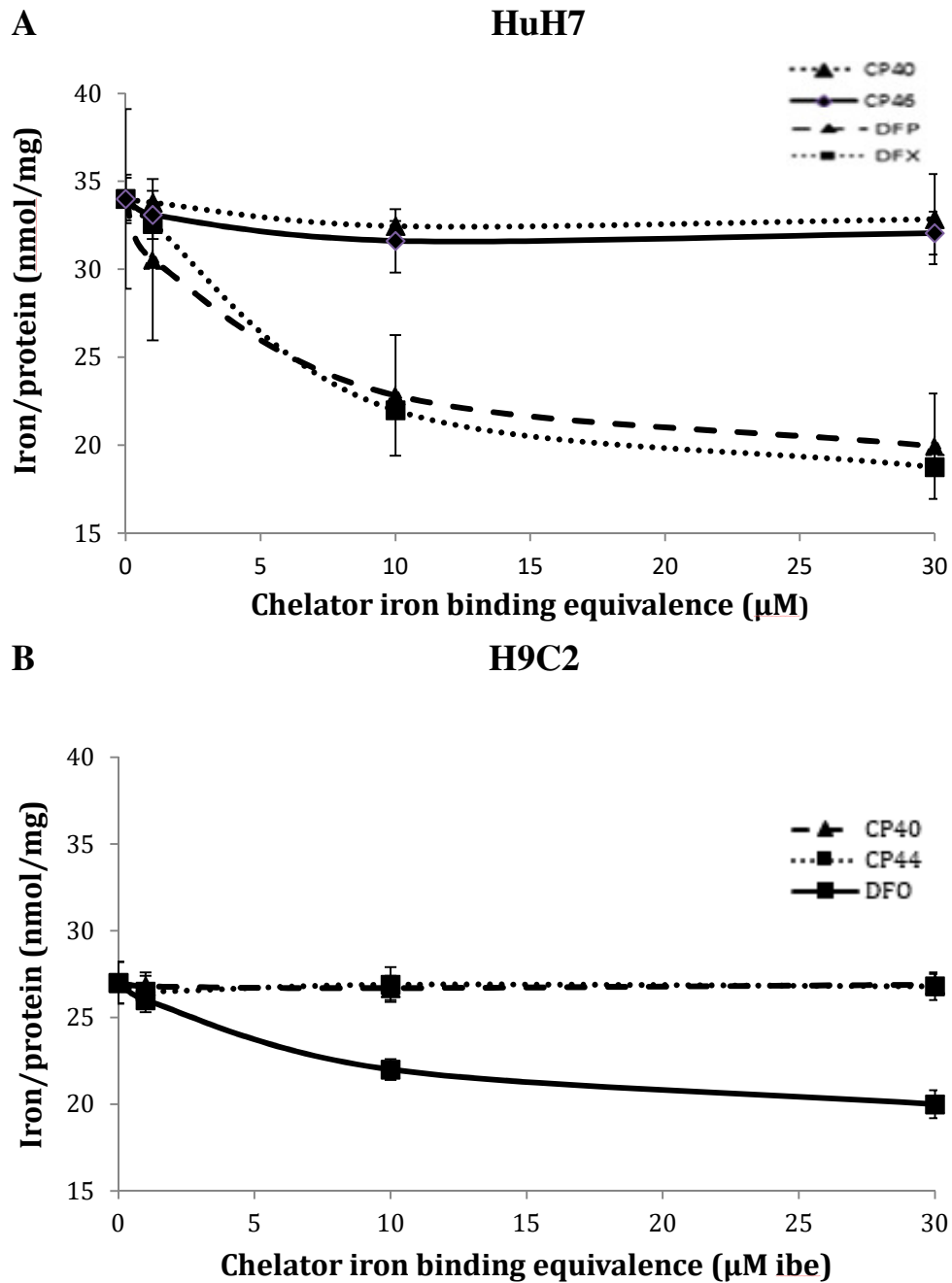
**Table 5 Percentage of intracellular iron removed by chelators in HuH7 and H9C2.** Cells were loaded with iron using two 10-hour changes of FBS containing media, rinsed before and after chelation treatment, exposed to chelators for 8 hours, and cellular iron/protein determined as in **Figure 15**. Results shown are the mean  $\pm$  SEM of 4 replicates in one experiment.

	% iron removed following 8 hours of chelator monotherapy at 30 $\mu$ M ibe	
	Hepatocytes (HUH7)	Cardiomyocytes (H9C2)
<b>DFO</b>	39.0 +/- 2.1	20.3 +/- 0.9
<b>DFP</b>	44.4 +/- 3.2	25.9 +/- 2.2
<b>DFX</b>	47.2 +/- 2.9	18.6 +/- 0.9

### 3.11 Iron release with low membrane-permeable hydrophilic iron chelators

Hydroxypyridinones with low cell penetration, such as CP40, CP44 or CP46 are known to not access intracellular pools directly due to their high hydrophilicity (pK) and thus cannot mobilise iron at observable rates in the cell culture system (**Table 6**). These were predicted to have negligible iron mobilising properties as shown previously with radio-labelled cells (Porter et al, 1988). However, we wished to confirm that the current cell system behaved as we predicted and that factors such as leaky cell membrane or extracellular iron adherence to the cell membrane did not contribute to iron mobilised from cells. In **Figure 21** it can be seen that unlike DFO, no recordable iron chelation effect was noted following 8 hours of treatment with CP40/CP44/CP46. This demonstrates that our washing techniques adequately remove any extracellular iron that could be available for chelation and be mistaken for an intracellular iron removal effect and further validates the integrity of the cell membrane in the cell culture model, because any cells with damaged or leaky cell membranes would allow intracellular iron to be chelated by the hydrophilic chelators. This also allows us to conclude that in our assay the chelation effects of DFO, DFX and DFP observed in **Figure 17, Figure 18, Figure 19, Figure 20**, are exclusively of the intracellular iron pools. This is consistent with observations using other models where these chelators had little or no effect (Porter et al, 1988).

**Figure 21 Decrements in cellular iron after an 8 hour treatment with 100 $\mu$ M CP40/CP46 in A. HuH7 B. H9C2.** Cells were loaded with iron using two media changes containing 10% FBS. Cells were loaded with iron using two 10-hour changes of FBS containing media, rinsed before and after chelation treatment, exposed to chelators for 8 hours, and cellular iron/protein determined as in Figure 15. Results shown are the mean  $\pm$  SEM of 3 replicates in one experiment





### **3.12 Effect of iron loading or iron chelation of cellular ferritin in HuH7 and H9C2 cells.**

#### **3.12.1 Effect of iron loading on cellular ferritin in HuH7 and H9C2 cells.**

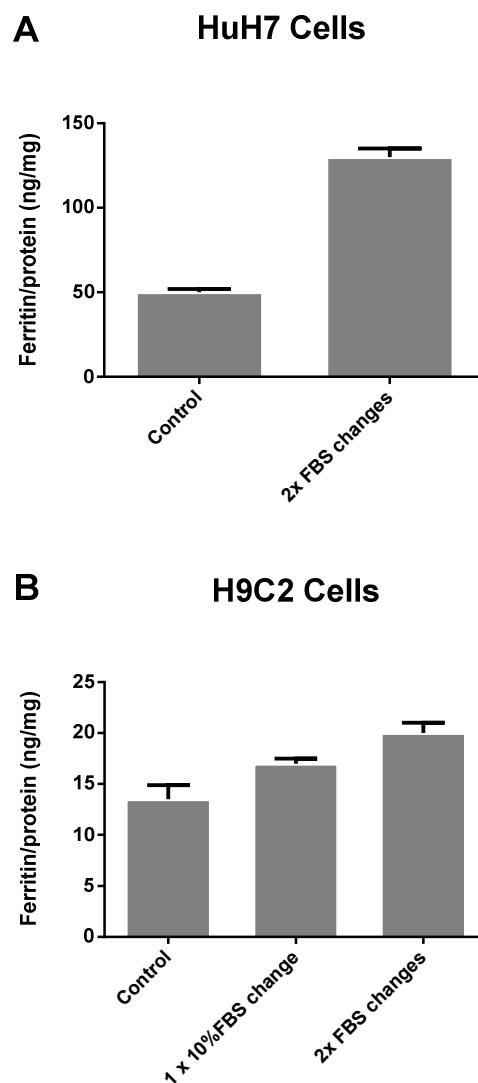
It is important to understand whether the total cellular iron mobilising effects of chelators above are associated with changes in storage iron and in particular cellular ferritin. Iron in ferritin is predicted to be less rapidly accessible to chelation than other iron pools such as labile intracellular iron, but ultimately storage iron must be decreased if iron overload is to be treated clinically. Using iron loading established previously in the chapter, changes in cell ferritin were measured by ELISA which was species specific for HuH7 (Human) and H9C2 (Rat) (see **Section 2.5**).

For the iron loading experiments, cells were cultured as described in previous sections and monolayers treated with one or two 10 hour applications of media containing 10% FBS. Two changes of FBS media increased the ferritin concentration in human HuH7 hepatocytes by 2.5-fold (250%) and 1.5-fold (150%) in rat H9C2 cardiomyocytes (**Figure 22**). It is also clear however that ferritin content adjusted for total cell protein is about 3 times higher at baseline in HuH7 cells than H9C2 cells as well as being more responsive to the effects of iron loading. This is consistent with the known iron storage function of hepatocytes in iron overload conditions which is not a feature of cardiomyocytes. It is also of interest that under similar iron loading conditions with two changes in FBS, the increments in total cellular iron noted in **Section 3.6** in HuH7 cells and H9C2 cells were 2.33 fold (230%) and 1.6 fold (160%) respectively (**Section 3.8**). Thus the relative increments in cell ferritin parallel the increments in total cell iron in each cell type, with the increments in both cell iron and ferritin being greater in HuH7 cells than H9C2 cells.

It appears therefore that in this model increments in cell ferritin respond proportionately to iron loading in both cell types. The lower proportion and absolute increase in cell iron and ferritin in H9C2 cells is consistent with their less specialised role in iron storage than hepatocytes. Ferritin degradation involves autophagic and non-autophagic pathways, and turnover of the ferritin protein is a constant process in the cell. Autophagy is upregulated in iron deficiency increasing iron availability by reducing storage

capacity (Mancias et al, 2014). In iron excess, non-autophagic pathways predominate, modulating factors such as the nuclear receptor coactivator 4 (NCOA4), leading to less ferritin breakdown and upregulating synthesis. Chelators such as DFO and DFX have been shown to modulate NCOA4 (Mancias et al, 2014).

**Figure 22 Effect of one and two 10 hours treatments of 10% FBS containing media on ferritin concentration in (A) HuH7 and (B) H9C2 cells.** Cells were loaded with iron 1 or 2 ten hour changes of 10% FBS containing media and were rinsed four times, including one wash containing DFO at 30 $\mu$ M and 3 PBS washes. Ferritin concentration was determined using commercially available ELISA kits as described in the methods, and adjusted for cellular protein

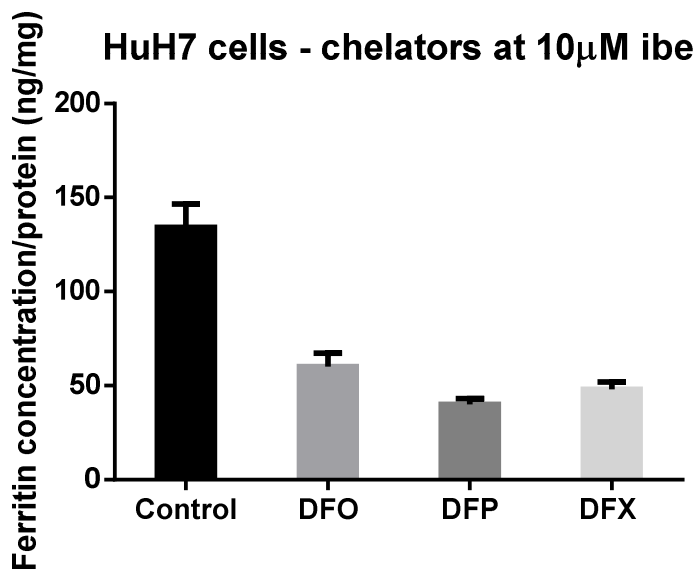


### **3.12.2 Effect of chelator treatment on cellular ferritin in HuH7 and H9C2 cells**

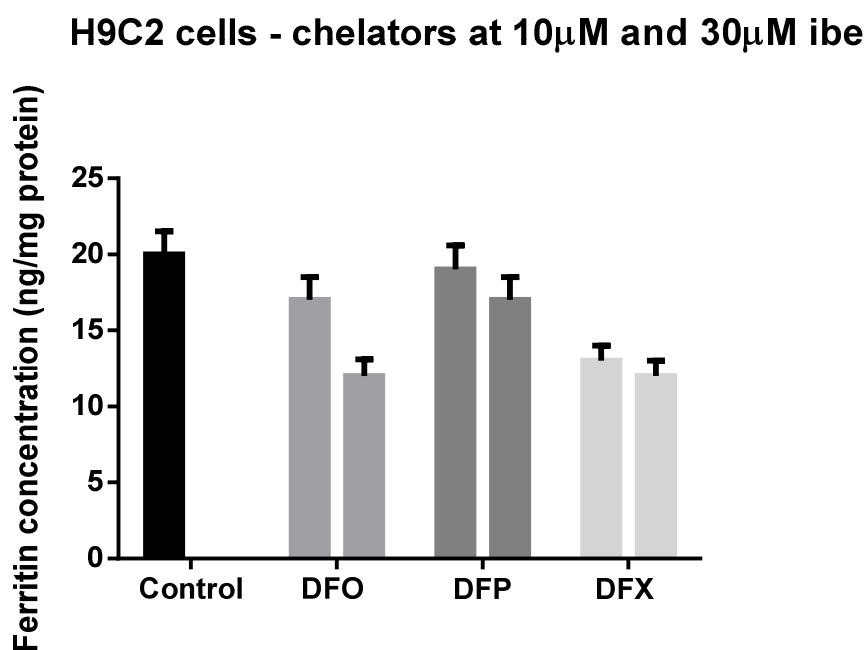
The response of cellular ferritin to iron chelators is studied in HuH7 (**Figure 23 A**) and H9C2 (**Figure 23 B**) cells. Decrements with commercially available chelators were clear in both cell types. In HuH7 hepatocytes, 10 $\mu$ M of commercially available chelators lead to ferritin decrements of almost 50% (**Figure 23 A**) with a 30% reduction in total cellular iron. However, in H9C2 cardiomyocytes ferritin decrements appeared both proportionately smaller as well as smaller in absolute terms: 30 $\mu$ M of chelators was required to reduce cellular ferritin by 10-35% (**Figure 23 B**) and total cellular iron by 18-26%. In both cell types, ferritin decrements are proportionately greater in HuH7 than H9C2 cells. Evidently, therefore, hepatocyte ferritin is more responsive, both to iron loading and iron unloading than in cardiomyocytes. This is consistent with the known high iron storage capacity of hepatocytes compared with cardiomyocytes.

**Figure 23 Ferritin in (A) HuH7 and (B) H9C2 cells treated with commercially available chelators for 8 hours.** Cells were loaded with iron with two 10-hour incubations with media containing 10% FBS. Adherent cells were rinsed four times, including one wash containing DFO at 30 $\mu$ M ibe and 3 PBS washes, and subsequently exposed to chelators at 10 $\mu$ M for 8 hours. Chelator supernatants were then removed, and the cells washed four times as above. Ferritin concentration was then determined using a commercially available ELISA kit as described in the methods, and adjusted for cellular protein.

**A**



**B**



### 3.13 Discussion

From the work in this chapter, it is clear that treating cells with media containing 10% FBS offers an optimal and physiologically and pathophysiologically relevant method for obtaining a high enough iron concentration in hepatocytes as well as cardiomyocytes to study iron release with chelators. This is likely attributed to a greater extent to NTBI uptake as opposed to transferrin iron uptake found in the fetal bovine serum. In RPMI 1640 for example, supplemented with 10% FBS, the total cellular iron was 25 $\mu$ M with a concentration of 0.29 $\mu$ M NTBI. Whilst Tf uptake is a known mechanism of iron acquisition, NTBI is very rapidly taken up form of iron (Brissot et al, 1985). Furthermore, the increase in total cellular iron noted in cardiomyocytes (**Figure 15**) and not just in hepatocytes supports this, as the presence of transferrin receptors in cardiomyocytes during G0 phase is limited (Gatter et al, 1983). In both cell types, total cellular iron increased to a greater extent when treating with media containing 10% FBS than when treating with FAC (**Figure 11, Figure 15**). Indeed the iron in FAC can be considered a species of NTBI; however, this is likely to be of a different form to that present in the FBS containing media. Regarding the washing of cells prior to and after chelator treatment, a 30 $\mu$ M DFO containing wash together with three PBS washes was chose, as this method proved to be the most effective at ensuring removal of extracellular iron, which can interfere with assessment of intracellular iron (**Figure 14**).

All licenced chelators were effective as monotherapy in this cell system, at concentrations that are clinically relevant. The studies on the effect of chelators on cellular iron mobilisation show some important contrasts amongst chelators which are in agreement with findings in other cell models. Very little iron removal occurs with DFO before 4 hours of treatment, findings consistent with previous studies reporting a much slower access to intracellular iron than for example with DFP and other hydroxypyridinones (Cooper et al, 1996; Hoyes & Porter, 1993). Factors such as the positive charge of DFO, its low lipid solubility, and larger size than DFP influence its uptake and distribution in cells (Porter et al, 1996; Porter et al, 2005). Furthermore, the Ferrioxamine complex (DFO-Fe) has a much slower egress rate from cells (Cooper et al, 1996; Hoyes & Porter, 1993). Similar to previous studies, the hydrophilic chelators CP40 and CP46, which are otherwise similar to DFP in terms of iron binding, induce no iron mobilisation as monotherapy treatment ((Dobbin et al, 1993; Porter et al, 1988).

This highlights the necessity of chelators to access the intracellular iron directly by crossing the cell membrane both in the free form as well as when bound to iron. The relative ranking order of chelators in terms of iron mobilisation showed only small differences at 8h, with DFP being the most effective in H9C2 cells but not in HuH7 cells. As will be discussed in a later chapter (**Chapter 5**) in more detail, HuH7 cells possess metabolic pathways lacking or relatively diminished in H9C2 cells. As DFP is metabolised by glucuronidation at an iron binding site, and enzymes responsible for its metabolism are much more widely available in the liver, its chelating and iron mobilising action is more likely to be reduced here.

In this chapter, I have shown that ferritin increases significantly in both hepatocytes and cardiomyocytes following treatment with 10% FBS containing media. The relative ferritin increments parallel the increase in total cellular iron in each cell type, with increments of both total iron and ferritin being greater in HuH7 cells. Following chelator treatment for 8 hours, ferritin decreases significantly in both cell lines. Decrements are significantly larger in hepatocytes compared to cardiomyocytes and reflect the larger iron storage capacity of this cell type. As ferritin concentration is a function of ferritin synthesis and opposing degradation, the decrease in its concentration, in this case, is likely to be due to an increase in degradation as a result of chelator-induced ferritin entry into lysosomes (De Domenico et al, 2009).

### **3.14 Conclusion**

In this chapter, a model for evaluating iron release from hepatocytes and cardiomyocytes by iron chelators, without the need for radioactive tracers has been presented. This model looks at total cellular iron and not only at radio-labelled iron pools. Ferritin changes parallel iron loading and unloading (measured biochemically), supporting the interpretation that intracellular iron is being recorded and that loading and unloading reflects predominantly changes in storage iron pools. Using two different cell types provides further insight into the effects of drug metabolism and cellular iron mobilisation. This model aids the selection of iron chelators designed to fulfill particular requirements as well as the development of novel chelators. The next chapter addresses the comparison between synergy and additivity of licensed chelator action on iron release, while closely studying chelator physiochemical properties.

## **Chapter 4 THE INFLUENCE OF COMBINATION OF COMMERCIALY AVAILABLE IRON CHELATORS ON RELEASE OF CELLULAR IRON.**

### **4.1 Introduction**

In clinical practice, iron chelators are increasingly used in combination, but the optimal conditions required for maximal cellular iron mobilisation and actual mechanisms of interaction between chelators are unclear. Examination of speciation plots for iron(III) binding of paired combinations of the commercially available iron chelators DFO, DFP, and DFX can suggest the conditions under which chelators can combine and act as ‘shuttle’ and ‘sink’ molecules. However, this approach does not consider their relative access and interaction with cellular iron pools. I addressed this issue using a sensitive ferrozine-based detection system for intracellular iron removal from the human hepatocyte (HuH-7) and cardiomyocyte (H9C2) cell lines (see previous chapter). I distinguished between antagonism, synergism or additivity of action of paired chelator combinations using mathematical isobologram analysis, over clinically relevant chelator concentrations.

### **4.2 Chelator speciation plots and their relevance to synergistic chelator combinations**

Speciation plots for combination pairs of chelators predict the binding of iron(III) by each chelator at equilibrium under defined conditions, namely 10 $\mu$ M iron(III) and at pH 7.4. These concentrations provide an indication of which chelator has the potential to act as a ‘shuttle’ or as a ‘sink’ for chelatable iron over the range of concentrations of each chelator pair shown. These proportions are calculated based on the known stability constants and chelation denticity (ratio of binding for chelator: iron) for each chelator. This analysis does not take into account the rate (kinetics) of this interaction or the restrictions to chelation imposed by the cellular compartmentalisation of iron in cells or elsewhere. The speciation plots were created by Prof. Hider from King’s College London University using HYSS (2016b), in which the concentration of iron and the concentration of the second chelator are varied. The stability constants used for the calculations are from published data shown in **Table 6** (Motekaitis & Martell, 1991).

The molar fraction of 10 $\mu$ M iron(III) bound to 10 $\mu$ M DFO in the presence of increasing concentrations of DFX is presented in **Figure 24 A**. It can be seen that at 10 $\mu$ M DFO, equilibrium favors the formation of iron complexes of DFO until those of DFX exceed about 15 $\mu$ M. This predicts that DFX will act as a shuttle for iron(III) onto DFO at concentrations below 20 $\mu$ M but at higher concentrations may compete with DFO as a sink for iron(III) binding. Thus at clinically achieved trough concentrations (about 20 $\mu$ M) (Galanello et al, 2006; Waldmeier et al, 2010), using standard daily dosing of DFX, about half of iron(III) is predicted to be bound to DFO and half to DFX in solution at neutral pH such as plasma. At peak clinical concentrations of DFX (about 60 $\mu$ M), equilibrium will favour the predominance of DFX iron complexes over those of DFO. Thus, trough concentrations of DFX will have the potential to donate iron(III) to DFO whereas this is less likely to happen at peak concentrations of DFX. It is important to realise that this prediction is for a cell-free system and does not predict the rates at which equilibrium is obtained. Hence the need to examine chelator interactions in a cell based system (see below).

The influences of varying the concentrations of DFP and DFX on the proportion of iron(III) bound to mixtures of each chelator is presented in **Figure 24 B, C**. **Figure 24 B** shows the molar fraction bound to 30 $\mu$ M DFP at increasing concentrations of DFX. This plot indicates that at equilibrium, and at for example 10 $\mu$ M DFX, about half of the iron(III) is bound to each chelator but when DFX exceeds 10 $\mu$ M the iron complex of DFX increasingly predominates. Thus at clinically relevant trough and peak concentrations of DFX about 40% and >98% respectively of iron(III) is predicted to be bound to DFX at equilibrium in a cell-free system. **Figure 24 C** shows the speciation of iron-chelate complexes at constant concentrations of 20 $\mu$ M DFX with increasing concentrations of DFP. These confirm the analysis in **Figure 24 B** but also allow examination of higher concentrations of DFP. Peak clinical concentrations of DFP of 100 $\mu$ M have been reported (Jirasomprasert et al, 2009; Limenta et al, 2011b) and under these concentrations and at trough concentrations of DFX about 60% of iron(III) is predicted to be bound to DFP in a cell-free system. This analysis suggests a ‘push–pull’ effect for iron-free binding over the range of clinically achieved concentrations of the two drugs, providing a circumstance under which both shuttle and sink effects may occur.

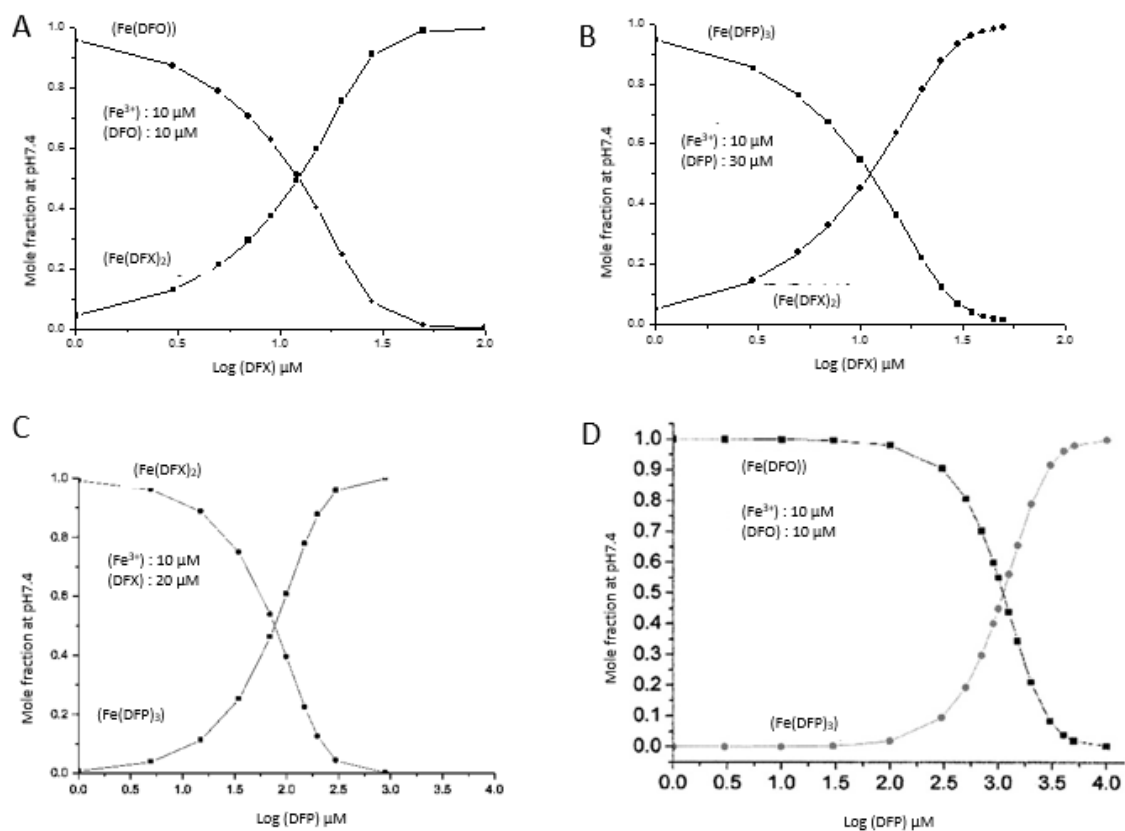


The speciation plot for the molar fraction of iron(III) bound to DFO at increasing concentrations of DFP is presented in **Figure 24 D** and has been previously published by our group (Evans et al, 2010). It can be seen that at clinically relevant concentrations of 10 $\mu$ M iron(III) and 10 $\mu$ M DFO, the iron binding will be predominantly to DFO until the concentration of DFP exceeds 1mM, a DFP concentration not achieved clinically. At clinically relevant peak DFP concentrations of 100 $\mu$ M, about 5% of iron(III) will be bound by DFP at equilibrium. This implies that a considerably higher concentration of DFP is required than that of DFX to compete with DFO for iron(III). Thus in a cell-free system, combinations of DFO with DFX or with DFP differ, because while the iron(III) complexes of DFO will predominate at all clinically achievable concentrations of DFP, iron(III) will bind preferentially to either DFX or DFO depending on whether DFX is at peak or trough levels. The effects of these considerations on iron release from cells are examined below.

**Table 6 Iron chelator characteristics.** (Vlachodimitropoulou Koumoutsea et al, 2015)

Chelator	Molecular Weight	Chelator : iron(III) binding ratio	Stability Constant $\log \beta_n$	pM	Charge of free ligand	Charge of iron complex	Lipid Solubility of free ligand ( $K_{part}$ )	Lipid Solubility of iron complex ( $K_{part}$ )
DFO	561*	1 : 1	33 <sup>(1)</sup>	26.6	1+	1+	0.01	0.03
DFP	139	3 : 1	37.2	20.5	0	0	0.17	0.08
DFX	373	2 : 1	26.5	22.5	1-	3-	6.3	NK
CP40	169	3 : 1	36.7	19.9	0	0	0.08	0.001
CP46	182	3 : 1	36.5	20.1	1+	3+	0.008	0.0007

**Figure 24** DFO, DFX, and DFP combination speciation plots at pH 7.4.  
 (Vlachodimitropoulou Koumoutsea et al, 2015)

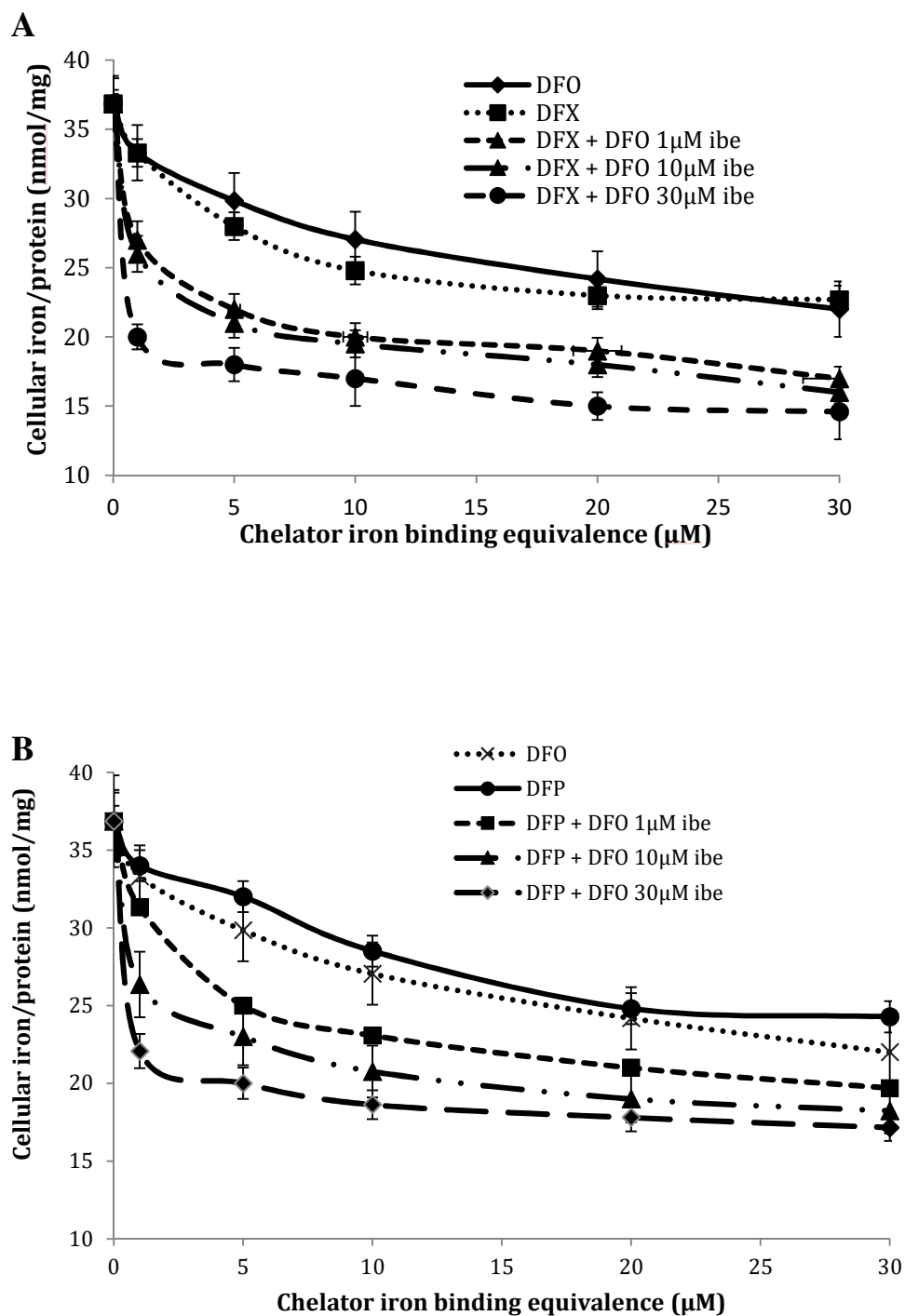


### 4.3 Comparison of cellular iron mobilisation with monotherapy and combinations in HuH7 cells

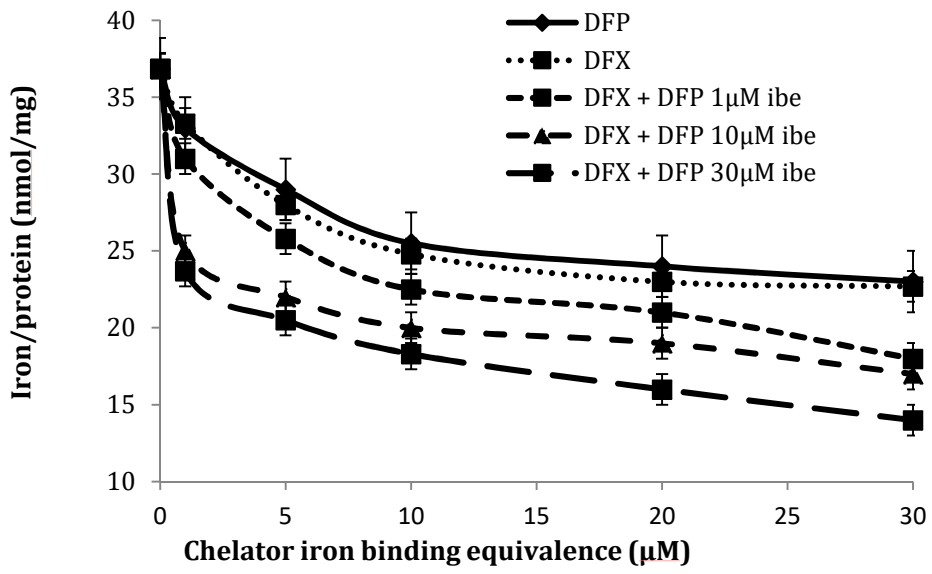
HuH7 cells were iron loaded as described in the methods section. Intracellular iron was determined using the ferrozine assay following 8 hours of treatment of chelator monotherapies and combinations. Intracellular iron is shown in **Figure 25 A, B, C, D** as a function of  $\log_{10}$  vs. iron/protein. In these experiments, the concentration of one of the two chelators is kept constant. Monotherapy treatment with DFO showed a concentration-dependent cellular iron removal at 8 hours (**A**) in contrast to findings at 4 hours (**Figure 17**). Iron mobilisation with DFX or DFP (**Figure 18, Figure 19, Figure 20, Figure 25**) also showed concentration dependence in monotherapy. When a second chelator was added, there was a significant additional decrease in intracellular iron, noted across the range of concentrations of the first chelator. This was the case for all combinations of the three commercially available chelators. Using non-linear regression, small increments of one chelator have statistically and biologically significant chelation effects. **Figure 25 D** shows that at 4 hours when DFO alone is not able to mobilise iron, a significant additional iron removal is seen when combined with DFP. Thus, DFO can act as an extracellular sink at short time intervals, when cell uptake and direct access to intracellular iron with DFO is limited.

**Figure 25 Treatment of HuH7 cells with a combination of (A) DFO and DFX, (B) DFO and DFP, and (C) DFP and DFX for 8 hours and (D) DFP and DFP for 4 hours.**

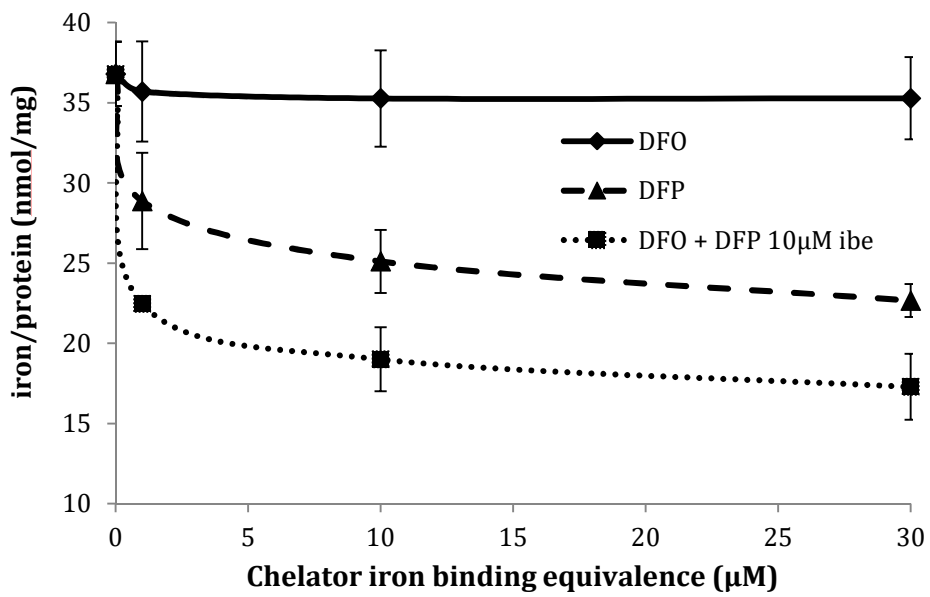
Cells were loaded with iron with two 10-hour treatments of 10% FBS containing media. Adherent cells were rinsed four times, including one wash containing DFO at 30 $\mu$ M ibe and 3 x PBS washes, and subsequently exposed to chelators for 8 hours. Chelator supernatants were then removed, and the cells washed four times as above before lysing with 200mM NaOH. Intracellular iron concentration was then determined using the ferrozine assay and normalised for total cellular protein in each well. Results shown are the mean  $\pm$  SEM of 4 replicates in one experiment.



C



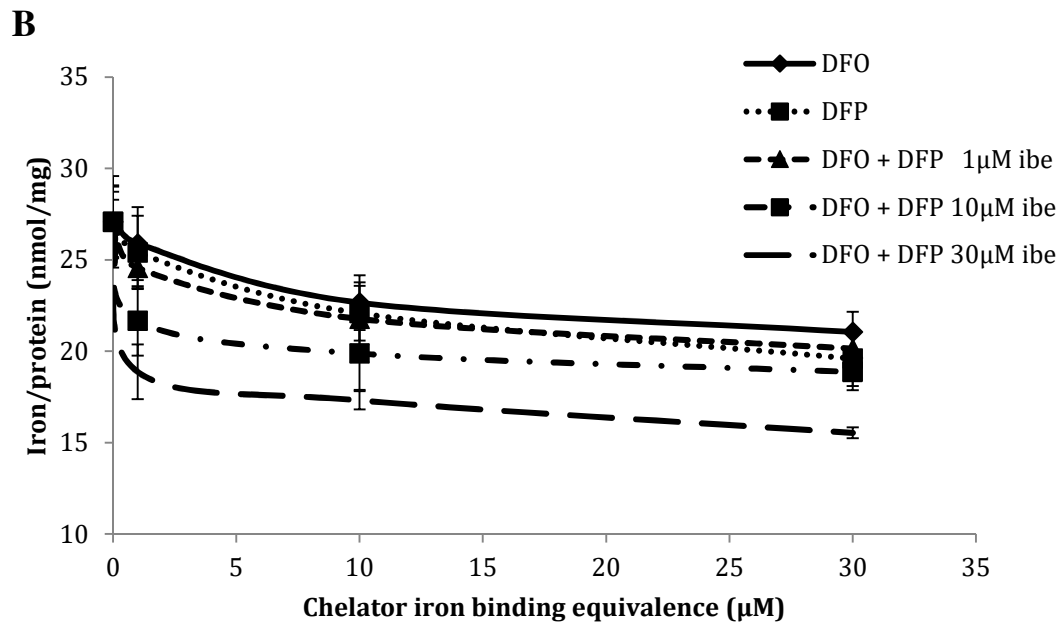
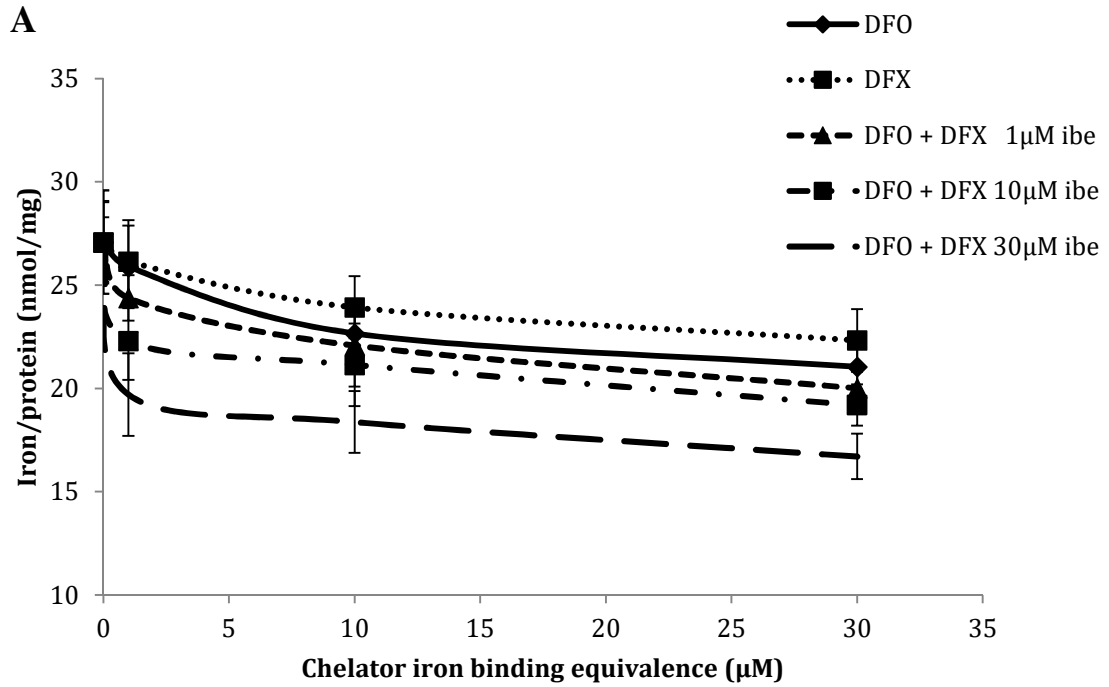
D

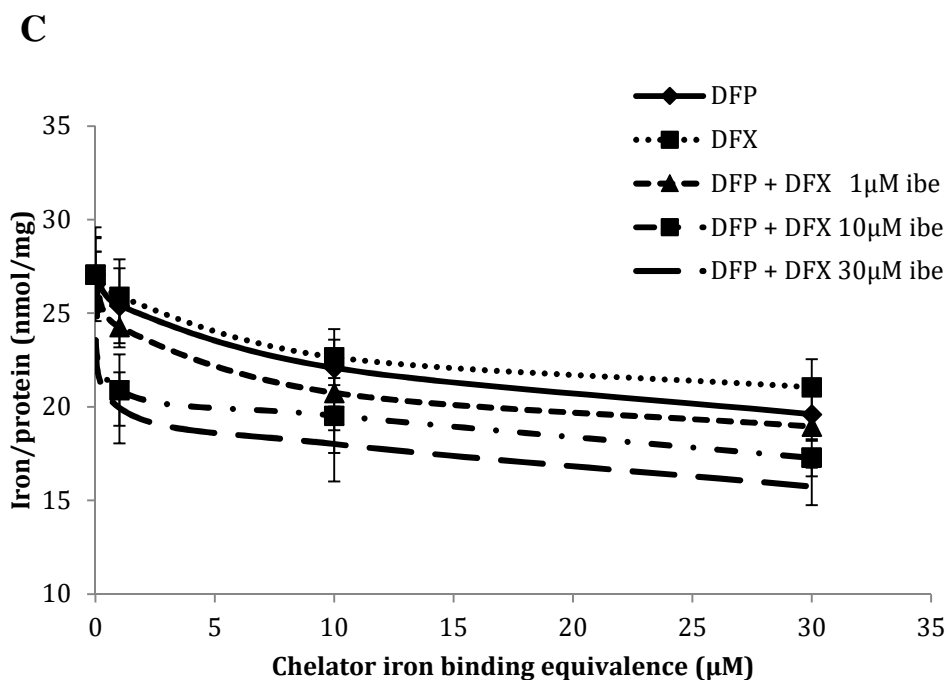


#### **4.4 Effect of chelator combinations on the intracellular iron pool after 8 hours in cardiomyocytes (H9C2)**

H9C2 cells were iron loaded with serial media changes as described in the methods section and exposed to chelator combinations of DFP, DFX, and DFO at different concentrations over a period of 8 hours. This response is plotted in **Figure 26 A, B, C** as a function of chelator iron binding equivalents (ibe) vs. iron/protein. In contrast to the findings at 4h, DFO mobilised cellular iron in a concentration dependent manner at 8h (**Figure 26 A, B**). Iron mobilization with DFX (**Figure 26 A, C**) or DFP (**Figure 26 B, C**) was greater than monotherapy at 4h and showed concentration dependence. There was a significant reduction in intracellular iron, with increasing concentrations of each one of the chelators while the other chelator was kept constant. Statistical analysis of the curves in **Figure 26 A, B, C** using non-linear regression analysis was performed, and it was demonstrated, similarly to hepatocytes, that small increments of one chelator in cardiomyocytes were sufficient to elicit statistically significant chelation effects for the combination as a whole, and were detected well above the sensitivity of our assay.

**Figure 26 Treatment of H9C2 cells with a combination of (A) DFO and DFX, (B) DFO and DFP and (C) DFP and DFX for 8 hours. Cells were loaded with iron, treated with chelators and intracellular iron/protein determined as in Figure 25.**





#### 4.5 Differentiation of synergy vs. additivity of chelator combinations using isobolograms

The issue of synergy vs. additivity was further addressed by the use of isobolograms. Two drugs with similar actions can sometimes produce an exaggerated or diminished effect when used in combination. As discussed in the methods section, the isobologram is a mathematical model used to distinguish between synergistic, additive or sub-additive response of drug combinations (Tallarida, 2006) where rectangular coordinates of dose combinations (a,b) that produce the same chosen effect level are shown; in this case 50% of the maximum response. **Figure 9** in the methods section shows the classic isobologram plot a straight line of additivity connecting the x and y-intercepts that represent the IC<sub>50</sub> values of each chelator monotherapy. This line is the reference for distinguishing additive from synergistic or sub-additive interactions.

**Figure 27** shows the isobolograms for combinations of the three commercially used chelators for a 50% chelation effect (defined as half maximal of the total chelatable cellular iron pool). The cells were iron loaded with serial media changes and treated with chelators for 8 hours. The axis intercepts represent the IC<sub>50</sub> for each chelator in this cell type when used in isolation (i.e., the potency; e.g., 12.5µM ibe for DFX). The



straight line of the isobologram connecting these intercept points is known as the line of potential additivity. This straight line represents the locus of all such dose pairs, which based on their known potencies, should give the same 50% chelation effect when used in combination. In all three cases, when the commercially available chelators were combined, a curved response was produced below the line of additivity, indicating a synergistic action.

**Figure 28** presents the isobolograms constructed for the combinations of the three commercially used chelators in H9C2 cells. These were constructed once again for the 50% chelation effect (half maximal of the chelatable iron pool) following 8 hours of chelator treatment; the axis intercepts again represent the  $IC_{50}$  for each chelator compound when used in isolation (i.e., the potency; e.g.,  $25\mu\text{M}$  ibe for DFX). Similarly to hepatocytes, in all three cases, combined use of chelators produce a curved response below the line of additivity, indicating synergism. The degree of synergism in both hepatocytes and cardiomyocytes is further examined below by looking at the synergy index  $\alpha$ , combination index, and dose reduction index.

**Figure 27** Commercial chelator combination isobolograms in HuH7 cells.

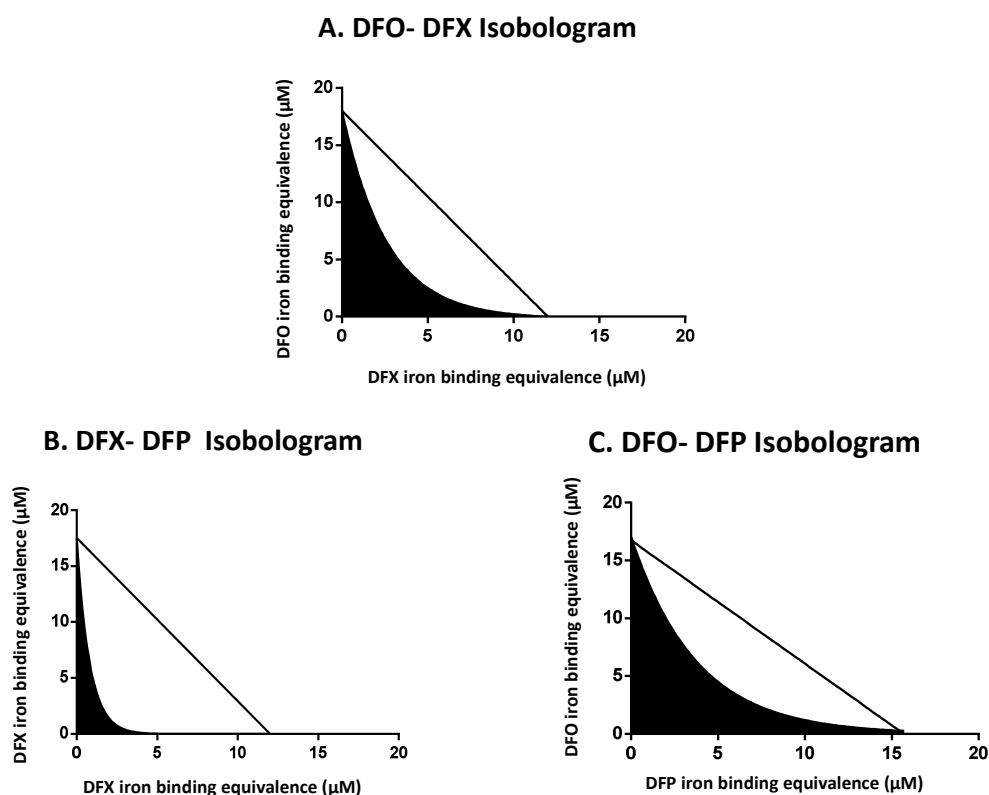
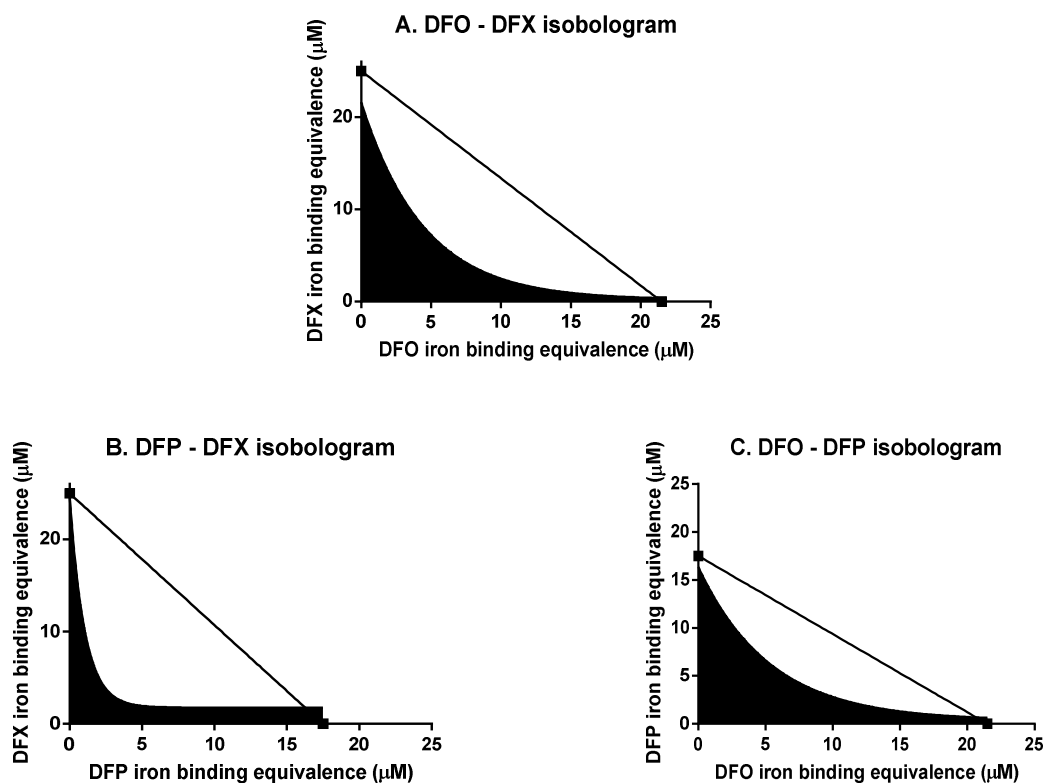


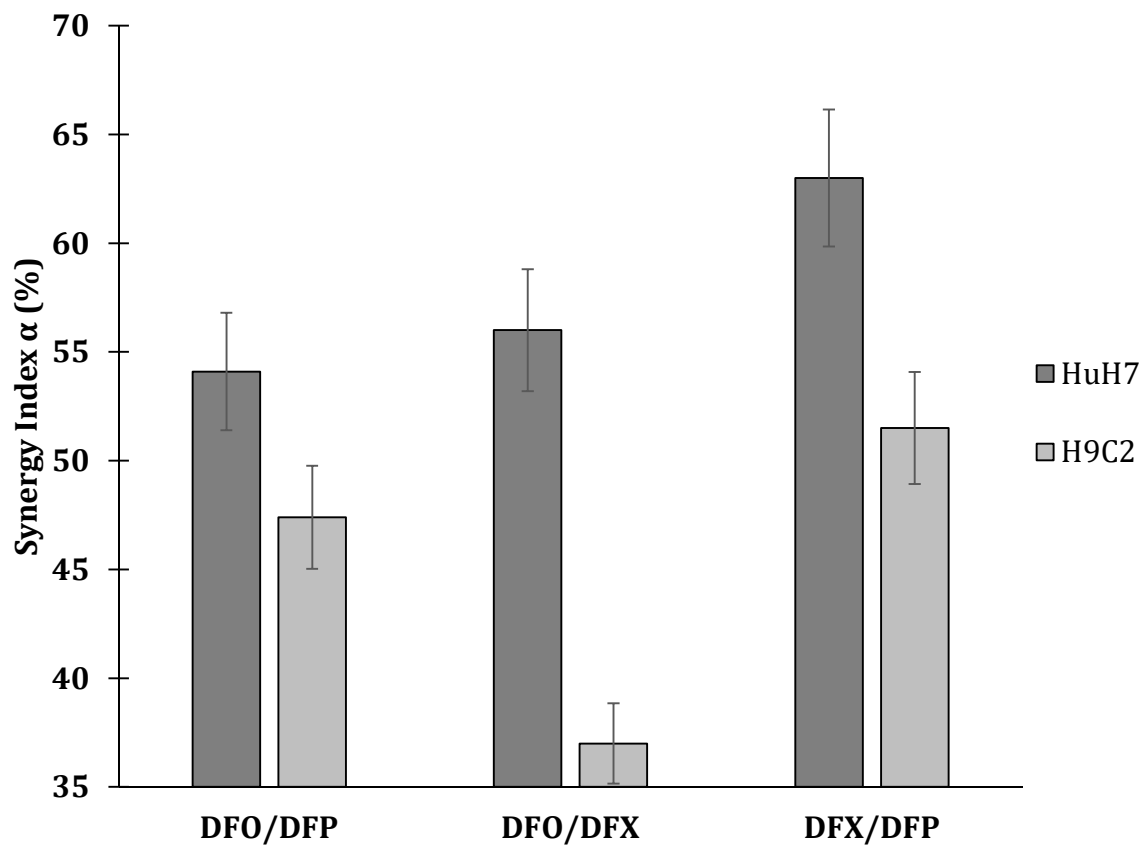
Figure 28 Commercial chelator combination isobolograms in H9C2 cells.



#### 4.6.1 Synergy Index $\alpha$

This index is an indication of how much the obtained effect exceeds that expected by additivity of the two compounds. To further quantify this effect we looked at the synergy index  $\alpha$ , which is equivalent to  $(1 - 1/R) \times 100$  where  $R =$  difference of area under the line and area under the curve of the isobologram. This index has been previously used to further examine synergy (Tallarida, 2001), and was derived using data generated from the program 'Prism 5' which was used to create the isobolograms. It was noted that when DFX and DFO are combined, 37% of the chelation effect is due to synergy in cardiomyocytes vs 56% in hepatocytes. In the DFP-DFO combination, 47.4 % of the total effect was due to synergy in hepatocytes vs 54.1% in cardiomyocytes. Most interestingly, in both hepatocytes and cardiomyocytes the synergistic effect is even greater, at 51.5% and 63% respectively in the case of the two oral chelators DFP and DFX when in combination (**Figure 29**).

**Figure 29 Synergy Index 'α' for the combination treatment of commercially available chelators in hepatocyte (HuH7) and cardiomyocyte (H9C2) cells.**



#### 4.6.2 Combination index

This data above showing synergistic action of chelators is supported by analysis of the combination effects in cardiomyocytes and hepatocytes using the software calcusyn 2.1 purchased from [www.biosoft.com](http://www.biosoft.com) (2016a). This software was used to provide a combination index 'CI' for each chelator set. A CI < 1 indicates synergy while a CI > 1 indicates antagonism. Thus, the lower the CI value <1, the greater the synergistic effect. The CIs for a 20% (ED<sub>20</sub>), 30% (ED<sub>30</sub>) and a 50% (ED<sub>50</sub>) effect are shown in **Table 7** for cardiomyocytes and **Table 8** for hepatocytes. The combination with the lowest CI and hence greatest synergy is DFP plus DFX, in both cell types. It was once again indicated that the most synergistic pair was the combination of the two oral chelators DFP and DFX with a CI of 0.26 in cardiomyocytes (**Table 7**) and 0.38 in hepatocytes (**Table 8**).

**Table 7** Combination Indices of chelators in cardiomyocytes (H9C2).

Chelator Combination	Combination Index (CI)			
	ED <sub>20</sub>	ED <sub>30</sub>	ED <sub>50</sub>	R (each combination fit)
DFO + DFX	0.87	0.62	0.29	0.94
DFO + DFP	0.98	0.71	0.31	0.88
DFX + DFP	0.79	0.58	0.26	0.91

**Table 8** Combination indices of chelators in hepatocytes (HuH7).

Chelator Combination	Combination Index (CI)			
	ED <sub>20</sub>	ED <sub>30</sub>	ED <sub>50</sub>	R (each combination fit)
DFO + DFX	0.18	0.27	0.50	0.91
DFO + DFP	0.16	0.29	0.47	0.89
DFX + DFP	0.086	0.15	0.38	0.93

#### 4.6.3 Dose reduction index

To demonstrate how combined chelation could impact on the dose of a chelator required to achieve a given effect, a dose reduction index was calculated. **Table 9** shows the dose reduction index (DRI) for all combinations of commercially used iron chelators in combination in hepatocytes. The dose reduction index (DRI) is a measure of the absolute dose reduction of one chelator required to produce a 50% of maximal chelation effect when the concentration of the other is increased. Looking at **Table 9**, for the combination of the two oral chelators, when DFP is added to DFX, the dose of DFX can be reduced by 3.8 fold when only 1 $\mu$ M ibe DFP is achieved in the blood. This suggests that the typical dose of 25mg/kg/day of DFX can be reduced to about 5mg/kg/day if DFP is added to the regime, achieving the concentration shown in column 3 of **Table 9**. We further proceeded to analyse the DFP/DFX combination of the two oral chelators in cardiomyocytes (**Table 10**). In this cell line, we also calculated what reduction in oral dose of DFX this combination corresponds to, given that a once daily dosing regimen of 20mg/kg of DFX leads to trough plasma levels of 20 $\mu$ M (Galanello et al, 2006). It can be seen that the presence of 10 $\mu$ M DFP can reduce the dose of DFX required to produce a 50% of the maximal chelation effect by 23.9 mg/kg. This concentration of DFP is clinically achievable (Bellanti et al, 2014; Limenta et al, 2011a).

These three indexes provide novel evidence to suggest that combined use of DFP and DFX will be particularly effective at mobilising cellular iron.

**Table 9 Chelator DRI in hepatocytes (HuH7).**

<b>Chelator Combination</b>	<b>Dose Reduction Index (DRI) of sink chelator</b>	<b>Shuttle Chelator Concentration (<math>\mu\text{M}</math> ibe) when in combination</b>	<b>Sink Chelator Concentration (<math>\mu\text{M}</math> ibe) when in combination</b>
<b>DFO + DFX</b>	3.2 (DFO)	DFX 1.8 $\mu\text{M}$ ibe	DFO 5 $\mu\text{M}$ ibe
<b>DFO + DFP</b>	2.8 (DFO)	DFP 1.2 $\mu\text{M}$ ibe	DFO 5.7 $\mu\text{M}$ ibe
<b>DFX + DFP</b>	3.8 (DFX)	DFP 0.9 $\mu\text{M}$ ibe	DFX 3.4 $\mu\text{M}$ ibe

**Table 10 Chelator Dose reduction in cardiomyocytes (H9C2).**

<b>DFP Concentration (<math>\mu\text{M}</math> ibe)</b>	<b>DFX Chelator Concentration (<math>\mu\text{M}</math> ibe) required when in combination with DFP to achieve a 50% effect</b>	<b>DRI: (DFX dose in combination required to achieve 50% effect)</b>	<b>Reduction of oral dose of DFX required to achieve 50% chelation effect in the presence of DFP</b>
<b>0</b>	25.1	-	
<b>1</b>	10.0	15.1	15.1 mg/kg
<b>5</b>	7.2	17.9	17.9 mg/kg
<b>10</b>	1.2	23.9	23.9 mg/kg

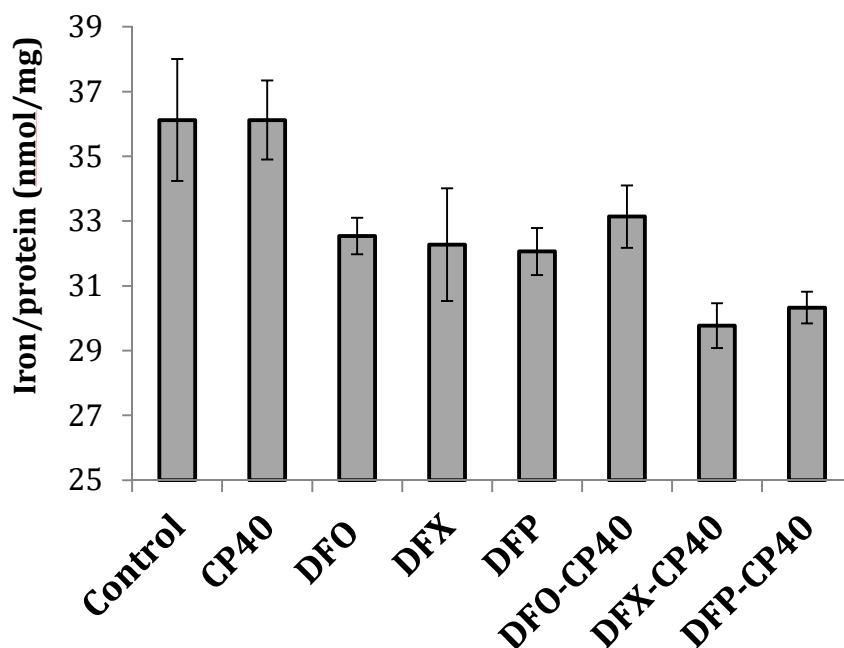
#### **4.7 Insights into synergistic mechanisms using the hydroxypyridinones CP40 and CP44 as probes**

The highly hydrophilic bidentate hydroxypyridine chelators CP40 and CP44 were used to probe the mechanism of combined chelator actions because they have previously been shown to mobilise no iron from hepatocytes or in iron-overloaded mice. This is due to low lipid solubility relative to the closely related DFP and consequent inability

to penetrate the cell membrane (Porter et al, 1988) (Porter et al, 1990). In **Figure 21** and **Figure 32**, it can be seen that, in contrast to DFO, CP40 and CP44 do not enhance cellular iron removal confirming previous observations in primary hepatocytes (Porter et al, 1990). When CP40 100 $\mu$ M was combined with DFO, no increased iron release was observed over that seen with DFO alone over an 8 hour period in hepatocytes (**Figure 30**). When CP40 was combined with DFP or DFX however, a small increase in cellular iron removal was seen. This provides mechanistic insight into how combinations of chelators interact. Firstly it supports the concept that the role of DFO in combined therapy is to act as an acceptor or 'sink' for iron(III). DFO can only act as an acceptor for iron(III) due to its hexadentate structure and high pM (**Table 6, Figure 24**). Thus because CP40 has very little access to intracellular iron when used alone, it cannot act as an intracellular iron shuttle onto DFO. As the properties of CP40 are similar to DFP, these observations also support the notion that the additional iron mobilisation seen when DFP when combined with DFO is to shuttle intracellular iron onto DFO, which is predominantly extracellular, particularly at short time intervals.

The small increase in cellular iron mobilisation observed when CP40 100 $\mu$ M was combined with DFX 10 $\mu$ M in **Figure 30** is likely due to an increase in the 'sink' total concentration in the extracellular medium. Consideration of the speciation plots in **Figure 24** for DFP (which has similar iron binding properties to CP40) suggests that at 30 $\mu$ M DFP and 30 $\mu$ M DFX, about 20% of the iron(III) will bind to DFP (and hence CP40) rather than DFX. The small increase in iron mobilisation when CP40 is added to DFP is also consistent with an increase in the concentration of 'sink' chelation in the extracellular medium. Here DFP can act as an intracellular shuttle onto CP40, which remains exclusively extracellular.

**Figure 30 Treatment of chelator monotherapy combined with CP40 for 8 hours in HuH7 cells.** Cells were loaded with iron, treated with chelators and intracellular iron/protein determined as in Figure 25.



#### 4.8 Discussion

The findings with chelator monotherapies provide a framework for understanding the potential effects for combined pairs of chelators. This system was developed using the cardiomyocyte cell line H9C2 and the hepatocyte cell line HuH7. It was developed because heart failure secondary to iron overload is the main cause of death in transfusional iron overload. This system has the advantage of measuring total cellular iron and does not require radioactive tracers. In this system, all three clinically available chelators are effective as monotherapy at cellular iron mobilisation and at clinically relevant concentrations. However, very little cellular iron removal is seen with DFO before 4 hours which is consistent with previous reports of slower access of DFO to intracellular iron than that with DFP or other hydroxypyridinones (Cooper et al, 1996; Hoyes & Porter, 1993) and is attributable to the relatively low lipid solubility of DFO and its larger size than DFP (Porter et al, 2005). Furthermore, the iron complex of DFO is slow to egress from cells (Cooper et al, 1996; Hoyes & Porter, 1993) due to its positive charge and low lipid solubility (Cooper et al, 1996) (Porter et al, 2005). As with previous studies, the highly hydrophilic chelators CP40 and CP46, which in other aspects of chelation are similar in their iron binding properties to DFP, were found to have no effect on iron release when used as monotherapies (Porter et al, 1988) (Dobbin



et al, 1993). This has been previously attributed to the necessity of chelators to access intracellular iron directly by transiting the cell membrane in the iron free and complexed states.

For paired combinations of these three clinically licensed chelators, our findings are consistent with synergistic interaction and to our knowledge, this is the first attempt made to formally distinguish between synergy and additivity of these commercially used chelators. Concentrations of chelators for these experiments were chosen to be clinically relevant. The conclusion of synergy is based firstly on the shapes of isobologram plots using established general methods for comparing drug interactions (Tallarida, 2006). Secondly, this is supported by the results with the combination index, which is a computed method designed to assess interactions of pairs of drugs. This is further supported by the synergy index findings derived from the isobolograms. In all three analyses, the combination of DFX and DFP shows greater effects than the other combinations at 8 hours, although all combinations appear synergistic.

Our overall results suggest that the mechanisms and consequences of chelator interaction depend on their relative concentrations, their iron binding affinities, and their ability to access intracellular iron pools directly. At least one of the paired chelators needs to enter cells and exit bound to iron for synergistic interaction to take place. Synergism with DFO and DFP combinations is consistent with rapid access of DFP to intracellular iron and the subsequent donation of iron(III) to DFO, the latter providing a predominantly extracellular sink for chelated iron. This mechanism has been previously demonstrated for NTBI in a cell-free system where DFP can access some NTBI species more rapidly than DFO (Evans et al, 2010). DFP by virtue of its low molecular weight, neutral charge and lack of extreme hydrophilicity can enter cells and exit rapidly as the iron complex. Additionally, it has more rapid access to iron pools within (Hoyes & Porter, 1993) (Porter et al, 2005) (Glickstein et al, 2005) (Glickstein et al, 2006) and outside cells (Evans et al, 2010) more rapidly than DFO and is thus an ideal molecule for shuttling purposes. Inspection of speciation plots shows that at equilibrium, iron is ultimately destined to binding to DFO when paired with DFP.

The synergism seen when DFX is combined with DFO depends firstly on the faster access to cellular iron of DFX than DFO and then the faster rate of egress of iron-chelate

complex of DFX. For synergism to occur, this chelated cellular iron then needs to be donated to DFO extracellularly. The higher lipid solubility and lower molecular weight of DFX compared with DFO is predicted to allow faster access to intracellular iron, and this is shown in the monotherapy experiments. The subsequent donation of chelated iron to DFO is consistent with the speciation plots and iron binding stoichiometry of these two chelators. Because of the hexadentate iron binding of DFO, the iron complexes are highly stable at neutral pH and will not act as an iron 'shuttle'. However because of its tridentate 2:1 stoichiometry, the iron complex of DFX is less thermodynamically stable than iron complexes of DFO and hence some or all of the iron chelated by DFX (depending on relative concentrations) is donated onto DFO. This provides the circumstances for shuttling and hence for synergy with this combination. Nevertheless, the speciation plots suggest that within cells DFX may compete to some extent for iron binding with DFO when DFX concentrations exceed about 10 $\mu$ M. However, the main mechanism for the observed synergy is for DFO to provide an extracellular sink as an acceptor for some or all of the iron rapidly chelated by DFX, subsequently freeing DFX to shuttle back for further rounds of intracellular chelation.

Closely looking at the synergistic action of DFP when combined with DFX it is evident that this is more complex because both chelators can rapidly access intracellular iron and both are able to act as either shuttles or sinks for iron(III), depending on their relative concentrations. These orally absorbed chelators can access cellular iron including the cytosol and organelles much faster than the larger parenterally administered DFO (Hoyes & Porter, 1993) (Porter et al, 2005) (Glickstein et al, 2005) (Glickstein et al, 2006), due to their lower molecular weight they have relatively higher lipid solubility. The monotherapy data in **Figure 20** shows that DFX monotherapy gains sufficient intracellular access to mobilise iron with similar kinetics to DFP. Consideration of speciation plots shows that the propensity of the two chelators to act as 'shuttles' or 'sinks' for iron(III) will depend on their relative concentrations over clinically relevant ranges: depending on when the last dose of each chelator was taken, relative concentrations can favor either chelator as a shuttle or sink. For example, over typical ranges seen clinically with DFX (20-60 $\mu$ M), speciation plots suggest that DFX will act more as a 'sink' for iron chelated by DFP except at peak concentrations of DFP (100 $\mu$ M) where this molecule will compete with DFX. The speciation analysis does

not take into account the rates of access or the compartmentalisation of chelatable cellular iron and it is possible that DFP can access additional intracellular iron pools that are only slowly available to DFX (Glickstein et al, 2005) (Glickstein et al, 2006).

The findings with CP40 and CP46 provide further mechanistic insight into the actions of DFP in combination therapy, particularly when DFP is combined with DFX. Even though CP40 and CP46 cannot gain access to intracellular iron when used alone (**Figure 21**), when combined with a chelator that can shuttle iron (DFX or DFP but not DFO) they increase cellular iron release (**Figure 32**). Speciation plots suggest for CP40 or CP46 (not shown, generated by R. Hider, King's College London, and are very similar to DFP) that CP40 and CP46 have the potential to contribute to an extracellular sink for iron chelated by DFX. For example at 20 $\mu$ M DFX, even at low concentrations of a hydroxypyridinone (10 $\mu$ M) about 10% of iron(III) will be bound to a hydroxypyridinone (**Figure 24 C**). Furthermore, at 100 $\mu$ M about 40% of the iron will bind to the hydroxypyridinone thereby effectively increasing the 'sink' chelator concentration. This extracellular 'sink' effect for CP40 and CP46 will also be seen with DFP when combined with DFX. Hence when combined with DFX, DFP has the potential to act both as a shuttle and a sink for iron(III). This may contribute to this combination being particularly effective.

In summary, these findings suggest that all three licenced chelators can act synergistically when their use is combined but that the combination of DFP with DFX is likely to be the most potent one. The presence of the clinically achievable 10 $\mu$ M DFP can lead to a reduction of 23.9 mg/kg of the daily dose of DFX to produce a 50% chelation effect. Further well-controlled clinical trials that also examine the safety of this combination are warranted.

#### **4.9 Conclusion**

In hepatocytes as well as cardiomyocytes, all combinations showed synergistic cellular iron mobilisation at 8h with clinically achievable concentrations of the 'sink' chelator and 'shuttle' chelator. The greatest synergism was achieved by combining DFP with DFX, where about 60 and 65% of the mobilised iron was attributable to synergistic interaction in hepatocytes and cardiomyocytes respectively. Our findings predict that

the dose of DFX had to be reduced by 3.8 fold to produce a half-maximal effect when the concentration of DFP is just 1 $\mu$ M in hepatocytes. Furthermore, It was noted that the presence of 5 $\mu$ M DFP could reduce the dose of DFX required to produce a 50% of the maximal chelation effect by 17.9 mg/kg in cardiomyocytes. This concentration of DFP is clinically achievable (Limenta et al, 2011a). Mechanisms for the synergy have been suggested by considering the iron-chelate speciation plots in conjunction with the size, charge and lipid solubilities for each chelator molecule. Hydroxypyridinones CP40 and CP 44 with low lipid solubilities but otherwise similar properties to DFP were used to validate the assay. These studies confirm that for synergistic cellular iron mobilisation, one chelator must have the physicochemical properties to enter cells, chelate intracellular iron and subsequently donate iron to a second 'sink' chelator.

## **Chapter 5 ELTROMBOPAG IS A POWERFUL CHELATOR OF IRON(III), THAT MOBILISES INTRACELLULAR STORAGE IRON ALONE OR IN COMBINATION WITH CLINICALLY ESTABLISHED CHELATORS.**

### **5.1 Introduction**

Eltrombopag (ELT) is a thrombopoietin receptor agonist that also decreases labile intracellular iron. Here we examine the previously undescribed iron(III) co-ordinating and cellular iron mobilising properties of ELT. Clinically achievable concentrations (1 $\mu$ M) mobilised total iron from hepatocyte and cardiomyocyte cell lines, while also rapidly decreasing intracellular reactive oxygen species (ROS). Decrements in cellular ferritin accounted for the majority of cellular iron removal, particularly in hepatocytes. Intracellular iron mobilisation by ELT was inhibited by free extracellular iron present in culture media but not by fresh human serum. Iron mobilisation from cardiomyocytes exceeded that obtained with deferiprone, desferrioxamine or deferasirox. When combined with these, ELT increased iron mobilisation 4-6 fold above single agent chelators. A synergistic mechanism, with ELT acting as a 'shuttle', is suggested by enhanced iron mobilisation when combined with the otherwise ineffective hydroxypyridinone, CP40. The high iron(III) binding constant (Log  $\beta_2$  34.9) and speciation plots, demonstrate equilibrium binding consistent with synergistic iron shuttling when combined with these chelators. ELT is a powerful intracellular iron chelator that decreases storage iron and also enhances iron removal with other chelators. In clinical use, donation of chelated iron by ELT to these chelators offers established routes for elimination of chelated iron.

ELT is an orally bioavailable small molecule approved for the treatment of Idiopathic Thrombocytopenia (ITP) and thrombocytopenia associated with chronic hepatitis C. An under appreciated property of ELT is its binding to metal ions and in particular to iron(III). It was reported that oral consumption of ELT with calcium, aluminium, and magnesium containing foods reduced absorption of these metals (Williams et al, 2009; Wire et al, 2012) and it was suggested that this could be due to chelation of metal ions (Williams et al, 2009). ELT has also been found to decrease labile iron within leukemia cells (Roth et al, 2012) and in principle, iron chelating properties of ELT may be relevant to antiproliferative and apoptotic effects in acute myeloid leukemia (AML)

(Roth et al, 2012) (Kalota et al, 2015) as well as its role in the treatment of hepatocellular carcinoma (Kurokawa et al, 2015). Some of the beneficial effects on haematopoiesis in MDS (Svensson et al, 2014) and aplastic anaemia (Leitch & Vickars, 2009) could also derive from an iron chelating mechanism. Preliminary findings by our group suggested that ELT at low concentrations could effectively mobilise iron from cardiomyocytes in culture (Vlachodimitropoulou et al, 2014) (Vlachodimitropoulou et al, 2015). However remarkably little is known about the iron binding properties of ELT. These unknowns include the iron coordination mechanism, iron(III) binding constant, effects on iron-induced ROS, effects on storage iron, relative interaction with different cell types and mechanisms of interaction with other iron chelators.

Here we have characterised the iron chelating properties of ELT in a cell-free system as well as in cell lines of two key cell types that are targets for iron overload, namely hepatocytes and cardiomyocytes. We have examined the ability of ELT to chelate cellular storage iron and to diminish intracellular ROS. An ability of ELT to act in concert with other chelators, by donating chelated iron to such molecules, could be important for the efficient elimination of chelated iron in urine or faeces because it is not known whether and how iron complexes of ELT would be eliminated. We have therefore also examined the ability and conditions under which ELT can shuttle iron out of cells and onto clinically licensed iron chelators.

## **5.2 Material and methods**

### **5.2.1 The cellular model**

The rat cardiomyocyte cell line (H9C2) and a human hepatocarcinoma (HuH7) cell line were chosen for investigation. Cardiomyocytes are a target tissue for transfusional iron overload and provide a particular therapeutic challenge. Hepatocytes represent the cell type with the largest quantity of iron deposition. HuH7 or H9C2 cells were plated at 200 000 cells/well in RPMI 1640 medium/DMEM supplemented with 10% fetal bovine serum (FBS). Cells were treated with DMEM media containing 10% FBS for one or two 10- hour periods and rinsed four times, including one wash containing DFO at 30 $\mu$ M and 3 x PBS washes. The cells were then lysed with

200mM NaOH. Intracellular iron concentration was determined using the ferrozine assay and adjusted for cellular protein (Vlachodimitropoulou Koumoutsea et al, 2015).

### **5.2.2 Cell damage and viability**

Viability has a critical influence on cellular iron release (Porter et al, 1988), and >98% was achieved in all reported experiments. Viability was assessed using the 'LDH Cytotoxicity Detection Kit' by Takara Bio Inc, which gives a quantitative comparison of early cell damage between 'treatment' and 'control.' This is a colorimetric assay and measures LDH activity leaked by damaged cells into the supernatant (W.J. Reeves Jr., 1966).

### **5.2.3 Determination of Intracellular Iron – The Ferrozine Assay**

Cells were lysed overnight with 200µl of 200 mmol/l NaOH. The ferrozine assay (on 190µl aliquots) was performed as previously described (Riemer et al, 2004) as well as in the methods **Section 2.3.5**. In brief, An aliquot (120 µl) of iron detection reagent was added for 30 min. Absorbance was recorded at 562 nm and lysate iron content calculated by standard curve interpolation against atomic absorption iron standards. Intracellular iron was normalized against protein content.

### **5.2.4 Protein assay**

The Coomassie (Bradford) protocol was used to determine cellular protein. Briefly, 250µl of Bradford reagent were added to 5µl of cell lysate and absorbance recorded at 595 nm.

### **5.2.5 Detection of Reactive Oxygen Species using a fluorimetric method**

To monitor the intracellular ROS, we utilised a cell-permeable oxidation-sensitive fluorescent probe 5,6-carboxy-2',7'- dichlorofluoresceindiacetate (DCFH-DA); (Molecular Probes, Leiden, Netherlands) as previously described. Nonfluorescent DCFH-DA, hydrolyzed to DCFH inside of cells, yields highly fluorescent DCF in the presence of intracellular hydrogen peroxide (H<sub>2</sub>O<sub>2</sub>). Therefore, the dichlorofluorescein (DCF) fluorescence intensity is proportional to the amount of intracellular ROS. Cells in Corning 24-well plates (Sigma-Aldrich, MA, USA) were preincubated with 4 mM

H2DCF-DA for 30 minutes at 37°C as per protocol. Chelators were then added, and the plate placed into the plate reader where fluorescence was recorded over a period of 1 hour (excitation at 504 nm, emission at 526 nm). The time between the addition of chelators and commencing ROS level recording was between 3 and 5 minutes at room temperature. The rate of ROS production was compared between chelator treated and untreated cells.

### **5.2.6 Ferritin Quantification**

Human and rat tissue ferritin were measured using commercially available enzyme-linked immunosorbent assay (ELISA) kits (Cusabio, Wuhan, China and My BioSource, San Diego, USA respectively) according to the instructions provided by the manufacturer for recording ferritin of cell lysates.

### **5.2.7 NTBI iron content of FBS, albumin, and human plasma**

This was kindly performed by Dr. Garbowski at UCL Cancer Institute, London. Free iron in media or sera (NTBI) was quantified as previously described (Gosriwatana et al, 1999) with slight modifications. On the day of the assay centrifugal filters (Modified PES 30K, 500µL low protein binding, VWR) were washed with 10mM NTA (200µL) and spun at 20300g for 10 min at 4°C followed by 2 rinses with 400µL HPLC-grade water and vacuum-aspirated till dry. Then 180µL serum was added in duplicate followed by admixture of 20µL 800mM NTA (containing 20µM Fe). This was left to equilibrate at 22°C for exactly 30 minutes; thereafter the ultrafilters were centrifuged at 20300g for 60 min at 4°C. Clear ultrafiltrate (about 180µL) was recovered and where it was yellow (indicating a breach of the membrane), the samples were redone. 100µL of unknowns or standards, 100µL 5mM chelexed MOPS pH 7.4, 50µL of 1:1 v/v mixture of 60mM BPT (bathophenanthroline disulphonic acid, or 4,7-Diphenyl-1, 10-phenanthroline disulphonic acid, disodium salt, Sigma) and 120mM TGA (thioglycolic acid or mercaptoacetic acid, Sigma) were added to an acid-washed 96-well plate and incubated on a shaker for 30 minutes to allow BPT-Fe complex formation and colour development. Standards were prepared using AA ferric chloride in 80mM NTA (0-20µM f.c.). Absorbance was recorded at 537 nm. The 800mM NTA solution used to treat the samples and prepare the standards is treated with up to 20µM iron to normalise



the background iron that contaminates reagents. This means that the zero standard gives a positive signal since it contains the added background iron as an NTA–complex. Free iron content of media in  $\mu\text{M}$  were as follows: water  $0.12\pm 0.1$ , RPMI  $0.57\pm 0.4$ , 10% FBS RPMI  $0.29\pm 0.05$  (100%FBS  $3.31\pm 0.23$ , 40g/L rHSA (recombinant human serum albumin) in RPMI (without FBS)  $0.79\pm 0.15$ , normal human serum NTBI  $-1.7\pm 0.12$ .

### **5.2.8 Spectrophotometric method for pKa and iron stability constant measurements**

This was kindly performed by Dr. Chen under the direction of Prof. Hider at King's College London. An automated titration system (Ma et al, 2014) was utilised under the conditions of constant temperature at  $25^\circ\text{C}$  and constant ionic strength at 0.1 M, using 0.1 M KCl, 0.1 M HCl, and 0.1 M KOH. The pH electrodes were calibrated using the GLEE program (2016c; Gans & O'Sullivan, 2000). The titration data were analysed using the pHab program (2016c). Species plots were calculated using the HYSS program (Alderighi et al, 2016). Analytical grade reagent materials were used in the preparation of all solutions.

## 5.3 Results

### 5.3.1 ELT effectively decreases hepatocellular and myocardial iron

The cellular iron release was studied in iron loaded HuH7 hepatocyte-like cells and the H9C2 cardiomyocyte cell line using a protocol developed by our group to investigate other chelators (Vlachodimitropoulou Koumoutsea et al, 2015). The ELT concentrations used for these experiments were informed by reported C<sub>max</sub> plasma values achieved clinically after oral ELT administration at 30, 50, and 75 mg/day in patients with ITP which correspond to blood plasma levels of 8, 18, and 28  $\mu\text{M}$ , respectively (Gibiansky et al, 2011). As we wished to identify the lowest concentration of ELT that would induce effective cellular iron mobilisation, initial experiments were performed at 10 $\mu\text{M}$  ELT, but subsequently, concentrations as low as 1 $\mu\text{M}$  were used. Based on the predominant 2:1 binding of ELT to iron(III) identified in this paper (**Figure 31, Table 11**), ELT has an iron binding equivalent (ibe) of 0.5 $\mu\text{M}$ . Following 8 hours of ELT treatment in HuH7 cells, intracellular iron was decreased in a dose-dependent manner with significant iron removal at clinically achievable concentrations (**Figure 32 A**). In cardiomyocytes, a time course showed iron mobilisation by as little as 1 $\mu\text{M}$  ELT at only 1 hour (**Figure 32 B**). In **Table 12**, iron mobilisation by 1 $\mu\text{M}$  ELT at 8 h as a single agent is compared with DFP, DFO and DFX as single agents at 1 $\mu\text{M}$  ibe. It can be seen that in cardiomyocytes ELT mobilises more iron at 8h than DFO, DFX or DFP. In hepatocytes at this low ELT concentration, iron mobilisation is less effective. For reasons discussed in detail below, this is likely to reflect greater metabolism of ELT within HuH7 cell than H9C2 cells, and the effects of metabolism are more likely to be identified at low chelator concentrations. However, this relatively low iron mobilisation in hepatocytes can be overcome at higher concentrations (**Figure 32 A**).

As the viability of cells may influence cellular iron release, independently of the chelation mechanism, experiments were therefore only performed where baseline viability exceeded > 98%, as assessed by the LDH assay described in the methods section. Hepatocytes showed no signs of toxicity following 8 hours of ELT treatment at concentrations up to 30 $\mu\text{M}$  (**Figure 33 A**). By contrast cardiomyocyte viability after 8 hours of exposure to 30 $\mu\text{M}$  ELT was compromised to 93% (**Figure 33 B**). Thus some

effects of iron release in cardiomyocytes noted in **Figure 32 B** by ELT at concentrations of  $30\mu\text{M}$  could be partially attributed to toxicity of the drug on the monolayer. Such effects are not seen at  $1\mu\text{M}$  and  $10\mu\text{M}$ .

**Figure 31 Structure of Eltrombopag and its iron complex.** The free ligand possesses 2 tautomers (**1** and **2**). Three iron(III) complexes have been identified **3** ( $\text{FeELT}$ ), **4** ( $\text{FeELT}_2\text{H}$ ) and **5** ( $\text{FeELT}_2$ )

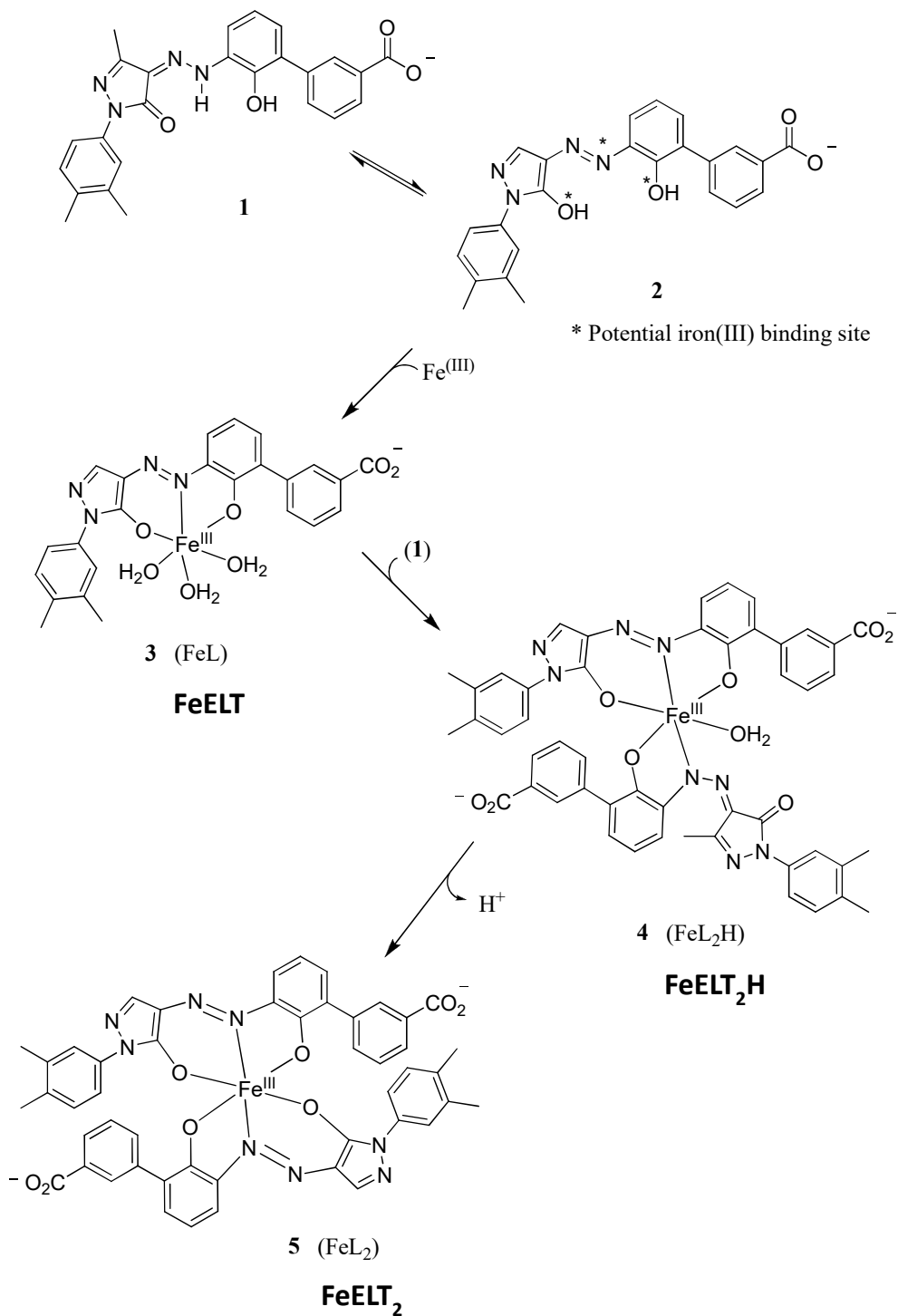


**Table 11 Comparison of the structure and iron binding properties of ELT and other chelators.** The relative stabilities of iron(III) binding are represented by the pFe, where the pFe of a given chelator for iron(III) is the negative log of the uncoordinated metal concentration under defined conditions (Martell, 1981). The higher pFe values, the lower the concentration of uncoordinated iron(III) and hence the greater stability for the iron-chelate complex. When pairs of chelators are combined in solution, iron(III) will bind preferentially to the chelator with the higher pFe value. This is highest for DFO and lowest for DFP, with DFX having an intermediate value. (Ihnat et al, 2002) (Motekaitis & Martell, 1991) (Nick et al, 2002).

	<b>DFO</b>	<b>DFP</b>	<b>DFX</b>	<b>ELT</b>
Molecular wt	561	139	373	442
Chelator/Iron(III) ratio	1:1	3:1	2:1	2:1 and 1:1
Log stability constant for iron(III)	30.6	37.2	36.5	34.9
pM (pmol/L)	26.6	20.7	23.1	22.0
Charge of free ligand at pH7.4	1+	0	1-	1-
Charge Iron complex at pH7.4	1+	0	3-	3- (2:1); 0 (1:1)
Lipid solubility free ligand (Kpart)	0.001	0.17	6.3	5.5

**Figure 32 Cellular iron release from hepatocyte HuH7 (A) or cardiomyocyte H9C2 cells (B) by ELT is shown as a function of ELT concentration.** Cells were loaded with iron as described in methods. Adherent cells were rinsed four times, including one wash containing DFO at 30µM and 3 PBS washes, and subsequently exposed to ELT and other chelators for the times shown. Chelator supernatants were then removed, and the cells washed four times as above before lysing with 200mM NaOH. Intracellular iron concentration was then determined using the ferrozine assay and normalised for total cellular protein in each well. Results shown are the mean ± SEM of 6 replicates in one experiment.

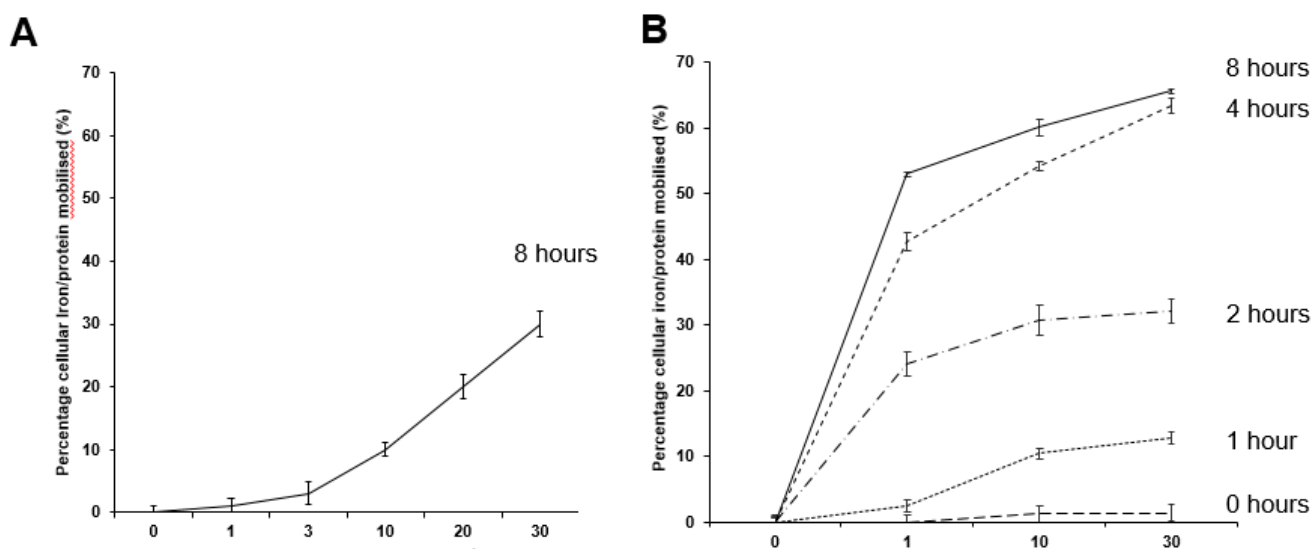
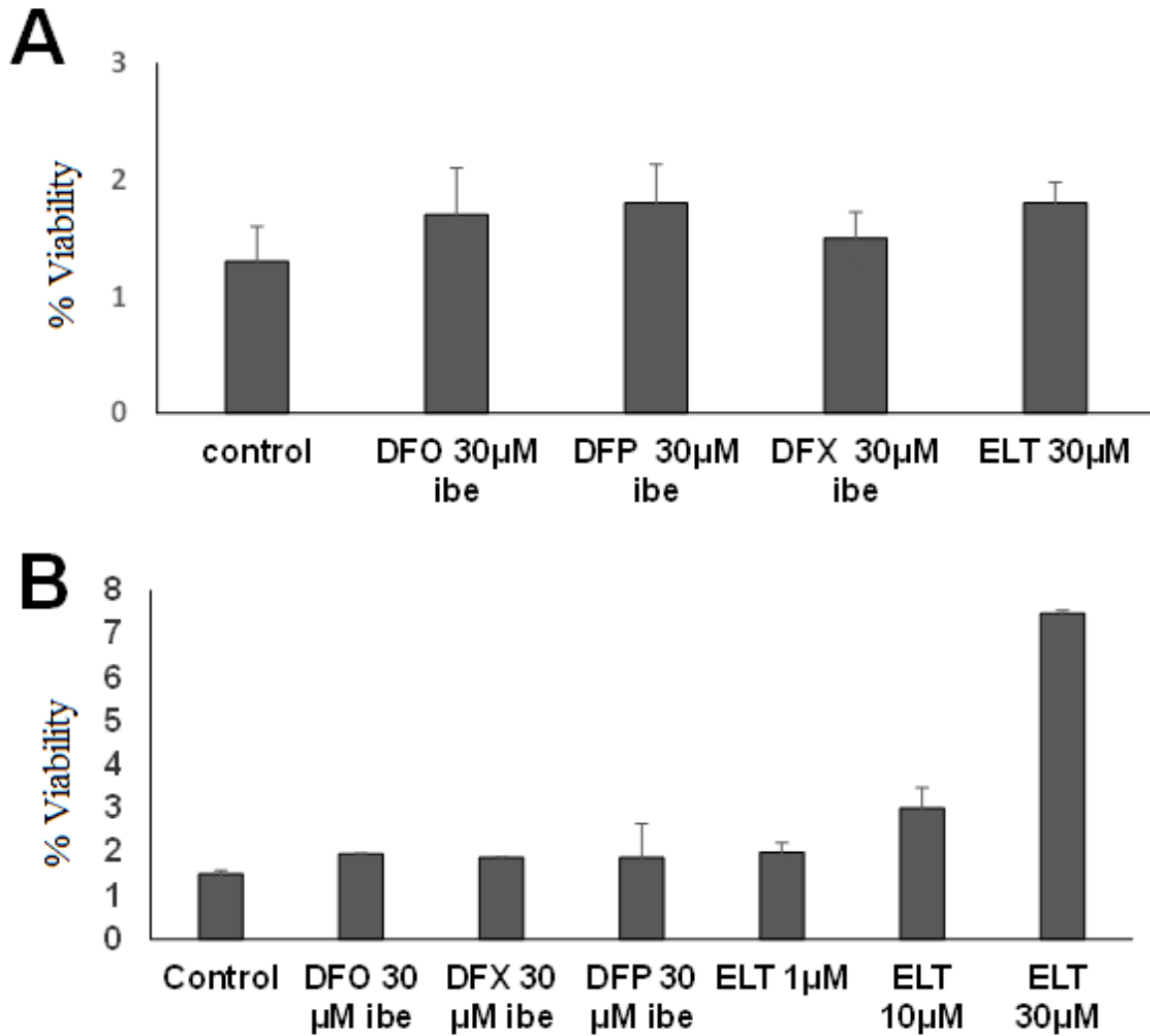


**Figure 33 Hepatocyte HuH7 (A) and Cardiomyocyte H9C2 (B) cell viability following an 8-hour treatment with ELT.** Following iron loading and chelator treatment as described in **Figure 32**, supernatants were removed and viability compared using the LDH assay as described in the methods section.



### 5.3.2 ELT decreases intracellular ferritin

We wished to understand whether the decrease in cellular iron seen above is predominantly due to mobilisation of storage iron (ferritin). HuH7 cells and H9C2 cells were iron-loaded as described in the methods section above using two media changes containing 10% FBS. This increased tissue ferritin by 75% in hepatocytes and by 33% in cardiomyocytes (data not shown), and increased total cellular iron by 4 and 2.5 fold respectively. Cells were then treated with ELT for 8 hours and cellular ferritin assayed as described in methods. In HuH7, 10 $\mu$ M ELT achieved a decrease of 85% in tissue ferritin compared with 46% decrease in H9C2 cardiomyocytes (**Figure 34**). In cardiomyocytes, there was a 46% reduction in ferritin with a 65% of total cellular iron. Thus chelation with ELT decreases both total cellular iron and cellular ferritin in both cell types with ferritin decrements being proportionately greater in HuH7 than H9C2 cells. Evidently, therefore, hepatocyte ferritin is more responsive, both to iron loading and iron unloading than in cardiomyocytes, which is consistent with the known high iron storage capacity of hepatocytes compared with cardiomyocytes.

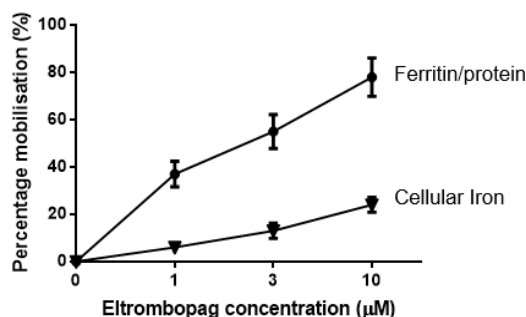
**Table 12 Comparison of percentage of intracellular iron mobilised at 8h in a cardiomyocyte (H9C2) and a hepatocyte (HuH7) cell lines by clinically available chelators or ELT, alone (top panel) or in combination (lower panel). Chelator concentrations are expressed as iron binding equivalence (ibe). Cells were pre-loaded with iron, rinsed, incubated with chelators and cellular iron determined as described in Figure 32. Results shown as the % iron released expressed as a % of T0 cellular iron and are the mean  $\pm$  SEM of 4 replicates in one experiment.**

<b>% iron release following 8 hours of chelator treatment</b>		
	<b>Cardiomyocytes</b>	<b>Hepatocytes</b>
DFO 1 $\mu$ M ibe	14.2 $\pm$ 1.2	28.6 $\pm$ 1.4
DFP 1 $\mu$ M ibe	17.1 $\pm$ 1.5	25.7 $\pm$ 1.2
DFX 1 $\mu$ M ibe	11.7 $\pm$ 1.0	22.8 $\pm$ 1.7
ELT 1 $\mu$ M	42.1 $\pm$ 2.1	6.9 $\pm$ 0.3
ELT 1 $\mu$ M + DFO 1 $\mu$ M ibe	58.2 $\pm$ 2.5	34.3 $\pm$ 1.1
ELT 1 $\mu$ M + DFP 1 $\mu$ M ibe	59.9 $\pm$ 3.1	38.2 $\pm$ 1.5
ELT 1 $\mu$ M + DFX 1 $\mu$ M ibe	66.4 $\pm$ 2.4	51.4 $\pm$ 1.9

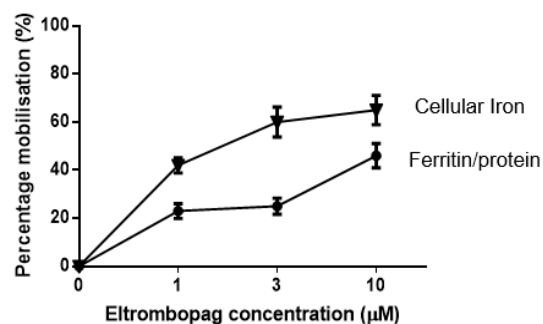
**Figure 34 Comparison of the effect of ELT on ferritin and total cellular iron mobilisation in hepatocyte HuH7 (A) and cardiomyocyte H9C2 cells (B) is shown.**

Following iron loading as described in the methods section, the cells were rinsed four times including one wash containing DFO at 30 $\mu$ M ibe and 3 PBS washes and subsequently exposed to ELT over an 8 hour period. At the end of the incubation, the supernatant was removed, and the cells further washed four times as above. Iron content was assessed using the ferrozine assay as described in methods. Ferritin was quantified using commercially available ELISA kits appropriate for our rat and human cell lined, as described in methods. The results are the mean  $\pm$  SEM of 3 replicates in one experiment.

**A. HuH7**



**B. H9C2**



### 5.3.3 ELT decreases ROS rapidly compared with other chelators

Intracellular ROS generation by iron is predominantly determined by the concentration of the intracellular labile iron pool (Cabantchik, 2014). Unlike measurement of total cellular iron or ferritin iron, continuous real-time measurement of ROS is achievable, allowing insight into the kinetics of intracellular chelation. A cell-permeable oxidation and hydrolysis sensitive fluorescent probe was used for this purpose as described in methods. After preloading cells with the non-fluorescent DCFH-DA (Molecular Probes, Leiden, Netherlands) for 30 minutes at 37°C, allowing time for commencement of hydrolysis to the highly fluorescent DCFH, chelators were added to each well and then placed into the plate reader where fluorescence was recorded over 1 hour at 37°C. The interval between addition of chelators and commencing ROS recording on the plate reader was between 3 and 5 minutes.

In **Figure 35** it can be seen that the rate of ROS generation is decreased by ELT in HuH7 and H9C2 cells compared with control. Even at the first measurable time-points, the fluorescence signal with ELT is less than control, suggesting very rapid entry of sufficient ELT to decrease ROS. It is also clear that inhibition of intracellular ROS generation by DFO is relatively slow and that DFP and DFX have intermediate effects on the rates of ROS generation. In **Figure 36** the relative inhibitory effects of different chelators on the rates of ROS generation are summarised for HuH7 and H9C2 cells. In these experiments 10µM ELT was used and 10µM iron binding equivalents of other chelators (except CP40 where 100µM (33µM ibe) was used). It can be seen that the rate of ROS generation is inhibited with ELT by 73% in HuH7 and by 61% in H9C2 cells, which is more than that obtained with other chelators, even though these were used at higher iron binding equivalents. In **Table 13**, experiments are shown which were conducted at even lower chelator concentrations of ELT (1µM) with exposure for 1 hour. It can be seen that among the chelator monotherapies, ELT again has the greatest rate in decreasing ROS generation in both cell types studied. The ROS decrease is similar in cardiomyocytes and hepatocytes, unlike effects of iron mobilization, which were greater in cardiomyocytes. This is consistent with rapid access of ELT to labile iron pools before significant metabolism has taken place in HuH7 as detailed in the discussion below.



**Figure 35 The time-course for ROS inhibition by ELT and other chelators.**

Cells were iron loaded and then rinsed four times as described in methods. Chelators were then added, and the rate of change of ROS production was recorded as fluorescence change (excitation at 504 nm, emission at 526 nm) continuously over 1 hour in the plate reader at 37°C in cardiomyocytes (A) and hepatocytes (B). DFO, DFP, and DFX were used at 10µM ipe, and ELT at 10µM. The rate of ROS production was compared between chelator treated and untreated cells. Data shown are readings from individual plates.

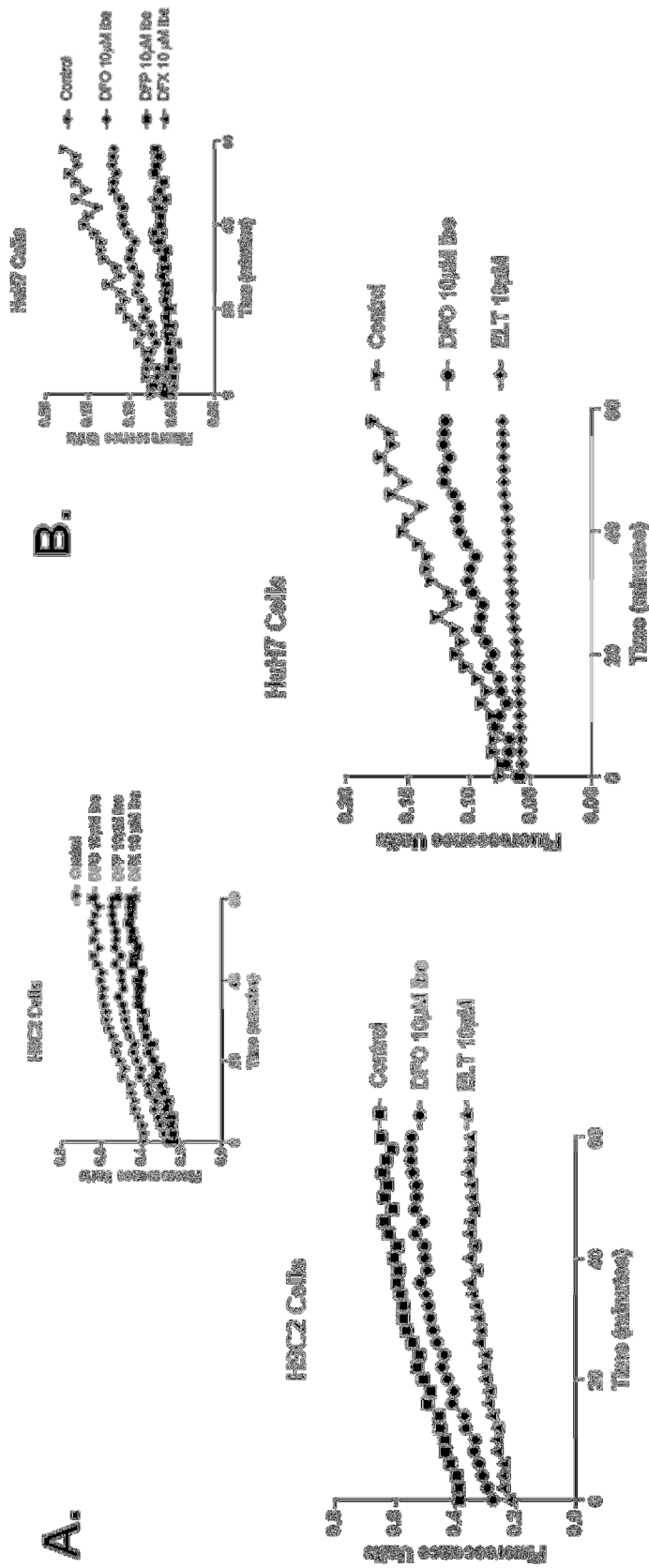
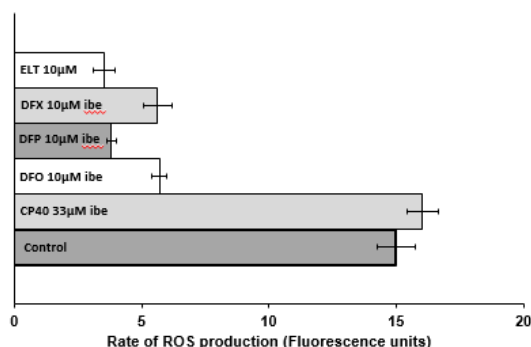


**Figure 36 Rate of ROS production following chelation treatment in (A) HuH7 and (B) H9C2 cells.** Rate of ROS generation determined as in **Figure 35**. ROS rate inhibition at 1h with CP40, DFO, DFP, DFX, and ELT are shown at 10 $\mu$ M ibe for each chelator, 10 $\mu$ M ELT and 33 $\mu$ M ibe CP40. Results are the mean  $\pm$  SEM of 4 observations in one experiment.

**A. HuH7**



**B. H9C2**

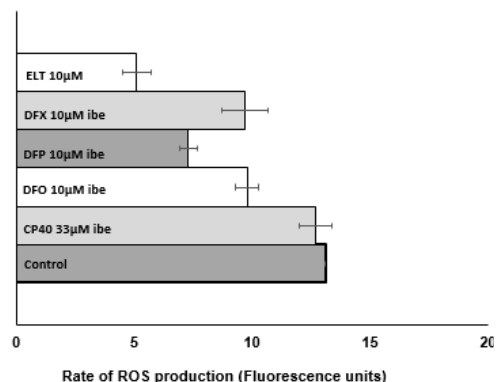


**Table 13 Comparison of ROS generation in cardiomyocyte (H9C2) and a hepatocyte (HuH7) cell lines is shown after addition of clinically available chelators or ELT, alone (top panel) or in combination (lower panel) over 90 minutes at the concentrations shown.** Experimental design and determination of ROS is otherwise as described in **Figure 5**. Results are the mean  $\pm$  SEM of 4 observations in one experiment.

<b>% decrease in ROS generation rate</b>		
	<b>Cardiomyocytes</b>	<b>Hepatocytes</b>
DFO 1 $\mu$ M ibe	16.4 +/- 1.1	11.3 +/- 0.9
DFP 1 $\mu$ M ibe	30.2 +/- 2.3	26 +/- 1.7
DFX 1 $\mu$ M ibe	12.2 +/- 1.1	40.3 +/- 2.9
ELT 1 $\mu$ M	44.2 +/- 2.7	41.2 +/- 3.1
ELT 1 $\mu$ M + DFO 1 $\mu$ M <u>ibe</u>	63.7 +/- 4.1	61.6 +/- 4.1
ELT 1 $\mu$ M + DFP 1 $\mu$ M <u>ibe</u>	60.3 +/- 5.2	57.9 +/- 4.6
ELT 1 $\mu$ M + DFX 1 $\mu$ M ibe	55.3 +/- 3.1	52.6 +/- 2.1

#### **5.3.4 Iron contamination in albumin or BSA inhibits cellular iron mobilisation by ELT**

Following reports that serum may inhibit the thrombopoietin agonist effects of ELT (Kalota et al, 2015), we reasoned that free iron contamination in media (unbound to transferrin) could be available for binding to ELT and that such binding might account for loss of action. We, therefore, investigated the inhibitory effects of several media or media supplements on cellular iron mobilisation by ELT.

An inhibitory effect of serum (FBS) on the iron mobilisation properties of ELT was noted in HuH7 cells (**Figure 38 A**). This effect was greater with increasing %FBS concentrations in the media, leading to a 4 fold inhibition at 25% FBS (**Figure 39 A**). As 100% FBS contains  $3.31 \pm 0.23 \mu\text{M}$  of free iron (see methods), the concentration in 25% FBS will be approximately  $0.8 \mu\text{M}$  and sufficient to partially inhibit  $1 \mu\text{M}$  ELT. However in order to ensure that the inhibition of ELT action was not secondary to protein binding, we examined the effects of recombinant albumin and fresh human serum on cellular iron mobilisation by ELT. Recombinant human albumin at 40g/L in RPMI contained  $0.79 \pm 0.15 \mu\text{M}$  iron and inhibited iron mobilisation from HuH7 cells by  $10 \mu\text{M}$  ELT ( $5 \mu\text{M}$  ibe) by about 50% (**Figure 38 B**). By contrast, fresh human serum contained no measurable free iron (only transferrin bound iron), had negligible iron releasing properties of its own (about 2%) and also had no inhibitory effects on iron release by ELT (**Figure 38 C**). We, therefore, conclude that inhibitory effects of sera and protein containing media on the iron mobilising effects of ELT are due to iron contamination in media and not from protein binding. These observations could also be important to studies where the thrombopoietin agonist effect of ELT is investigated. This is because 'free' iron contamination in media will lead to complexation of ELT by iron(III) (**Figure 31**) which is likely to abrogate interaction with the thrombopoietic receptor. In patients where plasma NTBI is present, higher concentrations of ELT may be needed than would be the case in patients lacking NTBI to induce iron cellular mobilisation or indeed effects resulting from binding to the thrombopoietin receptor.

### 5.3.5 Iron(III) binding and speciation plots for ELT alone or combined with other chelators

In order to explain the observations in cell culture, we wished to formally establish the iron(III) binding properties of ELT in a cell-free system, as these have not been previously reported. The approach for determining iron(III) binding is briefly described in methods. The normal chemical representation of ELT is presented in structure 1 (**Figure 31**), this lacks a high-affinity iron(III) binding site. However, ELT can be represented as a mixture of two tautomers which are in  $K_{\text{FeL}_2\text{H}} = 43.4$  and  $K_{\text{FeL}_2} = 34.9$  equilibrium with each other; the second tautomer **2** possesses a potential tridentate iron(III) binding site and is fully conjugated. Titration with iron(III) yielded three equilibrium constants,  $K_{\text{FeL}} = 25.6$ ,  $K_{\text{FeL}_2\text{H}} = 43.4$  and  $K_{\text{FeL}_2} = 34.9$ ; and ELT has three pKa values 2.6, 8.7, 11.1. Using this data, a pFe value of 22.0 was determined which is greater than that of deferiprone (20.4) and very similar to that of DFX (23.1). The speciation plot for iron(III)/ELT (**Figure 37**) indicates that a mixture of the 1:1 and 2:1 complexes are present at pH 7.4. Significantly the 1:1 complex (**3**) possesses zero net charge and has a molecular weight lower than 500 and so like the deferiprone iron complex, the 1:1 ELT iron complex is predicted to readily permeate membranes. The pFe value for ELT as well as for DFO, DFX, and DFP is presented in **Table 11**. The pFe value is the negative log of the iron(III) concentration under defined conditions (1 $\mu\text{M}$  iron(III) and 10 $\mu\text{M}$  chelator) (Vlachodimitropoulou et al, 2015). The pFe (pM) for ELT is 22.0, which is greater than that of DFP but less than that of DFX and DFO, the consequences of which are shown in **Figure 39** as speciation plots of iron(III) (1 $\mu\text{M}$ ) binding at increasing concentrations of ELT (1-10 $\mu\text{M}$ ) in the presence of (a) DFO 1 $\mu\text{M}$  (b) DFP 3 $\mu\text{M}$  (c) DFX 2 $\mu\text{M}$ . It can be seen in (a) that at equilibrium under these conditions, ELT will donate iron(III) to DFO over the entire range of ELT concentrations, with ELT acting as a shuttle and DFO as the sink for iron(III). By contrast, when combined with DFP (b), ELT will act as a sink for iron(III) when ELT concentrations exceed 1 $\mu\text{M}$ . However, in (c) it can be seen that ELT, when in the presence of DFX (Exjade), can act as either a shuttle or a sink for iron(III) depending on the relative concentration of ELT and complexation to ELT will be favoured when ELT concentrations exceed 7 $\mu\text{M}$ . The exchange of iron(III) from the ELT FeL complex (**3**) to competing ligands is likely to be fast as only 3 iron coordination sites are occupied

by ELT. The remaining 3 sites are occupied by water (3) and will be readily available for displacement by strong iron chelating ligands.

**Figure 37** The speciation of iron(III) in the presence of ELT as a function of pH.  $[\text{Fe}]_{\text{total}}=1\mu\text{M}$ ;  $[\text{ELT}]_{\text{total}}=10\mu\text{M}$ . (Kind donation of Professor Hider, King's College London).

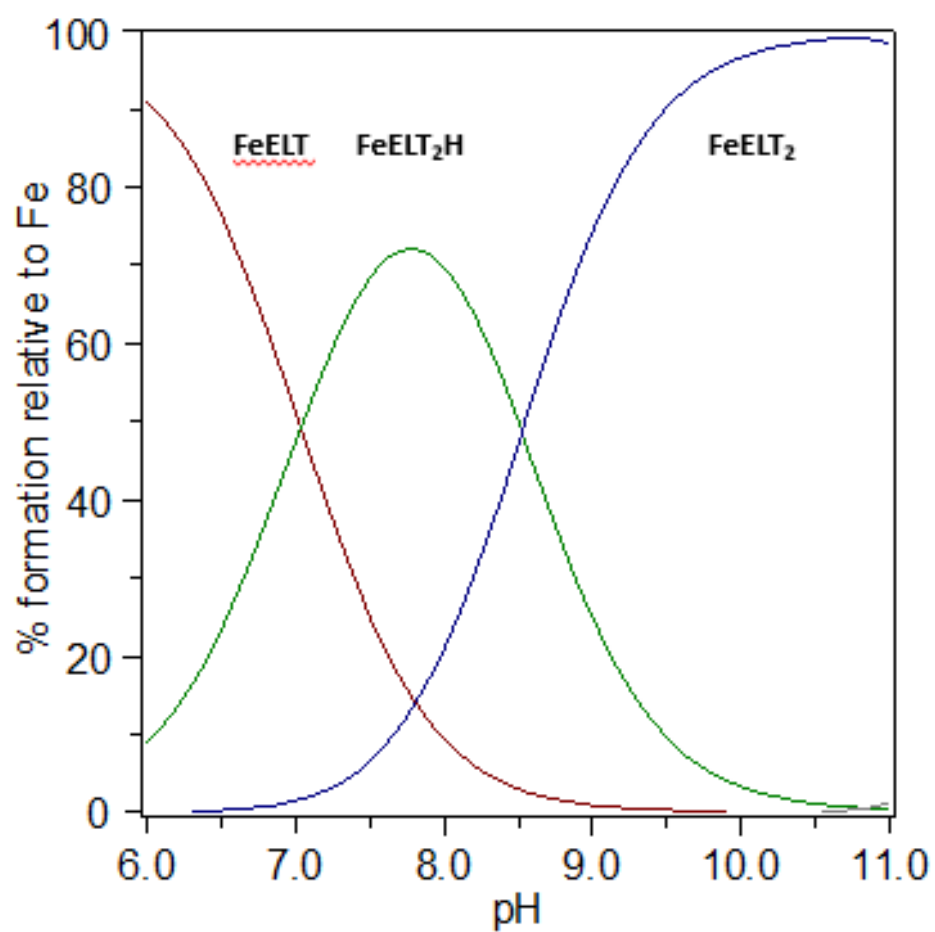


**Figure 39** The effect of serum and albumin on the iron mobilisation by ELT is shown in HuH7 cells. Following iron loading and rising as described above cells were subsequently exposed to ELT at 30  $\mu\text{M}$  in RPMI over an 8 hour period with media containing (A) increasing concentrations of FBS (0-25%): (B) Recombinant Human Albumin (rHSA) (Sigma) (C) heat-inactivated human serum (see methods). Cellular iron content at 8h was determined as described above. Results are mean  $\pm$  SEM of 4 observations in one experiment.

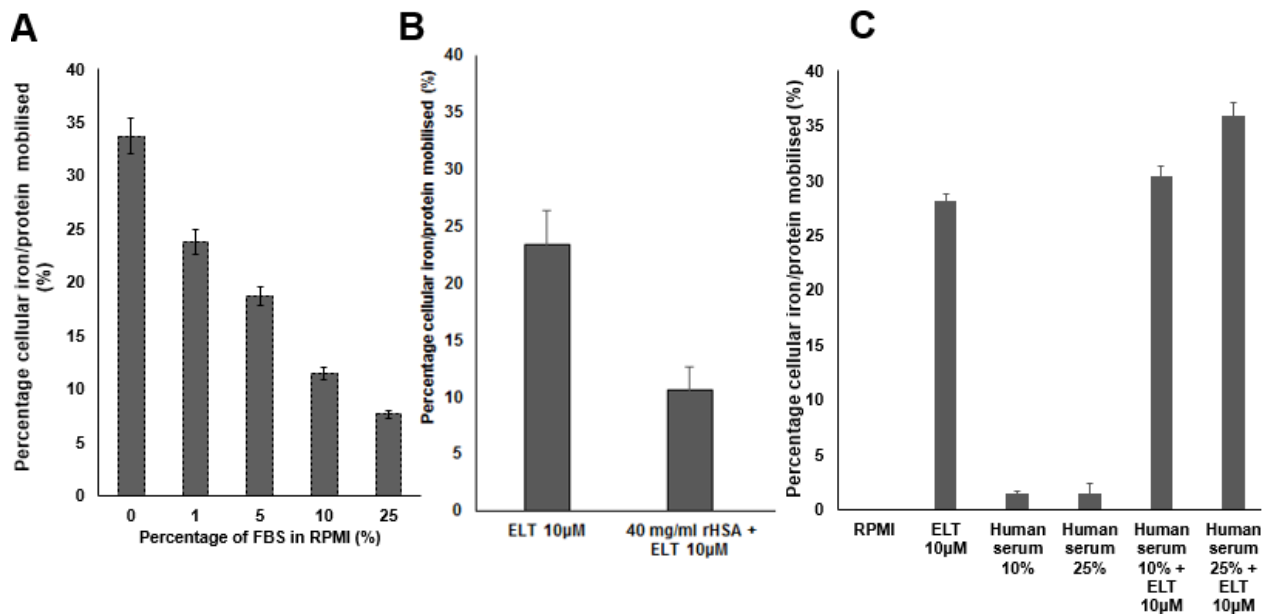
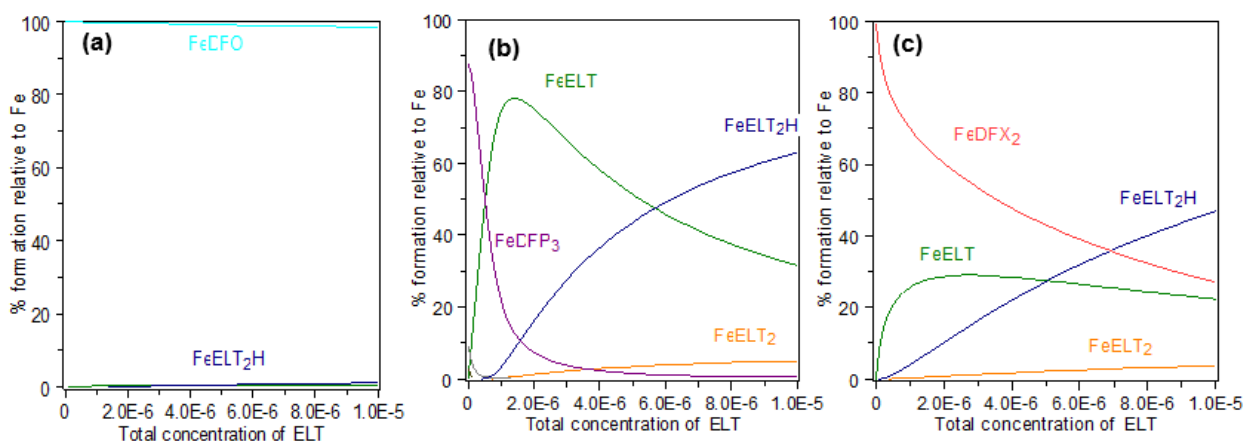


**Figure 38** The proportions of ELT species bound to iron(III) at equilibrium, with increasing ELT concentrations, in the presence of (a) 1 $\mu\text{M}$  DFO, (b) 3 $\mu\text{M}$  DFP, (c) 2 $\mu\text{M}$  DFX. Proportions are calculated from the iron binding constants for iron chelate complexes of the respective chelators shown in Table 11. (Kind donation of Professor Hider, King's College London).



### **5.3.6 Combination of ELT with clinically available chelators enhances iron mobilisation**

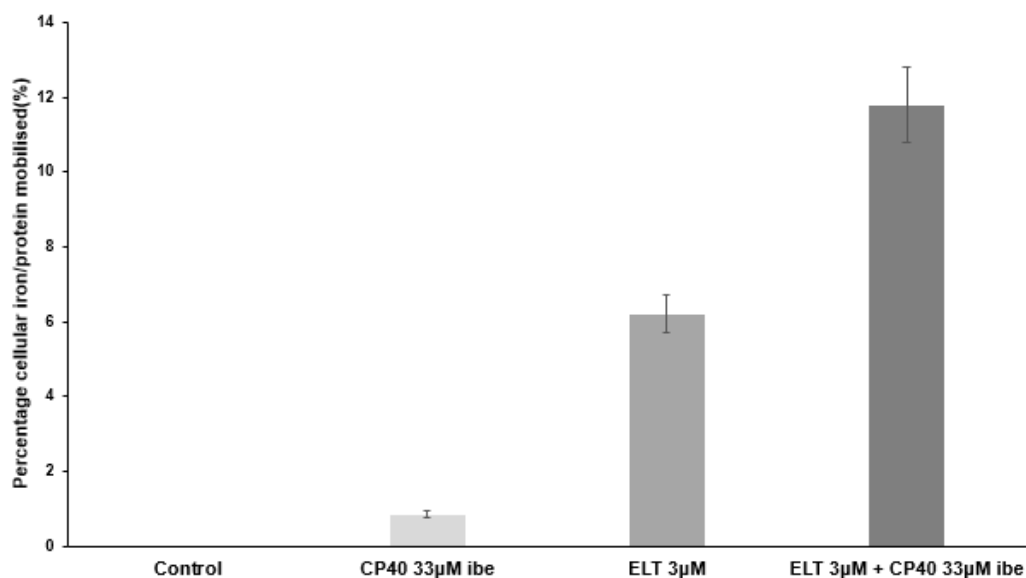
The relative effects of chelator combinations with ELT on cellular iron removal are shown in **Table 12** for the two cell lines. Findings are consistent with the predictions from speciation plots shown above. Thus when ELT at just 1 $\mu$ M is combined with DFO, DFP, and DFX at 1 $\mu$ M, iron mobilisation is between 4 and 6 times greater than monotherapy of commercially available chelators. In both cell lines, the most effective combination appeared to be that of ELT and the orally available chelator DFX. Based on speciation plots in **Figure 39**, the mechanism for enhanced iron mobilisation is predicted to be the shuttling of iron(III) between chelators. Under the conditions of these experiments at 1 $\mu$ M of these clinically available chelators, the speciation plots predict that ELT will behave as iron(III) shuttle to these chelators acting as sinks. Under the conditions used in **Table 12**, DFP is predicted from speciation plots to be a less effective sink chelator than DFX, which could explain the lower efficacy of this combination. However at transient peak concentrations of DFP reported clinically of approximately 100 $\mu$ M will have significant 'sink' effect. Iron release observed in **Table 12** when ELT is combined with DFO is consistent with speciation data in **Figure 39 A** which predicts that DFO will be an effective sink for iron(III) forming ferrioxamine (FO) when combined with ELT. The reason that ELT is less effective in combination with DFO than DFX is most likely related to slow rates of access of DFO to intracellular iron (Hoyes & Porter, 1993) and slow egress of intracellular FO from cells (Cooper et al, 1996) as previously described.

### **5.3.7 Synergistic chelation of ELT combined with otherwise ineffective hydroxypyridinone CP40**

In order to demonstrate synergistic iron chelation when ELT is combined with a second chelator, we examined a hydroxypyridone chelator with a high iron binding constant that is ineffective at mobilising cellular iron due to its inability to permeate cell membranes (Porter et al, 1988; Porter et al, 1990). In **Figure 40**, it can be seen that CP40 alone does not enhance cellular iron removal, confirming previous observations in primary hepatocytes (Porter et al, 1988; Porter et al, 1990). When CP40 was combined with ELT, however, an increase in cellular iron removal was seen, greater than with ELT alone. This provides mechanistic insight into how combinations of

commercial chelators with ELT interact. Firstly it supports the concept that the role of ELT in combined therapy is its potential to act as an iron shuttle. In monotherapy, CP40 has very little access to intracellular iron and thus it cannot act as an intracellular iron shuttle but can act as a passive extracellular acceptor of iron when delivered by another chelator. The increase in cellular iron mobilisation observed when CP40 33 $\mu$ M ibe was combined with ELT 3 $\mu$ M is likely due to an increase in the 'sink' availability in the extracellular medium as described for other chelator combinations (6). Here, therefore, ELT can shuttle iron intracellularly onto CP40, which remains exclusively extracellular.

**Figure 40 Cellular iron retention mobilisation is shown in previously iron loaded HuH7 cells, after 8 hours of exposure to ELT 3 $\mu$ M and/or CP40 33 $\mu$ M ibe as single agents and combination over an 8 hour period.** Chelator supernatants were then removed and cellular iron determined as described above. Results are the mean  $\pm$  SEM of 4 replicates in one experiment.





## 5.4 Discussion

In this paper, we have demonstrated progressive removal of total cellular iron by ELT in both cardiomyocyte (H9C2) and hepatocyte (HuH7) cell lines. This iron removal is associated with lowering of intracellular ferritin, consistent with decrements in storage iron in both cell types. Surprisingly ELT proved superior at mobilising cellular iron in the cardiomyocyte cell line to iron chelators that are currently used in clinical practice, namely DFO, DFP and DFX, and at remarkably low concentrations (1 $\mu$ M) (**Table 12**). Iron removal from the hepatocellular line (HuH7) was less effective than from H9C2 cardiomyocytes at low concentrations of 1 $\mu$ M (**Table 12**) but at higher concentrations, ELT were increasingly effective (**Figure 32 B**). The greater efficacy in cardiomyocyte than hepatocyte cell lines at low ELT concentrations may relate to greater rates of ELT metabolism in hepatocytes than in cardiomyocytes. It is known that ELT is metabolised by mono-oxygenation, glucuronidation, hydralazine cleavage and conjugation in the liver before being fully eliminated in faeces and urine (Deng et al, 2011). Glucuronidation and ELT cleavage will generate metabolites which are unable to bind iron(III). Liver hepatocytes are typically more active in drug metabolism than cardiomyocytes, and it is known that HuH7 cells contain most of the Phase I and Phase II enzymes that are present in hepatocytes (Guo et al, 2011). Thus greater metabolic inactivation of ELT would be expected in HuH7 cells than H9C2 cells. Indeed, while CYP2B1, 2B2, 2E1, and 2J3 are expressed in H9C2 cells and heart myocardium at comparable levels, these are significantly lower than in the liver (Zordoky & El-Kadi, 2007). Therefore the greater relative iron mobilisation from H9C2 than HuH7 cells, at low ELT concentrations, is consistent with greater metabolic inactivation in HuH7 than H9C2 cells. In clinical use, however, metabolic inactivation of ELT is unlikely to be a major issue limiting iron chelation, as unmetabolised ELT accounts for >94 % of drug at 4h with 64% remaining unmetabolised at 24h (Deng et al, 2011).

The data with ROS add insight into the interaction of ELT with iron pools in hepatocytes and cardiomyocytes. The kinetics of ROS inhibition with ELT in both cell types are rapid, occurring at the first measurable time point after addition of ELT (**Figure 35**) and consistent with the high pM value and low molecular weight of ELT (**Table 11**) allowing rapid access of ELT to intracellular iron pools. These findings are also consistent with Kalota et al. where, while investigating antiproliferative effects of ELT

in acute myeloid leukaemia cells, demonstrated rapid ROS decrements with a decreased H<sub>2</sub>O<sub>2</sub> levels (Kalota et al, 2015). By contrast, total cellular iron removal is gradual and progressive (**Figure 32 B**) allowing time for metabolism and inactivation of ELT particularly in the HuH7 hepatocyte-like cells. Thus while ELT-induced ROS decrements are rapid and similar in H9C2 and HuH7 cells (**Figure 36**) (**Table 13**), the total cellular iron mobilisation from HuH7 is less than in H9C2 cells, due to the slower rate at which storage iron is removed and the opportunity therefore afforded for ELT metabolism, particularly in HuH7 cells.

The iron binding and speciation data for ELT show Fe<sub>2</sub>LH to be the predominant species at physiological pH, indicative of tridentate chelation (**Figure 33**). The free ligand possesses 2 tautomers (**1** and **2**). Three iron(III) complexes have been identified **3** (FeELT), **4** (FeELT2H) and **5** (FeELT2) (**Figure 39**). The overall pFe for ELT is greater than DFP but less than for DFX and DFO (**Table 11**). This has implications for iron shuttling helps to explain the observed relative cellular iron release when ELT is combined with these chelators. The phenomenon of iron shuttling has been described with other chelator combinations (Srichairatanakool et al, 1997) (Giardina & Grady, 2001) (Vlachodimitropoulou Koumoutsea et al, 2015) (Evans et al, 2010), where one chelator possessing rapid access to iron pools subsequently donates iron to a 'sink' chelator that possesses greater stability for iron(III) binding but slower kinetic access. Iron(III) shuttling could occur both within or outside cells and it is not essential for the sink chelator to enter cells for synergism to occur (Vlachodimitropoulou Koumoutsea et al, 2015). The neutral charge of ELT as an iron complex is a characteristics well suited for iron shuttling across cell membranes (Vlachodimitropoulou Koumoutsea et al, 2015) when the sink chelator has slow intracellular access. A good example of such enhanced synergistic chelation is when CP40 (**Figure 40**) which has no inherent iron mobilising effects of its own, is combined with ELT. Such shuttling onto CP40, acting as a sink, has been previously described with other iron chelator combinations (Vlachodimitropoulou Koumoutsea et al, 2015).

For combinations of ELT with other chelators, the speciation plots (**Figure 39**) predict that at 1µM iron and 1µM iron binding equivalents of DFO or DFX, that iron can be shuttled onto these chelators by ELT at 1-10µM but that ELT is more likely to act as a

'sink' when combined with DFP (at the concentrations described in **Figure 39 B**). Our iron(III) release data (**Table 12**) show that while benefits of combining ELT with DFO and DFP appear additive in both cardiomyocytes and hepatocytes, with DFX, this exceeds the additive effects of either drug, suggesting synergism (**Table 12**). For example in hepatocytes, ELT alone had a small iron mobilising effect (7% reduction), and DFX alone had 23% reduction, but the effect of the two combined was suggestive of synergism with 51% reduction. Interestingly, in contrast when ROS decrements at 1 hour are considered for the ELT and DFX combination, the effects seem merely additive (**Table 13**). This is because while the inhibition of ROS is dependent on the summated iron binding capacity within cells, net cellular iron mobilisation over time is less limited by the iron binding capacity of intracellular chelation as, once ELT has donated iron to a second chelator, the free ligand is again available for a fresh round of chelation. Greater iron release with combinations of ELT and DFX than of ELT with DFO are not explained by speciation plots, as DFO is a highly effective sink for iron(III) (**Figure 39 B**). Rather this could be explained by faster access of DFX to intracellular iron pools (Glickstein et al, 2006) when compared with the slower access by DFO (Hoyes & Porter, 1993). Intracellular as well as extracellular iron shuttling from ELT onto DFX would explain the difference from ELT with DFO, where shuttling is likely to be predominantly extracellular. At steady state clinical concentrations of DFX (20µM) (Galanello et al, 2003) (Piga et al, 2006), DFX is likely to be an even more effective sink for iron(III). Combination of DFP with ELT was less effective than for ELT with DFX, and this is most likely explained by the speciation data rather than access to intracellular iron pools, which for DFP is known to be rapid. **Figure 39** shows that DFP is a less effective sink (B) than DFX (C) under the conditions shown. However, at the high transient peak plasma concentrations reported clinically for DFP (al-Refaie et al, 1995) it is likely that the 'sink' properties of DFP will be enhanced.

Our data are consistent with the iron chelating effects of ELT being independent of the TPO-R effect because the latter is highly species specific. The thrombopoietic actions of ELT occur only in humans and primates with no effect in rodents, whereas the iron mobilising effects in our experiments were seen both in human HuH7 cells and murine H9C2 cardiomyocyte cells. This suggests that the mechanism of action for iron removal is distinct to its thrombopoietic effect. It has been suggested (Kalota et al, 2015) that the

thrombopoietic actions of ELT could be inhibited by binding to plasma proteins. Our experiments show that inhibition of cellular iron mobilisation by ELT is a consequence of the binding of ELT to 'free' non-transferrin bound iron that contaminates FBS and albumin preparations rather than to albumin itself. Fresh human serum has no inhibitory effects on the iron removal properties of ELT. Thus when transferrin is not fully saturated, it is unlikely that serum will inhibit the actions of ELT. When NTBI is present in patient's serum, higher concentrations of ELT may be required to achieve the desired effect, be it iron chelation or enhanced thrombopoiesis. However as NTBI values rarely exceed 5 $\mu$ M in iron overload, and thus plasma concentrations of ELT to overcome this effect should be obtainable.

The chelating actions of ELT have not been explored clinically but may be beneficial in several settings. An obvious application would be the treatment of transfusional iron overload or patients with dysregulated cellular iron metabolism, such as in sideroblastic anaemia. The elimination of route for iron complexes of ELT is unknown and requires studies in animal models and in humans. However if iron chelated by ELT were donated to another chelator, as suggested by our cell culture experiments, then the iron complex of ELT would not need to be eliminated in urine or faeces directly but through the second chelator, for which elimination routes are well established. Other consequences of iron chelation by ELT require consideration. In addition to increasing platelet counts, ELT can also increase red blood cell and neutrophil counts and has recently been approved in the US for the treatment of severe aplastic anaemia (Design, 2016). Some of the beneficial effects of ELT on haematopoiesis in MDS and aplastic anaemia could also be derived from this iron chelating mechanism. Antileukemic effects mediated through modulation of intracellular iron content have also been postulated (Roth et al, 2012). The antioxidant and iron chelation properties of ELT are tightly linked to cell death in leukaemia cells (Roth et al, 2012) as the anti-proliferative and apoptotic effects of iron chelators are well described (Maclean et al, 2001) , through mechanisms that include inhibition of ribonucleotide reductase (Hoyes et al, 1992; Kayyali et al, 2001). However, in patients with ITP, iron chelation could create or exacerbate iron deficiency, and this needs to be explored. Importantly the 1 $\mu$ M concentration of ELT which was effective at mobilising cellular iron is nearly twenty-fold less than peak plasma concentrations obtained following 30mg ELT orally, a dose used to treat

thrombocytopenia (Gibiensky et al, 2011). At this dose, increments in platelet counts do not typically exceed 1.2 x the baseline values in healthy volunteers with repeat dosing (Jenkins et al, 2007). Hence it is predicted that effective chelating doses of ELT could be given without promoting unacceptably thrombocytosis, although this would require careful study before making recommendations. In principle, still lower concentrations could be used for iron chelation if ELT were combined with another clinically licensed iron chelator. ELT has been generally well tolerated, in long-term clinical treatments (Saleh et al, 2013). The most common reported adverse events with ELT are headache, gastrointestinal symptoms, and upper respiratory tract infections, occurring in up to 26, 14, and 23% of patients, respectively (Saleh et al, 2013). Regarding the risk of thromboembolic events, published studies (Bussel et al, 2007; Bussel et al, 2009; Bussel et al, 2013; Cheng et al, 2011) did not demonstrate any correlation between ELT treatment and occurrence of such events. This suggests that ELT doses could be administered to patients without thrombocytopenia that induced significant intracellular chelation, without appreciable increments in platelet counts.

## **5.5 Conclusion**

We have demonstrated the iron binding properties of ELT in solution and the iron mobilising properties from cells for the first time. Remarkably low concentrations of ELT are required to mobilise cellular iron; single agent ELT is at least as effective as clinically licensed iron chelators at mobilising cardiomyocyte iron. Additive or synergistic intracellular chelation is shown when ELT is combined with clinically available chelators. The doses of ELT, alone or in combination with other chelators, are sufficiently low to suggest ELT could be used as an iron chelator in patients who are not thrombocytopenic.

## **Chapter 6 THE INFLUENCE OF FLAVONOIDS ON CELLULAR IRON MOBILISATION ALONE OR IN COMBINATION WITH CLINICALLY AVAILABLE IRON CHELATORS**

### **6.1 Introduction**

I have developed a cellular model of iron overload in hepatocyte (HuH7) and cardiomyocyte (H9C2) cells that can accurately reflect iron mobilisation by chelating molecules at clinically relevant concentrations. In previous chapters, this model was used to look closely at interactions between chelators when in combination and to distinguish between the principles of ‘synergy’ and ‘additivity’ of chelator action. This system was then utilised to interrogate the potential of a drug (Eltrombopag), typically used to manage ITP, to act as a ‘shuttle’ of iron onto ‘sink chelators’. A novel finding was its potential application in the management of transfusional iron overload.

In this chapter, I have now applied the above system to examine a group of compounds that possess iron chelating properties that occur naturally in the daily human diet, namely the flavonoids. These are known to have both iron-chelating<sup>22</sup> as well as anti-oxidant properties, but the extent to which these two broad properties functionally overlap is not fully understood. In principle, the system that I have developed, whereby the iron chelating properties of such compounds can be examined independently from real-time effects as antioxidants in the same cells, provides an opportunity to study structure-functions relationships of flavonoids. The metabolism of these compounds yields structures where the iron binding sites are modified, thus abrogating iron binding, but where the basic structure of the flavonoids is otherwise unperturbed. In principle, therefore, it is possible to dissect the iron binding properties from the antioxidant properties. It was reasoned that this would provide insight into how these common components of the human diet contribute anti-oxidant versus iron chelating effects and may suggest how these overlapping properties might best be applied selectively to benefit human health.

### **6.2 Chemistry of flavonoids**

Flavonoids are abundant micronutrients in the diet of humans that have attracted

increasing attention in the recent years due to their iron chelating (Guo et al, 2007), antioxidant, anti-inflammatory and anticarcinogenic properties (Middleton, 1998). Their potential protective role has also been postulated in oxidative stress-related chronic diseases such as diabetes and ischaemic heart disease (Yao et al, 2004). Quercetin is one of the predominant flavonoids present in the diet, with the richest sources being in red wine, onions, apples and tea (Boots et al, 2008). **Table 14** shows the classification, structure and most common food sources of some of the dietary flavonoids. The flavonoid structure is based on the flavonoid nucleus consisting of three phenolic rings A,B and C (**Figure 41**). The bioavailability, biological activity, and metabolism are highly dependent on the configuration of the molecule, the number of hydroxyl groups, and the substitution of functional groups about their nuclear structure. Flavonoids in the diet (Hollman et al, 1999) are commonly present in their glycosylated form. The aglycone, glycoside as well as methyl, glucuronide and sulphate conjugates (Mullen et al, 2006) forms have been reported in human plasma after ingestion of flavonoids.

**Table 14 Food sources of dietary flavonoids.** (Figure adapted from Kumar and Pandey, 2013)

Class	Flavonoid	Dietary source
Flavanol	(+)-Catechin (-)-Epicatechin Epigallocatechin	Tea
Flavone	Chrysin, apigenin Rutin, luteolin, and luteolin glucosides	Fruit skins, red wine, buckwheat, red peppe
Flavonol	Kaempferol, quercetin, myricetin, and tamarixetin	Onion, red wine, olive oil, berries, and grap
Flavanone	Naringin, naringenin, taxifolin, and hesperidin	Citrus fruits, grapefruits, lemons, and oran
Isoflavone	Genistin, daidzin	Soyabean
Anthocyanidin	Apigenidin, cyanidin	Cherry, easberry, and strawberry

There is a great variety of phenolic structures amongst the molecules that come under the flavonoid category, and to date, more than 4000 varieties have been identified (Middleton, 1998). Their structure is based on a fifteen carbon backbone that consists of two benzene rings, named A and B, which are linked by one pyrene ring (C). Flavonoids can be divided into a number of classes, namely flavones, flavonols, flavanones, isoflavones, etc. (**Figure 42**). These classes differ between them in the substitution pattern and level of oxidation of the C ring. However, differences between molecules within a class differ in the substitution pattern of the A and B rings. Furthermore, flavonoids can occur as aglycones, glycosides, and methylated derivatives. Spectroscopic studies have revealed that flavonoids exhibit two major absorption bands: Band I (320-385nm) corresponding to the A ring absorption and Band II (250-285nm) representing the B ring absorption. The functional groups attached to the different derivatives cause a shift in the absorption spectra, e.g., kaempferol 367nm (3,5,7,4'-hydroxyl groups) to 371 for quercetin (3,5,7,3',4'-hydroxyl groups) and 374 (3,5,7,3',4', 5'-hydroxyl groups) for myrecetin (Yao et al, 2004).

**Figure 41 Core flavonoid structure.**

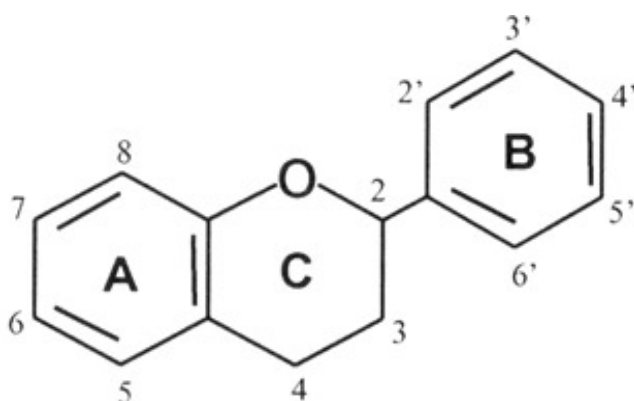
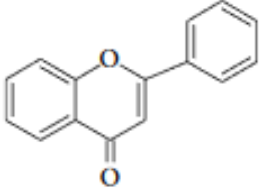
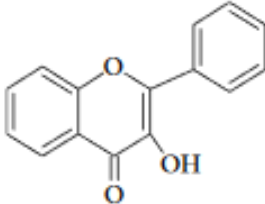
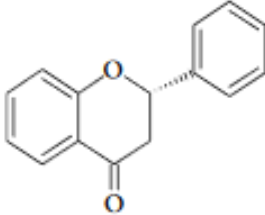
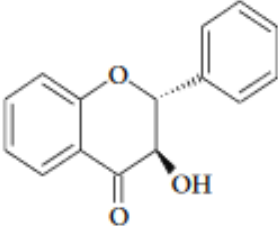
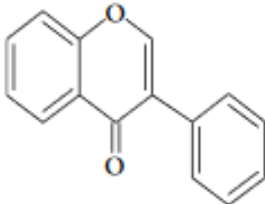
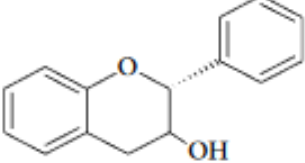




Figure 42 Structures of the different flavonoid groups.

Group of flavanoid	Structure backbone
Flavones	
Flavonols	
Flavanones	
Flavanonol	
Isoflavones	
Flavan-3-ols	

### 6.3 Dietary uptake and metabolism of flavonoids in humans

As with any molecule, the oral bioavailability of flavonoids is greatly dependent on molecular size, lipophilicity, configuration, solubility, and pKa. Following dietary consumption, certain flavonoids are taken up via the small intestine whilst others have to go through the colon. This is greatly dependent on whether the flavonoid is in its glycosylated form or aglycone, which can be easily taken up by the small intestine. Glycosylated compounds must be converted to the aglycone form prior to absorption (Hollman et al, 1999).

The hydrophilic flavonoid glucosides, such as quercetin, are transported through the Na<sup>+</sup> powered glucose cotransporter (SGLT1). Alternatively, glucosides are commonly hydrolysed by the enzyme lactase phloridzin hydrolase (LPH), a  $\beta$ -glucosidase commonly found on the brush border of the small intestine (Day et al, 2000). Once the aglycone is liberated, it can then be absorbed across the small intestine. The glycosides that are not substrates of LPH are transported towards the colon where there are bacteria with the ability of molecule hydrolysis and release of the aglycone, however often the aglycone itself will also be degraded (Scheline, 1973). As a result, there is only minimal absorption of glycosides in the colon compared to the small intestine.

Following absorption, the flavonoids are generally conjugated by the liver via glucuronidation, sulphation or methylation or are further metabolised to smaller phenolics. If a flavonoid is secreted in the bile, and it cannot be absorbed by the small intestine, it will subsequently be degraded in the colon by the intestinal microflora that will also destroy the flavonoid ring structure. Oligomeric compounds may be hydrolysed to monomers in the acidic conditions of the stomach and larger molecules may reach the colon and be degraded by bacteria. Dimerisation is thought to reduce bioavailability (Spencer et al, 2000). Despite the relatively low molecular weight of a number of the flavonoids, their low solubility in water coupled with a short residence time in the intestine may significantly reduce their therapeutic efficacy and presents a problem for medicinal application.

## 6.4 Flavonoids and their biological activities

### *Antioxidant activity*

Acting as an antioxidant is probably one of the best-described properties of flavonoids. Antioxidant activity amongst the group can be variable and is highly dependent upon the availability of hydroxyl groups as well as the configuration of the molecule and the biotransformations and substitutions. The core structure of flavonoids favours electron delocalisation and allows for greater flavonoid radical stability due to the configuration of its  $\pi$  bonds in the carbon backbone which are in line (**Figure 41**) and allow electron spread across the molecule. The most important groups that allow ROS scavenging, as reported in the literature, are located on the B ring of the structure (Kumar & Pandey, 2013), and this involves the donation of a hydrogen and an electron to stabilise other groups such as hydroxyl, peroxy and peroxy nitrite radicals.

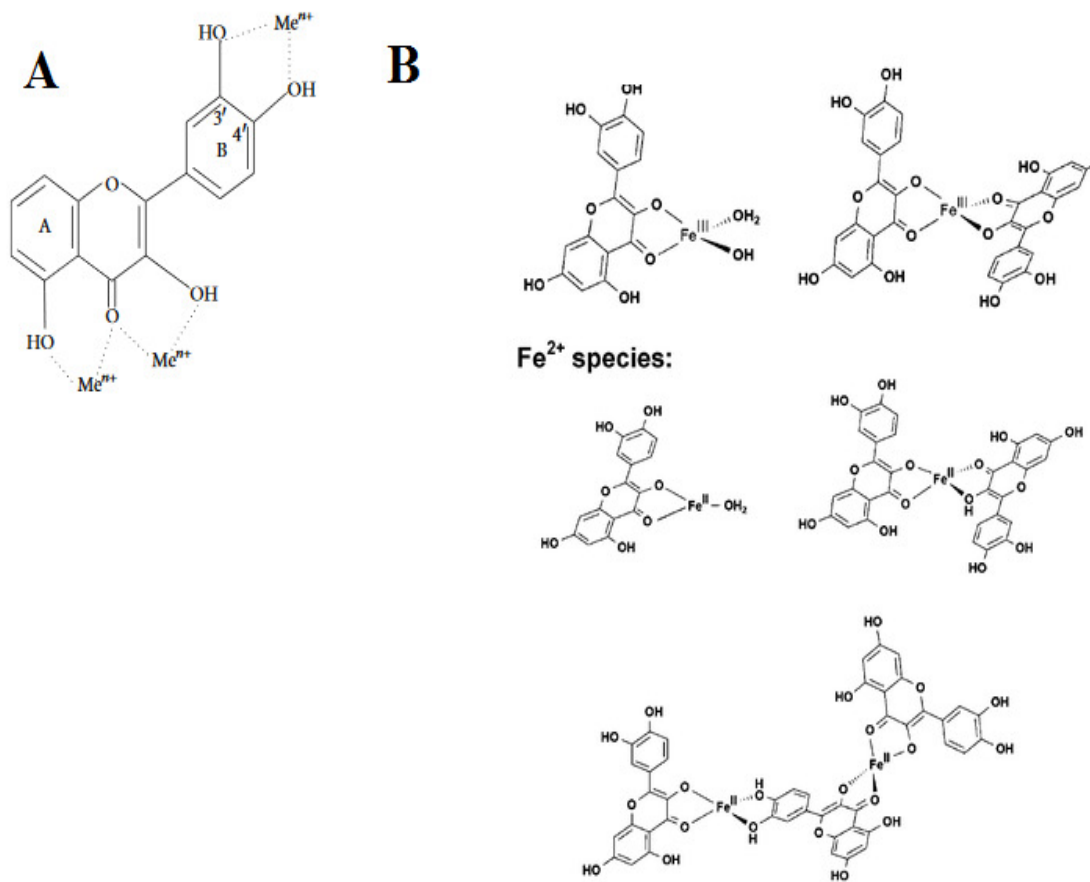
Flavonoids and quercetin, in particular, are strong inhibitors of lipid peroxidation because of their capacity to reduce radicals such as hydroxyl and superoxide radicals by hydrogen atom donation, forming stable flavonoid radicals themselves (Mishra et al, 2013a). It has been reported that antioxidant activity of the molecule declines proportionately to the number of glucose moieties present (Ratty & Das, 1988). However, antioxidant activity is not only limited to ROS suppression by free radical scavenging, but it is often closely related to chelation of elements which are themselves involved in ROS generation. In the presence of transition metals, the extent that iron chelation and free radical scavenging each contribute to the antioxidant effects of a molecule are unclear, and this will further be addressed in this chapter.

### *Iron chelation*

Iron chelating and ion stabilising properties of flavonoids, quercetin, in particular, have been previously well documented, independent of its antioxidant effects. Metals bind at specific points of the structure, as indicated in Figure 43 A. The ratio of iron binding to quercetin and binding constants for Fe(II) and Fe(III) were first characterised by Guo et al. in 2009 using electrospray ionisation mass spectroscopy (Guo et al, 2007). There are three iron-binding motifs on the quercetin molecule that

can bind iron strongly under physiological conditions. Quercetin can form 1:1 complexes and 1:2 complexes with Fe(III). Similarly, 1:1 (binding constant  $2 \times 10^6/M$ ) and 1:2 (binding constant  $5 \times 10^{10}/M^2$ ) complexes are formed with Fe(II), but also 2:3 ratio complexes (Guo et al, 2007) (Figure 43 **B**). The iron binding constants of Fe(II) for the 3 different iron binding sites are all similar for a 2:1 complex but follow the following order of preference: 1) 3-hydroxyl and carbonyl site C ring 2) 5-hydroxyl and carbonyl site A and C rings) and 3) 3',4'-dihydroxy site on the B ring. The order of binding constants for Fe(III) for a 1:1 complex has been proposed by some authors to possibly follow a different order: 3',4'-dihydroxy site on the B ring > 3-hydroxyl and carbonyl site on the C ring (Guo et al, 2007). Quercetin has also been noted to bind  $Ga^{3+}$  and  $Zn^{2+}$ . Interestingly, quercetin binds Fe(II) more strongly than the chelator ferrozine and it is also known to completely suppress Fenton reactions at only  $\mu M$  concentrations. In this thesis, we investigate the potential role of quercetin and its metabolites in shuttling iron out of cells and the extent by which inhibition of chelation properties by substitution at the chelation sites with different moieties impacts on the antioxidant capacity of these naturally occurring compounds.

Figure 43 Flavonoid binding site for trace metal ions indicated by  $Me^{n+}$  (A)(Kumar & Pandey, 2013) and complexes formed between quercetin and Fe (III) and Fe (II) (B). (Guo et al, 2007)



### *Hepatoprotective, antibacterial, anti-inflammatory, anti-cancer and anti-viral properties*

A number of flavonoids including quercetin, catechin and rutin have been reported in the literature to have hepatoprotective activity (Tapas et al, 2008). This probably involves mechanism such as ROS suppression, decreased lipid peroxidation and inhibition of release of pro-inflammatory cytokines (Tapas et al, 2008). Furthermore, several flavonoids including flavonol glycosides and isoflavones have been known to be potent antimicrobials *in vitro*. This is not surprising given that they are known to be synthesised by plants in response to infection (Abhay K. Pandey, 2010; Mishra et al, 2011; Mishra et al, 2013a; Mishra et al, 2013b). This property is most likely related to inactivation of enzymes and transport proteins. Apart from their antioxidant effects, other pathways for the anti-inflammatory actions of flavonoids have also been postulated, such as suppression of the inflammatory gene microRNA-155 in murine macrophages, and reduction of mRNA and protein levels of tumour necrosis factor alpha and interleukin 1 $\beta$  and interleukin 6 (Boesch-Saadatmandi et al, 2011). Consumption of fruit and vegetable is inversely linked to cancer of the prostate, lung, stomach and breast (Brusselmans et al, 2005). Proposed mechanisms involved include quercetin metabolites inducing G2/M arrest by upregulating PPAR-gamma expression in human lung cancer cells (Yeh et al, 2011), tyrosine kinase inhibition, downregulation of the mutant p53 protein, and inhibition of oestrogen receptor binding capacity, even though this is debatable as even the quercetin metabolites have been shown to mimic the actions of endogenous oestrogens and stimulate oestrogen receptors in a human breast cancer cell line (Ruotolo et al, 2014). Lastly, the antiviral activity of flavonoids was recognised in the 1940s. Quercetin has been shown to have viral neutralisation effects against dengue viral infection and mouse hepatitis virus *in vitro* (Chiu et al, 2016).

#### **6.5 Dietary uptake, metabolism, and toxicology of Quercetin**

The estimated dietary intake of all flavonoids is 200-350mg/day, and intake of flavonols is 20mg/day of which quercetin amounts to over 50%, making its daily intake approximately 10 -16 mg/day (Kawabata et al, 2015; Nishimuro et al, 2015). However, due to its wide presence in numerous fruits and vegetables such as apples,

berries, and onions, high consumption could increase intake to over 200mg/day. Quercetin is one of the most abundant and, best studied and metabolically active flavonoids.' The most prevalent form of quercetin in food is not the aglycone, but the glucoside (Kawabata et al, 2015), however, the aglycone is often purchased as a dietary supplement. Quercetin is deglycosylated by enzymatic pathways prior to its passive uptake through the small intestine. As mentioned above, enzymes that participate in this initial reaction include LPH or other gut-derived microbial enzymes. Naturally, the glucose moiety can substitute the hydroxyl group either at the 4' site on the B ring or site 3 on the C ring. The latter structure was used in the experiments to follow in this chapter.

Once it is deglycosylated in the small intestine, the quercetin aglycone undergoes significant biotransformation mainly by glucuronidation, sulphation, and methylation, involving the phase II enzymes UGT (uridine 5'-diphosphoglucuronosyltransferase), SULT (sulfotransferase), and COMT (catechol-O-methyltransferase). Isorhamnetin is the methylated derivative of quercetin, at the 3' site of the B ring whilst quercetin glucuronide has a glucuronide substitution at site 3 of the C ring. Kaempferol has a hydrogen substitution at the 3' hydroxyl group site on the B ring.

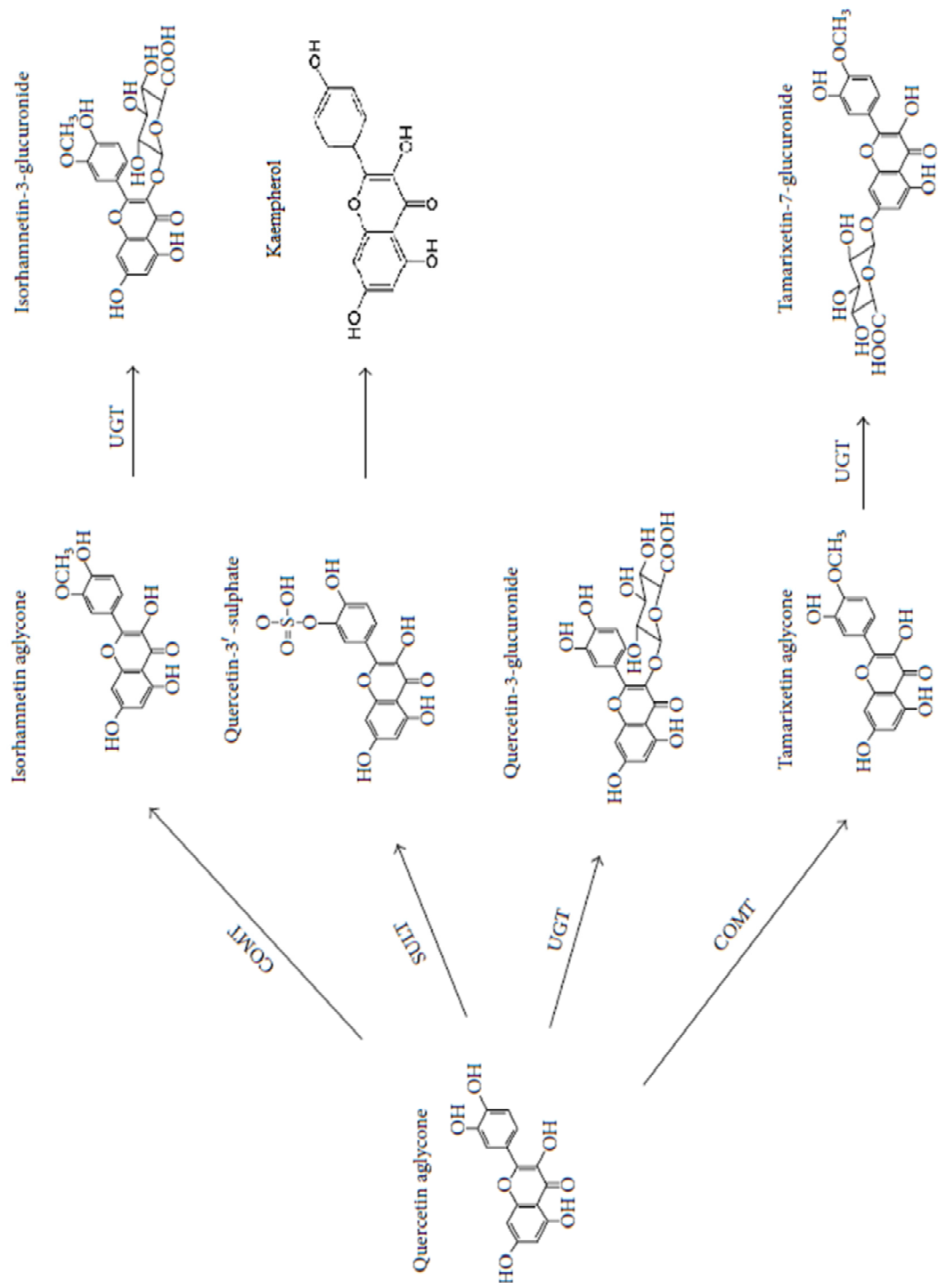
Figure 44 shows the structure of quercetin aglycone and its principle metabolites that are derived from some of the above biotransformation reactions. A number of animal studies mainly in rats and pig have shown the presence of quercetin in several tissues including the lung, kidney, liver as well as the brain (de Boer et al, 2005). Diet-derived quercetin is present in the plasma at concentrations in the nanomolar range (<100nM), however, this is increased by supplementation of the glucoside or the aglycone to about 5µM (Conquer et al, 1998; Manach et al, 2005). Supplementation of quercetin leads to the presence of similar metabolites in the mouse, rat as well as the gerbil, to humans (Yeh et al, 2016). The plasma half-life of quercetin is between 11 and 28 hours, making further increases to plasma concentration feasible (Manach et al, 2004; Manach et al, 2005). There is some controversy regarding the presence and concentration of the quercetin aglycone found circulating in plasma (Kelly, 2011; Shanely et al, 2010), however, the metabolite moieties such as the methylated and glucuronidated form are prominent. Nonetheless, studies have previously supported

the antioxidant and other beneficial effects of not only the aglycone but also its metabolites (glucuronidated, sulphated, methylated) *in vitro* and *in vivo* (2014; Boesch-Saadatmandi et al, 2011; Moon et al, 2001; Shirai et al, 2006; Yeh et al, 2011). Quercetin and 12 of its metabolites have been identified in urine, within 24 hours of onion consumption in humans (Mullen et al, 2006).

The toxicological profile of quercetin is virtually unremarkable as previously documented in the literature (Harwood et al, 2007; Shirai et al, 2006). Similarly to other flavonoids, quercetin has a number of reported beneficial effects relating to the cardiovascular system, cancer, diabetes and the nervous system (Boots et al, 2008; Kelly, 2011; Russo et al, 2012). We are particularly interested in the ion chelating properties of quercetin and its metabolites, and the potential of these molecules to act as 'shuttles' of iron(III), and therefore be candidates for combination treatment to current chelation therapy.



**Figure 44 Structure of quercetin and its principal metabolites**  
 (Boesch-Saadatmandi et al, 2011)



## 6.6 Materials and Methods

### 6.6.1 Flavonoid compounds

- VI. *Quercetin, Isorhamnetin, Quercetin 3-β-D- glucoside (Sigma-Aldrich, USA)*
- VII. *Quercetin-3-D-glucuronide, (HWI Pharma Solutions, Germany)*
- VIII. *Kaempferol (Calbiochem, Canada)*

### 6.6.2 The cellular model

The rat (H9C2) cardiomyocyte cell line and a human hepatocellular carcinoma (HuH7) cell line were chosen for investigation of the iron mobilisation properties of quercetin and its metabolites. Cardiomyocytes are a target tissue for transfusional iron overload and provide a particular therapeutic challenge, and hepatocytes represent the cell type with the largest quantity of iron deposition. The development of our HuH7/H9C2 cell models to assess iron mobilisation has previously been described in **Chapter 3**; a brief description of the finalised model is given below. Cells were plated at 200 000 cells/well in RPMI 1640 medium (HuH7)/DMEM (H9C2) supplemented with 10% fetal bovine serum (FBS) and allowed to attach for 24 h. In these experiments, the supernatant (media/10% FBS) was changed twice at 10-hour intervals. A threefold increase in intracellular iron concentration was achieved by this method in hepatocytes and a two-fold in cardiomyocytes (data not shown). The cells were sequentially washed with phosphate-buffered saline (PBS), 30 μM DFO ibe/PBS for 1 min then 2x PBS. After incubation with test compounds, further washes with PBS, 30 μM DFO ibe/PBS then 2x PBS were performed. Cellular iron loading and iron mobilisation were measured as a decrease in cellular iron content using the ferrozine assay (**Section 2.3.5**), adjusted for cellular protein (Vlachodimitropoulou Koumoutsea et al, 2015).

### 6.6.3 Cell damage and viability

As described in **Chapter 3**, viability is of critical importance when addressing iron release (Porter et al, 1988). Viability was ensured > 98% using the 'LDH Cytotoxicity Detection Kit' by Takara Bio Inc, which gives a quantitative comparison of early cell damage between 'treatment' and 'control.' This is a colorimetric assay and measures LDH activity leaked by damaged cells into the supernatant (W.J. Reeves Jr., 1966). The tryptan blue solution of 50/50 (vol./vol.) in PBS assay was also used, where non-

viable cells take up the dye and appear blue when directly visualised under the microscope.

#### **6.6.4 Determination of intracellular iron – The ferrozine assay**

The ferrozine assay is described in detail in the methods **Section 2.3.5**. In brief, cells were lysed overnight with 200µl of 200 mmol/l NaOH and iron detection reagent (6.5 mmol/l ferrozine, 6.5 mmol/l neocuproine, 2.5 mol/l ammonium acetate and 1 mol/l ascorbic acid dissolved in iron-free high-performance liquid chromatography grade water) was added for 30 min. Absorbance was recorded at 562 nm and lysate iron content calculated by standard curve interpolation against atomic absorption iron standards. Intracellular iron was normalised against protein content using the Coomassie (Bradford) assay.

#### **6.6.5 Detection of ROS using a fluorimetric method**

As previously described in **Section 2.6**, we utilised a cell-permeable oxidation-sensitive fluorescent probe 5,6-carboxy-2',7'- dichlorofluoresceindiacetate (DCFH-DA) (Molecular Probes, Leiden, Netherlands) to monitor the intracellular rate of ROS production. Cells in Corning 24-well plates (Sigma-Aldrich, MA, USA) were pre-incubated with 4µM H<sub>2</sub>DCF-DA for 30 minutes at 37°C as per protocol. Test compounds were then added, and fluorescence was recorded continuously over a period of 1 hour (excitation at 504 nm, emission at 526 nm). The time between the addition of chelators and commencing ROS level recording was between 3 and 5 minutes at room temperature. The rate of ROS production was compared between chelator treated and untreated cells.

#### **6.6.6 Ferritin quantification**

The ferritin quantification method is described in **Section 2.5**. Commercially available enzyme-linked immunosorbent assay (ELISA) kits (Cusabio, Wuhan, China and My BioSource, San Diego, USA) were used to measure human and rat tissue ferritin respectively in cell lysates, according to the instructions provided by the manufacturer.

## **6.7 Results**

### **6.7.1 Viability of hepatocytes and cardiomyocytes following exposure to quercetin and its metabolites**

As the viability of cells may influence cellular iron release, prior to conducting iron mobilisation studies with quercetin and its metabolites, we ensured that viability was maintained >98% using the Trypan blue and LDH assays following treatment. HuH7 showed no signs of toxicity following 12 hours of treatment with all metabolites at 30µM using the LDH assay (**Table 15**) as well as the Trypan blue method (Figure 45). Similarly, quercetin, as well as the tested metabolites, did not appear to be toxic to H9C2 cells (**Table 15**) at the concentrations evaluated.

**Figure 45 Tryptan blue viability staining in HuH7 cells following a 12 hour treatment with quercetin and its metabolites at 30 $\mu$ M.** Cells were loaded with RPMI media containing 10% FBS (2x 10 hour changes). Adherent cells were rinsed four times, including one wash containing DFO at 30 $\mu$ M ibe and 3 x PBS washes, and subsequently exposed to test compounds for 12 hours. Supernatants were then removed, and the cells stained with Tryptan blue as described in the methods.

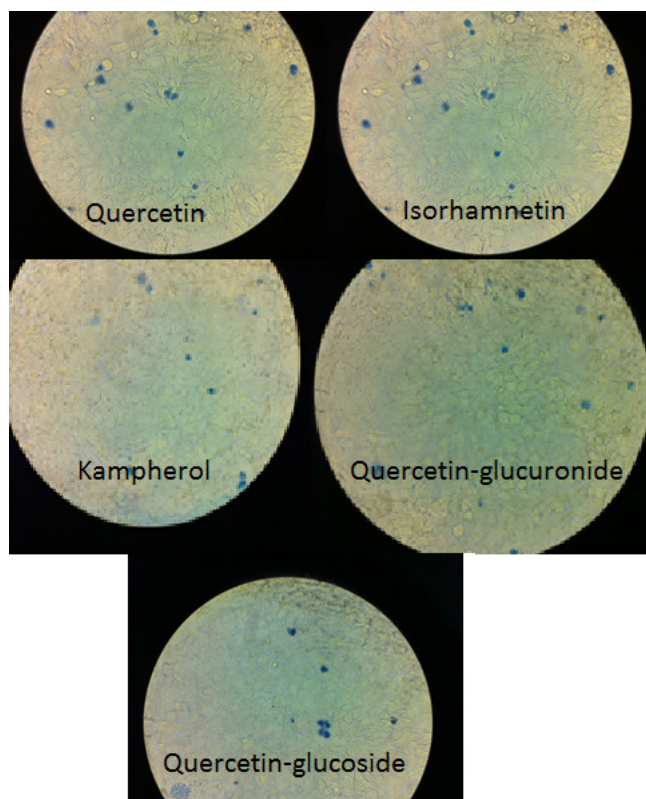


**Table 15 Percentage viability assessed by the LDH assay following 12 hours of treatment with quercetin and its metabolites at 30 $\mu$ M.** Cells were loaded with iron and treated with metabolites as in (Figure 45). Supernatants were then removed, and viability determined using the LDH assay as described in the methods.

	% viability following 12 hours of treatment at 30 $\mu$ M using the LDH assay	
	Hepatocytes (HuH7)	Cardiomyocytes (H9C2)
Quercetin	98.1 +/- 0.2	99.2 +/- 0.6
Isorhamnetin	99.2 +/- 1.1	98.7 +/- 0.8
Quercetin-glucoside	98.7 +/- 0.4	98.3 +/- 0.4
Kampherol	99.5 +/- 0.8	99.2 +/- 0.4
Quercetin-glucuronide	98.9 +/- 0.6	99.4 +/- 0.9

### 6.7.2 Quercetin decreases hepatocellular and myocardial iron in a time and concentration-dependent manner.

**Table 16 Percentage iron release from hepatocyte (HuH7) and cardiomyocyte (H9C2) cells following 8 hours of treatment with commercially available chelators at 30 $\mu$ M ibe and quercetin at 30 $\mu$ M.** Cells were loaded with iron as described in methods. Adherent cells were rinsed four times, including one wash containing DFO at 30 $\mu$ M ibe and 3 x PBS washes, and subsequently exposed to chelators for 8 hours. Chelator supernatants were then removed, and the cells washed four times as above before lysing with 200mM NaOH. Intracellular iron concentration was then determined using the ferrozine assay and normalised for total cellular protein in each well. Results shown are expressed as the % of T0 cellular iron released and are the mean  $\pm$  SEM of 4 replicates in one experiment. **Table 16** shows percentage iron release from hepatocyte (HuH7) and cardiomyocyte (H9C2) cells following 8 hours of treatment with commercially available chelators and quercetin. The cells were exposed to two 10 hour treatment periods with RPMI/DMEM containing 10% FBS to iron load the cells, and were then incubated with media without FBS, but with chelators at 30 $\mu$ M ibe or quercetin 30 $\mu$ M

for 8 hours. Following an 8 hour treatment, the iron removal was relatively similar for all three commercially available iron chelators in each cell type. Iron mobilisation with quercetin was found to be at 16.6% and 41.9% of total cellular iron in cardiomyocytes and hepatocytes respectively, making it only mildly a less effective chelator than DFO, DFX, and DFP in this model (**Table 16**). Given the availability of the all three ‘iron-binding motifs’ on the flavonoid structure; (1) 3-hydroxyl and carbonyl site (C ring) 2) 5-hydroxyl and carbonyl site (A and C rings) and 3) 3',4'-dihydroxy site on the B-ring, with a high affinity for binding of Fe(II) and Fe(III), the intracellular iron mobilisation noted in both cell types is not surprising.

**Table 16 Percentage iron release from hepatocyte (HuH7) and cardiomyocyte (H9C2) cells following 8 hours of treatment with commercially available chelators at 30µM ibe and quercetin at 30µM.** Cells were loaded with iron as described in methods. Adherent cells were rinsed four times, including one wash containing DFO at 30µM ibe and 3 x PBS washes, and subsequently exposed to chelators for 8 hours. Chelator supernatants were then removed, and the cells washed four times as above before lysing with 200mM NaOH. Intracellular iron concentration was then determined using the ferrozine assay and normalised for total cellular protein in each well. Results shown are expressed as the % of T0 cellular iron released and are the mean ± SEM of 4 replicates in one experiment.

	<b>% cellular iron removed following 8 hours of quercetin 30µM monotherapy compared with other chelators at 30µM ibe</b>	
	<b>Hepatocytes (HUH7)</b>	<b>Cardiomyocytes (H9C2)</b>
<b>DFO</b>	<b>47.3 +/- 2.9</b>	<b>22.2 +/- 1.3</b>
<b>DFP</b>	<b>44.6 +/- 1.2</b>	<b>17.5 +/- 0.9</b>
<b>DFX</b>	<b>44.4 +/- 2.3</b>	<b>27.6 +/- 1.7</b>
<b><i>Quercetin</i></b>	<b>41.9 +/- 0.7</b>	<b>16.6 +/- 0.6</b>

### 6.7.3 Cellular iron mobilisation by Quercetin metabolites.

The iron mobilisation properties of quercetin metabolites were next investigated. These included quercetin-3-glucoside and metabolites isorhamnetin, kaempferol and quercetin glucuronide. This allowed close interrogation of the effects of substitution of different hydroxyl groups at the iron binding sites on metal binding as a function of time and concentration. It can be seen that cellular iron is decreased by quercetin as early as 1h and at 3 $\mu$ M and 30 $\mu$ M. As expected, quercetin which has all three 'iron-binding' motifs available was the most effective at mobilising cellular iron in a time (**Figure 46**) as well as concentration-dependent fashion (**Figure 47**). Iron mobilisation sharply increases with as little as 3 $\mu$ M Quercetin (**Figure 47**) and appears to slow down after 4 hours at 30 $\mu$ M (**Figure 46**), similarly to DFO, DFX and DFP at 30 $\mu$ M (**Figure 18 B**). Quercetin-3- glucuronide, which has a glucuronide substitution at site 3 on the C ring (**Figure 42**), produced an only minimal reduction in cellular iron at 8 hours. Interestingly, quercetin-3 glucoside which has a glucose substitution at the same site was also inefficient at iron mobilisation. The efficacy of tested compounds increased in the following order: quercetin-3-glucuronide, kaempferol, quercetin-3-glucoside, isorhamnetin, and quercetin. Isorhamnetin mobilised 34.7% following 8 hours of treatment (vs. 41.9% with quercetin treatment) (**Figure 47**). The inhibition of iron chelating function of quercetin noted here by substitution of site 3 on the C ring in particular, following metabolism, for example to the glucuronide and glucoside structures, highlights the importance of this particular site which is known to be preferred in iron chelation (Guo et al, 2007). It is also noted that Kaempferol, that has no substitution on the C-ring and hence at site 3 or at site 5 on the A ring, is also poor at iron mobilisation. However, in the case of Kaempferol, the hydroxyl group on the 3' site of the B ring is absent. This finding highlights that iron mobilisation is not only dependent on substitutions at the known iron binding sites, but the configuration of the molecule and number of hydroxyl groups is also of pivotal importance for a molecule to function as an iron chelator and/or to shift iron from the intracellular to the extracellular compartment.



**Figure 46** Time course of change in intracellular iron content using monotherapy with quercetin and its metabolites at (A) 3  $\mu$ M and (B) 30 $\mu$ M and in HuH7 cells. Cells were loaded with iron, treated with chelators and intracellular iron concentration determines as in (Table 16). Results shown are the mean  $\pm$  SEM of 4 replicates in one experiment.

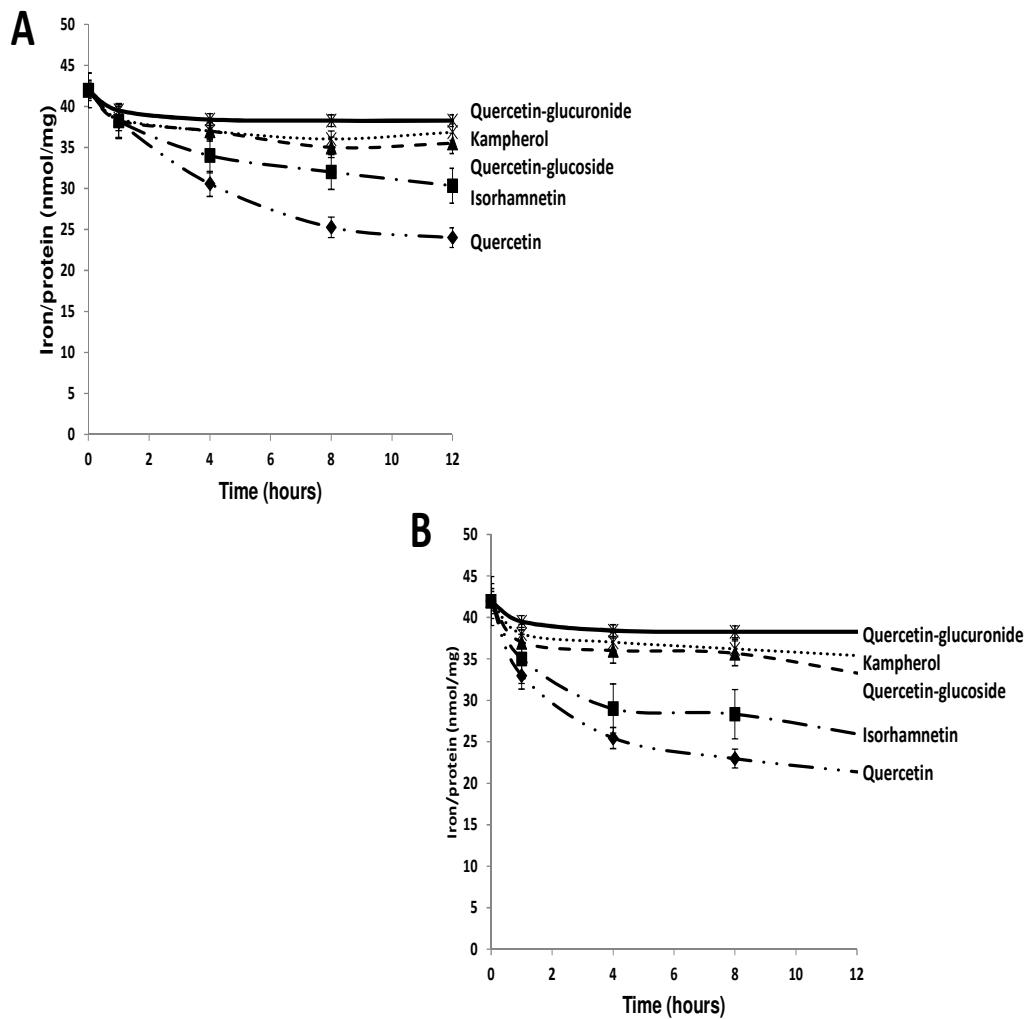
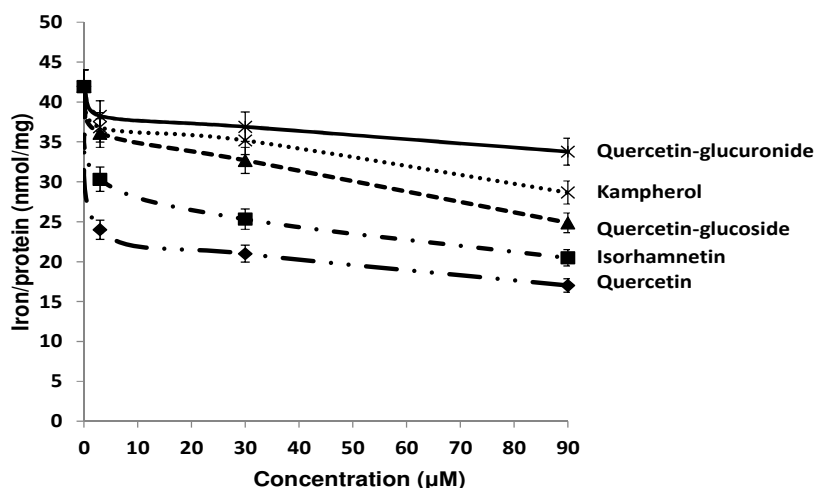


**Figure 47 Concentration dependence for change in cellular iron at 8h after monotherapy with quercetin and its metabolites in HuH7 cells.** Cells were loaded with iron, treated with chelators and intracellular iron concentration determines as in (Table 16). Results shown are the mean  $\pm$  SEM of 4 replicates in one experiment.

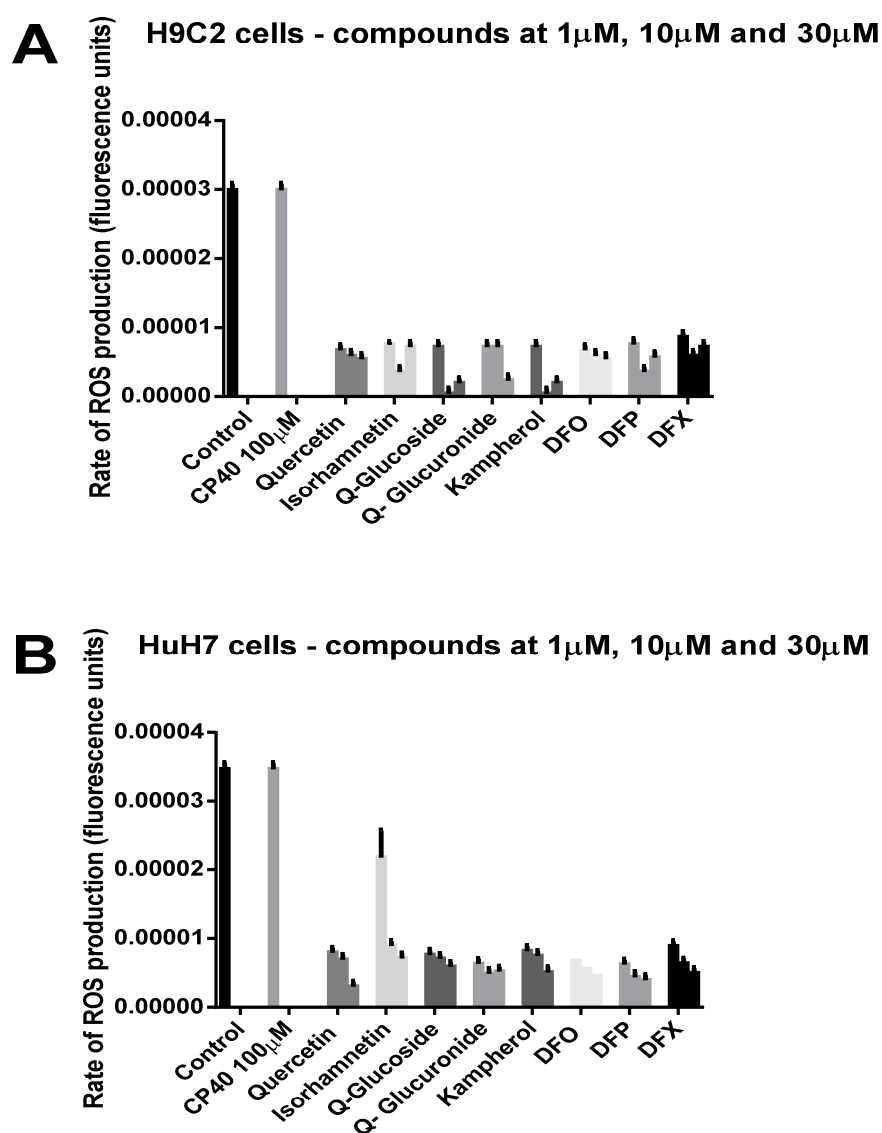


#### 6.7.4 Quercetin and its metabolites rapidly decreases ROS compared with other chelators

Following a close look at the effect of substitutions at the iron chelating motifs of the quercetin molecule and the impact on iron mobilisation, we wished to evaluate ROS scavenging properties of quercetin glucoside and the quercetin metabolites. The capacity of flavonoids to act as antioxidants is one that is very well recognised. A cell-permeable oxidation and hydrolysis sensitive fluorescent probe was used for this purpose as described in methods. After iron loading cells as previously described, they were preloaded with the non-fluorescent DCFH-DA (Molecular Probes, Leiden, Netherlands) for 30 minutes at 37<sup>0</sup>C, allowing time for commencement of hydrolysis to the highly fluorescent DCFH. Compounds were added to each well and then placed into the plate reader where fluorescence was recorded over 1 hour at 37<sup>0</sup>C. The interval between addition of chelators and commencing ROS recording on the plate reader was between 3 and 5 minutes.

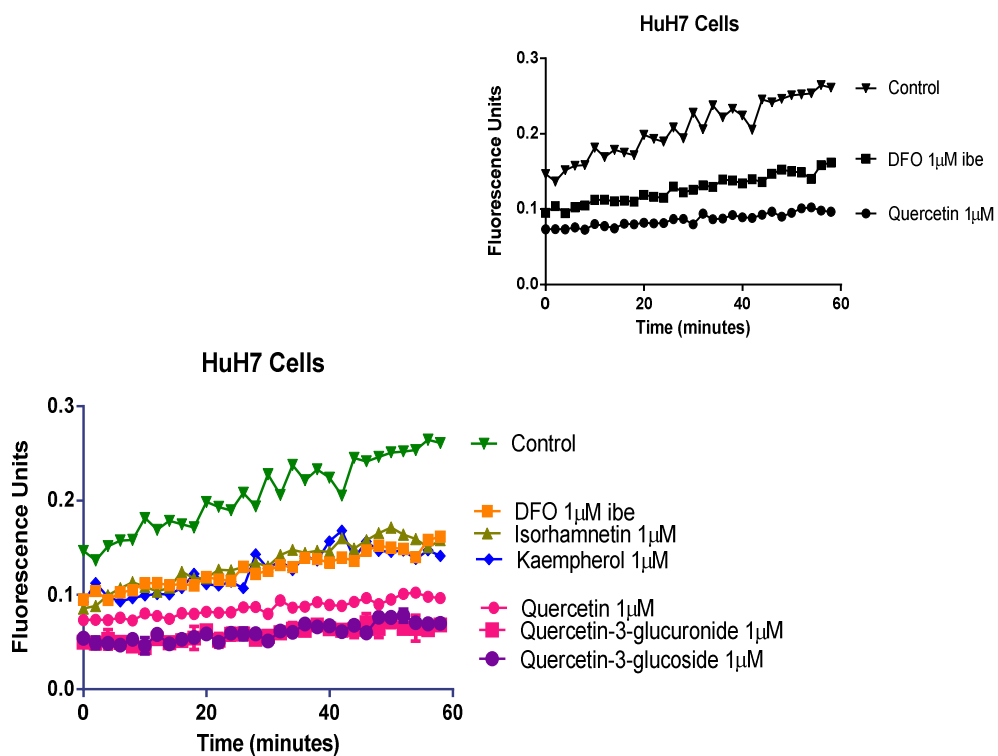
In **Figure 48** the concentration dependence of ROS inhibition by Quercetin-3-glucoside, Quercetin as well as all its metabolites in HuH7 and H9C2 cells is shown together with the commercially available chelators DFO, DFX, and DFP. Interestingly, the rate of ROS production at 1 hour is suppressed very effectively and equally amongst the flavonoids and the commercially used iron chelators.

**Figure 48** Concentration dependent ROS inhibition by Quercetin and its metabolites and commercially available chelators in cardiomyocytes (A) and hepatocytes (B). Cells were iron loaded and then rinsed four times as described in (Table 16). Chelators were then added, and the rate of change of ROS production was recorded as fluorescence change (excitation at 504 nm, emission at 526 nm) continuously over 1 hour in the plate reader at 37°C. DFO, DFP, and DFX were used at 1, 10, 30µM, and Quercetin and its metabolites at 1, 10, 30µM.



In (**Figure 49**) it can be seen that from the first measurable time-points, the fluorescence signal with all metabolites was less than control, suggesting very rapid entry of compounds to decrease ROS. Looking more closely at the time course of ROS production (**Figure 49**), despite all chelators decreasing ROS production at a comparable rate (i.e. the slope of the curve if the initial T0 value is normalised), it can be seen that in terms of absolute ROS amounts, the most potent scavengers were quercetin, quercetin-3-glucuronide, and quercetin-3-glucoside (cellular protein comparable between wells). Interestingly, Kaempferol and Isorhamnetin (molecule which effectively mobilises iron) which have substitutions at the 3' site of the B-ring lag behind, with rates comparable to DFO, when looking at absolute amounts of ROS. This could reflect slower uptake of these compounds into cells, comparable to those of DFO, or an inherently lower capacity to scavenge ROS. This highlights the importance of the hydroxyl groups in the 3' and 4' position of the B ring in terms of radical scavenging and provides structure-to-function insight regarding iron chelation and antioxidant capacity (see discussion).

**Figure 49** The time-course for ROS inhibition by DFO 1 $\mu$ M ibe, Quercetin, Quercetin-3-glucoside and Quercetin metabolites at 1 $\mu$ M in HuH7 cells. Cells were loaded iron, and ROS generation recorded over 1 hours as described in (Figure 48).

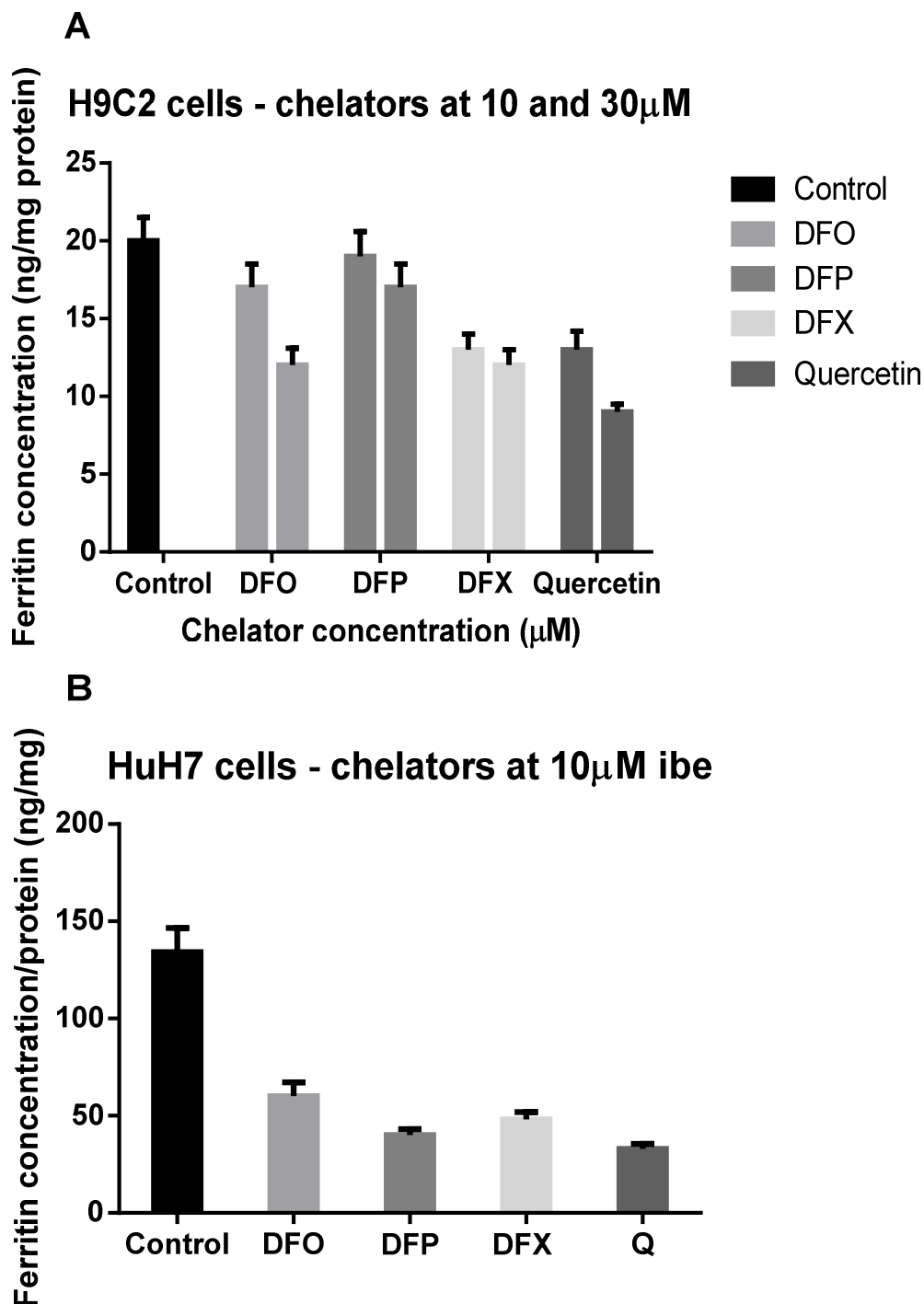


### 6.7.5 Quercetin and its metabolites decrease intracellular ferritin

It was important to understand how the decrease in cellular iron and ROS generation seen above reflects in the mobilisation of storage iron (ferritin). HuH7 cells and H9C2 cells were iron-loaded as described in the methods section above using two media changes containing 10% FBS. This increased tissue ferritin by 75% in hepatocytes and by 33% in cardiomyocytes (**Figure 22**), and increased total cellular iron by 4 and 2.5 fold respectively. Cells were then treated with DFO/DFP/DFX/quercetin monotherapy for 8 hours and cellular ferritin assayed as described in methods.

In HuH7, quercetin achieved a dose-dependent decrease in ferritin at 10 $\mu$ M and 30 $\mu$ M. At 30 $\mu$ M it was, in fact, more effective than all 3 commercially available iron chelators at mobilising cellular ferritin, reducing the total concentration by 45% (Figure 50). In cardiomyocytes, quercetin was particularly effective at decreasing ferritin at 10 $\mu$ M (75.4%) (Figure 50), similar to DFX at 10 $\mu$ M (70.1%). Thus chelation with quercetin decreases both total cellular iron (**Table 16**) and cellular ferritin (Figure 50) in both cell types with ferritin decrements being proportionately greater in HuH7 than H9C2 cells. Evidently, therefore, hepatocyte ferritin is more responsive, both to iron loading and iron unloading than in cardiomyocytes, which is consistent with the known high iron storage capacity of hepatocytes compared with cardiomyocytes. Ferritin decrements at 8h with quercetin compared with DFO/DFP/DFX in (A) cardiomyocyte H9C2 cells (B) hepatocyte HuH7 are shown in Figure 50.

**Figure 50 Ferritin decrements at 8h with quercetin or DFX, DFP or DFO in (A) cardiomyocyte H9C2 cells and (B) in hepatocyte HuH7.** Following iron loading as described in the methods section, the cells were rinsed four times including one wash containing DFO at 30 $\mu$ M ibe and 3 PBS washes and subsequently exposed to chelators over an 8 hour period. At the end of the incubation, the supernatant was removed, and the cells further washed four times as above. Ferritin was quantified using commercially available ELISA kits appropriate for our rat and human cell lines, as described in methods. The results are the mean  $\pm$  SEM of 3 replicates in one experiment.

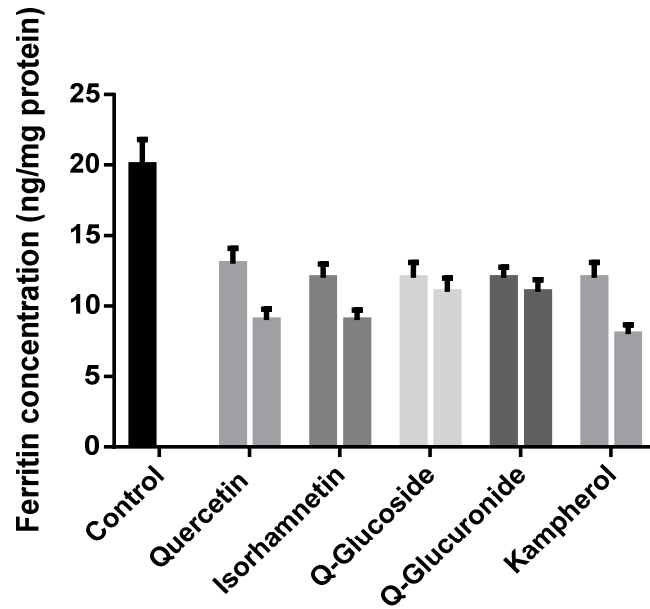


The effects of flavonoids, some of which had showed little iron binding and removal were then examined (**Figure 51**). quercetin-glucuronide, Kampherol, quercetin-3-glucoside, and isorhamnetin were also effective at mobilising storage iron (ferritin). Interestingly in both cell types, all derivatives are able to decrease ferritin concentration in a dose-dependent manner at 10 and 30 $\mu$ M, being nearly as effective as the unmetabolised ligand. While the effectiveness of for example quercetin and isorhamnetin could be attributed to cytoplasmic iron chelation leading to mobilisation of Fe(III) from ferritin, this is less likely when considering the weaker chelation properties of quercetin-glucuronide (**Figure 47**). Therefore, some of the ferritin decreasing effects could be unrelated directly to iron chelation and may relate to their strong antioxidant effects demonstrated above. This could occur because reduction in ROS levels is known to increase iron-responsive elements (IRP) which leads to a decrease in ferritin synthesis (see discussion) (Cairo et al, 1998).

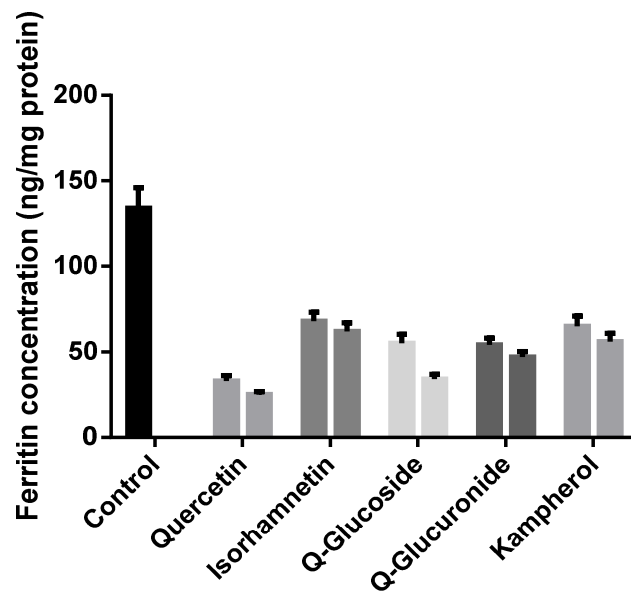


**Figure 51 Ferritin decrements at 8h with quercetin and its metabolites in (A) cardiomyocyte H9C2 cells and (B) in hepatocyte HuH7. Cells were loaded with iron, treated with chelators and ferritin determines as described in Figure 50. The results are the mean  $\pm$  SEM of 3 replicates in one experiment.**

**A H9C2 cells - compounds at 10 $\mu$ M and 30 $\mu$ M ibe**



**B HuH7 cells - compounds at 10 $\mu$ M and 30 $\mu$ M ibe**



### **6.7.6 Synergistic iron mobilisation by combinations of Quercetin or its metabolites with clinically available chelators.**

In principle the addition of Quercetin containing foods to standard clinically used chelation regimens could enhance the efficacy of the latter. In this section, the effects of Quercetin alone is compared with those of Quercetin when combined with clinically available iron chelators in terms of intracellular iron mobilisation.

### **6.7.7 Iron mobilisation by quercetin and its metabolites combined with commercially available chelators in HuH7 cells**

The relative effects of combining flavonoids at increasing concentrations with DFO, DFP, and DFX at 10 $\mu$ M ibe on cellular iron removal from HuH7 cells are shown in **Figure 52**. Cells were loaded with iron as described in methods, with two media changes containing 10% FBS for 10 hours. Adherent cells were rinsed four times, including one wash containing DFO at 30 $\mu$ M ibe and 3 x PBS washes, and subsequently exposed to chelators for 12 hours.

When quercetin or its metabolites were combined with either DFO, DFP or DFX at 10 $\mu$ M ibe, quercetin produced greater increase in cellular iron mobilisation than all other quercetin derivatives. For example, at the lowest concentration tested of 3 $\mu$ M, Quercetin improved mobilisation by 2.6, 2.5 and 2.3 fold when combined with DFO, DFX or DFP at 10 $\mu$ M ibe.

The metabolite isorhamnetin was also particularly effective, in contrast to for example quercetin-glucuronide which only mildly enhanced iron mobilisation when combined with 10 $\mu$ M ibe of commercially available chelators. As isorhamnetin is one of the main metabolites of quercetin in human plasma (Burak et al, 2015), we wished to examine its potential to act as a shuttle for iron(III) more extensively when combined with DFO/DFX/DFP, in hepatocytes. Cells were loaded with iron as described in methods and treated with chelator combinations for 8 hours. Intracellular iron concentration was then determined using the ferrozine assay and normalised for total cellular protein. **Figure 53** shows that isorhamnetin is able to enhance iron mobilisation when combined with DFO/DFX/DFP in a concentration-dependent manner. Following 8 hours of treatment at only 1 $\mu$ M it enhances iron decrements by

2.1, 1.3 and 1.6 fold when combined with 10 $\mu$ M of DFO, DFP and DFX respectively, making it almost as potent as quercetin in enhancing iron mobilisation at small concentrations.

Overall this data suggest that quercetin and its derivatives possess the ability to increase iron mobilisation from cells when combined with clinically available chelators. The relative efficacy of the derivatives of quercetin when combined with other chelators, reflect the relative efficacy of these compounds when used alone. The data obtained comparing different metabolites show the importance of preservation of the hydroxyl group in site 3 of the C ring for effective iron chelation (see **Figure 42**).

**Figure 52 Decrements in HuH7 cellular iron by DFO/DFX/DFP combined with Quercetin or its metabolites.** Cells were loaded with iron, treated with chelators and intracellular iron concentration determines as in Figure 47. Results are the mean  $\pm$  SEM of 6 replicates in one experiment.

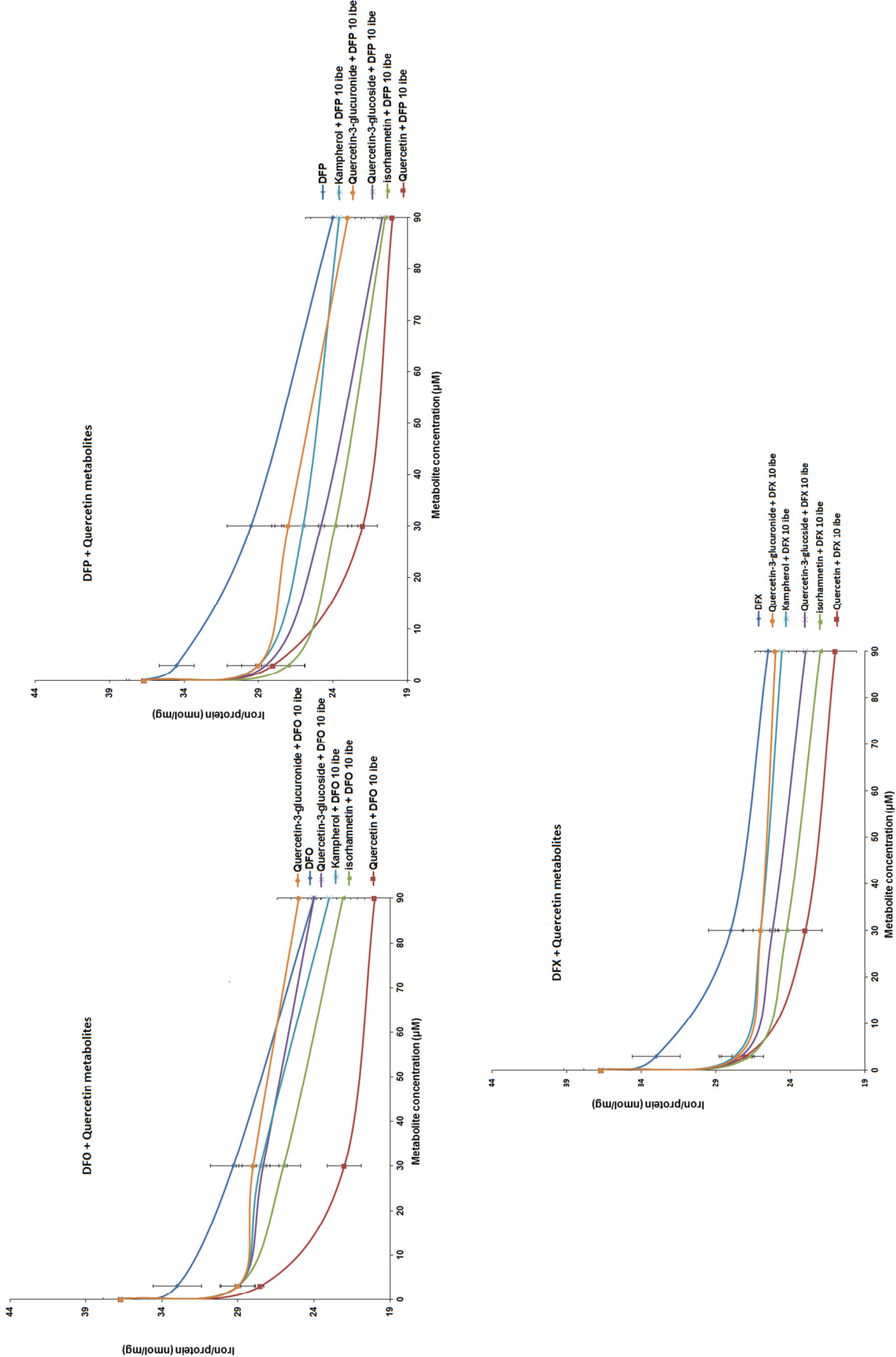
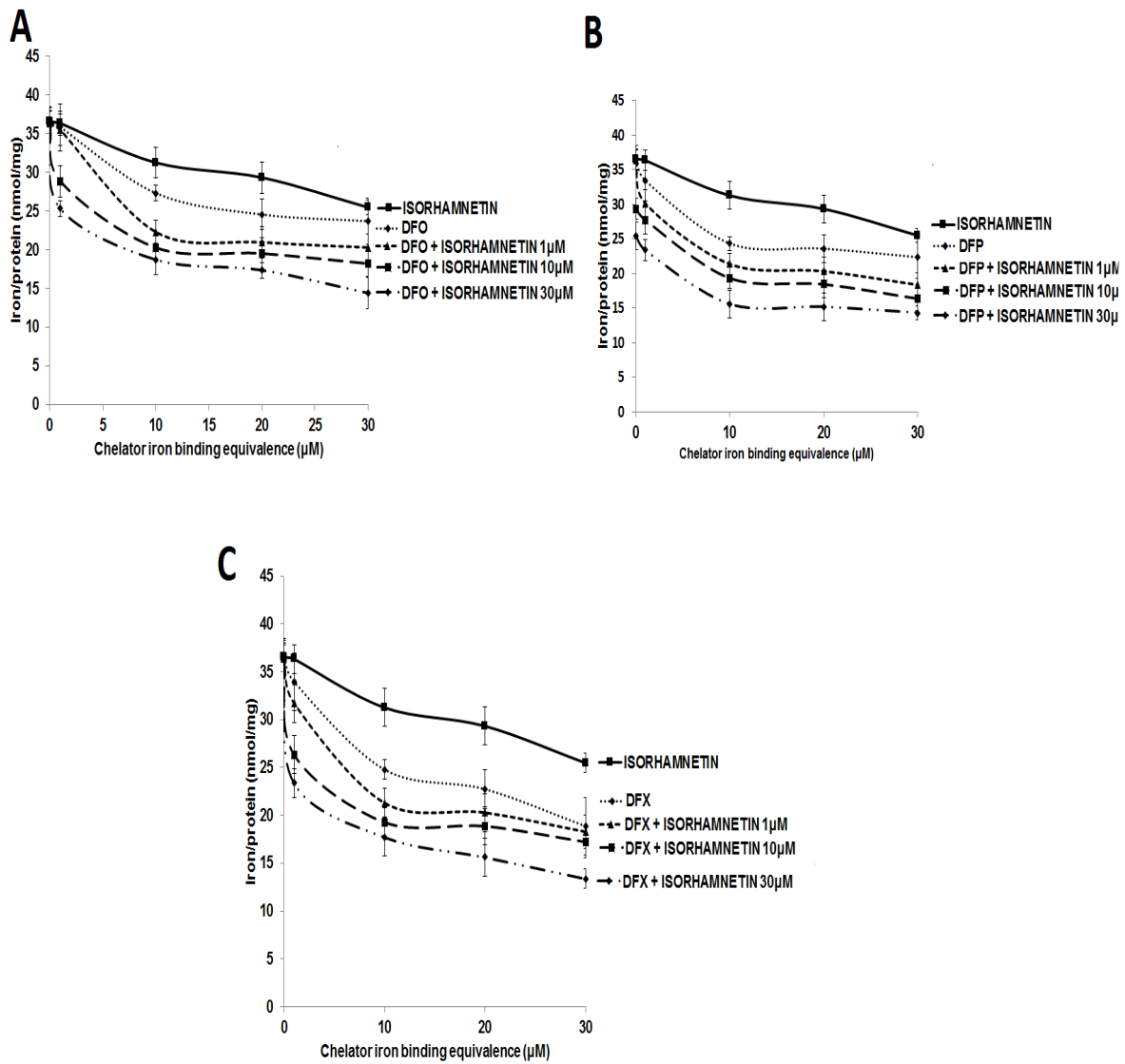


**Figure 53. Decrements in cellular iron in H9C2 cells by combinations of Isorhamnetin with clinically available iron chelators following 8 hours of treatment.** (A) DFO-Isorhamnetin, (B) DFP-Isorhamnetin, (C) DFX-Isorhamnetin. Cells were loaded with iron, treated with chelators and intracellular iron concentration determines as in **Figure 47**. Results are the mean  $\pm$  SEM of 3 replicates in one experiment.



### 6.7.8 Quercetin isobolograms and the synergy index $\alpha$

The issue of synergy vs. additivity of action of quercetin and commercially available iron chelators was further addressed by the use of isobolograms. As discussed in the methods section, the isobologram is a mathematical model used to distinguish between the synergistic, additive or subadditive response of drug combinations (Tallarida, 2006) where rectangular coordinates of dose combinations (a,b) that produce the same chosen effect level are shown; in this case 50% of the maximum response. **Figure 53** shows the isobolograms for combinations of the three commercially used chelators for a 50% chelation effect with quercetin. HuH7 cells were iron loaded with serial media changes as previously described and treated with chelators for 8 hours. In all three cases, a curved response was produced below the line of additivity, indicating a synergistic action. The axis intercepts again represent the IC<sub>50</sub> for each chelator compound when used in isolation (i.e., the potency; e.g., 16.7 $\mu$ M ibe for DFP). The degree of synergism was further examined below by looking at the synergy index  $\alpha$ .

As previously discussed (**Section 4.6.1**), this index is a representation of how much of the obtained effect exceeds that expected by additivity of the two compounds. It is equivalent to  $(1 - 1/R) \times 100$  where R = difference of area under the line and area under the curve of the isobologram (Tallarida, 2001) and was derived using data generated from the program 'Prism 5'. It was noted that when quercetin and DFO are combined, 56.3% of the chelation effect is due to synergy. In the quercetin-DFP combination, 60.6 % of the total effect was due to synergy and interestingly this appears to be the most synergistic combination, even when comparing commercially available iron chelator combinations. The synergy of action noted is very likely to be attributed to the potential of quercetin to act as an effective 'shuttle' of iron to a 'sink'.

**Figure 54** Quercetin and commercially available chelator combination isobolograms in HuH7 cells.

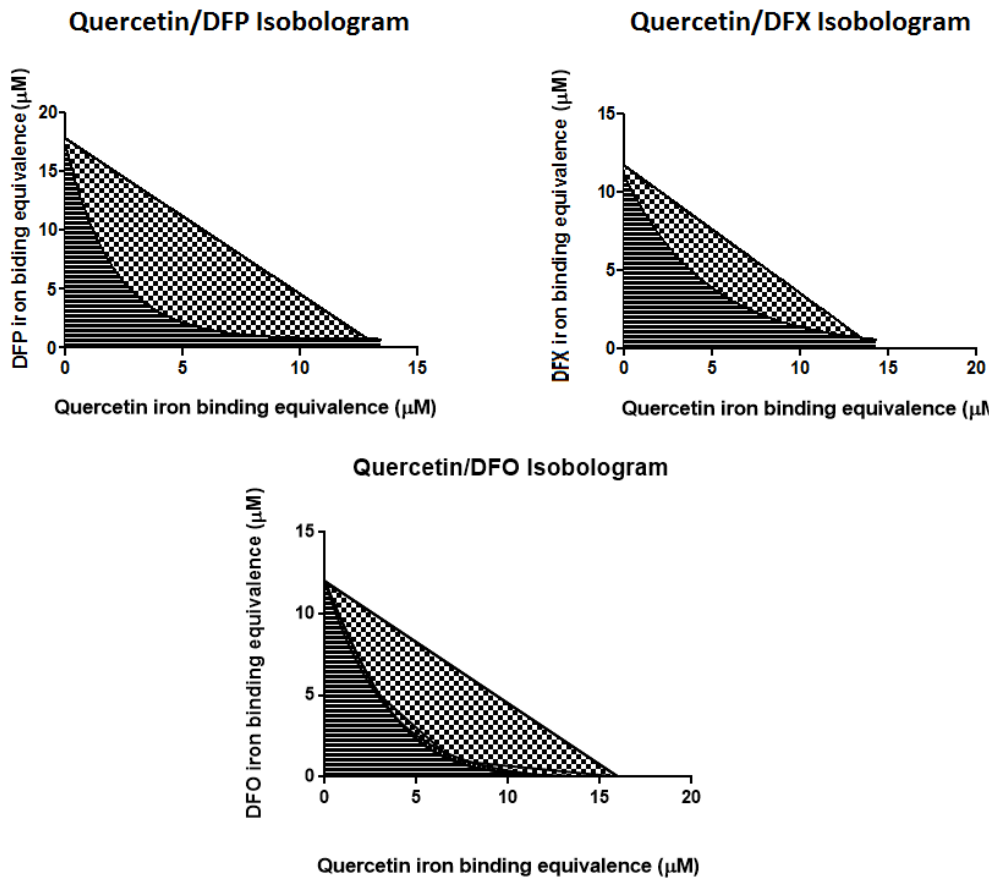


**Table 17 Synergy Index ‘ $\alpha$ ’ for the combination treatment of commercially available chelators with quercetin in cardiomyocyte (H9C2) cells.** This index is a representation of how much of the obtained effect exceeds that expected by additivity of the two compounds (Section 4.6.1).

Chelator Combination	Synergy Index ( $\alpha$ )
DFO - DFX	37.0 +/- 2.1
DFO - DFP	47.4 +/-3.2
DFX - DFP	51.5 +/- 2.9
Quercetin - DFO	56.3 +/- 3.2
Quercetin - DFP	60.6 +/- 1.9
Quercetin - DFX	45.9 +/- 2.7

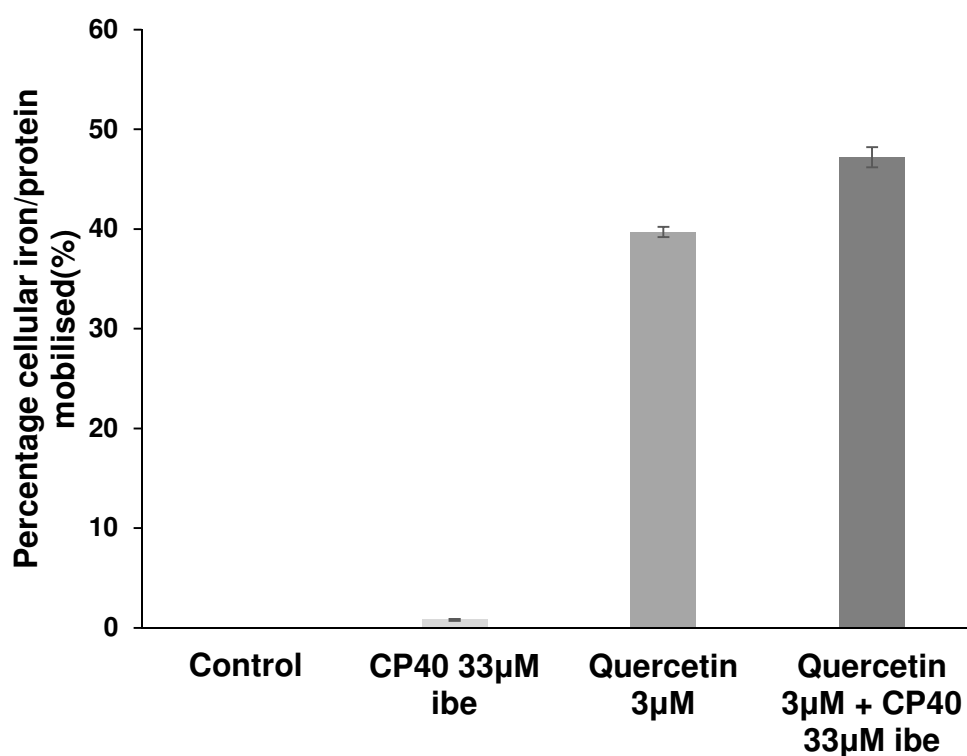
### 6.8 Synergistic chelation of Quercetin combined with otherwise ineffective hydroxyridinone CP40

To demonstrate synergistic iron chelation and distinguish from ‘additivity’ of action when quercetin is combined with a second chelator, we examined CP40 (a hydroxypyridone chelator with a high iron binding constant that is ineffective at mobilising cellular iron due to its inability to permeate cell membranes) (Porter et al, 1988; Porter et al, 1990). In Figure 55 , it can be seen that CP40 alone does not enhance cellular iron removal, confirming previous observations in **Chapter 4** in primary hepatocytes (Porter et al, 1988; Porter et al, 1990). When CP40 was combined with quercetin, however, an increase in cellular iron removal was seen, greater than with quercetin alone. This provides further mechanistic insight into how combinations of commercial chelators with quercetin interact. It supports the concept that quercetin in combined therapy has the potential to act as a shuttle here donating



iron chelated intracellularly to the extracellular CP40. Since CP40 has very little access to intracellular iron when used alone, it cannot act as an intracellular iron shuttle but as a passive extracellular acceptor of iron within cells by another chelator. The increase in cellular iron mobilisation observed when CP40 33 $\mu$ M ibe was combined with quercetin 3 $\mu$ M is likely due to an increase in the 'sink' total concentration in the extracellular medium. Therefore, quercetin can act as an intracellular shuttle onto CP40, which remains exclusively in the extracellular compartment.

**Figure 55 Cellular iron mobilisation is shown in previously iron loaded HuH7 cells, after 8 hours of exposure to quercetin 3 $\mu$ M and/or CP40 33 $\mu$ M ibe as single agents and combination. Chelator supernatants were then removed and cellular iron determined as described above. Results are the mean  $\pm$  SEM of 4 replicates in one experiment.**



## 6.9 Discussion

In this chapter, naturally occurring iron chelators, present in human diet, that are also known to be potent antioxidants were used to interrogate the relationship between the structure and function of naturally occurring flavonoid chelators in terms of iron mobilisation and ROS scavenging properties. The progressive removal of total cellular iron by quercetin in hepatocyte (HuH7) and cardiomyocyte (H9C2) cell lines has been shown. Surprisingly, quercetin monotherapy at 30 $\mu$ M proved only just inferior at mobilising cellular iron in the cardiomyocytes (16.6%) and hepatocytes cell line (41.9%) to DFP for example which mobilised 44.6% of hepatocyte and 17.5% of total cardiomyocyte iron at 30 $\mu$ M ibe following 8 hours of treatment (**Table 16**).

With respect to metabolites of quercetin, even with a low concentrations of 3 $\mu$ M of the quercetin aglycone, mobilisation of iron is seen as early as 1 hour of treatment (**Figure 46**). Closely investigating the iron mobilisation properties of isorhamnetin, quercetin-glucoside, kaempherol and quercetin glucuronide further, sheds light on the different iron binding motifs of phenolics and their importance for effective iron chelation. Isorhamnetin, which has a methyl group substituted at the 3' hydroxyl group on the B ring, is almost as effective in iron mobilisation as the quercetin aglycone in hepatocytes (34.7% vs. 41.9%). However, substitution of a glucuronide or a glucoside at site 3 on the C ring decreases iron mobilisation to 13% and 26% respectively following 8 hours of treatment in HuH7 cells at 30 $\mu$ M (**Figure 46**). The above results confirm that the preferred Fe(II) iron binding motif is indeed the 3-hydroxyl and carbonyl site on the C ring. Furthermore, it is not only key for iron chelation but also pivotal in iron binding and enabling the molecule to act as a shuttle. Isorhamnetin proved to at only 1 $\mu$ M enhance iron mobilisation by 2.1, 1.3 and 1.6 fold (quercetin enhanced by 2.6, 2.5 and 2.3) when combined with 10 $\mu$ M ibe of DFO, DFP, and DFX respectively. The synergistic potential of quercetin was once again confirmed by utilising the extracellular iron chelator CP40, which has no inherent iron mobilisation effects of its own, and lead to enhancement of iron mobilisation when it is combined with quercetin (**Figure 55**). This experiment provides evidence that quercetin indeed acts as a true 'shuttle' of iron out of cells. As CP40 cannot enter cells (Porter et al, 1988; Porter et al, 1990) and has no inherent iron mobilising properties the only way in which cellular iron mobilisation can be enhanced is by quercetin chelating iron

within cells and then donating iron(III) to the extracellular 'sink' that is CP40. We predict that quercetin binds more weakly to iron(III) than CP40 at low concentrations, as seen by the iron shuttling with quercetin at  $3\mu\text{M}$  and CP40  $33\mu\text{M}$  ibe, however speciation plots using increasing quercetin concentrations are required in order to predict at what concentration quercetin will begin to compete with CP40 for iron(III) binding.

The effect on ROS scavenging of the structurally related flavonoids that are metabolites of quercetin, provides insight into the rates of access of these compounds to intracellular iron pools as well as to the differences and similarities of antioxidant and chelating effects of these compounds. The findings adds insight into the relationship between the structure and function in this respect. The kinetics of rate of ROS inhibition with all tested compounds are very rapid, occurring at the first measurable time point (**Figure 48**) confirming that the hydroxyl groups on the B ring (Figure 44) is crucial for scavenging ROS, and as previously quoted in the literature the 3' and 4' hydroxyl groups are the ones to readily donate a hydrogen and an electron to neutralise radicals (Cao et al, 1997). Stable radical formation is favoured by the carbon backbone structure of flavonoids that allow for free movement of an electron across it (delocalisation), increasing stability. In terms of absolute values of ROS, it is noted that Kaempferol and Isorhamnetin are the least effective scavengers, once again highlighting the importance of the 3' hydroxyl group on the B ring (Figure 44). There is limited knowledge to date on the structure-activity relationship of quercetin (Brown et al, 1998), and this is the first report investigating this in the quercetin metabolites with regards to their iron mobilising and antioxidant/antiradical activity. Importantly, while quercetin glucuronide and quercetin-3-glucoside are effective ROS scavengers (**Figure 48**) they are ineffective at mobilising cellular iron (**Figure 46**). While this could in principle be due to the inability of iron complexes of these compounds to egress from cells, it is more likely that these compounds are ineffective iron chelators because as discussed above they are metabolised at the iron-binding sites of the C ring. This demonstrates therefore that metabolites of quercetin and presumably those of quercetin itself possess free radical scavenging properties that are independent of the iron chelating properties. Thus, with regards to iron mobilisation, the 3-hydroxyl and carbonyl site on the C-ring allows iron binding and enhances the property of a

flavonoid to act as an iron shuttle, but inhibition of this function is not correlated with antioxidant activity as this is mostly dependent on the 3' hydroxyl group on the B ring.

However, prediction of the physiochemical activity of a molecule is not purely based on its configuration and availability of hydroxyl groups. An important contributor to the pro/antioxidant activity of molecules is their partition coefficients ( $\log P$ ), where  $P$  is the ratio of the concentration of the molecule in octanol to the aqueous concentration at pH 7.4. The partition coefficient is used as an indicator of the affinity of a compound to cross membranes *in vivo* and determine their absorption, distribution, and biological effects. The partition coefficient and the ability to diffuse through plasma membranes cannot be considered similar for all flavonoids given their variation in structure and physiochemical properties. Only molecules of appropriate lipophilicity can diffuse across phospholipid membranes, and in general, flavonoid aglycones tend to be more lipophilic than any conjugates. Quercetin has a partition coefficient of  $1.82 \pm 0.32$  vs. Kaempferol  $3.11 \pm 0.54$  and quercetin-3-glucoside  $0.32 \pm 0.02$ , demonstrating the approximately equal distribution of quercetin between aqueous and lipophilic compartments. Quercetin-3-glucoside will, however, permeate cells more readily than both the quercetin aglycone and Kaempferol, and this is a property that can contribute to the enhanced ROS scavenging of quercetin-3-glucoside and quercetin-3-glucuronide noted above.

We wished to understand how the decrease in cellular iron and ROS generation seen above reflects in the mobilisation of storage iron (ferritin). In HuH7, quercetin achieved a dose-dependent decrease in ferritin at  $10\mu\text{M}$  and  $30\mu\text{M}$ . At  $30\mu\text{M}$  it was, in fact, more effective than all 3 commercially available iron chelators at mobilising cellular ferritin, reducing the total concentration by 45% (Figure 50). Given the strong iron mobilisation properties of quercetin, this is not surprising. Interestingly in both cell types, all the structurally related flavonoids tested were able to decrease ferritin concentration in a dose-dependent manner at 10 and  $30\mu\text{M}$ , being nearly as effective as the unmetabolised ligand. There are a number of potential explanations for this discussed below.

Ferritin stores Fe(III) in a 24 subunit multimer that is a combination of light and heavy chains. Iron must be released from ferritin to be biologically active. Ferritin

degradation involves autophagic and non-autophagic pathways, which are evolutionary pathways essential for maintaining iron homeostasis. Turnover of the ferritin protein is a constant process in the cell. Autophagy through lysosomal mechanisms appears to be the main degradation in iron deficiency; whereas non-autophagic pathways dominate in iron sufficiency. Recently, the nuclear receptor coactivator 4 (NCOA4) was identified as a key protein for mediation of ferritin autophagy (Mancias et al, 2014). Chelators such as DFO and DFX (Mancias et al, 2014) have been shown to activate NCOA4 mediating ferritin autophagy. Considering the iron chelating properties of our flavonoids, mediation of NCOA4 levels and stimulation of the ferritin autophagy pathway is a possible explanation for the low levels of ferritin noted following 8 hours of treatment in hepatocytes and cardiomyocytes (**Figure 51**).

Alternatively, some of the ferritin decrements may be unrelated to iron chelation and demonstrate a response to the strong antioxidant effects of the flavonoids demonstrated above. (This is consistent with data showing how some of ferritin synthesis is controlled by factors independent of iron that are more dependent on free radicals). Excess iron is 'sensed' by iron-responsive proteins (IRP) which bind to iron responsive elements (IRE) on the ferritin molecule modulating synthesis. IRP has been previously shown to be regulated by the redox state *in vitro* as well as in cell cultures (Hentze et al, 1989; Müllner et al, 1992). Furthermore, it has been demonstrated in rats that ferritin synthesis in the liver is stimulated by oxidative stress, and there is down-regulation of IRP binding. This effect could be partly modulated by iron chelation, however, it can also be attributed to ROS independently as they play a fundamental role in the maintenance of the conformation of IRP, being a direct target for ROS (Philpott et al, 1993). ROS lowers IRP levels, increasing iron sequestration (Cairo et al, 1998). In our model, the marked reduction in ROS is likely to lead to an increase in IRP and a reduction of ferritin synthesis/increased degradation. Our data suggest there may be differences between different cell types in the relative dependence of iron or free radical induced ferritin synthesis. Thus in the H9C2 cells all metabolites of quercetin are approximately as effective as each other in decreasing ferritin synthesis. In contrast, in HuH7 cell quercetin is the most effective. Since quercetin is also the most effective at iron mobilisation, and it is possible that ferritin

synthesis in the hepatocytes, like in HuH7 cells where iron is stored, is relatively more dependent on iron than in cardiomyocytes that are not significant sites of iron storage.

## **6.10 Conclusion**

In this chapter, we have demonstrated the iron mobilising properties of quercetin and its principle metabolites from cells for the first time and demonstrated their ability to act as an iron ‘shuttle’ when combined with clinically available chelators. Metabolism of quercetin will not abolish its iron mobilisation properties as a large number of its metabolites share its iron chelating properties. The doses of quercetin, alone or in combination with other chelators, are sufficiently low and clinically achievable to suggest quercetin could be used as an adjunct to iron chelation, with the DFP-Quercetin combination appearing to be the most synergistic. Furthermore, we have provided a unique structure-function analysis of flavonoids with regards to iron mobilisation and antioxidant capacity as a function of Fe(II) binding.

## **Chapter 7 DEVELOPMENT OF AN IRON-OVERLOADED MOUSE MODEL FOR TESTING THE ORAL EFFICACY OF IRON MOBILISATION WITH FLAVONOIDS ALONE OR IN COMBINATION WITH OTHER IRON CHELATION**

### **7.1 Rationale for developing a murine model where cardiac iron overload is achieved**

The current clinical management of  $\beta$  thalassaemia major involves a lifelong dependence on regular blood transfusions, a consequence of which is systemic iron overload which most importantly includes the liver and heart, and chronic use of iron chelators in order to manage this complication. Until very recently, death secondary to heart failure resulting from cardiac iron overload is the leading cause of mortality in patients with  $\beta$  thalassaemia major. A key requirement of iron chelators is the removal and prevention of excess cardiac iron loading. Therefore, a critical aspect of a putative model to study iron overload is cardiac iron loading within cardiomyocytes and not only in the interstitium of the myocardium and the epicardium.

### **7.2 Mouse models of cardiac iron-overload**

Early models for evaluating iron loading have been described in **Section 1.6.5**. Here we review some of the recent models using iron dextran, ferrocene and carbonyl iron to load iron into the heart.

The effect of DFX and DFO treatment has been studied on iron loaded gerbils with respect to cardiac iron (Wood et al, 2006). In this work, iron dextran 200mg/kg was injected (ip) weekly for 10 weeks to induce iron loading, and was followed by an iron redistribution period of 13 days. On Perls stain of the hearts, iron was noted to be absent from within the myocytes and likely accumulated within macrophages in the extracellular matrix. It may be possible that gerbils may excrete iron via the faecal route twice as rapidly as mice, therefore, a protocol of daily injections may have been more appropriate in the animal. Furthermore, 13 days may not have been sufficient for the iron from the iron dextran to have accumulated and be redistributed within the myocardium, and hence a longer re-equilibration period may need consideration.

In a heterozygous  $\beta$  thalassaemia mouse model (Yatmark et al, 2014), mice were injected with a total of 180mg of iron (20mg/daily) for two weeks, and there was a 3 day re-equilibration period prior to a 7-day treatment with DFO and DFP to investigate effects on liver and cardiac iron. A group of mice were sacrificed 10 days following the end of iron dextran treatment. The histology Perls stain images show large clumps of iron dextran making it difficult to assess the location of iron within the myocardium. Following 7 days of chelator treatment, small deposits are possibly seen within the myocytes, supporting the use of a heterozygous thalassaemic mouse and iron dextran as a medium for iron loading, but also supporting the notion for a longer time period for iron equilibration and re-distribution. Another group (Moon et al, 2011) found no relationship between iron loading non-thalassaemic mice and cardiac function, and administered daily injections of 10mg/day iron dextran, up to a total of either 100mg, 200mg or 300mg. Between two and four weeks were allowed for iron redistribution prior to animal culling, with the implication that mice that were more heavily iron loaded had the shortest re-equilibration period as all animals were sacrificed at the same time. Histology slides demonstrate iron depositions in the cardiac interstitium, but none is visible in the myocardium. This supports the hypothesis that the use of a thalassaemic mouse model and a longer re-equilibration period would have resulted in iron deposition within the cardiomyocytes, similar to that seen in human transfusional iron overload.

In another model, wild type mice were fed a ferrocene-supplemented diet (0.2%w/w) over a period of two months to induce iron overload and were then treated with DFP or curcumin for 4 months (Thephinlap et al, 2011). Although dietary iron supplementation is less technically challenging and time consuming than i.p. injections of iron dextran, and furthermore mice receive daily treatment, this study showed only minimal iron deposits in the cardiac interstitium.

In a haemochromatosis mouse model (Santos et al, 2000) fed a 2.5% (w/w) carbonyl iron diet for 12 weeks, a small amount of iron deposits were noted within lysosomes in the cardiomyocytes using an electron microscope. On examination of the histology Perls stain images, the majority of iron appears to be in the interstitium and there is no clear iron deposition within the cardiomyocyte. This study does however provide



promising evidence in support of the use of carbonyl iron as a vehicle for iron loading, however longer treatment periods may be necessary.

Given the short-comings of these various methodologies, iron dextran was chosen as the iron administration vehicle, at a dose of 10mg/day for 5 days/week, for 4 weeks. An extended iron re-equilibration period of 4 weeks was incorporated into the study protocol, and a group of animals was randomly selected for culling at the end of the iron dextran loading period for comparison of heart, liver and spleen tissue iron, in order to assess the effects of re-equilibration on iron distribution at an organ and cellular level (**Section 7.3.2**).

### **7.2.1 Rationale for using a beta thalassaemia mouse model.**

One of the goals of this work was to produce a murine model of thalassaemia that would develop cardiac iron loading within cardiomyocyte and represent the pathology of transfusional iron overload and its response to chelation as closely as possible to that seen in humans. Animal models for the study of iron overload and the effects of iron chelators are described in **Section 1.6.5**. In addition, several iron-containing vehicles have been used to induce iron overload (**Table 3**), but convincing evidence of iron loading within cardiomyocytes of these models is lacking. Described in this chapter is the development of an iron loading protocol utilising iron dextran, studied in a humanised  $\beta$  thalassaemia mouse model. In contrast to humans, iron overloaded wild-type mice rapidly unload excess iron in their faeces (Musumeci et al, 2014). By iron-loading humanised  $\beta$  thalassaemia mice, the ineffective erythropoiesis that occurs from the thalassaemic gene is predicted to change the balance between iron loss and iron absorption in favour of iron retention. This would predict a model where iron overload, particularly extra-hepatically, is obtained more readily than in wild-type mice.

### **7.2.2 Murine models of thalassaemia**

Modelling thalassaemia in mice is complicated by the fact that mice lack true fetal haemoglobin. Following birth, human erythroid cells undergo a fetal to adult haemoglobin switch. However, mice do not undergo such a change and continue expressing the same adult globin genes that were synthesised during fetal development.

The ideal mouse model of thalassaemia should demonstrate the following features: (a) only express human haemoglobin, (b) complete in a similar fashion to humans the transition from expression of fetal  $\gamma$  to adult  $\beta$  genes following birth, (c) synthesise no functioning adult  $\beta$  globin chains, (d) be transfusion dependent for life, (e) be heritable, (f) accumulate iron in cardiomyocytes and hepatocytes, and (g) lack a mechanism of iron excretion.

The humanised thalassaemia mouse model (Heterozygous knockin  $\gamma^{\text{HPFH}}\delta\beta^0/\gamma\beta^{\text{A}}$ ) which was generated by Huo et al (Huo et al, 2010) was chosen. This is, a relatively novel mouse model, created in 2008 (Huo et al, 2009), and represents one of the most clinically accurate models of  $\beta$  thalassaemia in a mouse to date. In this mouse, the adult  $\beta$  globin gene has been replaced by a human fetal to adult haemoglobin-switching cassette. In the homozygous form, the mice die around day 18 of life due to lethal anaemia, and life can only be sustained by repeated blood transfusions. However this is expensive, time consuming and requires great expertise. The heterozygous form exhibits a  $\beta$  thalassaemia intermedia-like phenotype and mice develop microcytic anaemia with mean haemoglobin of 7.9g/dL, compared to that of 13.8g/dL in wild-type mice. On blood film examination, there are hypochromic red cells with marked anisopoikilocytosis, and a 9-fold increase in the reticulocyte count. These mice also demonstrate erythroid hyperplasia as well as, similarly to humans, extramedullary haematopoiesis as a consequence of anaemia. Furthermore, there is splenomegaly with the enlargement of the spleen averaging 6-fold. Lastly, the premature destruction of erythroid cells leads to iron release, and there is mild iron deposition noted in the bone marrow, liver and spleen (Huo et al, 2009) but not the heart. In view of the ineffective erythropoiesis, this model is predicted to favour iron retention and more readily show iron accumulation extra-hepatically. Following a review of the currently available iron loading techniques (**Table 3**), intraperitoneal injections of iron dextran were chosen in an attempt to induce iron loading into the heart as described in the methods below, in the heterozygous mouse (**Figure 56**).

### **7.2.3 Value of MRI in assessing tissue iron in iron overloaded models.**

The use of clinical magnetic resonance imaging (MRI) to assess the extent of iron loading in organs has revolutionised the diagnosis, management, and treatment of  $\beta$

thalassaemia major patients (Papakonstantinou et al, 2009; Tanner et al, 2006; Voskaridou et al, 2004; Wood et al, 2005a). MRI has two primary advantages over other imaging or invasive diagnostic techniques; accurate measurement of cardiac structure and function; and direct quantification of iron loading due to shortening of magnetic relaxation times T1, T2, and T2\* in the presence of iron. In this chapter we show the application of clinically relevant MRI assessment methods to the novel  $\gamma^{\text{HPFH}}\delta\beta^0$  knockin mouse model of  $\beta$  thalassaemia in the presence of iron overload, and its correlation with tissue iron. We used the opportunity to collaborate with the Centre for Advanced Biomedical Imaging, also at UCL.

There is an urgent need for accurate non-invasive methods that will detect and quantify iron load, so that new therapies can be directly assessed *in vivo*, and this lead to the development of an MRI iron monitoring technique to determine changes in iron status. Ultimately, MRI iron monitoring will lead to reduction in animal use and a more effective short as well as long-term monitoring of iron status.

## 7.3 Development of the iron overloaded murine mouse model

### 7.3.1 Materials and Methods

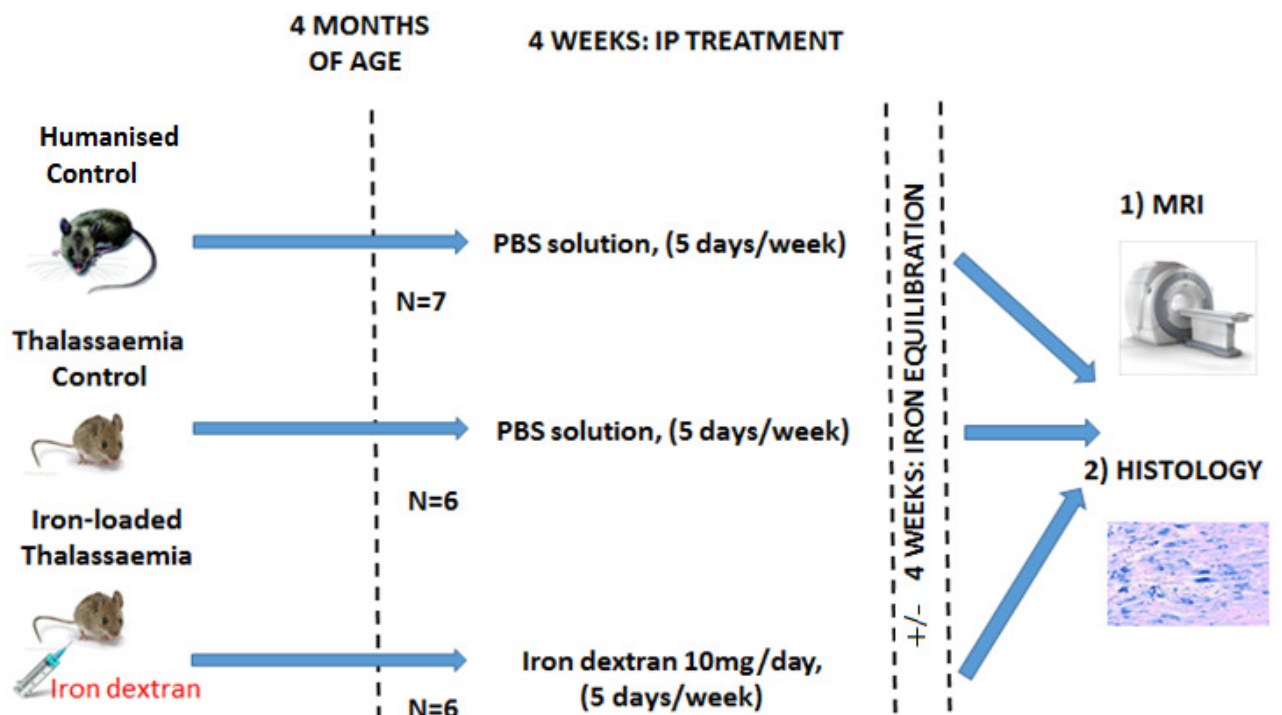
As stated earlier, collaboration was established with the Centre for Advanced Biomedical Imaging, University College London, to correlate iron overloaded murine tissue iron and histological findings with non-invasive and *in vivo* MRI (see below). I performed iron loading of mice, animal culling and blood sampling, tissue fixation, post mortem quantification of tissue iron, acquisition, and analysis of histology images and correlation of tissue iron with MRI findings. All imaging was carried out by Laurence Jackson, at University College London (UCL), as part of his doctoral studies. Blood sample analysis was performed by the Veterinary Clinical Pathology Lab, University of Cambridge.

### 7.3.2 Iron loading of humanized $\beta$ thalassaemic mice

The humanised thalassaemia mouse model (Heterozygous knockin  $\gamma^{\text{HPFH}}\delta\beta^0/\gamma\beta^{\text{A}}$ ) was kindly donated by Dr. Anna David, *Institute of Women's Health*, University College London. Male heterozygous knockin mice ( $\gamma^{\text{HPFH}}\delta\beta^0/\gamma\beta^{\text{A}}$ ) were housed in stainless steel cages in a temperature and humidity controlled environment with 12 hour light/dark cycles. The mice had access to water and standard chow diet *ad libidum*. All animal work was performed in accordance with the UK Home Office Animals Scientific Procedures Act (1986) and institutional guidelines. Twelve thalassaemic mice and seven control mice ( $\gamma\beta^{\text{A}}/\gamma\beta^{\text{A}}$ ) were randomized at 4 months of age to receive either iron dextran or PBS intraperitoneal (ip) injections for 5 out of 7 days/week for a total of 4 weeks to induce iron loading (**Figure 56**). The treatment groups are further annotated below. Three iron-loaded mice and 3 control thalassaemia as well as 2 humanised control mice were culled straight after the loading period. A further 4 week period was allowed for iron re-equilibration prior to MRI and animal sacrifice for tissue iron determination of the rest of the mice (**Section 2.8.3, Section 2.8.4**).

- a) *Humanised Control*: Humanised  $\gamma\beta^A/\gamma\beta^A$  control mice (n=7). 0.1ml of *ip* PBS 5 days/week for 4 weeks.
- b) *Control Thalassaemia*: Heterozygous knockin  $\gamma^{\text{HPFH}}\delta\beta^0/\gamma\beta^A$  thalassaemia mice (n=6). 0.1ml of *ip* PBS 5 days/week for 4 weeks.
- c) *Iron-loaded Thalassaemia*: Heterozygous knockin  $\gamma^{\text{HPFH}}\delta\beta^0/\gamma\beta^A$  thalassaemia mice (n=6) received *ip* injections of iron dextran solution (10mg/day for 4 weeks (5 days/week)) to induce iron loading.

Figure 56 Schematic representation of mouse iron loading model



### 7.3.3 Iron quantification, histology and blood sampling

Following MRI imaging I sacrificed the animals and fixed tissue samples of the heart, spleen and liver in 4% Paraformaldehyde for analysis. I measured non-haem tissue iron concentration using the iron assay described by Bothwell et al. (Bothwell et al, 1979) (**Section 2.8.5**) and iron deposits were observed histologically by Perls' staining carried out at the Veterinary Clinical Pathology Lab, University of Cambridge (**Section 2.8.6**). I scanned the slides using the slide scanner at the Biosciences division at UCL to

visualise tissue iron staining and further analysed the extent of iron deposition using the software 'Image J'. Blood samples were taken by me during animal culling.

#### **7.3.4 MRI measurements**

To correlate the histological findings of iron overloaded tissue with, non-invasive and *in vivo* preclinical MRI was used. Imaging was performed by Laurence Jackson prior to me culling the mice, using a 9.4T MR system (Agilent Technologies, Santa Clara, USA). A small animal physiological monitoring system (SA Instruments, Stony Brook, NY) was used to record the ECG tracing, respiration rate, and temperature during the scan. Animals were anaesthetised for the MRI by Laurence Jackson under a mixture of isoflurane and oxygen with physiological measurements monitored to maintain the depth of anaesthesia. A number of measurements were obtained by Laurence Jackson during the scan:

##### *I. Spleen volume*

In control and non-loaded thalassaemia mice these readings were easily obtained, however in iron-loaded mice due to the ultra-short T2/T2\* relaxation in the spleen, this proved initially more challenging. The ratio of spleen volume to total animal mass was used as a quantitative and animal-independent value for spleen size.

##### *II. MRI Relaxometry*

Transverse relaxation mechanisms T2 and T2\* are the time constants describing the rate of transverse MRI signal decay that depends on the microscopic magnetic environment in tissue. The large paramagnetic influence of molecules containing iron causes perturbations to the magnetic environment regardless of its biomolecular form. This results in faster transverse spin relaxation in direct proportion to iron concentration, making T2/T2\* quantifiable markers for iron-overload (Carpenter et al, 2014; Carpenter et al, 2011). T1 was also recorded using a different sequence.

##### *III. Cardiac Function*

Cardiac function was assessed with a gradient echo MRI sequence with the number of cine frames matched to cover the complete cardiac cycle. The left ventricular blood pool was segmented at systole and (Heiberg et al, 2010) the corresponding volumes used to calculate left ventricular ejection fraction (EF), stroke volume (SV) and end systolic/diastolic volumes (ESV/EDV) (Stuckey et al, 2012).

## 7.4 Results

### 7.4.1 Tissue iron and histology

Histological sections of spleen, heart and liver are shown in **Figure 57 A**, from animals culled 4 weeks post completion of the iron dextran iron loading regimen in the group of iron-loaded  $\beta$  thalassaemic mice, and 4 weeks after completion of PBS treatment in humanised control and  $\beta$  thalassaemic control mice. There is no iron deposition in the spleen, liver nor heart of humanised control mice. Small iron deposits are visible as blue regions in the liver and spleen of thalassaemia control group in the absence of iron loading, but there is no accumulation of iron in cardiomyocytes. This iron distribution in the non-iron loaded control heterozygous  $\beta$ -thalassaemic mouse is consistent with early stage organ iron deposition secondary to haemolytic iron release where the iron has not spread beyond the macrophage system of the liver and spleen. In the iron loaded thalassaemia group there are large iron deposits in the liver and spleen, but most importantly iron is also visible in cardiac macrophages, epicardium, and the myocardium (**Figure 58**).

Iron tissue concentration determined by the Bothwell non-haem assay for each organ examined in the respective study groups is shown in **Figure 57 B**. Control thalassaemia hearts did not show significantly higher iron content than humanised controls, but iron loaded thalassaemia animals showed large cardiac iron depositions (**Figure 57 B**, **Figure 58**). Hepatic iron content was higher than humanised controls in control thalassaemia and iron-loaded animals, while splenic iron showed an increasing trend but the results did not reach statistical significance. These results match the T2/T2\* relaxometry measurements presented below. Table 18 shows the tissue iron in the heart, liver, and spleen of animals culled directly after completion of iron dextran treatment compared to the group which underwent a 4 week iron redistribution period.

**Figure 57 Iron in the heart, liver and spleen following iron-loading in mice and a 4 week re-equilibration period.**  
 (A) Perls stain showing iron deposits in the spleen, liver and heart. Iron loading is noted in the cardiomyocytes only following iron treatment. Results of the Bothwell iron assay (B) show that iron content significantly increases following treatment with iron dextran in all three organs.

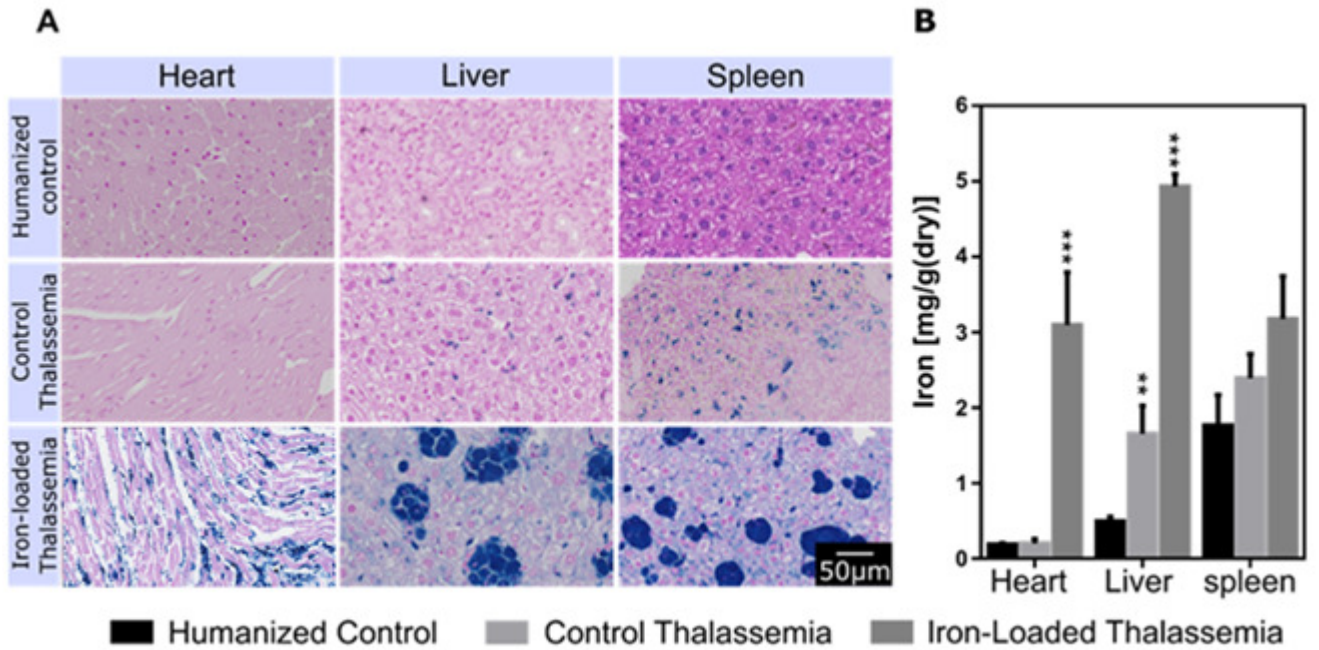
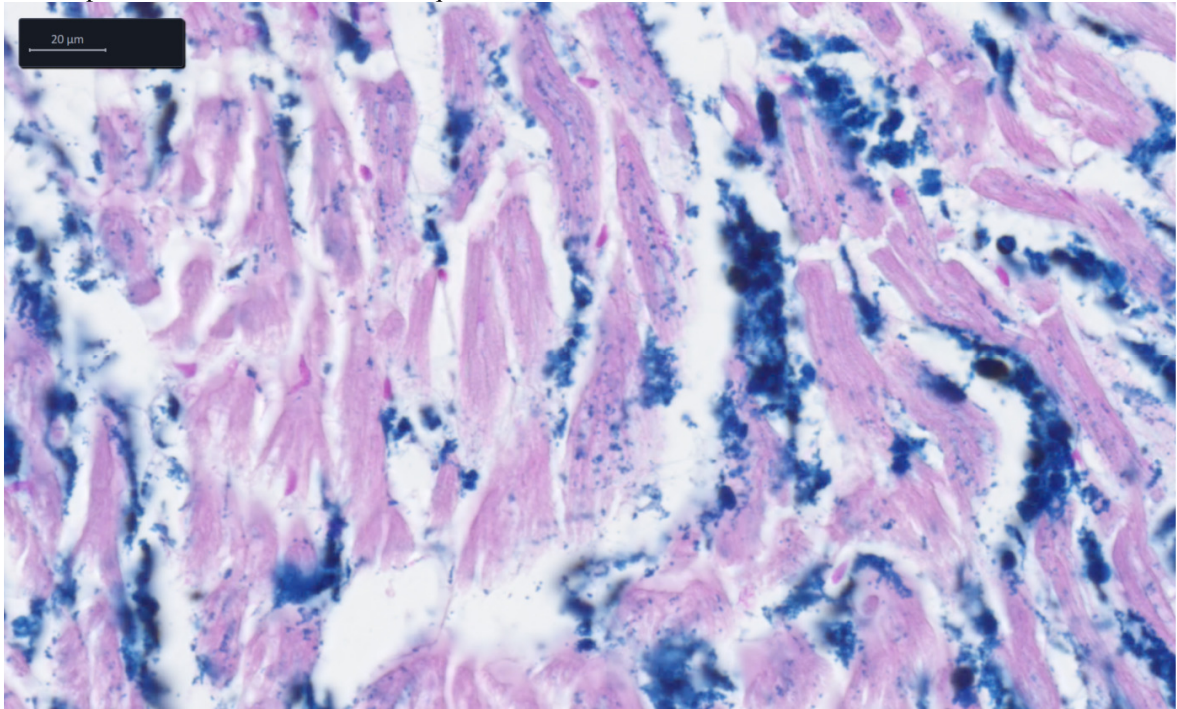




**Figure 58** Perls stain of the heart of iron loaded mice demonstrating iron in the myocardium. (20x magnification). The mice were iron loaded with IP injections of iron dextran 10mg/day for 5 days/ week and a 4 week period was allowed for iron re-equilibration.



#### **7.4.2 The effect of a immediate culling vs. following a 4 week re-equilibration period**

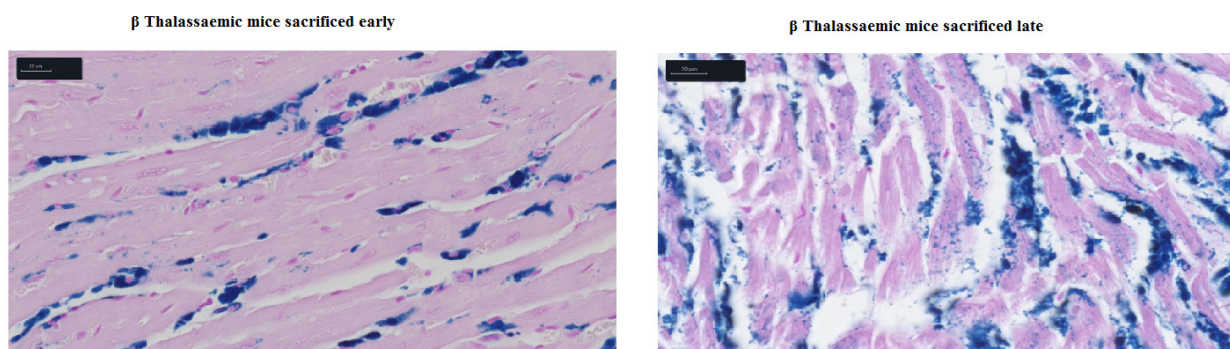
Three of the six  $\beta$  thalassaemic mice that received i.p. injections of iron dextran for 5 days/week at 10mg/day for 4 weeks, were sacrificed at the end of the iron loading regimen. The remaining 3 mice were culled 4 weeks after the end of the treatment, to allow for iron redistribution. Tissue iron was quantified using the Bothwell non-heam iron quantification method (**Section 2.8.4**). Interestingly, in the animals maintained for 4 weeks after iron loading for iron redistribution, the cardiac iron concentration increased significantly, by 2.2 fold (from 1.91 to 3.09,  $p < 0.05$ ) (Table 18). This is clearly visible in the Perl stains in **Figure 59**, where the myocardial iron is present at low levels initially, followed by iron dextran deposition in the interstitium as well as myocardium 4 weeks later. Both liver iron and spleen tissue iron concentration showed a decreasing trend in tissue iron from 5.04 to 4.83 ( $p > 0.05$ ) and 3.94 to 2.41 ( $p < 0.05$ )

(Table 18). These findings clearly demonstrate iron redistribution from the spleen/liver to the heart, commonly by macrophages.

**Table 18 Heart, liver and spleen tissue iron.** Heterozygous  $\beta$  thalassaemic mice (iron loaded with 10mg/day of iron dextran for 5 days/week for 4 weeks. Mice were either culled after completion of iron dextran treatment or after a further 4 week period for iron re-equilibration. Errors represent SEM.

	Heart iron [mg/g(dry weight)]	Liver iron iron [mg/g(dry weight)]	Spleen iron iron [mg/g(dry weight)]
<b>Culled straight after iron treatment (n=3)</b>	1.91 +/- 0.25	5.04 +/- 0.65	3.94 +/- 0.41
<b>Culled 4 weeks post treatment (n=3)</b>	4.28 +/- 0.81	4.83 +/- 0.11	2.41 +/- 0.51
<b>Average of above animals (n=6)</b>	3.09 +/- 0.71	4.93 +/- 0.51	3.17 +/- 0.42

**Figure 59** Perls stain of the heart of iron loaded mice demonstrating iron in the myocardium in mice sacrificed directly after the 4 week iron loading treatment or 4 weeks later.



### 7.4.3 Haematological parameters following iron dextran treatment

Following animal sacrifice either directly after the four week iron loading period with iron dextran or following 4 weeks allowed for iron re-equilibration, blood samples were taken by me during the culling process. FBC analysis of these samples was performed at the Veterinary Clinical Pathology Lab, University of Cambridge and the results can be seen in Table 19. Iron treatment significantly increased the haemoglobin (Hb) from 8.53 to 10.27 g/dL in control vs. treatment ( $p=0.01$ ), approaching the average level for the humanised control mice 11.3 g/dL. Red blood cell count (RBC) significantly increased from 6.86 to  $9.62 \times 10^{12}/L$  ( $p=0.009$ ). The mean corpuscular volume (MCV) and mean corpuscular haemoglobin (MCH) remained unaffected by iron dextran treatment, however, there was a significant increase in haematocrit from 30.17 to 35.45, which was slightly mean value of 38.13 for the humanised control group. Of note, the reticulocyte proportion was more than two-fold higher in untreated compared to treated mice (15.89% vs. 6.90%), and the mean reticulocytes proportion was recorded as 3.85% in the humanised controls. Furthermore, iron treatment appeared to induce a significant increase in white cell count ( $15.19 \times 10^9/L$  vs.  $3.16 \times 10^9/L$ ) coupled by an increase in neutrophils ( $3.52 \times 10^9/L$  vs.  $0.18 \times 10^9/L$ ) as well as lymphocytes ( $9.60 \times 10^9/L$  vs.  $2.83 \times 10^9/L$ ). The interpretation of the above findings is discussed in **Section 7.5**.

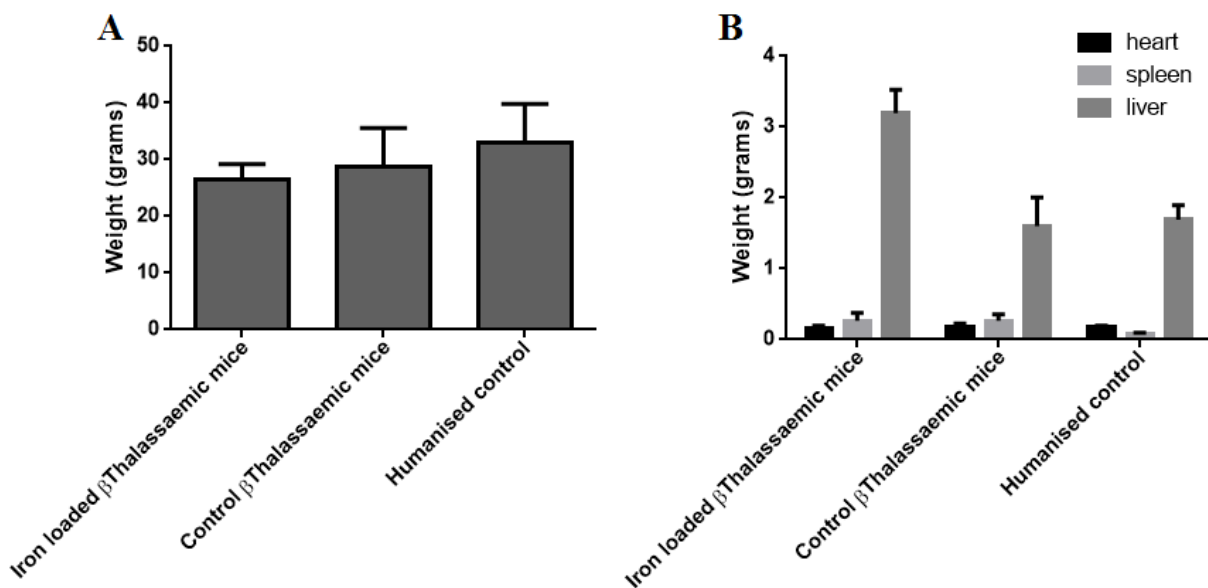
**Table 19 Changes in haematological parameters secondary to iron loading with iron dextran.** Heterozygous  $\beta$  thalassaemic mice were iron loaded with 10mg/day of iron dextran for 5 days/week for 4 weeks. Thalassaemia control mice and humanised controls were treated with PBS for 4 weeks. Mice were either culled after completion of iron dextran/PBS treatment or a further 4 week period for was allowed prior to culling. \* indicates  $p < 0.05$  when comparing the mean of thalassaemia iron loaded and the mean of thalassaemia control mice.

	Thalassaemia iron loaded			Thalassaemia control			Humanised control		
	Mean	Culled 4w	Culled 8w	Mean	Culled 4w	Culled 8w	Mean	Culled 4w	Culled 8w
<b>Hb (g/dL)</b>	<b>10.27*</b>	10.1	10.43	<b>8.53</b>	8.53	8.53	<b>11.3</b>	11.17	11.80
<b>MCV (fL)</b>	<b>41.20</b>	40.2	42.2	<b>43.9</b>	45.20	43.25	<b>45.7</b>	46.40	44.50
<b>MCH (pg)</b>	<b>12.4</b>	12.40	12.40	<b>11.93</b>	11.40	12.20	<b>12.93</b>	12.85	13.10
<b>RBC (<math>\times 10^{12}/L</math>)</b>	<b>9.62*</b>	9.04	8.20	<b>6.86</b>	6.66	6.97	<b>8.33</b>	7.99	9.02
<b>WBC (<math>\times 10^9/L</math>)</b>	<b>15.19*</b>	12.83	17.54	<b>3.16</b>	5.95	1.76	<b>1.74</b>	2.40	0.43
<b>Neutrophils (<math>\times 10^9/L</math>)</b>	<b>3.52*</b>	4.39	2.65	<b>0.18</b>	0.18	0.18	<b>0.13</b>	0.17	0.05
<b>Lymphocytes (<math>\times 10^9/L</math>)</b>	<b>9.60*</b>	6.10	13.1	<b>2.83</b>	5.60	1.45	<b>1.47</b>	2.00	0.40
<b>Haematocrit (L/L)</b>	<b>35.45*</b>	36.3	34.6	<b>30.17</b>	30.1	30.20	<b>38.13</b>	37.15	40.10
<b>Platelets (<math>\times 10^9/L</math>)</b>	<b>1538</b>	1518	1558	<b>1613</b>	1917	1462	<b>1285</b>	1071	1715
<b>% Reticulocytes</b>	<b>6.90*</b>	5.71	8.08	<b>15.89</b>	24.36	11.66	<b>3.85</b>	2.73	4.96
<b>reticulocytes</b>	<b>589*</b>	516	662	<b>1023</b>	1622	723.80	<b>319</b>	190	447

#### 7.4.4 Comparison of the weight of mice (A) and their heart, liver and spleen weights (B) post sacrifice.

Neither the weight (**Figure 60 A**) nor the heart size of  $\beta$  thalassaemic mice (**Figure 60 B**) was significantly different. The thalassaemic control mice had a 3-fold larger spleen compared to humanised controls (0.26g vs. 0.08g) ( $p < 0.01$ ). However, iron loading did not appear to further increase spleen size (**Figure 60 B**). These findings were also confirmed by MRI spleen volume measurements (**Section 7.4.5**). The liver weight was more than double in iron-loaded mice compared to thalassaemic controls (**Figure 60 B**) ( $p < 0.04$ ).

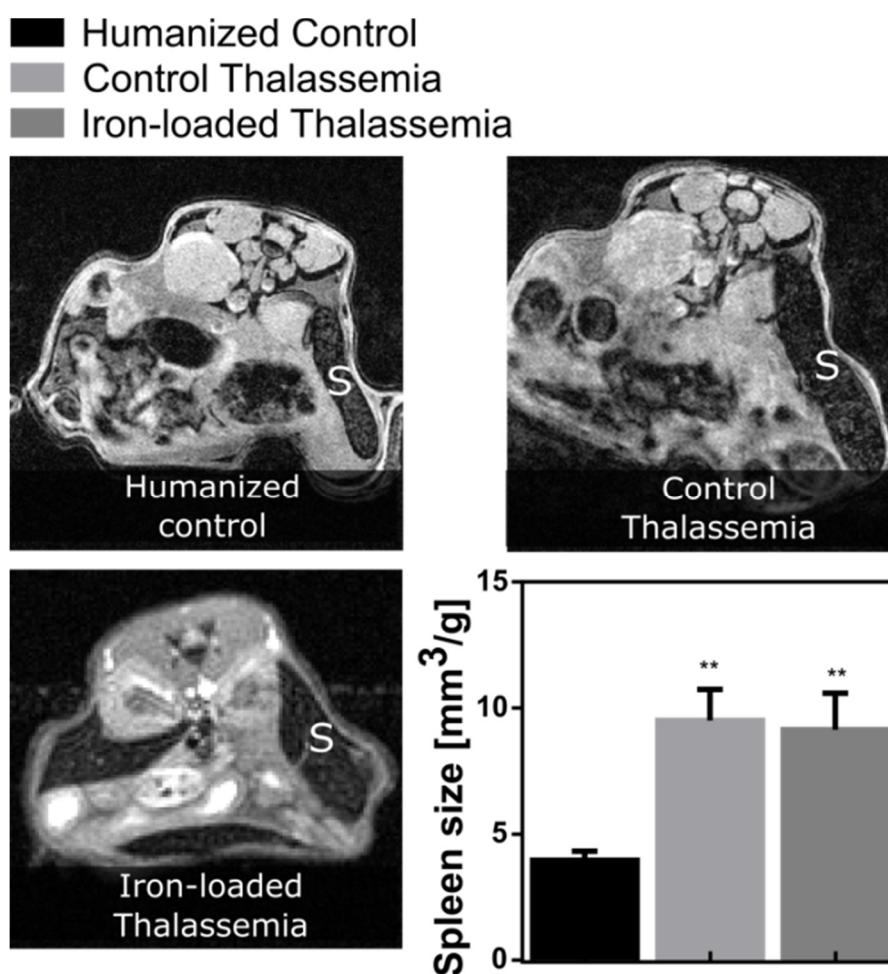
Figure 60 Comparison of the weight of mice (A) and their heart, liver and spleen weights (B) post sacrifice.



#### 7.4.5 Spleen volume by MRI (performed by Laurence Jackson)

A significant increase in spleen size was observed in the presence of the  $\gamma^{\text{HPFH}}\delta\beta^0$  gene (**Figure 61**). **Figure 61** shows a comparison of the axial spleen images and highlights the enlarged spleens in iron loaded and control thalassaemia mice. Spleen volume normalised to body mass was significantly increased in control thalassaemia ( $9.5\pm 1.2\text{mm}^3/\text{g}$ ) and iron loaded thalassaemia mice ( $9.1\pm 1.3\text{mm}^3/\text{g}$ ) relative to humanised control mice ( $4.0\pm 0.4\text{mm}^3/\text{g}$ ), however, there was no significant change in volume between iron loaded and control thalassaemia. This suggests that splenomegaly in this animal is probably a result of erythrocyte phagocytosis present in our heterozygous mouse model already.

**Figure 61 Mice spleen volumes.** Spleens (S) were significantly enlarged relative to humanised controls in control and iron-loaded thalassaemia mice. The spleen can be identified by its speckled texture due to the dense trabeculae. This was quantified by the ratio of spleen volume to animal mass (\*\* $p < 0.01$ ).



#### 7.4.6 T2/T2\* relaxation (performed by Laurence Jackson)

Measurements of cardiac, hepatic and splenic T2 and T2\* are shown in Figure 62 and **Figure 63** respectively, along with representative images from each group at identical echo time. Myocardial T2 was shortened in iron-loaded thalassaemia mice ( $3.3\pm 0.3\text{ms}$ ) versus humanised controls ( $18.0\pm 0.8\text{ms}$ ) and thalassaemia controls ( $17.2\pm 2.1\text{ms}$ ). Similarly, myocardial T2\* in iron overload ( $0.7\pm 0.2\text{ms}$ ) was shortened relative to humanised controls ( $11.5\pm 4.3\text{ms}$ ) and thalassaemia controls ( $10.1\pm 5.2\text{ms}$ ). This data demonstrates that T2 and T2\* measures are sensitive to iron loading in this animal model. It can be inferred from this that the heterozygous phenotype does not have any cardiac siderosis.

Hepatic T2 was shortened in both the control thalassaemia ( $9.4\pm 2.9\text{ms}$ ) and iron-loaded thalassaemia mice ( $1.3\pm 0.3\text{ms}$ ) relative to humanised controls ( $13.2\pm 0.10\text{ms}$ ). Similarly, hepatic T2\* was shortened in the control thalassaemia ( $4.7\pm 1.5\text{ms}$ ) and iron-loaded thalassaemia mice ( $0.6\pm 0.2\text{ms}$ ) models relative to humanised controls ( $7.6\pm 1.9\text{ms}$ ). This shortening of T2 and T2\* in the non-iron loaded thalassaemia group can be attributed to the premature destruction of erythroid cells leading to iron release and iron/ferritin deposition in the liver.

The role of the spleen in breaking down senescent erythrocytes renders it hyperactive in thalassaemia where a large population of erythrocytes is defective. Iron deposition is a byproduct of the metabolism of the hemoglobin in the spleen. The shortened T2 and T2\* in both thalassaemia groups reflects this process. Splenic T2 was shortened in control thalassaemia mice ( $3.9\pm 0.8\text{ms}$ ) and iron-loaded thalassaemia ( $1.7\pm 0.9\text{ms}$ ) compared with humanised controls ( $6.2\pm 0.8\text{ms}$ ). Splenic T2\* was shortened in iron overload mice ( $0.8\pm 0.1\text{ms}$ ) and control thalassaemia mice ( $0.6\pm 0.5\text{ms}$ ) relative to humanized controls ( $1.5\pm 0.3\text{ms}$ ).

Iron accumulation occurs initially in the macrophage system of the spleen, liver and bone marrow but subsequently in hepatocytes and ultimately in the heart and endocrine systems. These MRI measurements show that, in the absence of iron loading, at 5 months of age the liver and spleen are showing signs of iron loading, but the process has not saturated in order to accumulate iron in the heart.



**Figure 62 T2 relaxation times in iron-loaded mice.** T2 was shortened in the control thalassaemia animals and more severely shortened in the case of iron-loaded thalassaemia mice (\* $p < 0.05$ , \*\* $p < 0.01$ , \*\*\* $p < 0.001$ ).

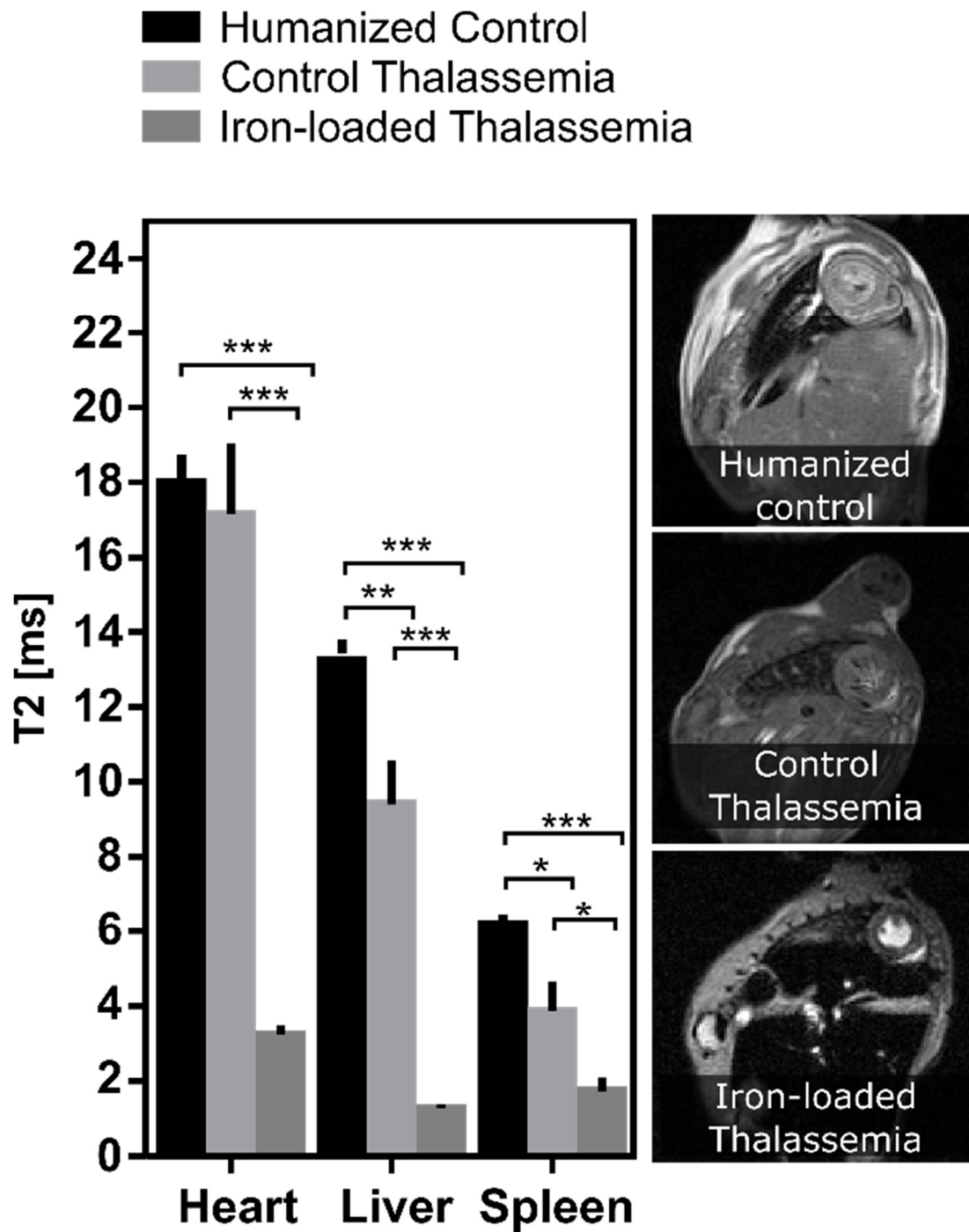
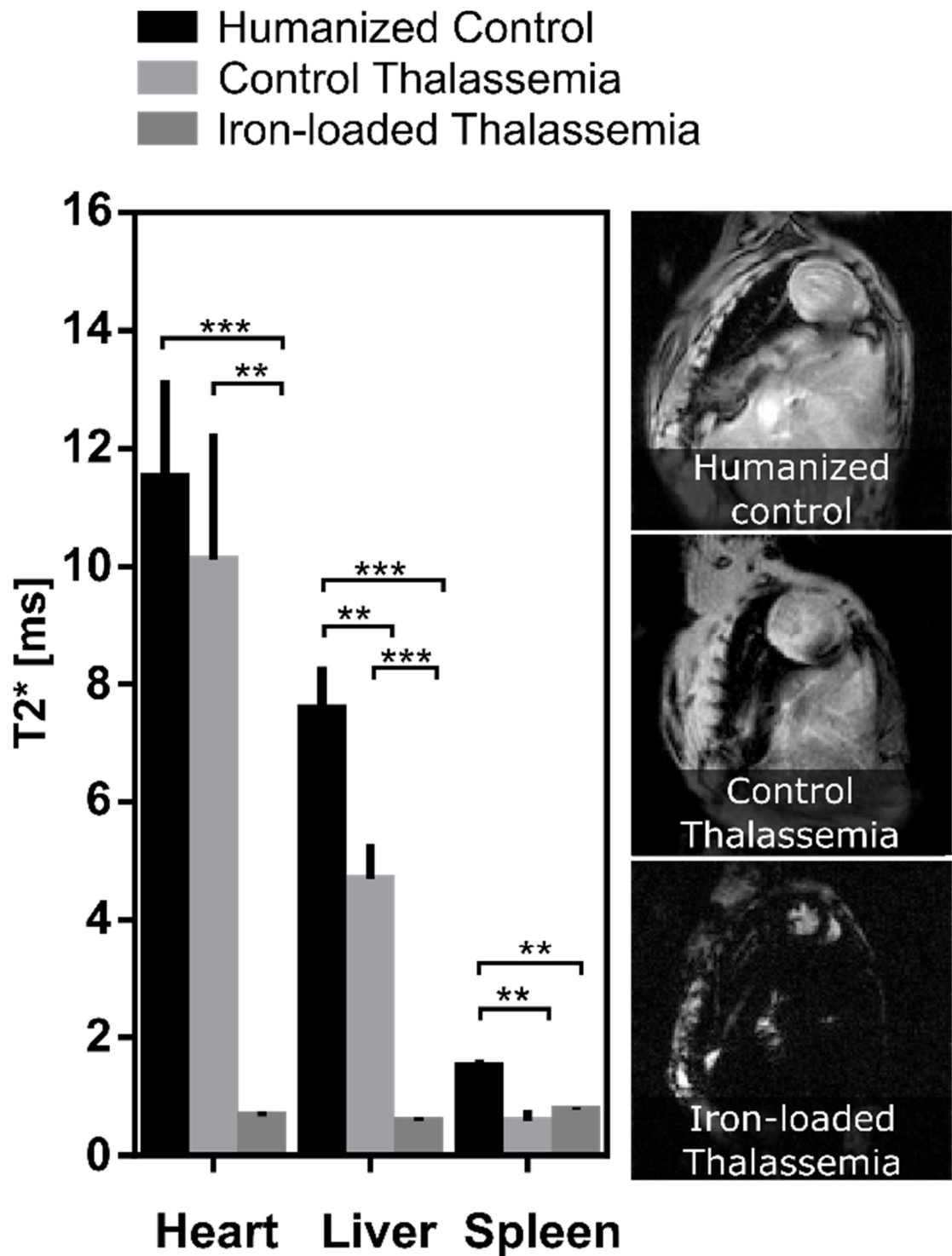




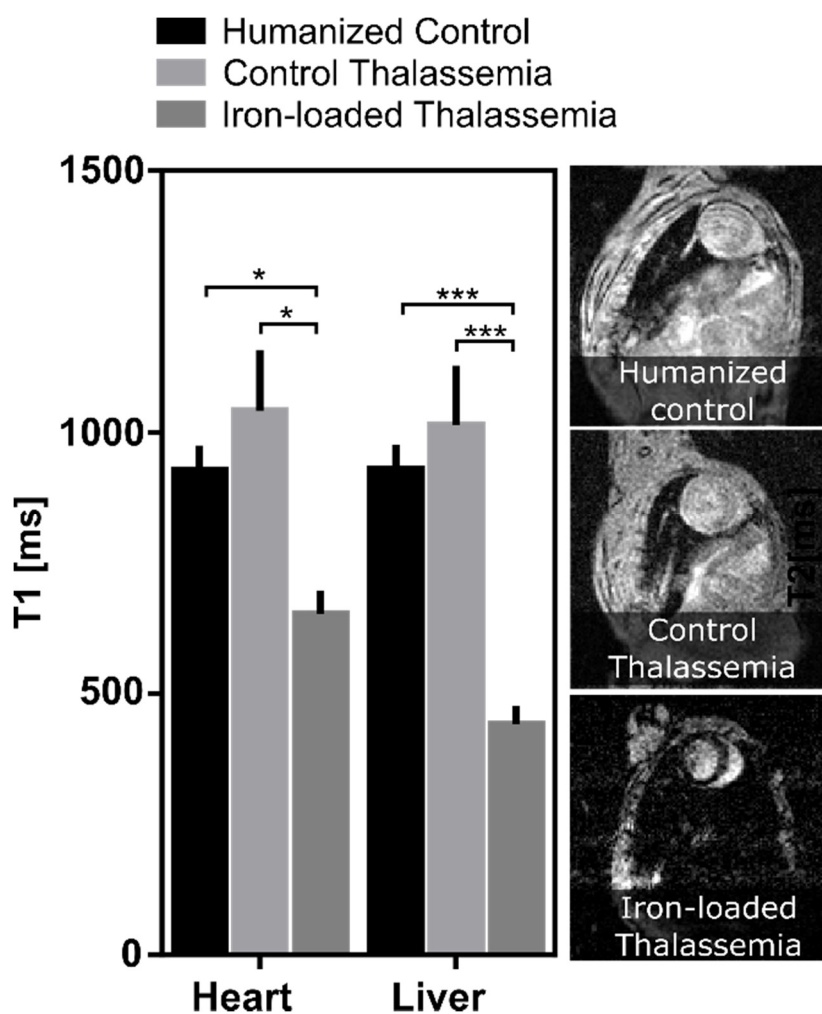
**Figure 63 T2\* relaxation times in iron-loaded mice.** T2\* relaxation was shortest in the iron-loaded thalassaemia animals in the heart, liver, and spleen (\*p<0.05, \*\*p<0.01, \*\*\*p<0.001).



#### 7.4.7 T1 relaxation (performed by Laurence Jackson)

T1 values were significantly shorter in the presence of iron loading (**Figure 64**). Cardiac T1 was shorter in iron-loaded mice ( $620\pm 125\text{ms}$ ) relative to control thalassaemia mice ( $1041\pm 261\text{ms}$ ) and humanised control animals ( $928\pm 115\text{ms}$ ). This was also the case for hepatic T1, with iron loaded thalassaemia animals having shorter T1 ( $456\pm 85\text{ms}$ ) than control thalassaemia ( $1014\pm 255\text{ms}$ ) and humanised control animals ( $929\pm 117\text{ms}$ ). This data shows that T1 is sensitive to the presence of iron loading, however, T1 changes in the presence of iron require direct interaction with ferric molecules, making its sensitivity lower than  $T2/T2^*$ . T1 measurements could be most useful at particularly high iron concentrations where  $T2/T2^*$  can be too short to accurately quantify tissue iron.

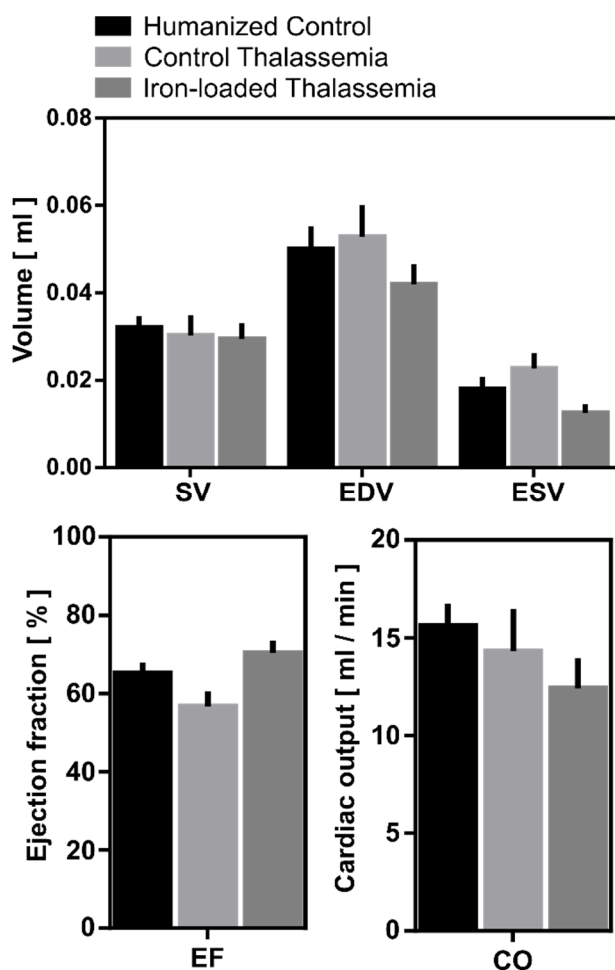
**Figure 64 T1 relaxation times in iron-loaded mice.** T1 relaxation in the heart and liver was significantly shortened in iron-loaded mice.



#### 7.4.8 Cardiac function (performed by Laurence Jackson)

Quantitative values describing left ventricular function are shown in **Figure 65**. Left ventricular end diastolic, end systolic and stroke volumes (SV) were preserved between groups. Cardiac output (CO), measured as the product of stroke volume and heart rate was not significantly altered in control thalassaemia mice ( $14.1 \pm 2.1$  ml/min) relative to humanised controls ( $15.6 \pm 1.1$  ml/min) and iron-loaded mice ( $12.4 \pm 1.5$  ml/min) indicating that at 5 months of age the heterozygous mouse has not developed the pathological high output state characteristic of anemia. Left ventricular ejection fraction (EF) was also unchanged in iron-loaded mice ( $70 \pm 2\%$ ) relative to control thalassaemia mice ( $57 \pm 4\%$ ) and humanised control animals ( $65 \pm 2\%$ ).

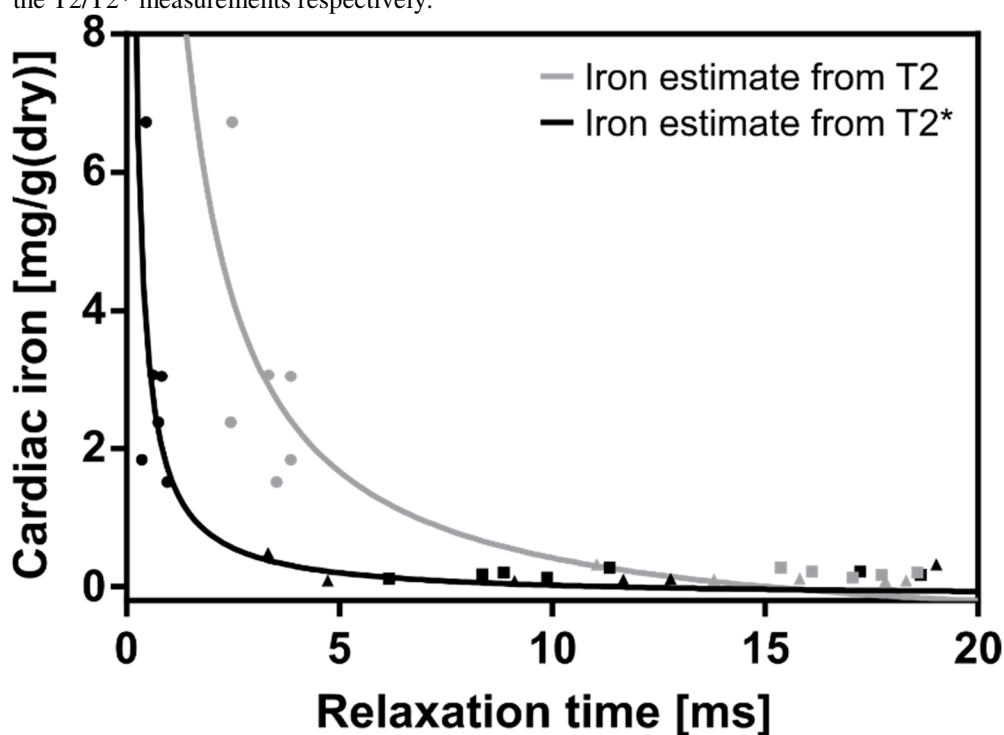
**Figure 65 Cardiac function following iron loading.** No significant changes in cardiac volumes were observed between groups, although the iron-loaded thalassaemia animals had an elevated ejection fraction relative to thalassaemia control mice (\* $p < 0.05$ ).



#### 7.4.9 Iron calibration

The tissue iron measurements generated by myself and the cardiac T2\* recorded by Laurence Jackson were used to generate a calibration curve to estimate the iron content of dry tissue. This relationship can be modeled using the following formula:  $[Fe]_{dry} = (1/T2^* - 1/T2_0^*)/K_{dry}$  where T2\* is the measured T2\* value, T2<sub>0</sub>\* is the T2\* of the heart in the absence of iron loading and K<sub>dry</sub> is a proportionality constant for dry tissue (Wood et al, 2005b). This curve was generated by Laurence Jackson who used the average T2\* of humanised controls as T2<sub>0</sub>\* and fitted K<sub>dry</sub> to the measured T2\* and dry iron concentrations. A representation of how the resulting calibration curve fits measured values is shown in **Figure 66**. It shows a sharp increase in estimated tissue iron at T2\* < 2ms. This is in agreement with the data of Carpenter et al, 2011 who correlated T2\* with tissue iron of 12 human hearts following retrieval from patients either post death or following cardiac transplantation (Carpenter et al, 2011). The process can be repeated for T2 measurements by substituting T2 for T2\* and in this case the iron concentration increases sharply at T2 < 5ms.

**Figure 66 Cardiac T2\* to iron calibration curve.** Points show individual animals, humanized controls(■), Thalassaemia controls(▲) and iron-loaded thalassaemia(●), grey/black points correspond to the T2/T2\* measurements respectively.



## 7.5 Discussion and conclusion

The goal of this work was to produce a quantitative platform for the assessment of  $\beta$  thalassaemia in a clinically relevant humanised mouse model which demonstrates cardiac iron siderosis, with the intention of accelerating the development of clinical therapies. Following administration of a total of 200mg of iron dextran 5days/week over a period of 4 weeks, we have managed to present the first model to our knowledge showing convincing evidence of iron loading within the cardiomyocytes of heterozygous  $\beta$  thalassaemic mice, and not simply within the interstitium. The total cardiac iron increased from  $0.02 \pm 0.001$  to  $3.09 \pm 0.6$  (**Figure 57 B**) and clear deposition within the myocardium is noted on Perls staining following 4 weeks of iron re-equilibration (**Figure 58**). The importance of allowing a long period for iron re-equilibration is highlighted by tissue iron measurements (Table 18) which show an increase from  $1.91 \pm 0.25$  to  $4.23 \pm 0.81$  before and after the re-equilibration period. Histology findings demonstrate that this time period is critical for allowing accumulation of iron in the cardiac myocytes, as noted by the increasing blue deposits on Perl staining (**Figure 59**).

Iron administration in our model interestingly resulted to an increase in Hb from 8.53 to 10.27 g/dL in control vs. treatment ( $p=0.01$ ). RBC significantly increased from  $6.86 \times 10^{12}/L$  to  $9.62 \times 10^{12}/L$  cells/L ( $p=0.009$ ) but MCV and MCH remained unaffected by iron treatment. These findings were coupled by a significant increase in haematocrit from 30.17 to 35.45 and a 2-fold decrease in reticulocyte count. It would therefore be possible to speculate that the increase in haematocrit could be attributed to an increase in RBC. Iron treatment appeared to also induce a significant increase in white cell count ( $15.19 \times 10^9/L$  vs.  $3.16 \times 10^9/L$ ) (Table 19). The increase in haemoglobin following iron administration has been noted previously, where iron dextran was administered 5 days/week for 4 weeks for a total of 130mg per animal in a transfusion independent model of  $\beta$  thalassaemia ( $Hbb^{th1/th1}$ ) (Ginzburg et al, 2009). The mean haemoglobin increase was 1.3g/dL and statistically significant, and compared to 1.7g/dL in the current work. Similarly, no change in MCH was noted, but a significant increase in MCV was observed. Furthermore, reticulocyte count was noted to increase from 2344 to 3613 cells/L, contrary to our study where the reticulocyte count dropped from 1023 to 589 cells/L following iron dextran administration. Ginzburg et al also noted an

expansion in extramedullary haematopoiesis in the liver and spleen, which in the liver was proportional to the dose of iron administered. This increase was not noted in the bone marrow and was coupled with a decrease in the erythroid precursor apoptosis (there is a known higher degree of apoptosis in haematopoietic erythroid precursors in thalassaemia) (Pootrakul et al, 2000; Yuan et al, 1993). Alternative explanations for the increase in Hb could relate to changes in red blood cell survival, or changes to hepcidin levels affecting gut iron uptake (which are already abnormally low in thalassaemia), but no further speculation is possible with the current available data. A further study administered recombinant human erythropoietin 3 times per week along with ferrous fumarate 305mg and folic acid 5mg daily for 11 months to 10 patients homozygous for  $\beta$  thalassaemia. Investigators noted an increase of Hb from 7.1 to 9.3g/dL, although it is difficult to comment on the isolated effect of iron administration in this context (Rachmilewitz et al, 1995).

The heterozygous thalassaemic mouse model was noted to have 3-fold heavier spleen at baseline, but this did not change following iron loading (**Figure 60 B**), and splenomegaly was also confirmed on MRI (**Figure 61**). This was originally described by (Huo et al, 2009), and has been attributed to the increase in extramedullary erythropoiesis in the spleen. Monitoring of cardiac function during MRI by Laurence Jackson showed no evidence of cardiac dysfunction with no change to SV, EDV, ESV, EF and CO. Other investigators similarly did not demonstrate any compromise in cardiac function following iron loading with *ip* iron dextran (Moon et al, 2011).

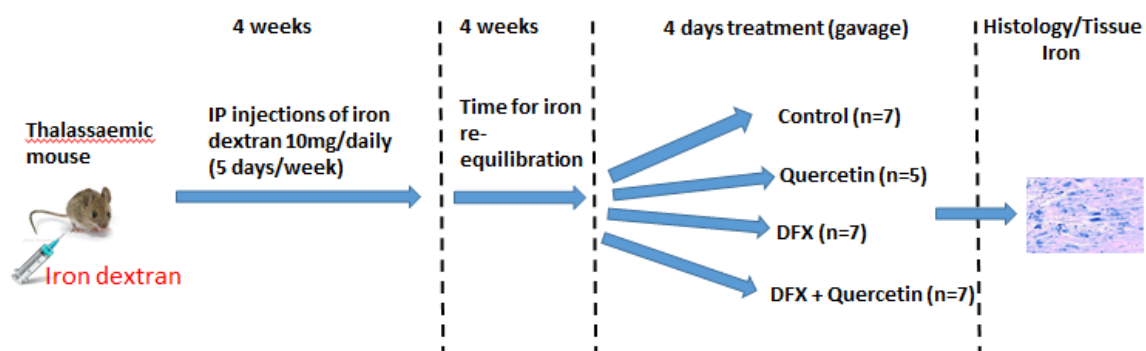
Changes in the quantitative MRI relaxation times T1, T2, and T2\* performed by Laurence Jackson were observed in the heart, liver, and spleen in our mouse model (**Figure 62, Figure 63, Figure 64**) following iron loading. The tissue iron data showed a strong correlation to MRI relaxation times ( $R=0.99$ ) (**Figure 66**). The T2 and T2\* calibration curves fitted in **Figure 66** are representative of calibration curves seen in humans (Carpenter et al, 2011) and this is a promising sign that the animal model is clinically representative and that serial measurements of tissue iron by MRI can establish trends in tissue iron loading/ unloading, enabling more clinically useful interpretation of efficacy of treatment and allowing for scarcer animal culling.

In conclusion, these results show a novel protocol for iron loading of an established  $\beta$  thalassaemia model demonstrating convincing evidence of cardiac siderosis. This model shows the importance of iron dextran as a vehicle for successful cardiac iron loading and highlights the importance of a long iron re-equilibration period prior to experimentation. Following a collaboration with the Centre for Advanced Biomedical Imaging, UCL, derivative calibration curves closely correlated tissue iron with cardiac T1, T2 and T2\*. Future preclinical studies into the safety of new agents will greatly benefit from this iron-overloaded mouse model and integration of MRI assessments, and will parallel investigation of toxicity and iron chelation efficacy serially *in vivo*.

## 7.6 Testing the flavonoid quercetin in our animal model

In this experiment, the relationship between the *in vitro* effects of quercetin in the hepatocyte and cardiomyocyte cellular models and its oral efficacy with regards to iron mobilisation, was studied in the novel *in vivo* model. Given that quercetin proved extremely effective at mobilising total cellular iron and demonstrated synergy when combined with all three commercially available iron chelators, the potential beneficial effects of this naturally occurring compound in terms of iron mobilisation from the heart, liver and spleen when in combination with the oral chelator DFX were examined. The materials and methods used have been described in **Section 7.3.1**. In principle, mice are iron loaded with iron dextran and thereafter are allowed a period of time for iron to be redistributed from mononuclear cells, where it is first taken up, into hepatocytes and then cardiomyocytes. **Figure 67** shows a schematic representation of the iron loading period with i.p. injections of iron dextran (10mg/daily, 5 days per week), and thereafter the re-equilibration 4 week period followed by the 4 days of chelator treatment by gavage. The mice were separated into 4 groups, namely: (a) control (vehicle gavage) (n=7), (b) Quercetin 300mg/kg/day (n=5), (c) DFX 30mg/kg/day (n=7), (d) DFX 30mg/kg/day + Quercetin 300mg/kg/day (n=7).

**Figure 67 Schematic representation of DFX/Quercetin combination treatment in iron-overloaded mice.**



### 7.6.1 Combination treatment of Quercetin and DFX in iron overloaded mice

Following iron loading with iron dextran and a re-equilibration period of four weeks, as described above, the mice received 4 days of treatment by gavage either with vehicle, Quercetin 300mg/kg/day, DFX 30mg/kg/day or a combination of Quercetin + DFX. All treatments were well tolerated with no noted toxicity during the time period. **Figure 68** shows a statistically significant reduction in total cardiac iron concentration between DFX (87.1  $\mu\text{g/g}$  wet tissue) and DFX + Quercetin (82.6  $\mu\text{g/g}$  wet tissue) ( $p=0.026$ ), and both treatments were significantly lower than control (**A**). In the liver (**B**), the control mice liver iron concentration was 1102  $\mu\text{g/g}$  tissue, which was reduced to 1028  $\mu\text{g/g}$  in DFX treated and 963  $\mu\text{g/g}$  tissue in DFX + Quercetin treated animals respectively, however this was not statistically significant. Similarly, in the spleen (**C**) tissue iron was reduced from 52 $\mu\text{g/g}$  tissue in control animals to 49.46  $\mu\text{g/g}$  tissue in DFX treated animals and 47.69  $\mu\text{g/g}$  tissue in DFX + Quercetin; however, the difference was not significant.

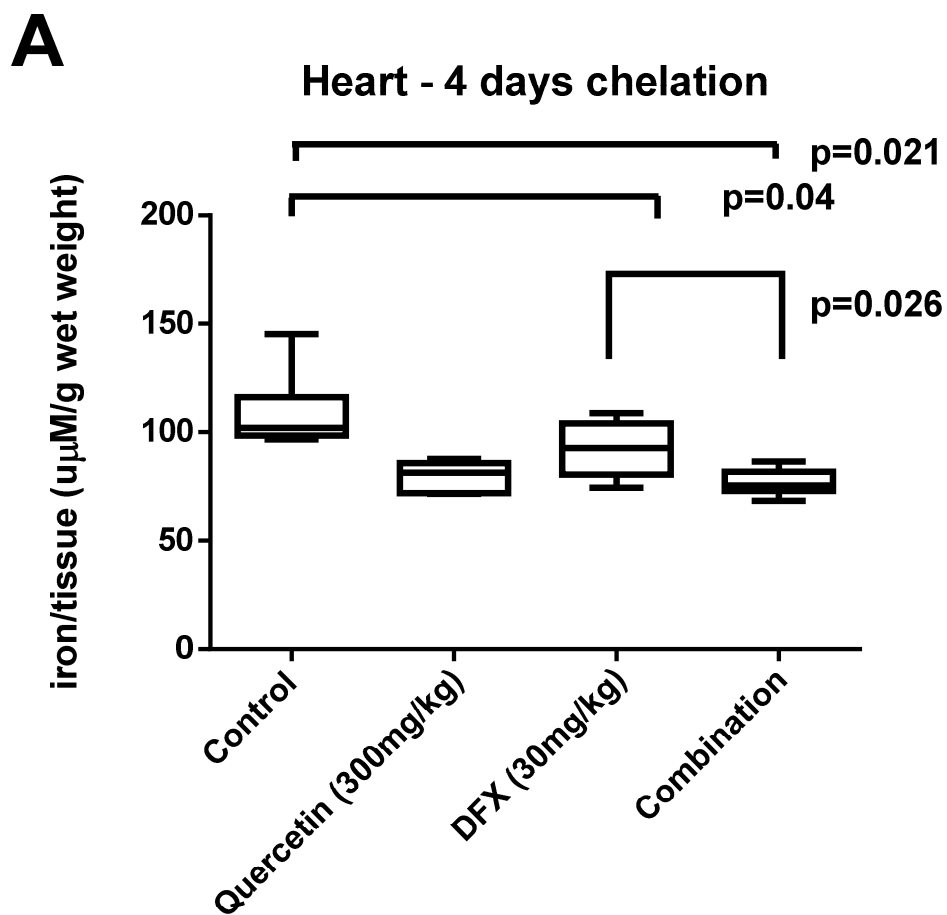
**Figure 69** shows the Perl stain slides of the heart, liver, and spleen following treatment. Inspection of the images suggests that there is a general improvement in tissue iron in combination therapy compared to control in all tissues. In order to quantify this observation, the images were analysed using the software 'Image J'. **Table 20** and **Table 21** show the results of Perls stain iron quantification by comparing the blue area

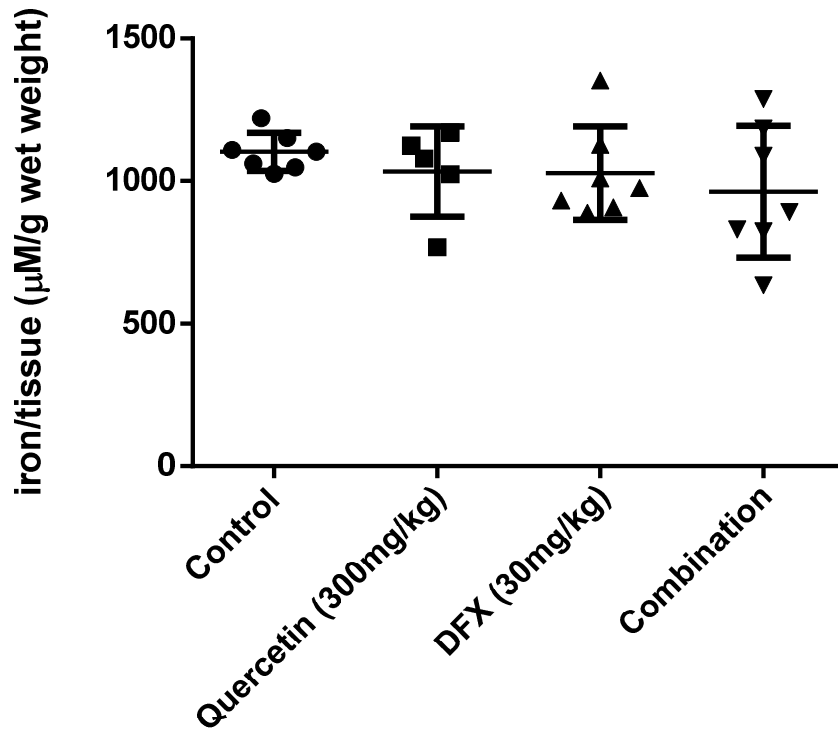
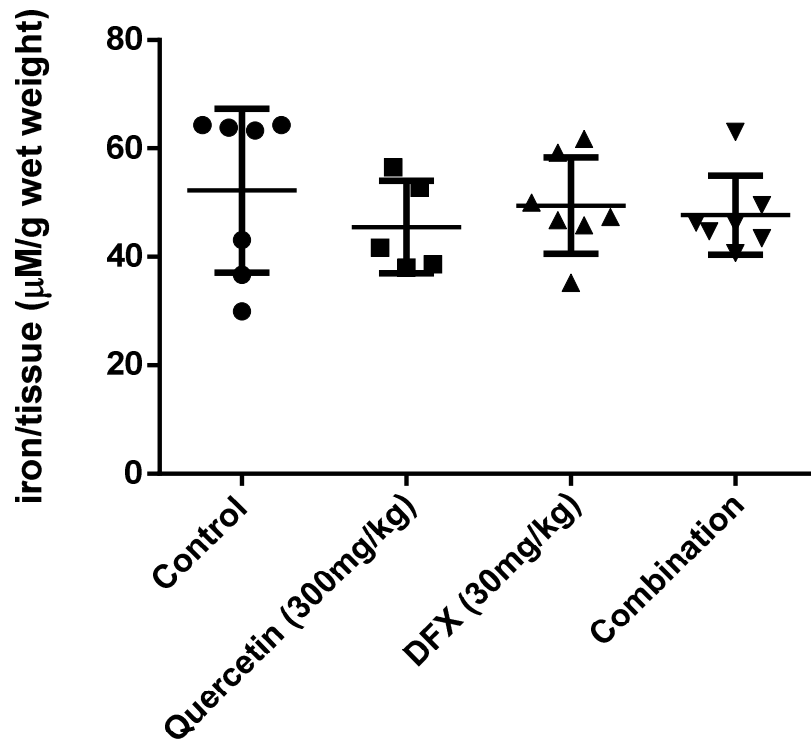


(iron deposition) in the slides or the number of blue pixels, respectively. Cardiac iron is 50 (arbitrary units) in control animals and 17 in DFX treatment, and this is further reduced to 2 in DFX + Quercetin treatment when comparing the blue area in the slides (**Table 20**). These findings are re-iterated by blue pixel counting in **Table 21**. In both the liver and spleen there is a notable reduction in tissue iron when comparing DFX treatment alone to combination with Quercetin. In the liver, quercetin appeared to increase tissue iron, however, the accuracy of this finding is uncertain in view of the large iron dextran deposits noted on this particular slide.

Quercetin has previously been studied in Sprague-Dawley male rats as a single dose of 50mg/kg where it was shown to modulate iron absorption in the duodenum by increasing apical iron uptake by decreasing subsequent basolateral iron efflux as well as ferroportin expression (Lesjak et al, 2014). Quercetin supplemented as 1% in the diet and fed to mice for 45 days, has been shown to reduce liver iron significantly and increase faecal iron excretion. The flavonoid curcumin has also been shown to be beneficial in the removal of interstitial cardiac iron and plasma NTBI following two months of treatment in BKO mice fed with a ferrocene-supplemented diet (Thephinlap et al, 2011). Notably, there is no study to date addressing iron mobilisation in cardiomyocytes by quercetin with or without a commercially used iron chelator (Zhang et al, 2006), and demonstrating the beneficial effects of this naturally occurring compound in terms of enhancing cardiac iron removal when in combination with a commercially available iron chelator. A potential future experiment would combine quercetin treatment with the other commercially available iron chelators and compare dosing and time of treatment to cardiac iron mobilisation. The MRI technique described earlier could prove valuable in monitoring response to treatment. It was not adopted in this particular case due to cost limitations.

**Figure 68 Tissue iron content of the (A) heart, (B) liver and (C) spleen of iron-loaded mice treated with DFX/Quercetin.** The mice were iron loaded with IP injections of iron dextran 10mg/day for 5 days/week and a 4 week period was allowed for iron re-equilibration. The mice were then treated for 4 days with vehicle, quercetin 300mg/kg daily, DFX 30mg/kg daily or a combination of DFX/Quercetin at the above concentrations. Tissue iron was quantified using the Bothwell method (McLaren, 1980).



**B****Liver - 4 days chelation****C****Spleen - 4 days chelation**

**Figure 69** Perls staining of heart, liver and spleen tissue in iron loaded mice following DFX/Quercetin treatment. The mice were iron loaded with IP injections of iron dextran 10mg/day for 5 days/ week and a 4 week period was allowed for iron re-equilibration prior to chelation treatment

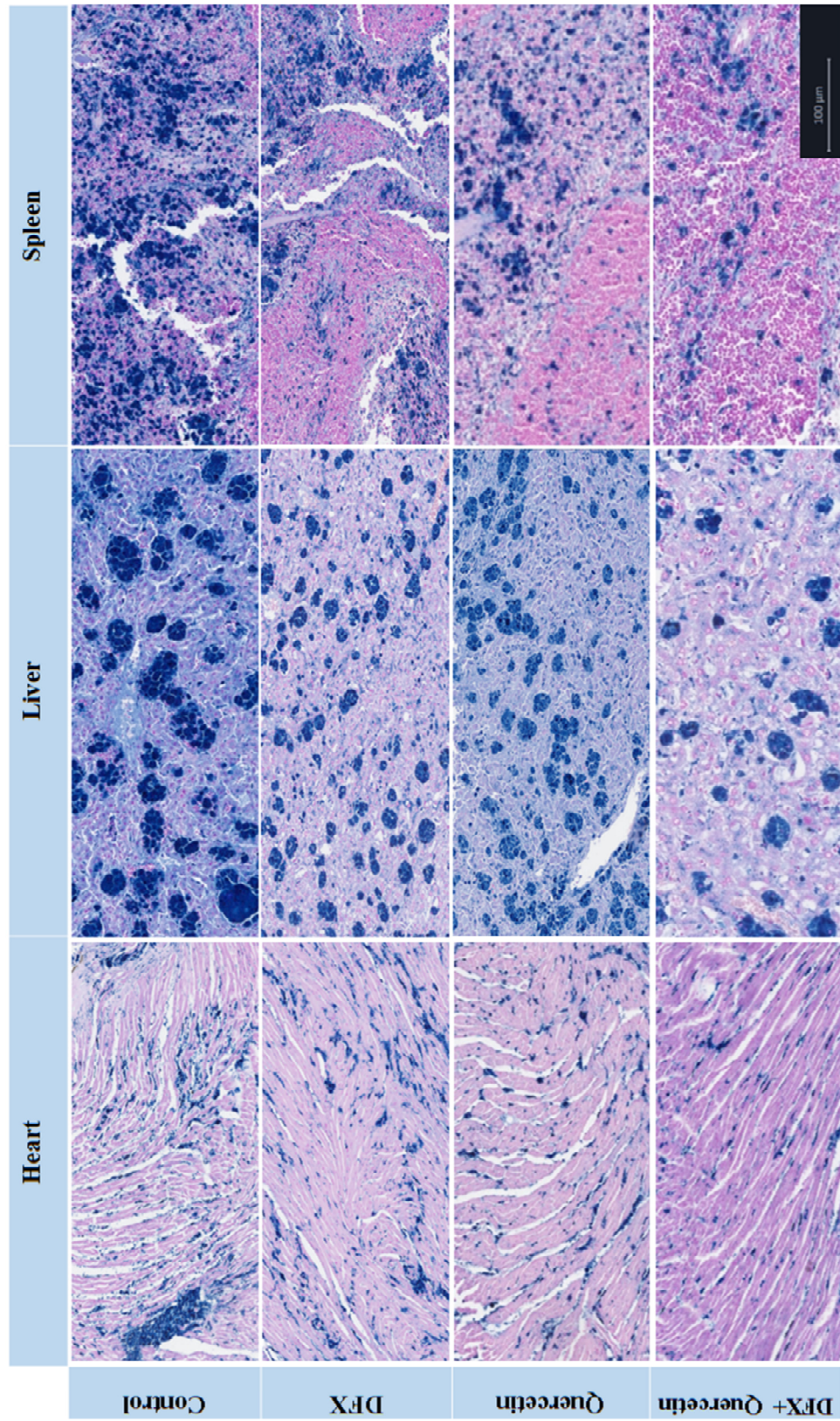
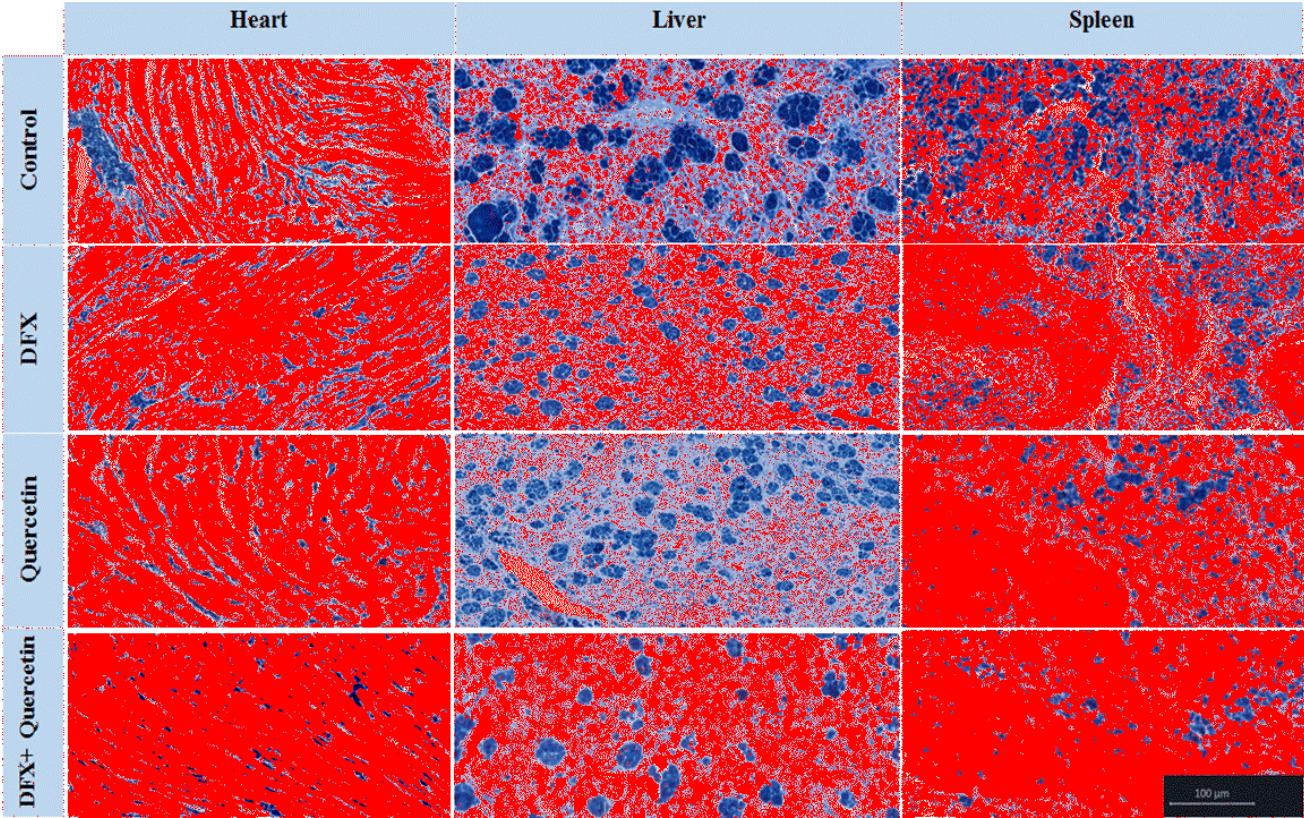




Figure 70 Perls stain images from Figure 69, following Image J modification to enable blue stained iron pixel quantification

(Acknowledgement to Prof Richard Naftalin, King's College London, for generating this suggestion)



**Table 20 Total 'blue' iron containing area count from the histology images in Figure 70 .**

<b>Total 'blue' Area</b>	<b>Heart</b>	<b>Liver</b>	<b>Spleen</b>
<b>Control</b>	<b>178</b>	<b>11340</b>	<b>1607</b>
<b>DFX</b>	<b>54</b>	<b>150</b>	<b>519</b>
<b>Quercetin</b>	<b>10</b>	<b>10465</b>	<b>18</b>
<b>DFX + Quercetin</b>	<b>3</b>	<b>78</b>	<b>57</b>

**Table 21 Total number of 'blue' pixels in the histology images in Figure 70 .**

<b>Number of 'blue' pixels</b>	<b>Heart</b>	<b>Liver</b>	<b>Spleen</b>
<b>Control</b>	<b>50</b>	<b>1217</b>	<b>284</b>
<b>DFX</b>	<b>17</b>	<b>65</b>	<b>95</b>
<b>Quercetin</b>	<b>7</b>	<b>2209</b>	<b>15</b>
<b>DFX + Quercetin</b>	<b>2</b>	<b>42</b>	<b>35</b>

### **7.6.2 Conclusions**

This novel mouse model was used to study the hypothesis that iron chelating compounds are effective at mobilising tissue iron when administered by the oral route, and to determine of the relative efficacy of addition of a flavonoid such as quercetin to commercially available oral treatment in terms of mobilising cardiac iron. It is clear from the above results that there could be value in the combination of DFX treatment with oral quercetin to improve iron mobilisation. Performing dose escalation of the flavonoid in addition to commercially used doses of DFX as well as assessing tissue

iron at longer time points will allow a more detailed study of the extent of iron mobilisation with potential reduction in experimental error. The Quercetin compound was selected on the basis of previous data using hepatocyte and cardiomyocyte cell cultures (**Chapter 6**) which demonstrated promising results in terms of iron mobilisation. It can be concluded that the findings in this chapter show that there is a close relationship between the efficacy of quercetin in cell culture and in the iron-overloaded mouse. The findings support the contention that hepatocytes/cardiomyocytes are a useful first model for screening new compounds both for their toxicity and efficacy. The cellular models are limited however in that they cannot be used to study eventualities such as oral efficacy and inactivation by metabolism.

## Chapter 8 CONCLUSIONS AND FUTURE PERSPECTIVES

### 8.1 The value of the *in vitro* cultures and *in vivo* mouse model for investigating iron chelators

The work in this thesis has characterised an *in vitro* model of iron loading that can evaluate iron chelators and their interactions in hepatocytes as well as cardiomyocytes. The value of this model has been tested by studying the optimal use for clinically available iron chelators to mobilise cardiac and hepatic iron. This model is also relevant to the development of new chelators as it has a number of features, detailed below, which are highly applicable in the early evaluation of novel compounds. Firstly, small quantities of chelator are required for screening, in contrast to animal models where at least 10 times the quantity of the drug is required. Furthermore, a number of compounds can be screened in one experiment, which is not readily applicable to the use of laboratory mice, where many more animals are required for *in vivo* screening. Therefore, compounds can be evaluated and excluded from further consideration without the potentially costly need to first scale up their synthesis. At the same time, compounds which are toxic to cells can be identified at an early stage and excluded from further development. Thus, as a first step in the evaluation of new compounds, this model has a number of advantages over *in vivo* systems. Of the *in vitro* systems available, it is clear that the hepatocyte and cardiomyocyte models are the most relevant for studying cellular iron mobilisation by iron chelators as hepatocytes are the cell type with the largest iron storage in transfusional iron overload, and removal of iron from the heart is one of the biggest challenges in reducing mortality from transfusional cardiac siderosis.

The cellular model was primarily used to elucidate several principles about the interactions of chelators within cells. It allowed for the first time a detailed interrogation of synergy as opposed to additivity of action of licensed chelators when used in combination, which has now been published. In HuH7 and H9C2 cells, all combinations of commercially available iron chelators showed synergistic cellular iron mobilisation at 8 hours, with most importantly, at clinically achievable concentrations of the ‘sink’ and ‘shuttle’ chelator. Interestingly, the greatest synergism was achieved by combining DFP with DFX, where about 60 and 65% of the mobilised iron was attributable to



synergistic interaction in hepatocytes and cardiomyocytes respectively. In our model, the dose of DFX had to be reduced by 3.8 fold to produce a half-maximal chelation effect when the concentration of DFP was just 1 $\mu$ M in HuH7 cells. Furthermore, it was noted that the presence of 5 $\mu$ M DFP could reduce the dose of DFX required to produce a 50% of the maximal chelation effect by 17.9 mg/kg in H9C2 cells. This concentration of DFP is clinically achievable (Limenta et al, 2011a). These studies confirm that for synergistic cellular iron mobilisation, one chelator must have the physicochemical properties to enter cells, chelate intracellular iron and subsequently donate iron to a second 'sink' chelator.

In this work, I demonstrate for the first time the iron binding properties of ELT in solution, a drug used to manage ITP, as well as its iron mobilising properties from cells. It was noted that remarkably low concentrations of ELT are required to mobilise cellular iron and as a single agent, ELT is at least as effective as clinically licensed iron chelators at mobilising cardiomyocyte iron. Additive or synergistic intracellular chelation is shown when ELT is combined with clinically available chelators. The doses of ELT, alone or in combination with other chelators, are sufficiently low and clinically achievable, suggesting that ELT could be used to enhance iron chelation in patients who are not thrombocytopenic.

I also investigated iron mobilising properties by the naturally occurring flavonoid quercetin and its principle metabolites. For the first time I show that quercetin can act as an iron 'shuttle' when combined with licensed iron chelators. Metabolism of quercetin does not abolish its iron mobilisation properties as a large number of its metabolites share its iron chelating properties. Once again, the doses of quercetin, alone or in combination with other chelators, are sufficiently low and clinically achievable to suggest quercetin could be used as an adjunct to iron chelation therapy, with the DFP-Quercetin combination appearing to be the most synergistic. Furthermore, I have shown a unique structure-function analysis of flavonoids with regards to iron and ferritin mobilisation and antioxidant capacity as a function of Fe(II) binding using our cellular models.

In the final two chapters of this thesis, I present a humanised model of  $\beta$  thalassaemia with cardiac iron loading that is highly suited for evaluating iron chelators and in conjunction with the MRI techniques developed on this model by our collaborators in the Centre for Advanced Biomedical Imaging, UCL, it should prove valuable in the assessment and prediction of response to novel clinical treatments in humans. This work shows novel and clear evidence of iron loading within the heart myocytes following *ip* administration of iron dextran. A number of modes of administration and forms of iron have been attempted to induce pathological iron overload including dietary carbonyl and ferrocene iron, however, the pattern of iron deposition has not been shown to include intracellular cardiomyocyte deposition. This could either be due to frequency of treatment, duration of treatment or inadequate time allowed for iron re-equilibration.

This novel mouse model was used to study the hypothesis that iron chelating compounds are effective at mobilising tissue iron when administered by the oral route, and to determine the relative efficacy of addition of a flavonoid such as quercetin to commercially available oral treatment in terms of mobilising cardiac iron. It is clear from the results in **Chapter 7** that there could be value in the combination of DFX treatment with oral quercetin to improve iron mobilisation. Performing dose escalation of the flavonoid in addition to commercially used doses of DFX as well as assessing tissue iron at longer time points will allow a more detailed study of the extent of iron mobilisation with potential reduction in experimental error. The quercetin compound was selected following results in cell culture (**Chapter 6**). It can be concluded that there is a close relationship between the efficacy of quercetin in cell culture and in the iron-overloaded mouse, and therefore the findings support the contention that our cellular models provide useful first screening of compounds for their toxicity and efficacy.

## **8.2 Limitations of the cellular culture system in investigating iron chelators**

From the discussions above, it appears that our cellular models are both predictive and relevant, but like all models, they have limitations and these must be considered.

An important aspect of the efficacy of chelators which may not be adequately addressed in cell cultures is the influence of their metabolism on this variable. Cultured

hepatocytes lose their cytochrome P450 progressively unless special culture conditions are maintained (Naughton et al, 1995; Tong et al, 1994). Thus, when using cell lines, the levels of cytochrome P450 are likely to have fallen to a fraction of physiological levels. This enzyme is important in 'Phase I' metabolism which includes oxidation of drugs in the liver through a process requiring NADPH and oxygen. This is unlikely to be of major significance with regards to hydroxypyridinones examined clinically, namely DFP (CP20), as the most important metabolic route occurs in 'Phase II metabolism' by glucuronidation, independently of cytochrome P450 (Choudhury & Singh, 1995; Hoyes & Porter, 1993). Similarly, the metabolism of DFX is heavily dependent on glucuronidation, and only a small fraction (<8%) is oxidative (cytochrome P450 dependent) in humans (Waldmeier et al, 2010).

The importance of determining chelator metabolism is further demonstrated by the interspecies variability for example in the case of the hydroxypyridinone (CP94). CP94 is extremely effective in mobilising liver iron in rats but by contrast, in guinea-pigs, the compound lacked any liver iron mobilisation effects. Close examination of the metabolism of this compound reveals that this can be attributed directly to inactivation of the iron binding site of the molecule by glucuronidation in the guinea pig (Porter et al, 1993; Waldmeier et al, 2010). The importance of drug metabolism is further demonstrated when looking at the effect of CP94 in thalassaemic patients. Due to rapid glucuronidation, its efficacy was once again poor when compared to DFO (Porter et al, 1994). Interestingly this was in contrast to the findings in *Cebus* monkeys, where CP94 was more effective than DFO (Bergeron et al, 1992). Furthermore, the widely used and effective iron chelator DFP used in humans had little impact in rats and monkeys (Bergeron et al, 1992).

Therefore any findings with respect to the efficacy of chelators in the mouse or cellular model should ideally be confirmed with metabolism studies in other species or using primary human cells. The way in which this is approached will depend on the resources available and the questions being addressed. Pharmacokinetic and metabolism studies can be performed in several species of laboratory animals to determine whether inactivation is likely to be problematic (Choudhury & Singh, 1995; Porter et al, 1993). Alternatively, metabolism of compounds in freshly isolated human hepatocytes or

human hepatocyte cultures (Gibson-D'Ambrosio et al, 1993) can be undertaken under special conditions so as to maintain cytochrome P450 levels if necessary (Gomez-Lechon et al, 1990; Naughton et al, 1995; Tong et al, 1994).

Finally, while the cellular models described in this work are a useful early step in screening for the unwanted toxic effects on cells, these cannot be expected to screen for all the toxic effects of iron chelators. It is known that iron chelators have important inhibitory effects on cell proliferation, affecting DNA synthesis and the cell cycle, as well as apoptosis, with clinical manifestations such as bone marrow suppression. This model is not intended to examine these effects. The novel mouse model could provide further insight on the above although animal and cellular models should be used together to best predict both beneficial and adverse effects of novel chelators for clinical use.

Numerous animal models have been developed to study iron loading and chelation, utilising different methodologies to model iron overload and its related complications. Rodent models are imperfect surrogates for studying the efficacy of chelators in humans as there are differences in iron accessibility and storage as well as in drug metabolism and half-life, which limits the extrapolation of results to humans. One such limitation of the humanised thalassaemia mouse model used in this work is that iron loading with iron-dextran leads to cardiac iron deposition, with a significant proportion occurring interstitially with subsequent redistribution into the myocyte. Although interstitial iron deposition in the heart is universal in thalassaemia patients (Buja & Roberts, 1971), it is less prominent than in rodents.

Furthermore, in rodents cardiac and liver iron appears to be much more closely correlated than in humans (WOOD et al, 2011), which suggests less asymmetry in the loading of organs as well as iron clearance compared to humans (Anderson et al, 2004; Wood et al, 2004). A further limitation of the mouse model is that no animal model accurately mimics human iron loading and often the loading follows a more strenuous regimen in experimental animals compared to patients. Furthermore, certain animals such as the gerbil spontaneously eliminate iron at high rates and this loss can potentially cause drug specific alterations and iron distribution effects that cannot be extrapolated

to human disease. In humans, iron loading secondary to transfusions overlaps with chelation protocols, thus introducing further variation and difficulty in creating a model.

### **8.3 Future developments and perspectives**

A further test of the value of the cellular and animal models is their future use beyond the immediate circumstances for which they were developed. The cellular models continue to be in use in the author's laboratory for identifying new compounds to improve the therapeutic safety margin of currently commercially available chelation therapy. Recent work in progress involves developing a pancreatic 'insulinoma' cell line model to investigate the impact of chelation treatment on insulin secretion. We aim in the near future to use our humanised  $\beta$  thalassaemia iron-overloaded mouse model to study the effects on cardiac iron overload by studying the addition of ELT to chelation treatment, such as, for example, the oral chelator DFX.

### **8.4 Conclusion**

In conclusion, the novel cellular models presented in this work are representative of 'unphysiological' iron overload and provide a useful initial step in the identification of new chelators which can mobilise iron, particularly when small quantities of novel drugs are available or when large numbers of compounds need to be primarily assessed. Furthermore, they can provide great insight into the interactions between chelators and their predicted additive/synergistic effects. These models are predictive of the iron mobilising properties of compounds with *in vivo* models and are extremely valuable in identifying principles concerning chelators' interactions with cardiomyocyte as well as hepatocyte iron pools. Both these models are currently in use in our laboratory at UCL and we have used them to generate data in support of the use of ELT as well as quercetin to enhance iron mobilisation by licensed chelators.

The novel humanised  $\beta$  thalassaemia iron-overloaded mouse model demonstrating cardiac iron loading is a first-in-kind development, and the novel application of MRI to ascertain T2\* in the mouse heart and liver, will provide a useful tool for studying iron chelators, the pathophysiology and disease progression, blood transfusion regimens and cellular/gene therapy in iron overload in the future.

## APPENDICES

- (2014) Glucuronidation does not suppress the estrogenic activity of quercetin in yeast and human breast cancer cell model systems, 559, 62–67.
- (2016a) *Biosoft: Software for Science*, 2016a. Available online: <http://www.biosoft.com/w/calculusyn.htm> [Accessed].
- (2016b) *HySS Hyperquad Simulation and Speciation*, 2016b. Available online: <http://www.hyperquad.co.uk/hyss.htm> [Accessed].
- (2016c) *pHAb Stability constants from pH and absorbance measurements*, 2016c. Available online: <http://www.hyperquad.co.uk/phab.htm> [Accessed].
- Abhay K. Pandey, A. K. M., Amita Mishra, Shashank Kumar, Amita Chandra (2010) Therapeutic potential of *C.Zeylanicum* extracts: an antifungal and antioxidant perspective.
- al-Refaie, F. N., Sheppard, L. N., Nortey, P., Wonke, B. & Hoffbrand, A. V. (1995) Pharmacokinetics of the oral iron chelator deferiprone (L1) in patients with iron overload. *Br J Haematol*, 89(2), 403-8.
- al-Refaie, F. N., Wonke, B., Hoffbrand, A. V., Wickens, D. G., Nortey, P. & Kontoghiorghes, G. J. (1992) Efficacy and possible adverse effects of the oral iron chelator 1,2-dimethyl-3-hydroxypyrid-4-one (L1) in thalassemia major. *Blood*, 80(3), 593-9.
- Alderighi, L., Gans, P., Ienco, A., Peters, D., Sabatini, A. & Vacca, A. (2016) Hyperquad simulation and speciation (HySS): a utility program for the investigation of equilibria involving soluble and partially soluble species.
- Anderson, L. J., Westwood, M. A., Holden, S., Davis, B., Prescott, E., Wonke, B., Porter, J. B., Walker, J. M. & Pennell, D. J. (2004) Myocardial iron clearance during reversal of siderotic cardiomyopathy with intravenous desferrioxamine: a prospective study using T2\* cardiovascular magnetic resonance. *Br J Haematol*, 127(3), 348-55.
- Arden, G. B., Wonke, B., Kennedy, C. & Huehns, E. R. (1984) Ocular changes in patients undergoing long-term desferrioxamine treatment. *Br J Ophthalmol*, 68(12), 873-7.
- Asare, G. A., Paterson, A. C., Kew, M. C., Khan, S. & Mossanda, K. S. (2006) Iron-free neoplastic nodules and hepatocellular carcinoma without cirrhosis in Wistar rats fed a diet high in iron. *J Pathol*, 208(1), 82-90.
- Awai, M., Narasaki, M., Yamanoi, Y. & Seno, S. (1979) Induction of diabetes in animals by parenteral administration of ferric nitrilotriacetate. A model of experimental hemochromatosis. *Am J Pathol*, 95(3), 663-73.
- Aydinok, Y., Evans, P., Manz, C. Y. & Porter, J. B. (2012a) Timed non-transferrin bound iron determinations probe the origin of chelatable iron pools during deferiprone regimens and predict chelation response. *Haematologica*, 97(6), 835-41.
- Aydinok, Y., Unal, S., Oymak, Y., Vergin, C., Turker, Z. D., Yildiz, D. & Yesilipek, A. (2012b) Observational study comparing long-term safety and efficacy of Deferasirox with Desferrioxamine therapy in chelation-naive children with transfusional iron overload. *European journal of haematology*, 88(5), 431-8.
- Bacon, B. R. & Tavill, A. S. (1984) Role of the liver in normal iron metabolism. *Semin Liver Dis*, 4(3), 181-92.
- Badylak, S. F. & Babbs, C. F. (1986) The effect of carbon dioxide, lidoflazine and deferoxamine upon long term survival following cardiorespiratory arrest in rats. *Resuscitation*, 13(3), 165-73.

- Bahram, S., Gilfillan, S., Kühn, L. C., Moret, R., Schulze, J. B., Lebeau, A. & Schümann, K. (1999) Experimental hemochromatosis due to MHC class I HFE deficiency: immune status and iron metabolism. *Proc Natl Acad Sci U S A*, 96(23), 13312-7.
- Bailey-Wood, R., White, G. P. & Jacobs, A. (1975) The use of Chang cells cultured in vitro for the investigation of cellular iron metabolism. *Br J Exp Pathol*, 56(4), 358-62.
- Bailey, S., Evans, R. W., Garratt, R. C., Gorinsky, B., Hasnain, S., Horsburgh, C., Jhoti, H., Lindley, P. F., Mydin, A., Sarra, R. & et al. (1988) Molecular structure of serum transferrin at 3.3-Å resolution. *Biochemistry*, 27(15), 5804-12.
- Baker, E., Page, M. & Morgan, E. H. (1985) Transferrin and iron release from rat hepatocytes in culture. *Am J Physiol*, 248(1 Pt 1), G93-7.
- Baker, E., Vicary, F. R. & Huehns, E. R. (1981) Iron release from isolated hepatocytes. *Br J Haematol*, 47(4), 493-504.
- Baker, E., Wong, A., Peter, H. & Jacobs, A. (1992) Desferrithiocin is an effective iron chelator in vivo and in vitro but ferrithiocin is toxic. *Br J Haematol*, 81(3), 424-31.
- Barry, M., Flynn, D. M., Letsky, E. A. & Risdon, R. A. (1974) Long-term chelation therapy in thalassaemia major: effect on liver iron concentration, liver histology, and clinical progress. *Br Med J*, 2(5909), 16-20.
- Barton, J. C. (2007) Drug evaluation: deferitricin (GT-56-252; NaHBED) for iron overload disorders. *IDrugs*, 10(4), 270-81.
- Batey, R. G., Shamir, S. & Wilms, J. (1981) Properties and hepatic metabolism of non-transferrin-bound iron. *Dig Dis Sci*, 26(12), 1084-8.
- Beinert, H. & Kennedy, M. C. (1989) 19th Sir Hans Krebs lecture. Engineering of protein bound iron-sulfur clusters. A tool for the study of protein and cluster chemistry and mechanism of iron-sulfur enzymes. *Eur J Biochem*, 186(1-2), 5-15.
- Bellanti, F., Danhof, M. & Della Pasqua, O. (2014) Population pharmacokinetics of deferiprone in healthy subjects. *Br J Clin Pharmacol*, 78(6), 1397-406.
- Berdoukas, V., Bentley, P., Frost, H. & Schnebli, H. P. (1993) Toxicity of oral iron chelator L1. *Lancet*, 341(8852), 1088.
- Bergeron, R. J., Streiff, R. R., Creary, E. A., Daniels, R. D., Jr., King, W., Luchetta, G., Wiegand, J., Moerker, T. & Peter, H. H. (1993) A comparative study of the iron-clearing properties of desferrithiocin analogues with desferrioxamine B in a Cebus monkey model. *Blood*, 81(8), 2166-73.
- Bergeron, R. J., Streiff, R. R., Wiegand, J., Luchetta, G., Creary, E. A. & Peter, H. H. (1992) A comparison of the iron-clearing properties of 1,2-dimethyl-3-hydroxypyrid-4-one, 1,2-diethyl-3-hydroxypyrid-4-one, and deferoxamine. *Blood*, 79(7), 1882-90.
- Bergeron, R. J., Wiegand, J., Dionis, J. B., Egli-Karmakka, M., Frei, J., Huxley-Tencer, A. & Peter, H. H. (1991) Evaluation of desferrithiocin and its synthetic analogues as orally effective iron chelators. *J Med Chem*, 34(7), 2072-8.
- Bergeron, R. J., Wiegand, J., Wollenweber, M., McManis, J. S., Algee, S. E. & Ratliff-Thompson, K. (1996) Synthesis and biological evaluation of naphthyldeferrithiocin iron chelators. *J Med Chem*, 39(8), 1575-81.
- Bernstein, S. E. (1987) Hereditary hypotransferrinemia with hemosiderosis, a murine disorder resembling human atransferrinemia. *J Lab Clin Med*, 110(6), 690-705.
- Blake, D. R., Winyard, P., Lunec, J., Williams, A., Good, P. A., Crewes, S. J., Gutteridge, J. M., Rowley, D., Halliwell, B., Cornish, A. & et al. (1985) Cerebral and ocular toxicity induced by desferrioxamine. *Q J Med*, 56(219), 345-55.
- Blatt, J. & Stitely, S. (1987) Antineuroblastoma activity of desferoxamine in human cell lines. *Cancer Res*, 47(7), 1749-50.

- Boesch-Saadatmandi, C., Loboda, A., Wagner, A. E., Stachurska, A., Jozkowicz, A., Dulak, J., Doring, F., Wolfram, S. & Rimbach, G. (2011) Effect of quercetin and its metabolites isorhamnetin and quercetin-3-glucuronide on inflammatory gene expression: role of miR-155. *J Nutr Biochem*, 22(3), 293-9.
- Bomford, A. B. & Munro, H. N. (1985) Transferrin and its receptor: their roles in cell function. *Hepatology*, 5(5), 870-5.
- Boots, A. W., Haenen, G. R. & Bast, A. (2008) Health effects of quercetin: from antioxidant to nutraceutical. *Eur J Pharmacol*, 585(2-3), 325-37.
- Borgna-Pignatti, C., Cappellini, M. D., De Stefano, P., Del Vecchio, G. C., Forni, G. L., Gamberini, M. R., Ghilardi, R., Piga, A., Romeo, M. A., Zhao, H. & Cnaan, A. (2006) Cardiac morbidity and mortality in deferoxamine- or deferiprone-treated patients with thalassemia major. *Blood*, 107(9), 3733-7.
- Borgna-Pignatti, C. & Marsella, M. (2015) Iron Chelation in Thalassemia Major. *Clin Ther*, 37(12), 2866-77.
- Bothwell, T. H., Charlton, R., Cook, J. & Finch, C. (1979) Iron metabolism in man. *Iron metabolism in man*.
- Bothwell, T. H., Roos, N. & Lifschitz, M. L. (1964) A METHOD FOR MEASURING THE STORAGE IRON CONTENT OF FORMALINISED TISSUES. *S Afr J Med Sci*, 29, 21-6.
- Bradford, M. M. (1976) A rapid and sensitive method for the quantitation of microgram quantities of protein utilizing the principle of protein-dye binding. *Anal Biochem*, 72, 248-54.
- Bradley, B., Prowse, S. J., Bauling, P. & Lafferty, K. J. (1986) Desferrioxamine treatment prevents chronic islet allograft damage. *Diabetes*, 35(5), 550-5.
- Breuer, W., Epsztejn, S. & Cabantchik, Z. I. (1995) Iron acquired from transferrin by K562 cells is delivered into a cytoplasmic pool of chelatable iron(II). *J Biol Chem*, 270(41), 24209-15.
- Breuer, W., Epsztejn, S. & Cabantchik, Z. I. (1996) Dynamics of the cytosolic chelatable iron pool of K562 cells. *FEBS Lett*, 382(3), 304-8.
- Brissot, P., Wright, T. L., Ma, W. L. & Weisiger, R. A. (1985) Efficient clearance of non-transferrin-bound iron by rat liver. Implications for hepatic iron loading in iron overload states. *J Clin Invest*, 76(4), 1463-70.
- Brittenham, G. M., Griffith, P. M., Nienhuis, A. W., McLaren, C. E., Young, N. S., Tucker, E. E., Allen, C. J., Farrell, D. E. & Harris, J. W. (1994) Efficacy of deferoxamine in preventing complications of iron overload in patients with thalassemia major. *N Engl J Med*, 331(9), 567-73.
- Brown, J. E., Khodr, H., Hider, R. C. & Rice-Evans, C. A. (1998) Structural dependence of flavonoid interactions with Cu<sup>2+</sup> ions: implications for their antioxidant properties. *Biochem J*, 330 ( Pt 3), 1173-8.
- Brusselmans, K., Vrolix, R., Verhoeven, G. & Swinnen, J. V. (2005) Induction of cancer cell apoptosis by flavonoids is associated with their ability to inhibit fatty acid synthase activity. *J Biol Chem*, 280(7), 5636-45.
- Buja, L. M. & Roberts, W. C. (1971) Iron in the heart. Etiology and clinical significance. *Am J Med*, 51(2), 209-21.
- Burak, C., Brüll, V., Langguth, P., Zimmermann, B. F., Stoffel-Wagner, B., Sausen, U., Stehle, P., Wolfram, S. & Egert, S. (2015) Higher plasma quercetin levels following oral administration of an onion skin extract compared with pure quercetin dihydrate in humans. *Eur J Nutr*.
- Bussel, J. B., Cheng, G., Saleh, M. N., Psaila, B., Kovaleva, L., Meddeb, B., Kloczko, J., Hassani, H., Mayer, B., Stone, N. L., Arning, M., Provan, D. & Jenkins, J. M. (2007)



- Eltrombopag for the treatment of chronic idiopathic thrombocytopenic purpura. *N Engl J Med*, 357(22), 2237-47.
- Bussel, J. B., Provan, D., Shamsi, T., Cheng, G., Psaila, B., Kovaleva, L., Salama, A., Jenkins, J. M., Roychowdhury, D., Mayer, B., Stone, N. & Arning, M. (2009) Effect of eltrombopag on platelet counts and bleeding during treatment of chronic idiopathic thrombocytopenic purpura: a randomised, double-blind, placebo-controlled trial. *Lancet*, 373(9664), 641-8.
- Bussel, J. B., Saleh, M. N., Vasey, S. Y., Mayer, B., Arning, M. & Stone, N. L. (2013) Repeated short-term use of eltrombopag in patients with chronic immune thrombocytopenia (ITP). *Br J Haematol*, 160(4), 538-46.
- Cabantchik, Z. I. (2014) Labile iron in cells and body fluids: physiology, pathology, and pharmacology. *Front Pharmacol*, 5, 45.
- Cairo, G., Tacchini, L., Recalcati, S., Azzimonti, B., Minotti, G. & Bernelli-Zazzera, A. (1998) Effect of reactive oxygen species on iron regulatory protein activity. *Ann N Y Acad Sci*, 851, 179-86.
- Cao, G., Sofic, E. & Prior, R. L. (1997) Antioxidant and prooxidant behavior of flavonoids: structure-activity relationships. *Free Radic Biol Med*, 22(5), 749-60.
- Cappellini, M. D., Bejaoui, M., Agaoglu, L., Canatan, D., Capra, M., Cohen, A., Drelichman, G., Economou, M., Fattoum, S., Kattamis, A., Kilinc, Y., Perrotta, S., Piga, A., Porter, J. B., Griffel, L., Dong, V., Clark, J. & Aydinok, Y. (2011) Iron chelation with deferasirox in adult and pediatric patients with thalassemia major: efficacy and safety during 5 years' follow-up. *Blood*, 118(4), 884-93.
- Cappellini, M. D., Cohen, A., Piga, A., Bejaoui, M., Perrotta, S., Agaoglu, L., Aydinok, Y., Kattamis, A., Kilinc, Y., Porter, J., Capra, M., Galanello, R., Fattoum, S., Drelichman, G., Magnano, C., Verissimo, M., Athanassiou-Metaxa, M., Giardina, P., Kourakli-Symeonidis, A., Janka-Schaub, G., Coates, T., Vermynen, C., Olivieri, N., Thuret, I., Opitz, H., Ressayre-Djaffer, C., Marks, P. & Alberti, D. (2006a) A phase 3 study of deferasirox (ICL670), a once-daily oral iron chelator, in patients with beta-thalassemia. *Blood*, 107(9), 3455-62.
- Cappellini, M. D., Cohen, A., Piga, A., Bejaoui, M., Perrotta, S., Agaoglu, L., Aydinok, Y., Kattamis, A., Kilinc, Y., Porter, J., Capra, M., Galanello, R., Fattoum, S., Drelichman, G., Magnano, C., Verissimo, M., Athanassiou-Metaxa, M., Giardina, P., Kourakli-Symeonidis, A., Janka-Schaub, G., Coates, T., Vermynen, C., Olivieri, N., Thuret, I., Opitz, H., Ressayre-Djaffer, C., Marks, P. & Alberti, D. (2006b) A phase 3 study of deferasirox (ICL670), a once-daily oral iron chelator, in patients with  $\beta$ -thalassemia.
- Carpenter, J.-P., He, T., Kirk, P., Roughton, M., Anderson, L. J., de Noronha, S. V., Baksi, A. J., Sheppard, M. N., Porter, J. B., Walker, J. M., Wood, J. C., Forni, G., Catani, G., Matta, G., Fucharoen, S., Fleming, A., House, M., Black, G., Firmin, D. N., St Pierre, T. G. & Pennell, D. J. (2014) Calibration of myocardial T2 and T1 against iron concentration. *J Cardiovasc Magn Reson*, 16, 62.
- Carpenter, J. P., He, T., Kirk, P., Roughton, M., Anderson, L. J., de Noronha, S. V., Sheppard, M. N., Porter, J. B., Walker, J. M., Wood, J. C., Galanello, R., Forni, G., Catani, G., Matta, G., Fucharoen, S., Fleming, A., House, M. J., Black, G., Firmin, D. N., St Pierre, T. G. & Pennell, D. J. (2011) On T2\* magnetic resonance and cardiac iron. *Circulation*, 123(14), 1519-28.
- Cavill, I., Worwood, M. & Jacobs, A. (1975) Internal regulation of iron absorption. *Nature*, 256(5515), 328-9.
- Cds, A. U. X. (2009) Supplemental Figure 1 Supplemental Figure 2, 2(C), 1--10.

- Cheng, G., Saleh, M. N., Marcher, C., Vasey, S., Mayer, B., Aivado, M., Arning, M., Stone, N. L. & Bussel, J. B. (2011) Eltrombopag for management of chronic immune thrombocytopenia (RAISE): a 6-month, randomised, phase 3 study. *Lancet*, 377(9763), 393-402.
- Chiew, K. H., Phoon, M. C., Putti, T., Tan, B. K. & Chow, V. T. (2016) Evaluation of antiviral activities of *Houttuynia cordata* Thunb. extract, quercetin, quercetrin and cinanserin on murine coronavirus and dengue virus infection. *Asian Pac J Trop Med*, 9(1), 1-7.
- Choudhury, R. & Singh, S. (1995) Effect of iron overload on the metabolism and urinary recovery of 3-hydroxypyridin-4-one chelating agents in the rat. *Drug Metab Dispos*, 23(3), 314-20.
- Cohen, A. R., Galanello, R., Piga, A., De Sanctis, V. & Tricta, F. (2003) Safety and effectiveness of long-term therapy with the oral iron chelator deferiprone. *Blood*, 102(5), 1583-7.
- Cohen, A. R., Mizanin, J. & Schwartz, E. (1989) Rapid removal of excessive iron with daily, high-dose intravenous chelation therapy. *J Pediatr*, 115(1), 151-5.
- Cole, E. S. & Glass, J. (1983) Transferrin binding and iron uptake in mouse hepatocytes. *Biochim Biophys Acta*, 762(1), 102-10.
- Conquer, J. A., Maiani, G., Azzini, E., Raguzzini, A. & Holub, B. J. (1998) Supplementation with quercetin markedly increases plasma quercetin concentration without effect on selected risk factors for heart disease in healthy subjects. *J Nutr*, 128(3), 593-7.
- Cooper, C. E., Lynagh, G. R., Hoyes, K. P., Hider, R. C., Cammack, R. & Porter, J. B. (1996) The relationship of intracellular iron chelation to the inhibition and regeneration of human ribonucleotide reductase. *J Biol Chem*, 271(34), 20291-9.
- Cragg, S. J., Covell, A. M., Burch, A., Owen, G. M., Jacobs, A. & Worwood, M. (1983) Turnover of <sup>131</sup>I-human spleen ferritin in plasma. *Br J Haematol*, 55(1), 83-92.
- Cragg, S. J., Wagstaff, M. & Worwood, M. (1981) Detection of a glycosylated subunit in human serum ferritin. *Biochem J*, 199(3), 565-71.
- Cumming, R. W., Thomson, J. & Koppel, J. L. (1978) Iron: a possible heterotropic effector of prolyl hydroxylase. *Biochim Biophys Acta*, 523(2), 533-7.
- Cunningham, J. M., al-Refaie, F. N., Hunter, A. E., Sheppard, L. N. & Hoffbrand, A. V. (1994) Differential toxicity of alpha-keto hydroxypyridine iron chelators and desferrioxamine to human haemopoietic precursors in vitro. *Eur J Haematol*, 52(3), 176-9.
- Dautry-Varsat, A., Ciechanover, A. & Lodish, H. F. (1983) pH and the recycling of transferrin during receptor-mediated endocytosis. *Proc Natl Acad Sci U S A*, 80(8), 2258-62.
- Davies, S. C., Marcus, R. E., Hungerford, J. L., Miller, H. M., Arden, G. B. & Huehns, E. R. (1983) Ocular toxicity of high-dose intravenous desferrioxamine. *Lancet*, 2, 181-184.
- Day, A. J., Canada, F. J., Diaz, J. C., Kroon, P. A., McLauchlan, R., Faulds, C. B., Plumb, G. W., Morgan, M. R. & Williamson, G. (2000) Dietary flavonoid and isoflavone glycosides are hydrolysed by the lactase site of lactase phlorizin hydrolase. *FEBS Lett*, 468(2-3), 166-70.
- de Boer, V. C., Dihal, A. A., van der Woude, H., Arts, I. C., Wolfram, S., Alink, G. M., Rietjens, I. M., Keijer, J. & Hollman, P. C. (2005) Tissue distribution of quercetin in rats and pigs. *J Nutr*, 135(7), 1718-25.

- De Domenico, I., Vaughn, M. B., Li, L., Bagley, D., Musci, G., Ward, D. M. & Kaplan, J. (2006) Ferroportin-mediated mobilization of ferritin iron precedes ferritin degradation by the proteasome. *Embo j*, 25(22), 5396-404.
- De Domenico, I., Ward, D. M. & Kaplan, J. (2009) Specific iron chelators determine the route of ferritin degradation.
- De Virgiliis, S., Congia, M., Frau, F., Argiolu, F., Diana, G., Cucca, F., Varsi, A., Sanna, G., Podda, G., Fodde, M. & et al. (1988) Deferoxamine-induced growth retardation in patients with thalassemia major. *J Pediatr*, 113(4), 661-9.
- De Virgiliis, S., Congia, M., Frau, F., Argiolu, F., Diana, G., Cucca, F., Varsi, A., Sanna, G., Podda, G. & Fodde, M. (1988) Desferrioxamine-induced growth retardation in patients with thalassaemia major. *Journal of Pediatrics*, 113, 661-669.
- Deng, Y., Madatian, A., Wire, M. B., Bowen, C., Park, J. W., Williams, D., Peng, B., Schubert, E., Gorycki, F., Levy, M. & Gorycki, P. D. (2011) Metabolism and disposition of eltrombopag, an oral, nonpeptide thrombopoietin receptor agonist, in healthy human subjects. *Drug Metab Dispos*, 39(9), 1734-46.
- Design, i. W. (2016) eltrombopag (Revolade (EU), Promacta (US)) UKMi New Drugs Online Database.
- Deugnier, Y., Turlin, B., Ropert, M., Cappellini, M. D., Porter, J. B., Giannone, V., Zhang, Y., Griffel, L. & Brissot, P. (2011) Improvement in liver pathology of patients with beta-thalassemia treated with deferasirox for at least 3 years. *Gastroenterology*, 141(4), 1202-11.
- Dobbin, P. S., Hider, R. C., Hall, A. D., Taylor, P. D., Sarpong, P., Porter, J. B., Xiao, G. & van der Helm, D. (1993) Synthesis, physicochemical properties, and biological evaluation of N- substituted 2-alkyl-3-hydroxy-4(1H)-pyridinones: orally active iron chelators with clinical potential. *J Med Chem*, 36(17), 2448-58.
- Drysdale, J. W. & Munro, H. N. (1965) Small-scale isolation of ferritin for the assay of the incorporation of <sup>14</sup>C-labelled amino acids. *Biochem J*, 95(3), 851-8.
- Edwards, J. A. & Hoke, J. E. (1972) Defect of intestinal mucosal iron uptake in mice with hereditary microcytic anemia. *Proc Soc Exp Biol Med*, 141(1), 81-4.
- Evans, P., Kayyali, R., Hider, R. C., Eccleston, J. & Porter, J. B. (2010) MECHANISMS FOR THE SHUTTILING OF PLASMA NON-TRANSFERRIN-BOUND IRON (NTBI) ONTO DEFEROXAMINE BY DEFERIPRONE. *Transl Res*, 156(2), 55-67.
- Fawwaz, R. A., Winchell, H. S., Pollycove, M. & Sargent, T. (1967) Hepatic iron deposition in humans. I. First-pass hepatic deposition of intestinally absorbed iron in patients with low plasma latent iron-binding capacity. *Blood*, 30(4), 417-24.
- Finch, C. A., Ragan, H. A., Dyer, I. A. & Cook, J. D. (1978) Body iron loss in animals. *Proc Soc Exp Biol Med*, 159(3), 335-8.
- Fleming, M. D., Romano, M. A., Su, M. A., Garrick, L. M., Garrick, M. D. & Andrews, N. C. (1998) Nramp2 is mutated in the anemic Belgrade (b) rat: evidence of a role for Nramp2 in endosomal iron transport. *Proc Natl Acad Sci U S A*, 95(3), 1148-53.
- Florence, A., Ward, R. J., Peters, T. J. & Crichton, R. R. (1992) Studies of in vivo iron mobilization by chelators in the ferrocene-loaded rat. *Biochem Pharmacol*, 44(6), 1023-7.
- Flynn, D. M., Hoffbrand, A. V. & Politis, D. (1982) Subcutaneous desferrioxamine: the effect of three years' treatment on liver, iron, serum ferritin, and comments on echocardiography. *Birth Defects Orig Artic Ser*, 18(7), 347-53.
- Gabutti, V. & Piga, A. (1996) Results of long-term iron-chelating therapy. *Acta Haematol*, 95(1), 26-36.
- Galanello, R., Piga, A., Alberti, D., Rouan, M. C., Bigler, H. & Sechaud, R. (2003) Safety, tolerability, and pharmacokinetics of ICL670, a new orally active iron-chelating

agent in patients with transfusion-dependent iron overload due to beta-thalassemia. *J Clin Pharmacol*, 43(6), 565-72.

Galanello, R., Piga, A., Forni, G. L., Bertrand, Y., Foschini, M. L., Bordone, E., Leoni, G., Lavagetto, A., Zappu, A., Longo, F., Maseruka, H., Hewson, N., Sechaud, R., Belleli, R. & Alberti, D. (2006) Phase II clinical evaluation of deferasirox, a once-daily oral chelating agent, in pediatric patients with beta-thalassemia major. *Haematologica*, 91(10), 1343-51.

Gans, P. & O'Sullivan, B. (2000) GLEE, a new computer program for glass electrode calibration. *Talanta*, 51(1), 33-7.

Garbowski, M. W., Ma, Y., Fucharoen, S., Srichairatanakool, S., Hider, R. & Porter, J. B. (2016) Clinical and methodological factors affecting non-transferrin-bound iron values using a novel fluorescent bead assay. *Transl Res*.

Gatter, K. C., Brown, G., Trowbridge, I. S., Woolston, R. E. & Mason, D. Y. (1983) Transferrin receptors in human tissues: their distribution and possible clinical relevance. *J Clin Pathol*, 36(5), 539-45.

Giardina, P. J. & Grady, R. W. (2001) Chelation therapy in beta-thalassemia: an optimistic update. *Semin Hematol*, 38(4), 360-6.

Gibiansky, E., Zhang, J., Williams, D., Wang, Z. & Ouellet, D. (2011) Population pharmacokinetics of eltrombopag in healthy subjects and patients with chronic idiopathic thrombocytopenic purpura. *J Clin Pharmacol*, 51(6), 842-56.

Gibson-D'Ambrosio, R. E., Crowe, D. L., Shuler, C. E. & D'Ambrosio, S. M. (1993) The establishment and continuous subculturing of normal human adult hepatocytes: expression of differentiated liver functions. *Cell Biol Toxicol*, 9(4), 385-403.

Ginzburg, Y. Z., Rybicki, A. C., Suzuka, S. M., Hall, C. B., Breuer, W., Cabantchik, Z. I., Bouhassira, E. E., Fabry, M. E. & Nagel, R. L. (2009) Exogenous iron increases hemoglobin in beta-thalassemic mice. *Exp Hematol*, 37(2), 172-83.

Glickstein, H., El, R. B., Link, G., Breuer, W., Konijn, A. M., Hershko, C., Nick, H. & Cabantchik, Z. I. (2006) Action of chelators in iron-loaded cardiac cells: Accessibility to intracellular labile iron and functional consequences. *Blood*, 108(9), 3195-203.

Glickstein, H., El, R. B., Shvartsman, M. & Cabantchik, Z. I. (2005) Intracellular labile iron pools as direct targets of iron chelators: a fluorescence study of chelator action in living cells. *Blood*, 106(9), 3242-50.

Goldberg, S. L., Giardina, P. J., Chirnomas, D., Esposito, J., Paley, C. & Vichinsky, E. (2013) The palatability and tolerability of deferasirox taken with different beverages or foods. *Pediatr Blood Cancer*, 60(9), 1507-12.

Gomez-Lechon, M. J., Lopez, P., Donato, T., Montoya, A., Larrauri, A., Gimenez, P., Trullenque, R., Fabra, R. & Castell, J. V. (1990) Culture of human hepatocytes from small surgical liver biopsies. Biochemical characterization and comparison with in vivo. *In Vitro Cell Dev Biol*, 26(1), 67-74.

Gordeuk, V. R., Bacon, B. R. & Brittenham, G. M. (1987) Iron overload: causes and consequences. *Annu Rev Nutr*, 7, 485-508.

Gosriwatana, I., Loreal, O., Lu, S., Brissot, P., Porter, J. & Hider, R. C. (1999) Quantification of non-transferrin-bound iron in the presence of unsaturated transferrin. *Anal Biochem*, 273(2), 212-20.

Grady, R. W., Graziano, J. H., Akers, H. A. & Cerami, A. (1976) The development of new iron-chelating drugs. *J Pharmacol Exp Ther*, 196(2), 478-85.

Grady, R. W., Peterson, C. M., Jones, R. L., Graziano, J. H., Bhargava, K. K., Berdoukas, V. A., Kokkini, G., Loukopoulos, D. & Cerami, A. (1979) Rhodotorulic acid--investigation of its potential as an iron-chelating drug. *J Pharmacol Exp Ther*, 209(3), 342-8.

- Gralla, E. J. & Burgess, D. H. (1982) Iron retention and excretion in mice transfused with homologous or heterologous blood and treated with chelators. *Methods Find Exp Clin Pharmacol*, 4(3), 151-9.
- Graziano, J. H., Grady, R. W. & Cerami, A. (1974) The identification of 2, 3-dihydroxybenzoic acid as a potentially useful iron-chelating drug. *J Pharmacol Exp Ther*, 190(3), 570-5.
- Guo, L., Dial, S., Shi, L., Branham, W., Liu, J., Fang, J. L., Green, B., Deng, H., Kaput, J. & Ning, B. (2011) Similarities and differences in the expression of drug-metabolizing enzymes between human hepatic cell lines and primary human hepatocytes. *Drug Metab Dispos*, 39(3), 528-38.
- Guo, M., Perez, C., Wei, Y., Rapoza, E., Su, G., Bou-Abdallah, F. & Chasteen, N. D. (2007) Iron-binding properties of plant phenolics and cranberry's bio-effects. *Dalton Trans*(43), 4951-61.
- Gutteridge, J. M. & Halliwell, B. (1989) Iron toxicity and oxygen radicals. *Baillieres Clin Haematol*, 2(2), 195-256.
- Gutteridge, J. M., Richmond, R. & Halliwell, B. (1979) Inhibition of the iron-catalysed formation of hydroxyl radicals from superoxide and of lipid peroxidation by desferrioxamine. *Biochem J*, 184(2), 469-72.
- Gyparakis, M., Porter, J. B., Hirani, S., Streater, M., Hider, R. C. & Huehns, E. R. (1987) In vivo evaluation of hydroxypyridone iron chelators in a mouse model. *Acta Haematol*, 78(2-3), 217-21.
- Hamilton, K. O., Stallibrass, L., Hassan, I., Jin, Y., Halleux, C. & Mackay, M. (1994) The transport of two iron chelators, desferrioxamine B and L1, across Caco-2 monolayers. *Br J Haematol*, 86(4), 851-7.
- Harwood, M., Danielewska-Nikiel, B., Borzelleca, J. F., Flamm, G. W., Williams, G. M. & Lines, T. C. (2007) A critical review of the data related to the safety of quercetin and lack of evidence of in vivo toxicity, including lack of genotoxic/carcinogenic properties. *Food Chem Toxicol*, 45(11), 2179-205.
- Heiberg, E., Sjögren, J., Ugander, M., Carlsson, M., Engblom, H. & Arheden, H. (2010) Design and validation of Segment--freely available software for cardiovascular image analysis. *BMC Med Imaging*, 10, 1.
- Hentze, M. W., Rouault, T. A., Harford, J. B. & Klausner, R. D. (1989) Oxidation-reduction and the molecular mechanism of a regulatory RNA-protein interaction. *Science*, 244(4902), 357-9.
- Hershko, C. (1978) Determinants of fecal and urinary iron excretion in desferrioxamine-treated rats. *Blood*, 51(3), 415-23.
- Hershko, C., Cook, J. D. & Finch, D. A. (1973) Storage iron kinetics. 3. Study of desferrioxamine action by selective radioiron labels of RE and parenchymal cells. *J Lab Clin Med*, 81(6), 876-86.
- Hershko, C., Konijn, A. M., Nick, H. P., Breuer, W., Cabantchik, Z. I. & Link, G. (2001) ICL670A: a new synthetic oral chelator: evaluation in hypertransfused rats with selective radioiron probes of hepatocellular and reticuloendothelial iron stores and in iron-loaded rat heart cells in culture. *Blood*, 97(4), 1115-22.
- Hershko, C., Link, G., Pinson, A., Peter, H. H., Dobbin, P. & Hider, R. C. (1991) Iron mobilization from myocardial cells by 3-hydroxypyridin-4-one chelators: studies in rat heart cells in culture. *Blood*, 77(9), 2049-53.
- Hider, R. C., Choudhury, R., Rai, B. L., Dehkordi, L. S. & Singh, S. (1996) Design of orally active iron chelators. *Acta Haematol*, 95(1), 6-12.
- Hider, R. C. & Hall, A. D. (1991) Clinically useful chelators of tripositive elements. *Prog Med Chem*, 28, 41-173.

- Hider, R. C., Kontoghiorghes, G., Stockham, M. A. & Limited, B. I. (2002) Pharmaceutical compositions.
- Hider, R. C. & Zhou, T. (2005) The design of orally active iron chelators. *Ann N Y Acad Sci*, 1054, 141-54.
- Ho, W. L., Lin, K. H., Wang, J. D., Hwang, J. S., Chung, C. W., Lin, D. T., Jou, S. T., Lu, M. Y. & Chern, J. P. (2006) Financial burden of national health insurance for treating patients with transfusion-dependent thalassemia in Taiwan. *Bone Marrow Transplant*, 37(6), 569-74.
- Hodgson, L. L., Quail, E. A. & Morgan, E. H. (1994) Receptor-independent uptake of transferrin-bound iron by reticulocytes. *Arch Biochem Biophys*, 308(1), 318-26.
- Hoffbrand, A. V. (1994) Prospects for oral iron chelation therapy. *J Lab Clin Med*, 123(4), 492-4.
- Hoffbrand, A. V., Bartlett, A. N., Veys, P. A., O'Connor, N. T. & Kontoghiorghes, G. J. (1989) Agranulocytosis and thrombocytopenia in patient with Blackfan-Diamond anaemia during oral chelator trial, *Lancet*. England, 457.
- Hollman, P. C., Bijlsman, M. N., van Gameren, Y., Cnossen, E. P., de Vries, J. H. & Katan, M. B. (1999) The sugar moiety is a major determinant of the absorption of dietary flavonoid glycosides in man. *Free Radic Res*, 31(6), 569-73.
- Hoy, T. G. & Jacobs, A. (1981) Ferritin polymers and the formation of haemosiderin. *Br J Haematol*, 49(4), 593-602.
- Hoyes, K. P., Hider, R. C. & Porter, J. B. (1992) Cell cycle synchronization and growth inhibition by 3-hydroxypyridin-4-one iron chelators in leukemia cell lines. *Cancer Res*, 52(17), 4591-9.
- Hoyes, K. P. & Porter, J. B. (1993) Subcellular distribution of desferrioxamine and hydroxypyridin-4-one chelators in K562 cells affects chelation of intracellular iron pools. *British Journal of Haematology*, 85(2), 393-400.
- Huo, Y., McConnell, S. C., Liu, S.-R., Yang, R., Zhang, T.-T., Sun, C.-W., Wu, L.-C. & Ryan, T. M. (2009) Humanized Mouse Model of Cooley's Anemia.
- Huo, Y., McConnell, S. C., Liu, S., Zhang, T., Yang, R., Ren, J. & Ryan, T. M. (2010) Humanized mouse models of Cooley's anemia: correct fetal-to-adult hemoglobin switching, disease onset, and disease pathology. *Ann N Y Acad Sci*, 1202, 45-51.
- Ihnat, P., Vennerstrom, J. & Robinson, D. (2002) Solution equilibria of deferoxamine amides. *J Pharm Sci* 91(1733-1741).
- Irie, S. & Tavassoli, M. (1987) Transferrin-mediated cellular iron uptake. *Am J Med Sci*, 293(2), 103-11.
- Jenkins, J. M., Williams, D., Deng, Y., Uhl, J., Kitchen, V., Collins, D. & Erickson-Miller, C. L. (2007) Phase 1 clinical study of eltrombopag, an oral, nonpeptide thrombopoietin receptor agonist. *Blood*, 109(11), 4739-41.
- Jirasomprasert, T., Morales, N. P., Limonta, L. M., Sirijaroonwong, S., Yamanont, P., Wilairat, P., Fucharoen, S. & Chantharaksri, U. (2009) Pharmacokinetic-related pro-oxidant activity of deferiprone in beta-thalassemia. *Free radical research*, 43(5), 485-91.
- Kalota, A., Selak, M. A., Garcia-Cid, L. A. & Carroll, M. (2015) Eltrombopag modulates reactive oxygen species and decreases acute myeloid leukemia cell survival. *PLoS One*, 10(4), e0126691.
- Kawabata, K., Mukai, R. & Ishisaka, A. (2015) Quercetin and related polyphenols: new insights and implications for their bioactivity and bioavailability. *Food Funct*, 6(5), 1399-417.
- Kayyali, R., Porter, J. B., Liu, Z. D., Davies, N. A., Nugent, J., Cooper, C. E. & Hider, R. C. (2001) Structure-function investigation of the interaction of 1- and 2- substituted

- 3-hydroxypyridin-4-ones with 5-lipoxygenase and ribonucleotide reductase. *J Biol Chem*, 15, 15.
- Keberle, H. (1964) THE BIOCHEMISTRY OF DESFERRIOXAMINE AND ITS RELATION TO IRON METABOLISM. *Ann N Y Acad Sci*, 119, 758-68.
- Kellenberger, C. J., Schmugge, M., Saurenmann, T., Di Gennaro, L., Eber, S. W., Willi, U. V. & Babyn, P. S. (2004) Radiographic and MRI features of deferiprone-related arthropathy of the knees in patients with beta-thalassemia. *AJR Am J Roentgenol*, 183(4), 989-94.
- Kelly, G. S. (2011) Quercetin. Monograph. *Altern Med Rev*, 16(2), 172-94.
- Klausner, R. D., Van Renswoude, J., Ashwell, G., Kempf, C., Schechter, A. N., Dean, A. & Bridges, K. R. (1983) Receptor-mediated endocytosis of transferrin in K562 cells. *J Biol Chem*, 258(8), 4715-24.
- Kleber, E. E., Torrance, J. D., Bothwell, T. H., Simon, M. O. & Charlton, R. W. (1981) Mobilisation of iron from peritoneal rat macrophages by desferrioxamine. *Scand J Haematol*, 27(3), 209-18.
- Kline, M. A. & Orvig, C. (1992) Complexation of iron with the orally active decorporation drug L1 (3-hydroxy-1,2-dimethyl-4-pyridinone). *Clin Chem*, 38(4), 562-5.
- Kontoghiorghes, G. J., Aldouri, M. A., Sheppard, L. & Hoffbrand, A. V. (1987) 1,2-Dimethyl-3-hydroxypyrid-4-one, an orally active chelator for treatment of iron overload. *Lancet*, 1(8545), 1294-5.
- Kontoghiorghes, G. J., Goddard, J. G., Bartlett, A. N. & Sheppard, L. (1990a) Pharmacokinetic studies in humans with the oral iron chelator 1,2-dimethyl-3-hydroxypyrid-4-one. *Clin Pharmacol Ther*, 48(3), 255-61.
- Kontoghiorghes, G. J., Goddard, J. G., Bartlett, A. N. & Sheppard, L. (1990b) Pharmacokinetic studies in humans with the oral iron chelator 1,2-dimethyl-3-hydroxypyrid-4-one. *Clinical Pharmacology*, 48, 255-261.
- Kumar, S. & Pandey, A. K. (2013) Chemistry and biological activities of flavonoids: an overview. *ScientificWorldJournal*, 2013, 162750.
- Kurokawa, T., Murata, S., Zheng, Y. W., Iwasaki, K., Kohno, K., Fukunaga, K. & Ohkohchi, N. (2015) The Eltrombopag antitumor effect on hepatocellular carcinoma. *Int J Oncol*, 47(5), 1696-702.
- Laub, R., Schneider, Y. J., Octave, J. N., Trouet, A. & Crichton, R. R. (1985) Cellular pharmacology of desferrioxamine B and derivatives in cultured rat hepatocytes in relation to iron mobilization. *Biochem Pharmacol*, 34(8), 1175-83.
- Le Lan, C., Loréal, O., Cohen, T., Ropert, M., Glickstein, H., Lainé, F., Pouchard, M., Deugnier, Y., Le Treut, A., Breuer, W., Cabantchik, Z. I. & Brissot, P. (2005) Redox active plasma iron in C282Y/C282Y hemochromatosis. *Blood*, 105(11), 4527-31.
- Lee, P., Mohammed, N., Marshall, L., Abeysinghe, R. D., Hider, R. C., Porter, J. B. & Singh, S. (1993) Intravenous infusion pharmacokinetics of desferrioxamine in thalassaemic patients. *Drug Metab Dispos*, 21(4), 640-4.
- Leibman, A. & Aisen, P. (1979) Distribution of iron between the binding sites of transferrin in serum: methods and results in normal human subjects. *Blood*, 53(6), 1058-65.
- Leitch, H. A. & Vickars, L. M. (2009) Supportive care and chelation therapy in MDS: are we saving lives or just lowering iron?, *Hematology Am Soc Hematol Educ Program*. United States, 664-72.
- Leo, A., Hansch, C. & Elkins, D. (2002) Partition coefficients and their uses.

- Lesjak, M., Hoque, R., Balesaria, S., Skinner, V., Debnam, E. S., Srail, S. K. & Sharp, P. A. (2014) Quercetin inhibits intestinal iron absorption and ferroportin transporter expression in vivo and in vitro. *PLoS One*, 9(7), e102900.
- Leverence, R., Mason, A. B. & Kaltashov, I. A. (2010) Noncanonical interactions between serum transferrin and transferrin receptor evaluated with electrospray ionization mass spectrometry. *Proc Natl Acad Sci U S A*, 107(18), 8123-8.
- Levin, V. A. (1980) Relationship of octanol/water partition coefficient and molecular weight to rat brain capillary permeability. *J Med Chem*, 23(6), 682-4.
- Levy, J. E., Montross, L. K., Cohen, D. E., Fleming, M. D. & Andrews, N. C. (1999) The C282Y mutation causing hereditary hemochromatosis does not produce a null allele. *Blood*, 94(1), 9-11.
- Limenta, L. M., Jirasomprasert, T., Jittangprasert, P., Wilairat, P., Yamanont, P., Chantharaksri, U., Fucharoen, S. & Morales, N. P. (2011a) Pharmacokinetics of deferiprone in patients with beta-thalassaemia: impact of splenectomy and iron status. *Clin Pharmacokinet*, 50(1), 41-50.
- Limenta, L. M., Jirasomprasert, T., Jittangprasert, P., Wilairat, P., Yamanont, P., Chantharaksri, U., Fucharoen, S. & Morales, N. P. (2011b) Pharmacokinetics of deferiprone in patients with beta-thalassaemia: impact of splenectomy and iron status. *Clinical pharmacokinetics*, 50(1), 41-50.
- Link, G., Pinson, A. & Hershko, C. (1985) Heart cells in culture: a model of myocardial iron overload and chelation. *J Lab Clin Med*, 106(2), 147-53.
- Link, G., Pinson, A., Kahane, I. & Hershko, C. (1989) Iron loading modifies the fatty acid composition of cultured rat myocardial cells and liposomal vesicles: effect of ascorbate and alpha-tocopherol on myocardial lipid peroxidation. *J Lab Clin Med*, 114(3), 243-9.
- Liuzzi, J. P., Aydemir, F., Nam, H., Knutson, M. D. & Cousins, R. J. (2006) Zip14 (Slc39a14) mediates non-transferrin-bound iron uptake into cells. *Proc Natl Acad Sci U S A*, 103(37), 13612-7.
- Longueville, A. & Crichton, R. R. (1986) An animal model of iron overload and its application to study hepatic ferritin iron mobilization by chelators. *Biochem Pharmacol*, 35(21), 3669-78.
- Lucarelli, G., Galimberti, M., Polchi, P., Angelucci, E., Baronciani, D., Giardini, C., Andreani, M., Agostinelli, F., Albertini, F. & Clift, R. A. (1993) Marrow transplantation in patients with thalassemia responsive to iron chelation therapy. *N Engl J Med*, 329(12), 840-4.
- Luck, A. N. & Mason, A. B. (2012) Transferrin-mediated cellular iron delivery. *Curr Top Membr*, 69, 3-35.
- Ma, Y., Kong, X., Chen, Y.-l. & Hider, R. C. (2014) Synthesis and characterizations of pyridazine-based iron chelators.
- Macleod, K. H., Cleveland, J. L. & Porter, J. B. (2001) Cellular zinc content is a major determinant of iron chelator-induced apoptosis of thymocytes. *Blood*, 98(13), 3831-9.
- Magaro, M., Zoli, A., Altomonte, L., Mirone, L., Corvino, G., Storti, S., Marra, R., Riccerca, B. M., Pagano, L. & Di Cesare, L. (1990) Iron chelation in rheumatoid arthritis: clinical and laboratory evaluation. *Ann Rheum Dis*, 49(4), 268-9.
- Manach, C., Scalbert, A., Morand, C., Remesy, C. & Jimenez, L. (2004) Polyphenols: food sources and bioavailability. *Am J Clin Nutr*, 79(5), 727-47.
- Manach, C., Williamson, G., Morand, C., Scalbert, A. & Remesy, C. (2005) Bioavailability and bioefficacy of polyphenols in humans. I. Review of 97 bioavailability studies. *Am J Clin Nutr*, 81(1 Suppl), 230s-242s.



- Mancias, J. D., Wang, X., Gygi, S. P., Harper, J. W. & Kimmelman, A. C. (2014) Quantitative proteomics identifies NCOA4 as the cargo receptor mediating ferritinophagy. *Nature*, 509(7498), 105-9.
- Marcus, R. E., Davies, S. C., Bantock, H. M., Underwood, S. R., Walton, S. & Huehns, E. R. (1984) Desferrioxamine to improve cardiac function in iron-overloaded patients with thalassemia major, *Lancet*. England, 392-3.
- Martell, A. (1981) *The design and synthesis of chelating agents* Elsevier North Holland Inc.
- Marx, J. J. & van Asbeck, B. S. (1996) Use of iron chelators in preventing hydroxyl radical damage: adult respiratory distress syndrome as an experimental model for the pathophysiology and treatment of oxygen-radical-mediated tissue damage. *Acta Haematol*, 95(1), 49-62.
- May, P. M. & Williams, D. R. (1979) Synergistic chelation therapy or mixed ligand complexes for plutonium and cadmium poisoning? *Nature*, 278(5704), 581-2.
- McLaren, D. S. (1980) *Iron Metabolism in Man: T. H. Bothwell, R. W. Charlton, J. D. Cook and C. A. Finch, Blackwell Scientific Publications, 1979. Pp. ix + 576. £33.50.* Translated from en by, 65.
- Middleton, E., Jr. (1998) Effect of plant flavonoids on immune and inflammatory cell function. *Adv Exp Med Biol*, 439, 175-82.
- Mishra, A., Kumar, S., Bhargava, A., Sharma, B. & Pandey, A. K. (2011) Studies on in vitro antioxidant and antistaphylococcal activities of some important medicinal plants. *Cell Mol Biol (Noisy-le-grand)*, 57(1), 16-25.
- Mishra, A., Kumar, S. & Pandey, A. K. (2013a) Scientific validation of the medicinal efficacy of *Tinospora cordifolia*. *ScientificWorldJournal*, 2013, 292934.
- Mishra, A., Sharma, A. K., Kumar, S., Saxena, A. K. & Pandey, A. K. (2013b) *Bauhinia variegata* leaf extracts exhibit considerable antibacterial, antioxidant, and anticancer activities. *Biomed Res Int*, 2013, 915436.
- Modell, B. (1977) Total management of thalassaemia major. *Arch Dis Child*, 52(6), 489-500.
- Modell, B., Letsky, E. A., Flynn, D. M., Peto, R. & Weatherall, D. J. (1982) Survival and desferrioxamine in thalassaemia major. *Br Med J (Clin Res Ed)*, 284(6322), 1081-4.
- Moon, J. H., Tsushida, T., Nakahara, K. & Terao, J. (2001) Identification of quercetin 3-O-beta-D-glucuronide as an antioxidative metabolite in rat plasma after oral administration of quercetin. *Free Radic Biol Med*, 30(11), 1274-85.
- Moon, S. N., Han, J. W., Hwang, H. S., Kim, M. J., Lee, S. J., Lee, J. Y., Oh, C. K. & Jeong, D. C. (2011) Establishment of secondary iron overloaded mouse model: evaluation of cardiac function and analysis according to iron concentration. *Pediatr Cardiol*, 32(7), 947-52.
- Morley, C. G. & Bezkorovainy, A. (1985) Cellular iron uptake from transferrin: is endocytosis the only mechanism? *Int J Biochem*, 17(5), 553-64.
- Motekaitis, R. & Martell, A. (1991) Stabilities of the iron(III) chelates of 1,2-dimethyl-3-hydroxy-4-pyridinone and related ligands. *Inorganica Chimica Acta* 183, 71-80.
- Mullen, W., Edwards, C. A. & Crozier, A. (2006) Absorption, excretion and metabolite profiling of methyl-, glucuronyl-, glucosyl- and sulpho-conjugates of quercetin in human plasma and urine after ingestion of onions. *Br J Nutr*, 96(1), 107-16.
- Müllner, E. W., Rothenberger, S., Müller, A. M. & Kühn, L. C. (1992) In vivo and in vitro modulation of the mRNA-binding activity of iron-regulatory factor. Tissue distribution and effects of cell proliferation, iron levels and redox state. *Eur J Biochem*, 208(3), 597-605.

- Musumeci, M., Maccari, S., Massimi, A., Stati, T., Sestili, P., Corritore, E., Pastorelli, A., Stacchini, P., Marano, G. & Catalano, L. (2014) Iron excretion in iron dextran-overloaded mice. *Blood Transfus*, 12(4), 485-90.
- Myers, B. M., Prendergast, F. G., Holman, R., Kuntz, S. M. & LaRusso, N. F. (1991) Alterations in the structure, physicochemical properties, and pH of hepatocyte lysosomes in experimental iron overload. *J Clin Invest*, 88(4), 1207-15.
- Nangalia, J., Massie, C. E., Baxter, E. J., Nice, F. L., Gundem, G., Wedge, D. C., Avezov, E., Li, J., Kollmann, K., Kent, D. G., Aziz, A., Godfrey, A. L., Hinton, J., Martincorena, I., Van Loo, P., Jones, A. V., Guglielmelli, P., Tarpey, P., Harding, H. P., Fitzpatrick, J. D., Goudie, C. T., Ortmann, C. A., Loughran, S. J., Raine, K., Jones, D. R., Butler, A. P., Teague, J. W., O'Meara, S., McLaren, S., Bianchi, M., Silber, Y., Dimitropoulou, D., Bloxham, D., Mudie, L., Maddison, M., Robinson, B., Keohane, C., Maclean, C., Hill, K., Orchard, K., Tauro, S., Du, M. Q., Greaves, M., Bowen, D., Huntly, B. J., Harrison, C. N., Cross, N. C., Ron, D., Vannucchi, A. M., Papaemmanuil, E., Campbell, P. J. & Green, A. R. (2013) Somatic CALR mutations in myeloproliferative neoplasms with nonmutated JAK2. *N Engl J Med*, 369(25), 2391-405.
- Naughton, B. A., Sibanda, B., Weintraub, J. P., San Roman, J. & Kamali, V. (1995) A stereotypic, transplantable liver tissue-culture system. *Appl Biochem Biotechnol*, 54(1-3), 65-91.
- Nick, H., Acklin, P., Lattmann, R., Buehlmayer, P., Hauffe, S., Schupp, J. & Alberti, D. (2003) Development of tridentate iron chelators: from desferrithiocin to ICL670. *Curr Med Chem*, 10(12), 1065-76.
- Nick, H., Allegrini, P. R., Fozard, L., Junker, U., Rojkaer, L., Salie, R., Niederkofler, V. & O'Reilly, T. (2009) Deferasirox reduces iron overload in a murine model of juvenile hemochromatosis. *Exp Biol Med (Maywood)*, 234(5), 492-503.
- Nick, H., Wong, A., Acklin, P., Faller, B., Jin, Y., Lattmann, R., Sergejew, T., Hauffe, S., Thomas, H. & Schnebli, H. P. (2002) ICL670A: preclinical profile. *Adv Exp Med Biol*, 509, 185-203.
- Nielsen, P., Heinelt, S. & Dullmann, J. (1993) Chronic feeding of carbonyl-iron and TMH-ferrocene in rats. Comparison of two iron-overload models with different iron absorption. *Comp Biochem Physiol C*, 106(2), 429-36.
- Nishimuro, H., Ohnishi, H., Sato, M., Ohnishi-Kameyama, M., Matsunaga, I., Naito, S., Ippoushi, K., Oike, H., Nagata, T., Akasaka, H., Saitoh, S., Shimamoto, K. & Kobori, M. (2015) Estimated daily intake and seasonal food sources of quercetin in Japan. *Nutrients*, 7(4), 2345-58.
- Niu, X., Huang, W. H., De Boer, B., Delriviere, L., Mou, L. J. & Jeffrey, G. P. (2014) Iron-induced oxidative rat liver injury after non-heart-beating warm ischemia is mediated by tumor necrosis factor alpha and prevented by deferoxamine. *Liver Transpl*, 20(8), 904-11.
- Nocka, K. H. & Pelus, L. M. (1988) Cell cycle specific effects of deferoxamine on human and murine hematopoietic progenitor cells. *Cancer Res*, 48(13), 3571-5.
- Oldendorf, W. H. (1974) Lipid solubility and drug penetration of the blood brain barrier. *Proc Soc Exp Biol Med*, 147(3), 813-5.
- Olivieri, N., NisbetBrown, E., Srichairatanakool, S., Dragsten, P., Hallaway, P., Hedlund, B. & Porter, J. (1996) Studies of iron excretion and non-transferrin-bound plasma iron (NTBPI), following a single infusion of hydroxyethyl starch-deferoxamine (HES-DFO): A new approach to iron chelation therapy. *BLOOD*, 88 (10) 1228 - 1228. (1996).

Olivieri, N. F., Brittenham, G. M., McLaren, C. E., Templeton, D. M., Cameron, R. G., McClelland, R. A., Burt, A. D. & Fleming, K. A. (1998) Long-term safety and effectiveness of iron-chelation therapy with deferiprone for thalassemia major. *The New England journal of medicine*, 339(7), 417-23.

Olivieri, N. F., Buncic, J. R., Chew, E., Gallant, T., Harrison, R. V., Keenan, N., Logan, W., Mitchell, D., Ricci, G., Skarf, B. & et al. (1986) Visual and auditory neurotoxicity in patients receiving subcutaneous deferoxamine infusions. *N Engl J Med*, 314(14), 869-73.

Olivieri, N. F., Koren, G., Harris, J., Khattak, S., Freedman, M. H., Templeton, D. M., Bailey, J. D. & Reilly, B. J. (1992a) Growth failure and bony changes induced by deferoxamine. *Am J Pediatr Hematol Oncol*, 14(1), 48-56.

Olivieri, N. F., Koren, G., Harris, J., Khattak, S., Freedman, M. H., Templeton, D. M., Bailey, J. D. & Reilly, B. J. (1992b) Growth failure and bony changes induced by deferoxamine. *American Journal of Pediatric Hematology Oncology*, 14(1), 48-56.

Olivieri, N. F., Koren, G., Hermann, C., Bentur, Y., Chung, D., Klein, J., St Louis, P., Freedman, M. H., McClelland, R. A. & Templeton, D. M. (1990) Comparison of oral iron chelator L1 and desferrioxamine in iron-loaded patients. *Lancet*, 336(8726), 1275-9.

Olivieri, N. F., Nathan, D. G., MacMillan, J. H., Wayne, A. S., Liu, P. P., McGee, A., Martin, M., Koren, G. & Cohen, A. R. (1994) Survival in medically treated patients with homozygous beta-thalassemia. *N Engl J Med*, 331(9), 574-8.

Oshiro, S., Nakajima, H., Markello, T., Krasnewich, D., Bernardini, I. & Gahl, W. A. (1993) Redox, transferrin-independent, and receptor-mediated endocytosis iron uptake systems in cultured human fibroblasts. *J Biol Chem*, 268(29), 21586-91.

Otto-Duessel, M., Brewer, C., Gonzalez, I., Nick, H. & Wood, J. C. (2008) Safety and efficacy of combined chelation therapy with deferasirox and deferoxamine in a gerbil model of iron overload. *Acta Haematol*, 120(2), 123-8.

Oudit, G. Y., Sun, H., Trivieri, M. G., Koch, S. E., Dawood, F., Ackerley, C., Yazdanpanah, M., Wilson, G. J., Schwartz, A., Liu, P. P. & Backx, P. H. (2003) L-type Ca<sup>2+</sup> channels provide a major pathway for iron entry into cardiomyocytes in iron-overload cardiomyopathy. *Nat Med*, 9(9), 1187-94.

Oudit, G. Y., Trivieri, M. G., Khaper, N., Liu, P. P. & Backx, P. H. (2006) Role of L-type Ca<sup>2+</sup> channels in iron transport and iron-overload cardiomyopathy. *J Mol Med (Berl)*, 84(5), 349-64.

Papakonstantinou, O., Alexopoulou, E., Economopoulos, N., Benekos, O., Kattamis, A., Kostaridou, S., Ladis, V., Efstathopoulos, E., Gouliamos, A. & Kelekis, N. L. (2009) Assessment of iron distribution between liver, spleen, pancreas, bone marrow, and myocardium by means of R2 relaxometry with MRI in patients with beta-thalassemia major. *J Magn Reson Imaging*, 29(4), 853-9.

Pennell, D. J., Berdoukas, V., Karagiorga, M., Ladis, V., Piga, A., Aessopos, A., Gotsis, E. D., Tanner, M. A., Smith, G. C., Westwood, M. A., Wonke, B. & Galanello, R. (2006) Randomized controlled trial of deferiprone or deferoxamine in beta-thalassemia major patients with asymptomatic myocardial siderosis. *Blood*, 107(9), 3738-44.

Pennell, D. J., Porter, J. B., Cappellini, M. D., Chan, L. L., El-Beshlawy, A., Aydinok, Y., Ibrahim, H., Li, C. K., Viprakasit, V., Elalfy, M. S., Kattamis, A., Smith, G., Habr, D., Domokos, G., Roubert, B. & Taher, A. (2011) Continued improvement in myocardial T2\* over two years of deferasirox therapy in beta-thalassemia major patients with cardiac iron overload. *Haematologica*, 96(1), 48-54.

Pennell, D. J., Porter, J. B., Cappellini, M. D., Chan, L. L., El-Beshlawy, A., Aydinok, Y., Ibrahim, H., Li, C. K., Viprakasit, V., Elalfy, M. S., Kattamis, A., Smith, G., Habr,

- D., Domokos, G., Roubert, B. & Taher, A. (2012) Deferasirox for up to 3 years leads to continued improvement of myocardial T2\* in patients with beta-thalassemia major. *Haematologica*, 97(6), 842-8.
- Pennell, D. J., Porter, J. B., Cappellini, M. D., El-Beshlawy, A., Chan, L. L., Aydinok, Y., Elalfy, M. S., Sutcharitchan, P., Li, C. K., Ibrahim, H., Viprakasit, V., Kattamis, A., Smith, G., Habr, D., Domokos, G., Roubert, B. & Taher, A. (2010) Efficacy of deferasirox in reducing and preventing cardiac iron overload in beta-thalassemia. *Blood*, 115(12), 2364-71.
- Pennell, D. J., Porter, J. B., Piga, A., Lai, Y., El-Beshlawy, A., Belhoul, K. M., Elalfy, M., Yesilipek, A., Kilinc, Y., Lawniczek, T., Habr, D., Weisskopf, M., Zhang, Y. & Aydinok, Y. (2014) A 1-year randomized controlled trial of deferasirox versus deferoxamine for myocardial iron removal in beta-thalassemia major (CORDELIA). *Blood (In press)*.
- Pennell, D. J., Porter, J. B., Piga, A., Lai, Y. R., El-Beshlawy, A., Elalfy, M., Yesilipek, A., Kilinc, Y., Habr, D., Musallam, K. M., Shen, J., Aydinok, Y. & investigators, C. s. (2015) Sustained improvements in myocardial T2\* over 2 years in severely iron-overloaded patients with beta thalassemia major treated with deferasirox or deferoxamine. *Am J Hematol*, 90(2), 91-6.
- Philpott, C. C., Haile, D., Rouault, T. A. & Klausner, R. D. (1993) Modification of a free Fe-S cluster cysteine residue in the active iron-responsive element-binding protein prevents RNA binding. *J Biol Chem*, 268(24), 17655-8.
- Piga, A., Galanello, R., Forni, G. L., Cappellini, M. D., Origa, R., Zappu, A., Donato, G., Bordone, E., Lavagetto, A., Zanaboni, L., Sechaud, R., Hewson, N., Ford, J. M., Opitz, H. & Alberti, D. (2006) Randomized phase II trial of deferasirox (Exjade, ICL670), a once-daily, orally-administered iron chelator, in comparison to deferoxamine in thalassemia patients with transfusional iron overload. *Haematologica*, 91(7), 873-80.
- Piga, A., Luzzatto, L., Capalbo, P., Gambotto, S., Tricta, F. & Gabutti, V. (1988a) High-dose desferrioxamine as a cause of growth failure in thalassaemic patients. *Eur J Haematol*, 40(4), 380-1.
- Piga, A., Luzzatto, L., Capalbo, P., Gambotto, S., Tricta, F. & Gabutti, V. (1988b) High dose desferrioxamine as a cause of growth failure in thalassaemic patients. *European Journal Haematology*, 40, 380-381.
- Pinilla-Tenas, J. J., Sparkman, B. K., Shawki, A., Illing, A. C., Mitchell, C. J., Zhao, N., Liuzzi, J. P., Cousins, R. J., Knutson, M. D. & Mackenzie, B. (2011) Zip14 is a complex broad-scope metal-ion transporter whose functional properties support roles in the cellular uptake of zinc and nontransferrin-bound iron. *Am J Physiol Cell Physiol*, 301(4), C862-71.
- Pippard, M. J., Callender, S. T. & Finch, C. A. (1982) Ferrioxamine excretion in iron-loaded man. *Blood*, 60(2), 288-94.
- Pippard, M. J., Jackson, M. J., Hoffman, K., Petrou, M. & Modell, C. B. (1986) Iron chelation using subcutaneous infusions of diethylene triamine penta-acetic acid (DTPA). *Scand J Haematol*, 36(5), 466-72.
- Pippard, M. J., Pattanapanyssat, K., Tiperkae, J. & Hider, R. C. (1989) Metabolism of the iron chelates of desferrioxamine and hydroxypyridinones in the rat., *Proceedings of the European Iron Club*. Budapest, Hungary.
- Pippard, M. J. & Weatherall, D. J. (1984) Iron absorption in non-transfused iron loading anaemias: prediction of risk for iron loading, and response to iron chelation treatment, in beta thalassaemia intermedia and congenital sideroblastic anaemias. *Haematologia (Budap)*, 17(1), 17-24.

- Pitt, C. G., Gupta, G., Estes, W. E., Rosenkrantz, H., Metterville, J. J., Crumbliss, A. L., Palmer, R. A., Nordquest, K. W., Hardy, K. A., Whitcomb, D. R., Byers, B. R., Arceneaux, J. E., Gaines, C. G. & Sciortino, C. V. (1979) The selection and evaluation of new chelating agents for the treatment of iron overload. *J Pharmacol Exp Ther*, 208(1), 12-8.
- Pootrakul, P., Sirankapracha, P., Hemsorach, S., Mounsub, W., Kumbunlue, R., Piangitjagum, A., Wasi, P., Ma, L. & Schrier, S. L. (2000) A correlation of erythrokinetics, ineffective erythropoiesis, and erythroid precursor apoptosis in thai patients with thalassemia. *Blood*, 96(7), 2606-12.
- Porter, J., Galanello, R., Saglio, G., Neufeld, E. J., Vichinsky, E., Cappellini, M. D., Olivieri, N., Piga, A., Cunningham, M. J., Soulières, D., Gattermann, N., Tchernia, G., Maertens, J., Giardina, P., Kwiatkowski, J., Quarta, G., Jeng, M., Forni, G. L., Stadler, M., Cario, H., Debusscher, L., Porta, M. D., Cazzola, M., Greenberg, P., Alimena, G., Rabault, B., Gathmann, I., Ford, J. M., Alberti, D. & Rose, C. (2008) Relative response of patients with myelodysplastic syndromes and other transfusion-dependent anaemias to deferasirox (ICL670): a 1-yr prospective study. *Eur J Haematol*, 80(2), 168-76.
- Porter, J., Waldmeier, F., Bruin, G., Hazell, K., Warrington, S., Delage, K., Sechaud, R., Peter, R., Ford, J., Alberti, D., Gross, G. & Schran, H. (2003) Pharmacokinetics, Metabolism and Elimination of the Iron Chelator Drug ICL670 in Patients, Following Single Oral Doses of 1000 mg [<sup>14</sup>C]Labelled Drug at Steady State. *Blood*, 102(11), 5b, Abstract 3720.
- Porter, J. B., Abeysinghe, R. D., Hoyes, K. P., Barra, C., Huehns, E. R., Brooks, P. N., Blackwell, M. P., Araneta, M., Brittenham, G., Singh, S. & et al. (1993) Contrasting interspecies efficacy and toxicology of 1,2-diethyl-3-hydroxypyridin-4-one, CP94, relates to differing metabolism of the iron chelating site. *Br J Haematol*, 85(1), 159-68.
- Porter, J. B., Abeysinghe, R. D., Marshall, L., Hider, R. C. & Singh, S. (1996) Kinetics of removal and reappearance of non-transferrin-bound plasma iron with deferoxamine therapy. *Blood*, 88(2), 705-13.
- Porter, J. B., Faherty, A., Stallibrass, L., Brookman, L., Hassan, I. & Howes, C. (1998) A trial to investigate the relationship between DFO pharmacokinetics and metabolism and DFO-related toxicity. *Ann N Y Acad Sci*, 850, 483-7.
- Porter, J. B., Gyparaki, M., Burke, L. C., Huehns, E. R., Sarpong, P., Saez, V. & Hider, R. C. (1988) Iron mobilization from hepatocyte monolayer cultures by chelators: the importance of membrane permeability and the iron-binding constant. *Blood*, 72(5), 1497-503.
- Porter, J. B., Hoyes, K. P., Abeysinghe, R., Huehns, E. R. & Hider, R. C. (1989a) Animal toxicology of iron chelator L1, *Lancet*. England, 156.
- Porter, J. B., Hoyes, K. P., Abeysinghe, R. D., Brooks, P. N., Huehns, E. R. & Hider, R. C. (1991) Comparison of the subacute toxicity and efficacy of 3-hydroxypyridin-4-one iron chelators in overloaded and nonoverloaded mice. *Blood*, 78(10), 2727-34.
- Porter, J. B., Jaswon, M. S., Huehns, E. R., East, C. A. & Hazell, J. W. (1989b) Desferrioxamine ototoxicity: evaluation of risk factors in thalassaemic patients and guidelines for safe dosage. *Br J Haematol*, 73(3), 403-9.
- Porter, J. B., Morgan, J., Hoyes, K. P., Burke, L. C., Huehns, E. R. & Hider, R. C. (1990) Relative oral efficacy and acute toxicity of hydroxypyridin-4-one iron chelators in mice. *Blood*, 76(11), 2389-96.
- Porter, J. B., Rafique, R., Srichairatanakool, S., Davis, B. A., Shah, F. T., Hair, T. & Evans, P. (2005) Recent insights into interactions of deferoxamine with cellular and plasma iron pools: Implications for clinical use. *Annals of the New York Academy of Sciences*, 1054, 155-68.

- Porter, J. B., Singh, S., Hoyes, K. P., Epemolu, O., Abeysinghe, R. D. & Hider, R. C. (1994) Lessons from preclinical and clinical studies with 1,2-diethyl-3-hydroxypyridin-4-one, CP94 and related compounds. *Adv Exp Med Biol*, 356, 361-70.
- Propper, R. D., Shurin, S. B. & Nathan, D. G. (1976) Reassessment of the use of desferrioxamine B in iron overload. *N Engl J Med*, 294(26), 1421-3.
- Rachmilewitz, E. A., Aker, M., Perry, D. & Dover, G. (1995) Sustained increase in haemoglobin and RBC following long-term administration of recombinant human erythropoietin to patients with homozygous beta-thalassaemia. *Br J Haematol*, 90(2), 341-5.
- Radisky, D. C. & Kaplan, J. (1998) Iron in cytosolic ferritin can be recycled through lysosomal degradation in human fibroblasts. *Biochem J*, 336 ( Pt 1), 201-5.
- Rama, R., Octave, J. N., Schneider, Y. J., Sibille, J. C., Limet, J. N., Mareschal, J. C., Trouet, A. & Crichton, R. R. (1981) Iron mobilization from cultured rat fibroblasts and hepatocytes. Effect of various drugs. *FEBS Lett*, 127(2), 204-6.
- Ratty, A. K. & Das, N. P. (1988) Effects of flavonoids on nonenzymatic lipid peroxidation: structure-activity relationship. *Biochem Med Metab Biol*, 39(1), 69-79.
- Riemer, J., Hoepken, H. H., Czerwinska, H., Robinson, S. R. & Dringen, R. (2004) Colorimetric ferrozine-based assay for the quantitation of iron in cultured cells. *Anal Biochem*, 331(2), 370-5.
- Ritter, C., da Cunha, A. A., Echer, I. C., Andrades, M., Reinke, A., Lucchiari, N., Rocha, J., Streck, E. L., Menna-Barreto, S., Moreira, J. C. & Dal-Pizzol, F. (2006) Effects of N-acetylcysteine plus deferoxamine in lipopolysaccharide-induced acute lung injury in the rat. *Crit Care Med*, 34(2), 471-7.
- Robins-Browne, R. M. & Prpic, J. K. (1983) Desferrioxamine and systemic yersiniosis. *Lancet*. England, 1372.
- Robins-Browne, R. M. & Prpic, J. K. (1985) Effects of iron and desferrioxamine on infections with *Yersinia enterocolitica*. *Infect Immun*, 47(3), 774-9.
- Roth, M., Will, B., Simkin, G., Narayanagari, S., Barreyro, L., Bartholdy, B., Tamari, R., Mitsiades, C. S., Verma, A. & Steidl, U. (2012) Eltrombopag inhibits the proliferation of leukemia cells via reduction of intracellular iron and induction of differentiation. *Blood*. United States, 386-94.
- Rouault, T. A. (2006) The role of iron regulatory proteins in mammalian iron homeostasis and disease. *Nat Chem Biol*, 2(8), 406-14.
- Ruotolo, R., Calani, L., Brighenti, F., Crozier, A., Ottonello, S. & Del Rio, D. (2014) Glucuronidation does not suppress the estrogenic activity of quercetin in yeast and human breast cancer cell model systems. *Arch Biochem Biophys*, 559, 62-7.
- Russo, M., Spagnuolo, C., Tedesco, I., Bilotto, S. & Russo, G. L. (2012) The flavonoid quercetin in disease prevention and therapy: facts and fancies. *Biochem Pharmacol*, 83(1), 6-15.
- Saito, K., Nishisato, T., Grasso, J. A. & Aisen, P. (1986) Interaction of transferrin with iron-loaded rat peritoneal macrophages. *Br J Haematol*, 62(2), 275-86.
- Saleh, M. N., Bussel, J. B., Cheng, G., Meyer, O., Bailey, C. K., Arning, M. & Brainsky, A. (2013) Safety and efficacy of eltrombopag for treatment of chronic immune thrombocytopenia: results of the long-term, open-label EXTEND study. *Blood*, 121(3), 537-45.
- Salis, O., Bedir, A., Kilinc, V., Alacam, H., Gulten, S. & Okuyucu, A. (2014) The anticancer effects of desferrioxamine on human breast adenocarcinoma and hepatocellular carcinoma cells. *Cancer Biomark*, 14(6), 419-26.

Santos, M. M., de Sousa, M., Rademakers, L. H., Clevers, H., Marx, J. J. & Schilham, M. W. (2000) Iron overload and heart fibrosis in mice deficient for both beta2-microglobulin and Rag1. *Am J Pathol*, 157(6), 1883-92.

Sanyear, C., Butthep, P., Nithipongvanich, R., Sirankapracha, P., Winichagoon, P., Fucharoen, S. & Svasti, S. (2013) Cardiomyocyte ultrastructural damage in  $\beta$ -thalassaemic mice. *Int J Exp Pathol*, 94(5), 336-42.

Schaefer, B., Effenberger, M. & Zoller, H. (2014) Iron metabolism in transplantation. *Transpl Int*, 27(11), 1109-17.

Scheline, R. R. (1973) Metabolism of foreign compounds by gastrointestinal microorganisms. *Pharmacol Rev*, 25(4), 451-523.

Schmidt, P. J., Racie, T., Westerman, M., Fitzgerald, K., Butler, J. S. & Fleming, M. D. (2015) Combination therapy with a Tmprss6 RNAi-therapeutic and the oral iron chelator deferiprone additively diminishes secondary iron overload in a mouse model of  $\beta$ -thalassemia intermedia. *Am J Hematol*, 90(4), 310-3.

Selden, C. & Peters, T. J. (1979) Separation and assay of iron proteins in needle biopsy specimens of human liver. *Clin Chim Acta*, 98(1-2), 47-52.

Shanely, R. A., Knab, A. M., Nieman, D. C., Jin, F., McAnulty, S. R. & Landram, M. J. (2010) Quercetin supplementation does not alter antioxidant status in humans. *Free Radic Res*, 44(2), 224-31.

Shirai, M., Kawai, Y., Yamanishi, R., Kinoshita, T., Chuman, H. & Terao, J. (2006) Effect of a conjugated quercetin metabolite, quercetin 3-glucuronide, on lipid hydroperoxide-dependent formation of reactive oxygen species in differentiated PC-12 cells. *Free Radic Res*, 40(10), 1047-53.

Silvestroni, E., Bianco, I., Graziani, B., Lerone, M., Valente, M., Congedo, P., Ponzini, D. & Costantini, S. (1982) Intensive iron chelation therapy in beta-thalassemia major: some effects on iron metabolism and blood transfusion dependence. *Acta Haematol*, 68(2), 115-23.

Sirivech, S., Frieden, E. & Osaki, S. (1974) The release of iron from horse spleen ferritin by reduced flavins. *Biochem J*, 143(2), 311-5.

Spencer, J. P., Chaudry, F., Pannala, A. S., Srail, S. K., Debnam, E. & Rice-Evans, C. (2000) Decomposition of cocoa procyanidins in the gastric milieu. *Biochem Biophys Res Commun*, 272(1), 236-41.

Srichairatanakool, S., Kemp, P. & Porter, J. B. (1997) Evidence for "shuttle" effect of NTBI onto desferrioxamine in thalassaemic plasma in the presence of NTA., *International Symposium: Iron in Biology and Medicine*. St. Malo, France.

Steward, A., Williamson, I., Madigan, T., Bretnall, A. & Hassan, I. F. (1996) An improved animal model for studying desferrioxamine. *Br J Haematol*, 95(4), 654-9.

Streater, M., Taylor, P. D., Hider, R. C. & Porter, J. (1990) Novel 3-hydroxy-2(1H)-pyridinones. Synthesis, iron(III)-chelating properties, and biological activity. *J Med Chem*, 33(6), 1749-55.

Stuckey, D. J., Carr, C. A., Camelliti, P., Tyler, D. J., Davies, K. E. & Clarke, K. (2012) In vivo MRI characterization of progressive cardiac dysfunction in the mdx mouse model of muscular dystrophy. *PLoS One*, 7(1), e28569.

Sumi, M., Tateishi, N., Shibata, H., Ohki, T. & Sata, M. (2013) Quercetin glucosides promote ischemia-induced angiogenesis, but do not promote tumor growth. *Life Sci*, 93(22), 814-9.

Summers, J. B., Gunn, B. P., Martin, J. G., Mazdiyasn, H., Stewart, A. O., Young, P. R., Goetze, A. M., Bouska, J. B., Dyer, R. D., Brooks, D. W. & et al. (1988) Orally active hydroxamic acid inhibitors of leukotriene biosynthesis. *J Med Chem*, 31(1), 3-5.

- Sutherland, R., Delia, D., Schneider, C., Newman, R., Kemshead, J. & Greaves, M. (1981) Ubiquitous cell-surface glycoprotein on tumor cells is proliferation-associated receptor for transferrin. *Proc Natl Acad Sci U S A*, 78(7), 4515-9.
- Svensson, T., Chowdhury, O., Garelius, H., Lorenz, F., Saft, L., Jacobsen, S. E., Hellstrom-Lindberg, E. & Cherif, H. (2014) A pilot phase I dose finding safety study of the thrombopoietin-receptor agonist, eltrombopag, in patients with myelodysplastic syndrome treated with azacitidine. *Eur J Haematol*, 93(5), 439-45.
- Taher, A., Cappellini, M. D., Vichinsky, E., Galanello, R., Piga, A., Lawniczek, T., Clark, J., Habr, D. & Porter, J. B. (2009a) Efficacy and safety of deferasirox doses of >30 mg/kg per d in patients with transfusion-dependent anaemia and iron overload. *Br J Haematol*, 147(5), 752-9.
- Taher, A., El-Beshlawy, A., Elalfy, M. S., Al Zir, K., Daar, S., Habr, D., Kriemler-Krahn, U., Hmissi, A. & Al Jefri, A. (2009b) Efficacy and safety of deferasirox, an oral iron chelator, in heavily iron-overloaded patients with  $\beta$ -thalassaemia: the ESCALATOR study. *Eur J Haematol*, 82(6), 458-65.
- Tallarida, R. J. (2001) Drug synergism: its detection and applications. *J Pharmacol Exp Ther*, 298(3), 865-72.
- Tallarida, R. J. (2006) An overview of drug combination analysis with isobolograms. *The Journal of pharmacology and experimental therapeutics*, 319(1), 1-7.
- Tanner, M. A., He, T., Westwood, M. A., Firmin, D. N., Pennell, D. J. & Investigators, T. I. F. H. T. (2006) Multi-center validation of the transferability of the magnetic resonance T2\* technique for the quantification of tissue iron. *Haematologica*, 91(10), 1388-91.
- Tapas, A., Sakarkar, D. & Kakde, R. (2008) Flavonoids as Nutraceuticals: A Review. 7.
- Taylor, P. D., Morrison, I. E. & Hider, R. C. (1988) Microcomputer application of non-linear regression analysis to metal-ligand equilibria. *Talanta*, 35(7), 507-12.
- Thelander, L. & Reichard, P. (1979) Reduction of ribonucleotides. *Annu Rev Biochem*, 48, 133-58.
- Thephinlap, C., Phisalaphong, C., Lailerd, N., Chattipakorn, N., Winichagoon, P., Vadolas, J., Fucharoen, S., Porter, J. B. & Srichairatanakool, S. (2011) Reversal of cardiac iron loading and dysfunction in thalassaemic mice by curcuminoids. *Med Chem*, 7(1), 62-9.
- Thorstensen, K. (1988) Hepatocytes and reticulocytes have different mechanisms for the uptake of iron from transferrin. *J Biol Chem*, 263(32), 16837-41.
- Thorstensen, K. & Romslo, I. (1988) Uptake of iron from transferrin by isolated rat hepatocytes. A redox-mediated plasma membrane process? *J Biol Chem*, 263(18), 8844-50.
- Thorstensen, K. & Romslo, I. (1990) The role of transferrin in the mechanism of cellular iron uptake. *Biochem J*, 271(1), 1-9.
- Tong, J. Z., Sarrazin, S., Cassio, D., Gauthier, F. & Alvarez, F. (1994) Application of spheroid culture to human hepatocytes and maintenance of their differentiation, *Biol Cell*. France, 77-81.
- Travis, S. & Menzies, I. (1992) Intestinal permeability: functional assessment and significance. *Clin Sci (Lond)*, 82(5), 471-88.
- Treffry, A. & Harrison, P. M. (1979) The binding of ferric iron by ferritin. *Biochem J*, 181(3), 709-16.
- Trinder, D., Batey, R. G., Morgan, E. H. & Baker, E. (1990) Effect of cellular iron concentration on iron uptake by hepatocytes. *Am J Physiol*, 259(4 Pt 1), G611-7.



- Trinder, D., Zak, O. & Aisen, P. (1996) Transferrin receptor-independent uptake of different transferrin by human hepatoma cells with antisense inhibition of receptor expression. *Hepatology*, 23(6), 1512-20.
- Tsukamoto, H., Horne, W., Kamimura, S., Niemela, O., Parkkila, S., Yla-Herttuala, S. & Brittenham, G. M. (1995) Experimental liver cirrhosis induced by alcohol and iron. *J Clin Invest*, 96(1), 620-30.
- Unger, A. & Hershko, C. (1974) Hepatocellular uptake of ferritin in the rat. *Br J Haematol*, 28(2), 169-79.
- Van Wyk, C. P., Linder-Horowitz, M. & Munro, H. N. (1971) Effect of iron loading on non-heme iron compounds in different liver cell populations. *J Biol Chem*, 246(4), 1025-31.
- Vlachodimitropoulou, E., Cooper, N., Psaila, B., Sola-Visner, M. & Porter, J. (2014) Eltrombopag Mobilizes Intracellular Iron Stores at Concentrations Lower Than Those Required with Other Clinically Available Iron Chelators. *Blood*, 124(21).
- Vlachodimitropoulou, E., JB, P., Cooper, N., Psaila, B. & Sola-Visner, M. (2015) A Potential Novel Application of Eltrombopag: A Combination Agent to Enhance Iron Chelation Therapy. *Blood*, 126(3), 353.
- Vlachodimitropoulou, E., Sharp, P. A. & Naftalin, R. J. (2011) Quercetin-iron chelates are transported via glucose transporters. *Free Radic Biol Med*, 50(8), 934-44.
- Vlachodimitropoulou Koumoutsea, E., Garbowski, M. & Porter, J. (2015) Synergistic intracellular iron chelation combinations: mechanisms and conditions for optimizing iron mobilization. *Br J Haematol*, 170(6), 874-83.
- Voskaridou, E., Douskou, M., Terpos, E., Papassotiriou, I., Stamoulakatou, A., Ourailidis, A., Loutradi, A. & Loukopoulos, D. (2004) Magnetic resonance imaging in the evaluation of iron overload in patients with beta thalassaemia and sickle cell disease. *Br J Haematol*, 126(5), 736-42.
- W.J. Reeves Jr., G. M. F. (1966) [54] L-Lactic dehydrogenase: Heart (H4). *Carbohydrate Metabolism*, 9, 288-294.
- Waldmeier, F., Bruin, G. J., Glaenzel, U., Hazell, K., Sechaud, R., Warrington, S. & Porter, J. B. (2010) Pharmacokinetics, metabolism, and disposition of deferasirox in beta-thalassemic patients with transfusion-dependent iron overload who are at pharmacokinetic steady state. *Drug Metab Dispos*, 38(5), 808-16.
- Waldmeier, P. C., Buchle, A. M. & Steulet, A. F. (1993) Inhibition of catechol-O-methyltransferase (COMT) as well as tyrosine and tryptophan hydroxylase by the orally active iron chelator, 1,2-dimethyl-3-hydroxypyridin-4-one (L1, CP20), in rat brain in vivo. *Biochem Pharmacol*, 45(12), 2417-24.
- Wanless, I. R., Sweeney, G., Dhillon, A. P., Guido, M., Piga, A., Galanello, R., Gamberini, M. R., Schwartz, E. & Cohen, A. R. (2002) Lack of progressive hepatic fibrosis during long-term therapy with deferasiprone in subjects with transfusion-dependent beta-thalassemia. *Blood*, 100(5), 1566-9.
- Weatherall, D. J. (2010) The inherited diseases of hemoglobin are an emerging global health burden. *Blood*, 115(22), 4331-6.
- Weir, M. P., Gibson, J. F. & Peters, T. J. (1984) Biochemical studies on the isolation and characterization of human spleen haemosiderin. *Biochem J*, 223(1), 31-8.
- White, G. P., Bailey-Wood, R. & Jacobs, A. (1976) The effect of chelating agents on cellular iron metabolism. *Clin Sci Mol Med*, 50(3), 145-52.
- Williams, D. D., Peng, B., Bailey, C. K., Wire, M. B., Deng, Y., Park, J. W., Collins, D. A., Kapsi, S. G. & Jenkins, J. M. (2009) Effects of food and antacids on the pharmacokinetics of eltrombopag in healthy adult subjects: two single-dose, open-label, randomized-sequence, crossover studies. *Clin Ther*, 31(4), 764-76.

- Wire, M. B., Bruce, J., Gauvin, J., Pendry, C. J., McGuire, S., Qian, Y. & Brainsky, A. (2012) A randomized, open-label, 5-period, balanced crossover study to evaluate the relative bioavailability of eltrombopag powder for oral suspension (PfOS) and tablet formulations and the effect of a high-calcium meal on eltrombopag pharmacokinetics when administered with or 2 hours before or after PfOS. *Clin Ther*, 34(3), 699-709.
- Wixom, R. L., Prutkin, L. & Munro, H. N. (1980) Hemosiderin: nature, formation, and significance. *Int Rev Exp Pathol*, 22, 193-225.
- Wolfe, L., Olivieri, N., Sallan, D., Colan, S., Rose, V., Propper, R., Freedman, M. H. & Nathan, D. G. (1985) Prevention of cardiac disease by subcutaneous deferoxamine in patients with thalassemia major. *N Engl J Med*, 312(25), 1600-3.
- Wong, A., Alder, V., Robertson, D., Papadimitriou, J., Maserei, J., Berdoukas, V., Kontoghiorghe, G., Taylor, E. & Baker, E. (1997) Liver iron depletion and toxicity of the iron chelator deferiprone (L1, CP20) in the guinea pig. *Biometals*, 10(4), 247-56.
- Wood, J. C., Enriquez, C., Ghugre, N., Tyzka, J. M., Carson, S., Nelson, M. D. & Coates, T. D. (2005a) MRI R2 and R2\* mapping accurately estimates hepatic iron concentration in transfusion-dependent thalassemia and sickle cell disease patients. *Blood*, 106(4), 1460-5.
- Wood, J. C., Otto-Duessel, M., Aguilar, M., Nick, H., Nelson, M. D., Coates, T. D., Pollack, H. & Moats, R. (2005b) Cardiac iron determines cardiac T2\*, T2, and T1 in the gerbil model of iron cardiomyopathy. *Circulation*, 112(4), 535-43.
- Wood, J. C., Otto-Duessel, M., Gonzalez, I., Aguilar, M. I., Shimada, H., Nick, H., Nelson, M. & Moats, R. (2006) Deferasirox and deferiprone remove cardiac iron in the iron-overloaded gerbil. *Transl Res*, 148(5), 272-80.
- WOOD, J. C., OTTO-DUESSEL, M., GONZALEZ, I., AGUILAR, M. I., SHIMADA, H., NICK, H., NELSON, M., MOATS, R. & Canada, G. o. C. N. R. C. (2011) Deferasirox and deferiprone remove cardiac iron in the iron-overloaded gerbil.
- Wood, J. C., Tyszka, J. M., Carson, S., Nelson, M. D. & Coates, T. D. (2004) Myocardial iron loading in transfusion-dependent thalassemia and sickle cell disease. *Blood*, 103(5), 1934-6.
- Worwood, M. (1982) Ferritin in human tissues and serum. *Clin Haematol*, 11(2), 275-307.
- Wright, T. L., Brissot, P., Ma, W. L. & Weisiger, R. A. (1986) Characterization of non-transferrin-bound iron clearance by rat liver. *J Biol Chem*, 261(23), 10909-14.
- Xu, W., Barrientos, T., Mao, L., Rockman, H. A., Sauve, A. A. & Andrews, N. C. (2015) Lethal cardiomyopathy in mice lacking transferrin receptor in the heart. *Cell Rep*, 13(3), 533-45.
- Yao, L. H., Jiang, Y. M., Shi, J., Tomas-Barberan, F. A., Datta, N., Singanusong, R. & Chen, S. S. (2004) Flavonoids in food and their health benefits. *Plant Foods Hum Nutr*, 59(3), 113-22.
- Yatmark, P., Morales, N. P., Chaisri, U., Wichaiyo, S., Hemstapat, W., Srichairatanakool, S., Svasti, S. & Fucharoen, S. (2014) Iron distribution and histopathological characterization of the liver and heart of beta-thalassemic mice with parenteral iron overload: Effects of deferoxamine and deferiprone. *Exp Toxicol Pathol*, 66(7), 333-43.
- Yatmark, P., Morales, N. P., Chaisri, U., Wichaiyo, S., Hemstapat, W., Srichairatanakool, S., Svasti, S. & Fucharoen, S. (2015) Effects of Iron Chelators on Pulmonary Iron Overload and Oxidative Stress in  $\beta$ -Thalassemic Mice. *Pharmacology*, 96(3-4), 192-9.
- Yeh, S. L., Lin, Y. C., Lin, Y. L., Li, C. C. & Chuang, C. H. (2016) Comparing the metabolism of quercetin in rats, mice and gerbils. *Eur J Nutr*, 55(1), 413-22.

- Yeh, S. L., Yeh, C. L., Chan, S. T. & Chuang, C. H. (2011) Plasma rich in quercetin metabolites induces G2/M arrest by upregulating PPAR-gamma expression in human A549 lung cancer cells. *Planta Med*, 77(10), 992-8.
- Yoshino, S., Blake, D. R. & Bacon, P. A. (1984) The effect of desferrioxamine on antigen-induced inflammation in the rat air pouch. *J Pharm Pharmacol*, 36(8), 543-5.
- Young, S. & Bomford, A. (1984) Transferrin and cellular iron exchange. *Clin Sci (Lond)*, 67(3), 273-8.
- Young, S. P. & Aisen, P. (1981) Transferrin receptors and the uptake and release of iron by isolated hepatocytes. *Hepatology*, 1(2), 114-9.
- Yuan, J., Angelucci, E., Lucarelli, G., Aljurf, M., Snyder, L. M., Kiefer, C. R., Ma, L. & Schrier, S. L. (1993) Accelerated programmed cell death (apoptosis) in erythroid precursors of patients with severe beta-thalassemia (Cooley's anemia). *Blood*, 82(2), 374-7.
- Zanninelli, G., Glickstein, H., Breuer, W., Milgram, P., Brissot, P., Hider, R. C., Konijn, A. M., Libman, J., Shanzer, A. & Cabantchik, Z. I. (1997) Iron acquired from transferrin by K562 cells is delivered into a cytoplasmic pool of chelatable iron(II). *Mol Pharmacol*, 51(5), 842-52.
- Zhang, Y., Li, H., Zhao, Y. & Gao, Z. (2006) Dietary supplementation of baicalin and quercetin attenuates iron overload induced mouse liver injury. *Eur J Pharmacol*, 535(1-3), 263-9.
- Zhou, X. Y., Tomatsu, S., Fleming, R. E., Parkkila, S., Waheed, A., Jiang, J., Fei, Y., Brunt, E. M., Ruddy, D. A., Prass, C. E., Schatzman, R. C., O'Neill, R., Britton, R. S., Bacon, B. R. & Sly, W. S. (1998) HFE gene knockout produces mouse model of hereditary hemochromatosis. *Proc Natl Acad Sci U S A*, 95(5), 2492-7.
- Zimelman, A. P., Zimmerman, H. J., McLean, R. & Weintraub, L. R. (1977) Effect of iron saturation of transferrin on hepatic iron uptake: an in vitro study. *Gastroenterology*, 72(1), 129-31.
- Zordoky, B. N. & El-Kadi, A. O. (2007) H9c2 cell line is a valuable in vitro model to study the drug metabolizing enzymes in the heart. *J Pharmacol Toxicol Methods*, 56(3), 317-22.
- Zurlo, M. G., De Stefano, P., Borgna-Pignatti, C., Di Palma, A., Piga, A., Melevendi, C., Di Gregorio, F., Burattini, M. G. & Terzoli, S. (1989) Survival and causes of death in thalassaemia major. *Lancet*, 2(8653), 27-30.
- Zuyderhoudt, F. M., Hengeveld, P., van Gool, J. & Jorning, G. G. (1978) A method for measurement of liver iron fractions in needle biopsy specimens and some results in acute liver disease. *Clin Chim Acta*, 86(3), 313-21.